

**Characterising the interaction between metastasis-associated protein S100A4 and non-muscle myosin IIA
in vitro and *in vivo***

Thesis submitted for the Degree of Doctor of Philosophy at the
University of Leicester

By

Andrew Francis Irvine BSc. (Hons) (Warwick)

Department of Cancer Studies and Molecular Medicine

&

Department of Biochemistry

University of Leicester

July 2012

Characterising the interaction between metastasis-associated protein S100A4 and non-muscle myosin IIA *in vitro* and *in vivo*

Andrew Francis Irvine

Abstract

S100A4 is a member of the S100 family of proteins and increases the motility of many cell types. This is also thought to explain its association with the epithelial-mesenchymal transition (EMT), a developmental program re-activated during tumourigenesis. Mechanistically, S100A4 interacts with a number of targets including Smad3 and liprin- β 1; however, the best characterised is non-muscle myosin IIA (NMIIA) which regulates many aspects of the cytoskeleton. There is a large body of *in vitro* data indicating that S100A4 promotes the monomeric state of NMIIA; however, *in vivo* evidence for the interaction in cells is lacking. Accordingly, the first aim of this study was to determine if S100A4 interacts with, and promotes the monomeric state of NMIIA in A431 cells undergoing SIP1-induced EMT. Intriguingly, co-localisation analysis of S100A4 and NMIIA in A431-SIP1 cells using immunoelectron microscopy indicated that NMIIA is present in a folded, 10S state, and unfolded 6S state, and S100A4 interacts with both. This represents the first evidence of 10S and 6S states of NMIIA in non-muscle cells. In addition, FRAP analysis demonstrated that cells with attenuated expression of S100A4 turned over NMIIA with a slower rate, consistent with S100A4 promoting the monomeric state. The second part of the study explored the mechanism of the S100A4-NMIIA interaction. *In vitro* analysis of phosphomimetic S1916D and S1943D NMIIA showed no differences in binding affinity with S100A4 compared to WT NMIIA, contrary to the published literature. Based on the NMR structure of S100A4 and NMIIA, V77 and C81 were identified as key S100A4 residues that mediated the interaction with NMIIA. Mutation of these sites abolished the interaction with NMIIA, an effect reflected in null-phenotypes for both proteins when over-expressed in A431 cells compared to WT S100A4. In conclusion, this study suggests S100A4 is an important regulator of NMIIA dynamics in cells.

Acknowledgements

First and foremost I would like to thank my supervisor, Dr Marina Kriajevska who not only gave me the opportunity to study at Leicester but has encouraged and supported me throughout the last four years. Marina instilled in me a passion for science and her enthusiasm and determination drove me to complete my studies, something I will always be grateful for.

I'm also indebted to the support of my co-supervisor, Professor Clive Bagshaw who oversaw all aspects of the project. From a scientific point of view, Clive taught me how to think of biology on the molecular scale, crucial in today's world of molecular bioscience. Beyond this, Clive was always there to offer kind words of support and displayed immense patience when responding to my many questions.

I'd also like to thank Dr Eugene Tulchinsky for his useful comments throughout the project and also entertaining both my scientific and non-scientific ramblings which often seemed to delay his departure from the lab in the evenings.

Many thanks to past and present members of Lab 314, especially Dr Emre Sayan and Dr Gareth Browne for their vast technical expertise and patience in answering my lab-related queries; Mrs Karen Kulbicki for helping to organise me and the lab (often, two conflicting objectives); fellow PhD students Wan Makhtar, Louise Hill, Gina Tse and the many MSc students who I had the pleasure of working with. From Clive's lab, I'd like to thank Dr Sandip Badyal who was a constant support throughout the first three years; Dr Jaswir Basran who always had time to share her knowledge and practical know-how and Mrs Nina Bhanji for her technical assistance. From the Leicester EM lab, I'd also like to thank Miss Natalie Allcock and Mr Stefan Hyman for their help and support with the TEM work.

Last but not least, I'd like to thank Dr Alex Fisher for his support and sound judgement; Dr Edward Green for his hob-cleaning skills; and my family: mother, father, Granny, brothers and sister.

Declaration

This thesis submitted for the degree of Doctor of Philosophy, entitled “Characterising the interaction between metastasis-associated protein S100A4 and non-muscle myosin IIA in vitro and in vivo” is based on work conducted by the author in the Departments of Cancer Studies and Molecular Medicine & Biochemistry at the University of Leicester during the period October 2008 and July 2012. All of the work recorded in this thesis is original unless otherwise acknowledged in the text or by references. None of the work has been submitted for another degree in this or any other University.

Signed:

Date:

Department of Cancer Studies and Molecular Medicine

Robert Kilpatrick Clinical Sciences Building

University of Leicester

Leicester

LE1 9HN

Table of Contents

Abstract.....	i
Acknowledgements.....	ii
Declaration.....	iii
Table of contents.....	iv
List of figures.....	xii
List of tables.....	xv
List of abbreviations.....	xvi
1 Introduction	1
1.1 Calcium and the S100 family	2
1.1.1 S100 protein structure	2
1.1.2 Calcium-binding	5
1.1.3 Quaternary structure: dimerisation and higher-order structures.....	7
1.1.4 S100 expression and distribution	9
1.1.5 S100 transcriptional regulation.....	10
1.1.6 Epigenetic regulation	11
1.1.7 Post-translational modifications	12
1.2 S100s and disease	14
1.2.1 Cancer.....	15
1.2.1.1 The Metastatic cascade.....	16
1.2.1.2 Cancer cell invasion	20
1.2.1.3 Epithelial-mesenchymal transition (EMT).....	21
1.2.1.3.1 EMT and metastasis.....	22
1.2.1.3.2 EMT and cell invasion	23
1.2.1.3.4 EMT and other factors	24
1.2.1.3.5 In vitro models of EMT	24
1.2.1.4.1 Experimental evidence.....	25
1.2.1.4.2 Clinical significance	26

1.2.1.4.3	S100A4 and EMT	27
1.3	S100 functions	30
1.3.1	S100A4 and cell migration	30
1.3.1.1	Principles of cell migration	32
1.3.1.1.1	Polarisation.....	32
1.3.1.1.2	Protrusion	36
1.3.1.1.3	Adhesion, translocation and retraction	38
1.3.1.2	Plasticity of cell migration.....	39
1.4	S100 protein targets	41
1.4.1	S100A4 protein targets.....	41
1.4.1.1	Non-muscle myosin IIA	42
1.4.1.1.1	Regulation of myosin II	44
1.4.1.1.1.1	Light chain regulation of myosin II	45
1.4.1.1.1.2	Heavy chain regulation of myosin IIA.....	49
1.4.1.1.1.2.1	Heavy chain phosphorylation	49
1.4.1.1.1.2.2	S100A4-myosin IIA interaction.....	50
1.4.1.1.1.2.3	S100A4-heavy chain phosphorylation interplay.....	52
1.4.1.1.1.2.4	In vivo evidence supporting the S100A4-myosin IIA interaction	54
1.5	Aims and objectives of thesis	56
2	Materials and Methods.....	58
2.1	Materials	59
2.1.1	Chemicals	59
2.1.2	Cell culture	59
2.1.2.1	Eukaryotic cell line.....	59
2.1.2.2	Cell culture reagents and supplements	60
2.1.2.3	Small-interfering RNA oligonucleotides.....	60

2.1.3	Protein analysis	60
2.1.3.1	SDS-PAGE and protein quantification	60
2.1.3.2	Western blotting.....	61
2.1.3.3	Immunoprecipitation	61
2.1.4	Immunocytochemistry and microscopy	61
2.1.5	Cloning and DNA analysis	61
2.1.6	Protein expression and purification.....	62
2.1.7	Kinetics and protein spectrophotometry	62
2.1.8	Antibodies.....	63
2.1.9	Oligonucleotides	69
2.1.10	Constructs	69
2.2	Mammalian cell culture techniques	70
2.2.1	Cell culture	70
2.2.2	Passaging and seeding of cells.....	70
2.2.3	Long-term storage and resuscitation of cells	70
2.2.4	Cell counting.....	71
2.2.5	Transfection	71
2.2.6	Invasion assay	71
2.2.7	Micropattern assay	72
2.2.7.1	Micropattern analysis	73
2.2.7.1.1	Collapse.....	73
2.2.7.1.2	Area.....	73
2.2.8	Stable integration of plasmid DNA.....	73
2.3	Protein analysis techniques	74
2.3.1	Preparation of protein lysates	74
2.3.2	Protein quantification	74
2.3.3	SDS-PAGE	74

2.3.3.1	Coomassie-blue staining.....	75
2.3.3.2	Western blotting.....	76
2.3.3.2.1	Re-probing membranes.....	77
2.3.4	Immunoprecipitation.....	77
2.4	Immunocytochemistry.....	78
2.4.1	Immunofluorescence.....	78
2.4.1.1	Co-localisation analysis of light microscopy imaging.....	79
2.4.2	Electron microscopy immunolabelling.....	79
2.4.2.1	Spatial Statistics and analysis.....	79
2.5	Live cell imaging.....	81
2.5.1	Time-lapse microscopy.....	81
2.5.2	FRAP.....	81
2.5.2.1	Analysis.....	81
2.6	Molecular biology techniques.....	84
2.6.1	Transformation of <i>E. coli</i>	84
2.6.2	DNA manipulation.....	84
2.6.2.1	Small and large-scale isolation of plasmid DNA.....	84
2.6.2.2	DNA gel electrophoresis.....	85
2.6.2.3	Site-directed mutagenesis.....	85
2.6.3	DNA sequencing.....	86
2.7	Recombinant protein expression and purification.....	87
2.7.1	Protein expression and purification.....	87
2.7.2	Quantification of protein and reagent concentration.....	88
2.8	Kinetic assays.....	89
2.8.1	Measuring myosin turbidity.....	89
2.8.2	Transient kinetics.....	89
2.8.2.1	Data Analysis of transient kinetics.....	89

2.8.2.2	Kinetic modelling.....	89
2.9	Analysis and statistics	90
2.9.1	Statistics.....	90
2.9.2	Sequence alignment	90
3	Characterising the expression of S100A4 in a model of Epithelial-Mesenchymal Transition (EMT)	91
3.1	Introduction	92
3.2	Results	94
3.2.1	S100A4 is activated during SIP1-induced EMT.....	94
3.2.2	S100A4 inhibition does not delay or block EMT	98
3.2.3	S100A4 promotes cell migration in A431-SIP1 cells.....	100
3.3	Discussion	101
3.3.1	Transcriptional regulation of S100A4 during EMT.....	101
3.3.2	Temporal regulation of S100A4 expression.....	102
3.3.3	Cell migration and S100A4	103
4	Investigating the interaction between S100A4 and myosin IIA in a model of EMT	105
4.1	Introduction	106
4.2	Results	108
4.2.1	Immunoprecipitation of the heavy chain of myosin IIA by S100A4.....	108
4.2.2	Co-localisation of S100A4 and myosin IIA <i>in vivo</i>	109
4.2.2.1	Use of quantitative analysis to assess protein-protein co-localisation in vivo	109
4.2.2.2	S100A4 and myosin IIA display partial co-localisation as assessed by confocal microscopy	110
4.2.2.3	An immunogold approach to assess co-localisation between S100A4 and myosin IIA.....	113
4.2.2.3.1	Generation of GFP-myosin IIA stable clones	115

4.2.2.3.2	Optimisation of fixation conditions for TEM	117
4.2.2.3.3	Optimisation of labelling conditions for TEM	119
4.2.2.3.4	Statistical methods to quantify co-localisation between S100A4 and GFP-myosin IIA.....	123
4.2.2.3.5	S100A4 and GFP-myosin IIA co-localise at distances consistent with the 10S and 6S forms of myosin	127
4.2.2.3.6	Phosphorylation of the RLC is largely mediated by Rho Kinase	131
4.2.2.3.7	Attenuation of RLC phosphorylation abolishes the co-localisation distance between S100A4 and a GFP-myosin IIA consistent with 6S myosin	132
4.2.2.3.8	S100A4 does not co-localise with GFP α -tubulin	134
4.2.3	S100A4 Modulates Myosin IIA Filament Formation <i>in vivo</i>	138
4.2.3.1	RNAi-mediated Knockdown of S100A4 Promotes Myosin IIA Filaments	138
4.2.3.2	Use of Fluorescence Recovery After Photobleaching (FRAP) to quantify the effect of S100A4 on myosin IIA recovery	140
4.2.3.2.1	Optimisation of the FRAP Protocol.....	141
4.2.3.2.2	S100A4 knockdown slows the recovery of myosin IIA	142
4.3	Discussion	147
4.3.1	Co-localisation of S100A4 and myosin IIA A431-SIP1 cells.....	147
4.3.2	The effect of S100A4 on myosin IIA turnover <i>in vivo</i>	153
5	Mechanism of the S100A4-myosin IIA interaction	155
5.1	Introduction	156
5.2	Results	158
5.2.1	Cloning of phosphomimetic M200 mutants	158
5.2.2	Protein expression trials	160
5.2.3	Large-scale expression and purification.....	161

5.2.4	Characterising the interaction between S100A4 and phosphomimetic Forms of M200.....	165
5.2.4.1	Effect of Ca ²⁺ -dissociation from the S100A4.Ca ²⁺ .M200 complex	166
5.2.4.2	Ionic dependence of S1916D and S1943D on filament formation.	168
5.2.4.3	Disassembly of filaments by S100A4	170
5.2.5	Characterising the interaction of S100A4 with a minimal binding peptide of myosin IIA	172
5.2.5.1	Kinetic characterisation of S100A4 and M39	175
5.2.5.1.1	Ca ²⁺ -dissociation from the S100A4.Ca ²⁺ .M39 complex	175
5.2.5.1.2	Calculation of the equilibrium dissociation constant for Ca ²⁺ -bound S100A4 interacting with M39.....	176
5.2.6	Rational design of S100A4 mutants to perturb the S100A4-myosin IIA interaction.....	178
5.2.6.1	Kinetic Characterisation of S100A4 mutants and M39	180
5.2.6.2	Investigating the interaction of S100A4 mutants in cells	182
5.2.6.2.1	Cloning of V77D and C81D S100A4 mutants	182
5.2.6.2.2	Effect of S100A4 mutation on the S100A4-myosin IIA interaction 183	
5.2.6.2.3	Intracellular Distribution of S100A4 mutants in vivo	184
5.2.6.2.4	Effect of S100A4 mutants on cell migration.....	186
5.2.6.2.5	Use of cell ECM micropatterns to study the effect of S100A4 on the cytoskeleton	188
5.3	Discussion	193
5.3.1	Heavy chain phosphorylation of myosin IIA and S100A4	193
5.3.2	Nanomolar affinity of the S100A4 and M39.....	194
5.3.3	Rational design of S100A4 mutants to abolish the interaction with myosin IIA	196
5.3.4	Myosin IIA-deficient mutants abolish the effect of WT S100A4 on cell migration and spreading.....	197

6	General Discussion	199
6.1	Cancer, EMT and S100A4	200
6.2	Evidence for S100A4 interaction with myosin IIA <i>in vivo</i>	202
6.2.1	Mechanism of the S100A4-myosin IIA interaction.....	204
6.2.2	Functional consequence of the S100A4-myosin IIA interaction.....	205
6.2.3	Regulation of the S100A4-myosin IIA interaction.....	207
6.3	S100A4 and cell migration.....	209
	Appendices.....	213
	References.....	215

List of figures

Figure 1.1:	Localisation of S100 genes on human chromosome 1.....	3
Figure 1.2:	Multiple sequence alignment of human S100 proteins.....	4
Figure 1.3:	Calcium induces a conformational change in S100A4 exposing a hydrophobic pocket.....	6
Figure 1.4:	Dimer structure of S100A4 in the presence of calcium.....	8
Figure 1.5:	The metastatic cascade.....	18
Figure 1.6:	Features of the cell migration cycle.....	34
Figure 1.7:	Regulation of Rho GTPases.....	35
Figure 1.8:	Graphical representation of non-muscle myosin II conformers.....	46
Figure 1.9:	Graphical representation of the 10S form of myosin II.....	47
Figure 1.10:	Sequence of the C-terminal region of myosin IIA.....	53
Figure 2.1:	Plasmid map for pEGFP- α -tubulin.....	71
Figure 2.2:	Plasmid map for pIRES-PURO2.....	71
Figure 2.3:	Plasmid map for pBI-S100A4.....	72
Figure 2.4:	Plasmid map for pEGFP-MIIA.....	72
Figure 2.5:	Plasmid map for pET28a-M200.....	73
Figure 2.6:	Graphical representation of FRAP data analysis.....	87
Figure 3.1:	Western blot analysis of S100A4 expression during EMT.....	98
Figure 3.2:	Temporal overview of SIP1-induced EMT.....	100
Figure 3.3:	Localisation of S100A4 and SIP1 during EMT.....	101
Figure 3.4:	Effect of S100A4 knockdown on progression of EMT.....	103
Figure 3.5:	RNAi-mediated knockdown of S100A4 reduces the rate of cell migration.....	104
Figure 4.1:	Immunoprecipitation of S100A4 from A431-SIP cells.....	112
Figure 4.2:	Immunofluorescence staining of S100A4 and Myosin IIA in A431-SIP1 cells.....	115
Figure 4.3:	Co-localisation analysis of S100A4 and Myosin IIA.....	116
Figure 4.4:	Schematic of N-terminally-tagged GFP-myosin IIA and S100A4 bound to the C-terminus.....	118
Figure 4.5:	Western blot analysis of A431-SIP1 and Cl.M cells.....	119
Figure 4.6:	Confocal analysis of Cl.M cells.....	120
Figure 4.7:	Optimisation of fixation conditions for TEM.....	122
Figure 4.8:	Immunogold labelling of Cl. M cells stained for S100A4.....	124
Figure 4.9:	Immunogold labelling of Cl. M cells stained for GFP.....	125
Figure 4.10:	Secondary-only control staining of Cl. M cells.....	126
Figure 4.11:	Co-localisation of S100A4 and GFP-myosin IIA.....	128
Figure 4.12:	Schematic representation of analysis used to assess co-localisation.....	130
Figure 4.13:	S100A4 and GFP-myosin IIA co-localise at two statistically significant distances.....	131
Figure 4.14:	Schematic representing the possible variability in measuring the distance between GFP and S100A4 gold particles.....	133

Figure 4.15:	Control to assess single-sided immunogold labelling.....	134
Figure 4.16:	ROCK is the major kinase involved in phosphorylation of the RMLC.....	135
Figure 4.17:	Attenuation of RMLC phosphorylation leads to colocalisation between GFP and S100A4 at only one specific distance consistent with 10S GFP-myosin IIA.....	136
Figure 4.18:	Selected images of GFP and S100A4 co-localised at distances consistent with 10S GFP-myosin IIA.....	137
Figure 4.19:	Characterisation of A431-SIP1 GFP- α -tubulin (Cl. T) cells.....	139
Figure 4.20:	Immunogold labelling of Cl.T Cells stained for S100A4 and GFP.....	140
Figure 4.21:	GFP- α -tubulin and S100A4 do not co-localise.....	141
Figure 4.22:	Knockdown of S100A4 causes an increase in myosin IIA filaments.....	143
Figure 4.23:	A graphical overview of the FRAP process.....	144
Figure 4.24:	Representative cell transfected with si non-targeting used for FRAP experiments....	147
Figure 4.25:	Representative cell transfected with si S100A4 used for FRAP experiments.....	148
Figure 4.26:	Kinetic traces from selected sells in the presence and absence of S100A4.....	149
Figure 4.27:	Knockdown of S100A4 significantly slows GFP-myosin IIA recovery.....	150
Figure 4.28:	Flexibility of myosin II around the HMM/LMM junction.....	154
Figure 4.29:	Schematic representing possible origins of the S100A4.6S myosin state.....	156
Figure 5.1:	Schematic representation of a M200, a C-terminal fragment of non-muscle myosin IIA.....	163
Figure 5.2:	Analysis of S1916D and S1943D plasmid DNA by gel electrophoresis.....	164
Figure 5.3:	Expression of S1916D and S1943D protein in the presence or absence of IPTG.....	165
Figure 5.4:	UV Spectroscopy of eluted fractions to assess the presence of S1916D or S1943D protein.....	166
Figure 5.5:	SDS-PAGE analysis of fractions containing S1916D and S1943D as identified by UV.....	167
Figure 5.6:	UV Spectropic and SDS-PAGE Analysis of Purified S1916D and S1943D.....	168
Figure 5.7:	Dissociation of Ca ²⁺ from S100A4 monitored Using Quin-2 fluorescence in the presence and absence of myosin proteins.....	171
Figure 5.8:	Turbidity of S1916D and S1943 as a function of [NaCl].....	173
Figure 5.9:	Dissociation of S1916D or S1943D filaments by S100A4.....	175
Figure 5.10:	Schematic Representation of the S100A4 Binding Site on Myosin IIA.....	177
Figure 5.11:	Structure of S100A4 complexed with a C-terminal fragment of myosin IIA, M39.....	178
Figure 5.12:	Dissociation of Ca ²⁺ from S100A4 monitored using quin-2 fluorescence in the presence and absence of M39.....	179
Figure 5.13:	Competition assay to determine the association rate constant for M39 binding to the S100A4.Ca ²⁺ Complex.....	181
Figure 5.14:	Schematic representation of the M39/S100A4 complex and mutated residues.....	183

Figure 5.15:	Dissociation of Ca ²⁺ from V77D and C81D monitored using quin-2 fluorescence in the presence or absence of M39.....	184
Figure 5.16:	Effect of increasing M39 Concentration on Ca ²⁺ Dissociation from V77D and C81D.....	185
Figure 5.17:	Analysis of V77D and C81D plasmid DNA by gel electrophoresis.....	186
Figure 5.18:	Immunoprecipitation analysis of WT S100A4, V77D and C81D.....	187
Figure 5.19:	Immunofluorescence analysis of WT S100A4, V77D and C81D.....	189
Figure 5.20:	Effect of WT S100A4, V77D and C81D on cell migration.....	191
Figure 5.21:	Representative images of transfected cells seeded on micropatterns.....	194
Figure 5.22:	S100A4 induces a collapsed-like phenotype on cells.....	195
Figure 5.23:	Effect of S100A4 on size of cells seeded on micropatterns.....	196
Figure 5.24:	Acidic residues point out into solution from the S100A4-M39 complex.....	199
Figure 6.1:	Mechanism for S100A4 promoting the turnover of myosin IIA in vivo.....	210
Figure 6.2:	Regulation of myosin IIA assembly/disassembly: The role of RLC/ MHC phosphorylation and S100A4-binding	215

List of tables

Table 1.1:	Summary of the transcriptional regulation of S100A4.....	11
Table 1.2:	Studies correlating S100A4 over-expression with poor prognosis.....	27
Table 1.3:	Studies identifying activation of S100A4 during EMT.....	29
Table 1.4:	Studies correlating S100A4 expression with increased rates of cell migration.....	31
Table 2.1:	Description of cell lines used in this study.....	63
Table 2.2:	Description of primary antibodies used during this study.....	67
Table 2.3:	Description of oligonucleotide primers used during this study.....	69
Table 2.4:	Description of plasmids used during this study.....	70
Table 2.5:	Volumes of PBS, TE and DMEM required for Cell Passaging.....	74
Table 2.6:	Volumes of water and acrylamide mix required for SDS-PAGE.....	79
Table 2.7:	PCR cycles for site-directed mutagenesis.....	90
Table 4.1:	Data summary for quantitative co-localisation of S100A4 and myosin IIA.....	116
Table 5.1:	Summary of rate constants and associated amplitudes from Figure 5.6.....	171

List of abbreviations

A	Amplitude
ACD	Assembly competent domain
ADAM	A disintegrin and metalloprotease domain
ADP	Adenosine diphosphate
APC	Adenomatous polyposis coli
aPKC	Atypical protein kinase C
APS	Ammonium persulphate
ATP	Adenosine triphosphate
ATTCC	American Type Tissue Culture Collection
AUC	Analytical ultracentrifugation
β -ME	β -mercaptoethanol
BSA	Bovine Serum Albumin
Ca^{2+}	Calcium ion
CBF	CCAAT-binding factor
CCL	Chemokine (C-C motif) ligand
CK2	Casein kinase 2
CRC	Colorectal cancer
CSC	Cancer stem cell
CSF	Colony-stimulated factor
CSR	Complete spatial randomness
CTC	Circulating tumour cells
DAPI	4',6-diamidino-2-phenylindol
DMEM	Dulbeccos modified Eagles medium
DMSO	Dimethyl sulphoxide
DNA	Deoxyribonucleic acid
DOX	Doxycycline
DTC	Disseminated tumour cells
E	Embryonic day

ECM	Extracellular matrix
EDTA	Ethylenediaminetetraacetic acid
EGF	Epidermal growth factor
EGTA	ethylene glycol tetraacetic acid
ELC	Essential light chain
EMT	Epithelial-mesenchymal transition
EREG	Epiregulin
ESC	Embryonic stem cell
FBS	Foetal bovine serum
FGF	Fibroblast growth factor
FRAP	Fluorescence recovery after photobleaching
FSP-1	Fibroblast-specific protein 1
FTS-1	Fibroblast transcription site-1
GAP	GTPase-activating protein
GDI	Guanosine nucleotide dissociation inhibitor
GEF	Guanine nucleotide exchange factor
GTP	Guanosine triphosphate
HDAC	Histone deacetylase
HMM	Heavy meromyosin
HNSCC	Head-neck squamous carcinoma cell
HRP	Horseradish peroxidase
ICA	Intensity correlation analysis
ICG	Intensity correlation quotient
Ig	Immunoglobulin
IL	Interleukin
IL-1B	Interleukin-1 β
kb	Kilobase
K _d	Equilibrium dissociation constant
LAR	Leukocyte antigen-related protein

LB	Luria broth
LMM	Light meromyosin
LOX	Lysyl oxidase-like
MBD	methyl-CpG-binding domain
MHC	Myosin heavy chain
MII	Non-muscle myosin II
MLCK	Myosin light chain kinase
MMP	Matrix metalloproteinases
MMTV	Mouse mammary tumour virus
mRNA	messenger RNA
MTOC	Microtubule-organising centre
MYPT1	Myosin phosphatase target subunit 1
NK	Natural killer cells
NM	Non-muscle myosin
NMII	Non-muscle myosin II
NOD	Non-obese diabetic
NT	Non-targeting
PAGE	Polyacrylamide gel electrophoresis
PBS	Phosphate buffered saline
PCC	Pearson's correlation coefficient
PDAC	Pancreatic ductal adenocarcinoma
PDM	Products differences of the mean
PI3-K	Phosphatidylinositol 3-kinase
PIP ₂	Phosphatidylinositol (4,5)-biphosphate
PIP ₃	Phosphatidylinositol (3,4,5)-triphosphate
PKC	Protein kinase C
PyMT	Polyoma virus middle T antigen
RAGE	Receptor for advanced glycation endproducts
RLC	Regulatory light chain

RNA	Ribonucleic acid
RNAi	RNA interference
ROCK	Rho-associated, coiled-coil kinase
ROI	Region of interest
SCID	Severe combined immunodeficiency
SDS	Sodium dodecyl sulphate
SIP1	Smad-interacting protein 1
siRNA	Small interfering ribonucleic acid
Sp1	Specificity protein 1
TAE	Tris acetic acid EDTA
TAM	Tumour-associated macrophages
TBS	Tris-buffered saline
TCF/LEF-1	T-cell factor/lymphoid enhancer factor
TE	Trypsin/EDTA
TEM	Transmission electron microscopy
TFP	Trifluoperazine
TGF- β	Transforming growth factor- β
TNC	Tenascin C
TNF- α	Tumour necrosis factor- α
UTR	Untranslated region
v/v	Volume by volume
VEGF	Vascular endothelial growth factor
w/v	Weight by volume
WASP	Wiskott–Aldrich syndrome protein
WAVE	WASP family verprolin-homologous protein
WT	Wild type

1 Introduction

1.1 Calcium and the S100 family

Calcium is a key secondary messenger regulating a variety of cellular processes including cell migration, muscle contraction and neurotransmitter release (Carafoli, 2002). As such, cellular concentrations of calcium are tightly regulated through the balance between calcium import and export, maintaining resting levels near 100 nM and signalling levels approaching 1 μ M (Berridge *et al.*, 2000). Decoding of the calcium signal is carried out by calcium-binding proteins, two types of which exist: buffers and effectors. Buffers serve to precisely co-ordinate the amplitude and recovery of the calcium signal while effectors are responsible for activating different calcium-sensitive processes. Around 200 of these proteins are encoded by the human genome (Berridge *et al.*, 2003).

The S100 family is the largest subfamily of calcium-binding proteins with over 23 members identified in *Homo sapiens* to date. Sixteen *S100s* cluster on chromosome 1q21.3 (Ravasi *et al.*, 2004), a locus known as the epidermal differentiation complex (Mischke *et al.*, 1996) (Figure 1.1). The genes evolved approximately 500 million years ago, coinciding with the origin of vertebrates in which they are exclusively expressed (Marenholz *et al.*, 2004). Mammalian *S100* genes share a common genomic structure consisting of three exons, the first of which encodes the 5' untranslated region while the second and third correspond to the open reading frame with the 3' untranslated region (UTR) located in the last part of the third exon (Ravasi *et al.*, 2004).

1.1.1 S100 protein structure

The *S100* genes encode small, acidic proteins that have a common structure consisting of a pseudo (N-terminal) and canonical (C-terminal) EF-hand, linked by a hinge region and ending in a C-terminal extension of varying length (Figure 1.2). The highest degree of sequence variability occurs within the hinge and C-terminal region and likely determines target specificity within the S100 family. EF hand domains are characterised by a helix-loop-helix motif of which the loop is responsible for calcium co-ordination. The pseudo EF hand is so-called because the loop contains 14 residues, as opposed to the typical 12 of the canonical EF hand and is specific to S100 and S100-

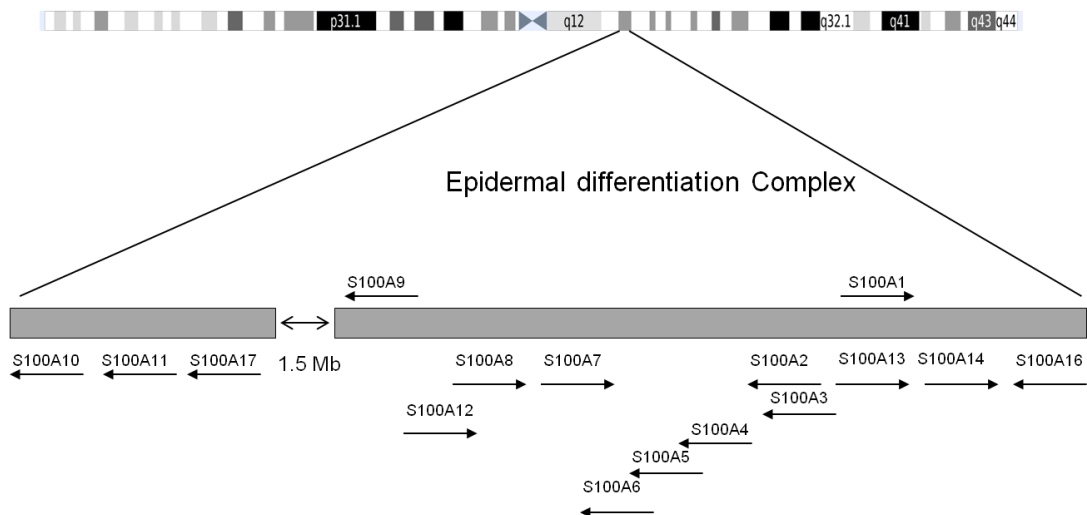
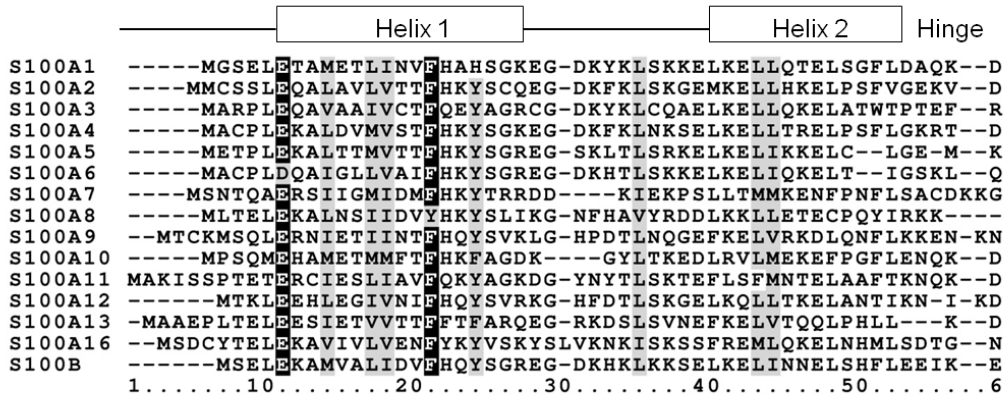


Figure 1.1: Localisation of *S100* genes on human chromosome 1

16 *S100* genes localise to region 1q21.3 of human chromosome 1, termed the epidermal differentiation complex (EDC). *S100A10*, *A11* and *A17* are approximately 1.5Mb upstream of the EDC. Arrows indicate direction of loci from 5'-UTR to 3'-UTR. Figure not to scale. Adapted from Ravasi *et al.*, (2004)

Pseudo EF-Hand



Canonical EF-Hand

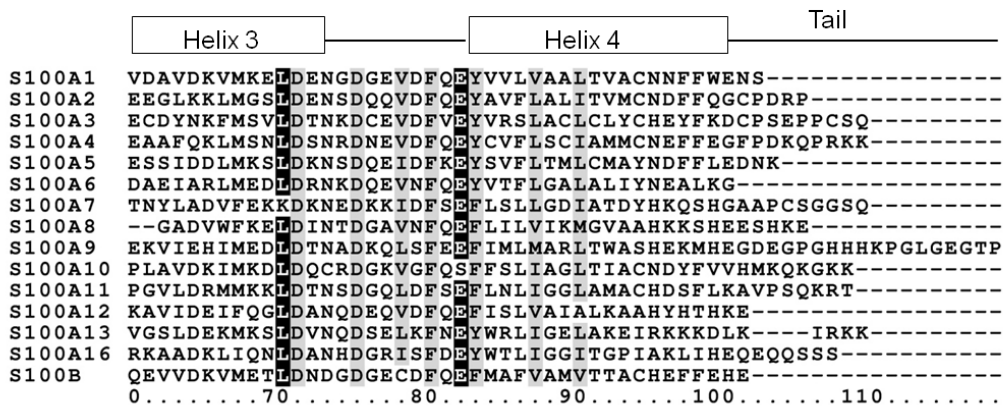


Figure 1.2: Multiple sequence alignment of human S100 proteins

S100 proteins consist of a pseudo (N-terminal) and canonical (C-terminal) EF hand each composed of a helix-loop-helix motif. Black shaded-residues indicate identical residues whilst gray-shaded are biochemically similar residues. Note the lack of sequence homology within the hinge and tail region.

like proteins (reviewed in (Marenholz *et al.*, 2004). Upon calcium binding, all S100 proteins [except S100A10 which is constitutively active (Rety *et al.*, 1999)] undergo a conformational change exposing a large hydrophobic pocket suitable for target binding (Donato, 1999). This is comparable to the activation of calmodulin in a calcium-dependent manner, also resulting in exposure of a hydrophobic surface used to recruit target proteins (Zhou *et al.*, 2006).

1.1.2 Calcium-binding

In the case of S100A4, calcium-binding causes a 60° re-orientation of helix 3 opening up a large cleft between helix 3, the hinge and helix 4 (Figure 1.3A,B) exposing a number of hydrophobic residues (Figure 1.3C). The pseudo EF (EF1) hand loop primarily co-ordinates calcium via backbone carbonyls whereas the canonical EF (EF2) hand loop binds calcium mainly via side chain carboxyls or carbonyls (Gingras *et al.*, 2008; Pathuri *et al.*, 2008). Within the literature, there are large discrepancies regarding calcium-binding properties of S100A4, in part due to the varying affinities of the pseudo and canonical EF hand to calcium (Badyal *et al.*, 2011). Garrett *et al.*, (2008) and Malashkevich *et al.*, (2008) considered there to be two classes of calcium-binding sites with the higher affinity site representing the canonical and lower affinity site representing the pseudo EF hand. Our group recently re-addressed this question demonstrating that mutation of the calcium co-ordinating residue, D63 in EF2 caused a significant reduction in calcium binding while mutation of E33 in EF1 led to only modest effects (Badyal *et al.*, 2011). These data are also supported by immunoprecipitation studies where the same D63N mutant abolished the interaction of S100A4 with one of its targets, non-muscle myosin IIA suggesting a fully functional canonical EF hand is required for a calcium-dependent interaction with its protein targets (Kim & Helfman, 2003). Despite this, there is likely co-operativity between EF1 and 2 (Badyal *et al.*, 2011) which could explain the result of Dutta *et al.*,(2002) who showed using NMR that N-terminal residues were perturbed at lower calcium ratios compared to those in the C-terminus, suggesting the N-terminal, pseudo EF hand is in fact the higher affinity site.

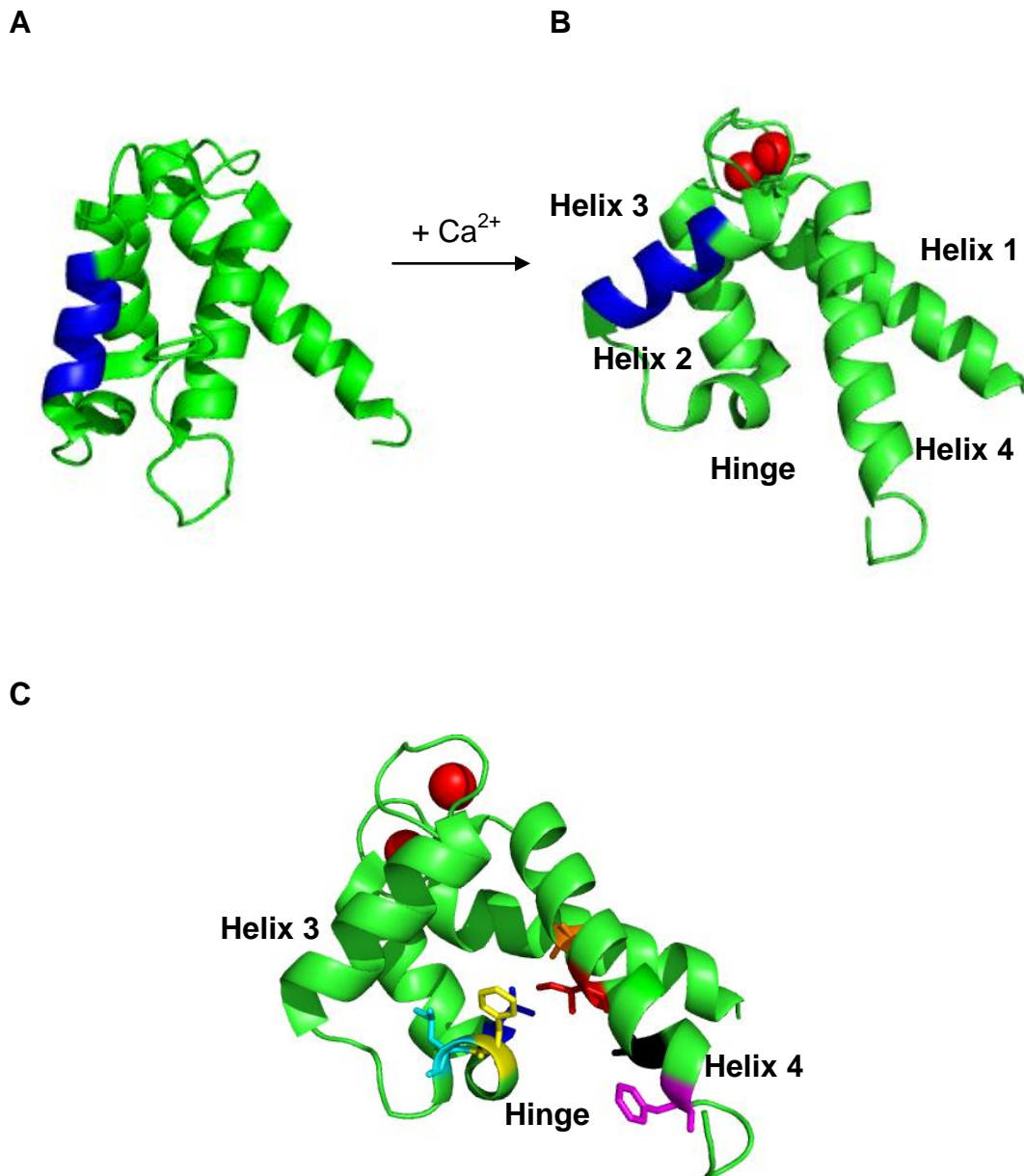


Figure 1.3: Calcium induces a conformational change in S100A4 exposing a hydrophobic pocket

Calcium-binding in apo S100A4 (**A**) causes helix 3 (highlighted in blue) to undergo a 60° re-orientation (**B**) opening up a large hydrophobic cleft between helix3, helix 4 and the hinge region. Calcium ions represented by red spheres. This pocket serves as an important site for protein-protein interactions (**C**). Highlighted residue as follows: Hinge: L41, blue; F45, yellow; L46, cyan. Helix 4: L79, orange; I82, red; C86, black; F89, purple. PDB code: Apo-S100A4, 1M31; Ca²⁺-S100A4, 3C1V

1.1.3 Quaternary structure: dimerisation and higher-order structures

In general, S100 proteins exist as symmetric homodimers in solution stabilised by non-covalent interactions between hydrophobic residues of helices 1 and 4 from each monomer (Gingras *et al.*, 2008) (Figure 1.4). In the case of S100A4, Tarabykina *et al.*, (2001) identified a number of key residues required for dimerisation within helix 4 including Phe72, Tyr75, Phe78 and Leu79 and complimentary residues from helix I, Ile12, Val13 and Phe16. Interestingly, mutation of Tyr75 to Phe was shown to stabilise the dimer attributed to the exposure of a fully hydrophobic cavity to solvent thus favouring dimerisation over free monomers (Tarabykina *et al.*, 2001). In terms of homodimerisation affinity, the equilibrium dissociation constant is approximately 4 μM , with dimerisation favoured in the presence of calcium (Streicher *et al.*, 2010).

Although S100s are generally thought to exist as homodimers, there are many reports of heterodimerisation within the family (Deloulme *et al.*, 2003). S100A8 and A9 are the best characterised S100 heterodimers with the complex having been shown to inhibit the S100A9-stimulated effect on neutrophil adhesion (Ryckman *et al.*, 2003). Moreover, the S100A1-S100B heterodimer inhibits the assembly of brain microtubules in the presence of zinc while S100A1-B homodimers alone have no such effect (Sorci *et al.*, 2000). Heterodimerisation between S100A6-S100B and S100A11-S100B has also been reported although interestingly, the C-terminal domain of S100B has been shown to be dispensable for the heterodimerisation with S100A1, but not for complexes formed with either S100A6 or S100A11, suggesting there are at least two distinct mechanisms for S100 heterodimer formation (Deloulme *et al.*, 2003). S100A4 has also been shown to heterodimerise with S100A1, an interaction that requires Cys76 and Cys81 since mutation of these residues abolishes heterodimerisation whilst not affecting S100A4 homodimerisation (Tarabykina *et al.*, 2000). Despite this evidence, the functional consequences of the S100A1-A4 heterodimer have yet to be explored.

In addition to dimerisation, it is now well established that S100 proteins are capable of forming higher order structures including tetramers and oligomers (Streicher *et al.*, 2010). Higher order states of S100s tend to be linked with their extracellular role, which in the case of S100B is functionally relevant since the tetramer binds its receptor with higher affinity than dimeric S100B (Ostendorp *et al.*, 2007). In general, calcium

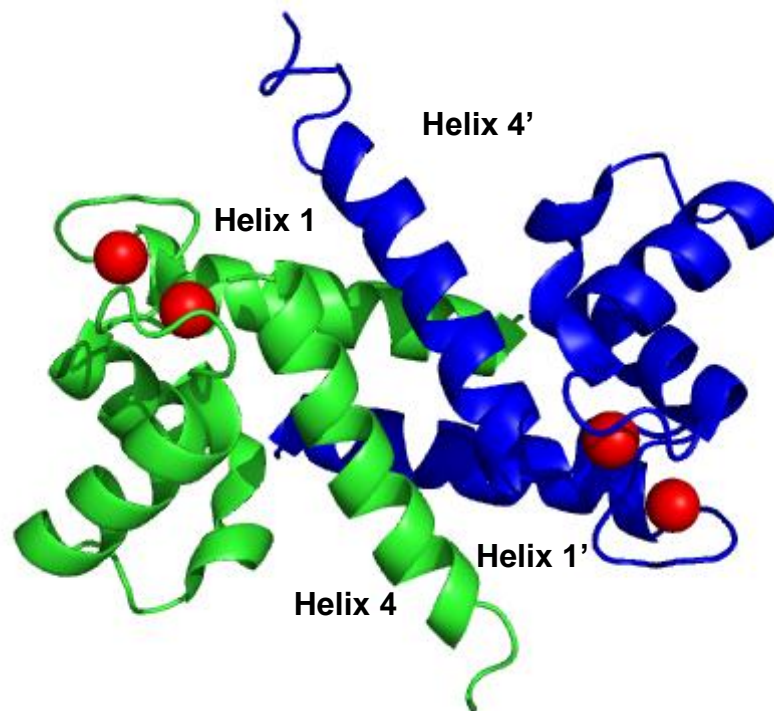


Figure 1.4: Dimer structure of S100A4 in the presence of calcium

The dimer of S100A4 in the Ca^{2+} -bound form is stabilised by non-covalent hydrophobic residues in helix 1 and helix 4. PDB code: Ca^{2+} -S100A4, 3C1V

changes the balance from a monomer-dimer to a dimer-oligomer equilibrium suggesting the calcium-induced conformational change alters the structure sufficiently to allow the formation of higher order structures (Streicher *et al.*, 2010). Indeed, a crystal structure of S100A4 in the calcium-bound state indicates that one of the hydrophobic pockets in each dimer interacts with the C-terminal tail of another, explaining why tetramerisation disrupts binding with target peptides (Gingras *et al.*, 2008). In agreement with this, it has recently been reported that trifluoperazine (TFP)-induced S100A4 oligomerisation prevents S100A4 from binding to one of its targets, non-muscle myosin IIA suggesting S100-induced oligomerisation could represent a regulatory mechanism in cells (Malashkevich *et al.*, 2010). Indeed, given the maximum concentrations of S100 proteins in cells (~10 μM), they are likely to exist as dimers without additional regulation (Streicher *et al.*, 2010).

1.1.4 S100 expression and distribution

Despite the high level of sequence and structural homology, S100 proteins exhibit exquisite tissue- and cell-specific expression (Donato, 2001). A common theme in expression of S100s is that their levels are often induced following cell or genotoxic stress (Donato, 2003). For instance, S100B is not expressed in normal cardiomyocytes but is strongly activated post-infarction (Tsoporis *et al.*, 2005) whilst S100A6 expression is activated in the adenocarcinoma cell line, HCT116 upon exposure to ionizing radiation (Orre *et al.*, 2007).

In the case of S100A4, early work focused on its potential use as a fibroblast marker, hence one of its alternative names: fibroblast specific protein-1 (FSP-1) [the use of which has been the source of some debate within the field (Österreicher *et al.*, 2011)]. This hypothesis originated from a study by Strutz *et al.*, (1995) who identified S100A4 as one of five specific transcripts in renal tubulointerstitial fibroblasts when compared to isogenic murine proximal tubular epithelium cells. Notwithstanding, S100A4 has since been shown to be expressed in a multitude of tissues and cell-types including parietal cells of the stomach, smooth muscle cells, endothelial cells and in many differentiated blood cells (neutrophils, macrophages, T-lymphocytes and platelets) thus strongly disproving the notion that S100A4 is a fibroblast specific protein (Schneider *et al.*, 2008).

1.1.5 S100 transcriptional regulation

Like other S100 proteins, S100A4 expression is commonly activated during a number of cell stress events, including chronic osmotic shock (Chen *et al.*, 2011), (Rivard *et al.*, 2007); hypoxia (Horiuchi *et al.*, 2012) and inflammation (Schneider *et al.*, 2008). Accordingly, a variety of studies have sort to determine the transcriptional regulation of S100A4 leading to a complex network of response elements and transcription factors controlling its expression as summarised in table 1.1. In general, S100A4 has been strongly implicated as a downstream target of many important cytokines and growth factors including, but not limited to TGF- β (Xie *et al.*, 2009b; Sato *et al.*, 2010), FGF (Ryan *et al.*, 2003), EGF (Hugo *et al.*, 2009) and IL-1 β (Franco-Barraza *et al.*, 2010) although the full signalling cascades have yet to be fully elucidated. Tulchinsky *et al.*, (1995) originally identified an AP-1 site as well as a complex of the NF-kB/Rel specific p50.p50 homo- and p50.p65 heterodimers bound to a kB-like element within the first intron of S100A4. Since this, additional *cis* elements interacting with transcription factors belonging to the SP-1 and CBF families were found (Cohn *et al.*, 2001). More recently, another *cis* element, the so-called fibroblast transcription site-1 (FTS-1) was identified approximately 1000 bps upstream of the TATA box and was shown to interact in a complex with the CBF- α subunit/KRAB-associated protein 1 (KAP-1) (Venkov *et al.*, 2007). Other signalling cascades are also important in controlling S100A4 expression with an *ErbB2* response element identified in the promoter (Hernan *et al.*, 2003) as well as a TCF binding site (Stein *et al.*, 2006) implicating the Wnt pathway in the transcriptional regulation of S100A4. Finally, ectopic expression of integrin $\alpha 6\beta 4$ in MDA-MB-45 cells has also been shown to induce expression of S100A4 via a NFAT5-dependent mechanism (Chen *et al.*, 2009).

Table 1.1: Summary of the transcriptional regulation of *S100A4*

Site	Description	Location	Reference
AP-1	Intronic enhancer	First intron	(Tulchinsky <i>et al.</i> , 1995)
kB-like element			(Cohn <i>et al.</i> , 2001)
SP-1			
CBF			
FTS-1	<i>Cis</i> element	1000 bps upstream of TATA box	(Venkov <i>et al.</i> , 2007)
ErbB2	Response element	Promoter	(Hernan <i>et al.</i> , 2003)
TCF	Binding site	Promoter	(Stein <i>et al.</i> , 2006)

1.1.6 Epigenetic regulation

In addition to transcriptional regulation, there is a large body of evidence suggesting many of the *S100* genes including *S100A4* are epigenetically regulated with DNA methylation the best characterised (Lindsey *et al.*, 2007). Mammalian genomes are generally depleted in CpG pairs except for short DNA repeats, known as CpG islands that frequently coincide with gene promoters. When such cytosine residues are methylated by DNA methyltransferases, these regions are often associated with transcriptional inhibition caused by one of two mechanisms. Firstly, methyl-CpG-binding domain proteins (MBDs) recruit additional proteins such as histone deacetylases (HDACs) which facilitate remodelling of chromatin to its repressed state, heterchromatin. Secondly, methylation can physically perturb binding of transcription factors to DNA thus preventing trans-activation (reviewed in (Robertson, 2005)).

The role of DNA methylation was first recognised for *S100s* when inhibition of DNA methyltransferases by 5'azacytidine resulted in activation of *S100A4* in lymphoma cells (Tulchinsky *et al.*, 1995). Since then, numerous studies have shown DNA methylation of *S100s* to be crucial in regulating their expression (Lindsey *et al.*, 2007) although each *S100* gene is likely to be controlled by CpG-specific DNA methylation rather than epigenetic silencing across the entire chromosome band. For instance, *S100A6* has been shown to be hypomethylated in fibroblasts but 30 kb away, *S100A2* is heavily methylated and therefore transcriptionally inactive supporting the notion that gene

specific, rather than global effects of chromatin structure control *S100* gene expression (Leśniak, 2011).

1.1.7 Post-translational modifications

Arguably the most common post-translational modification reported for S100 proteins are related to redox modifications of cysteine residues (Su *et al.*, 2009). The two most important of these include S-glutathionylation, the formation of a mixed disulphide with a glutathione molecule and S-nitrosylation, the addition of a nitrosyl group (reviewed in (Winterbourn & Hampton, 2008)). Cysteine residues are highly conserved between species and only S100A12 and A13 lack them (Su *et al.*, 2009). S100A8 and A9 are the best characterised S100s regarding redox modifications with S-nitrosylation important in regulating blood flow during inflammation (Lim *et al.*, 2008). The role of S100A1 as a calcium receptor is also dependent on S-glutathionylation, a modification thought to alter the flexibility of the N- and C-terminal calcium-binding loops thereby enhancing calcium co-ordination (Goch *et al.*, 2005). The neurotrophic effect of S100B is dependent on its oxidation to intramolecular disulphide-bridged monomers or dimers with Cys68 and Cys84 mutants lacking biological activity (Zhukova *et al.*, 2004). In a recent study it was demonstrated that S100A4 and A6 exist in both unmodified and glutathionylated forms in HCT116 cells, but upon exposure to ionizing radiation, the forms shifted towards cysteineylated S100A4 and A6 (Orre *et al.*, 2007). In the case of S100A6, this was shown to cause a nuclear to cytoplasmic translocation (the effect of cysteineylation on S100A4 was not explored).

In general, there are relatively little data regarding other post-translational modifications of S100 proteins. In one study by Sakaguchi *et al.*, (2000) phosphorylation of S100A11 in confluent fibroblasts was shown to lead to nuclear translocation and subsequent inhibition of DNA synthesis implicating S100A11 in contact inhibition of growth. Consistent with this, phosphorylation of S100A8 and A9 induced a cytoplasm-plasma membrane translocation, an effect dependent on changes in the calcium-binding properties of both proteins (van den Bos *et al.*, 1996). More recently, S100A4 was identified in a number of charge variants from both cell lines and tumour samples using native 2D-PAGE, consistent with protein phosphorylation although MALDI-TOF mass spectrometry failed to identify any such modifications

(Haugen *et al.*, 2008). To date, there has only been one study regarding the sumoylation of an S100 protein. Using primary articular chondrocytes, Miranda *et al.*, (2010) demonstrated that S100A4 sumoylation at Lys22 and Lys96 occurs after exposure to IL-1 β and leads to nuclear translocation of S100A4 resulting in transactivation of MMP-13 (Okada *et al.*, 1997).

1.2 S100s and disease

Since S100s are expressed in a variety of tissues and cells, deregulation of their expression is associated with a wide array of pathological disorders which can be broadly classified into four categories: neurodegeneration, cardiomyopathies, inflammatory diseases and cancer (Marenholz *et al.*, 2004).

In terms of neurodegeneration, S100B has long been associated with traumatic brain injuries with an increase seen in patients suffering from Down's syndrome, Alzheimer's or multiple sclerosis (Donato, 2001). It is also recognised as a marker for brain ischaemia and is predictive of clinical outcome (Donato, 2001).

Of the S100 proteins, S100A1 is most strongly associated with cardiomyopathies. It is abundantly expressed in cardiomyocytes where it is thought to modulate contractile performance of the heart. Indeed, increased expression of S100A1 is associated with right ventricular hypertrophy and its down-regulation with end-stage heart failure. The plasma level of S100A1 also correlates with acute myocardial ischaemia (reviewed in (Rohde *et al.*, 2010). Although not expressed in mature myocardium, S100B expression is induced after myocardial infarction and causes increased apoptosis and progressive deterioration of cardiac function (Tsoporis *et al.*, 2010). S100A6 has also been shown to be upregulated in damaged myocardium where it may also be involved in hypertrophy (Tsoporis *et al.*, 2005).

A third focus of S100-related research has centred on their role in inflammatory (and often autoimmune) disorders. Of the S100s involved, S100A8, A9 and A12 are most strongly associated with inflammation and are collectively known as the calgranulins; reflecting their calcium-binding capacity as well as their high expression in granulocytes. Indeed, S100A8 and A9 alone are considered to constitute ~45% of the cytosol of neutrophils (reviewed in (Goyette & Geczy, 2011). As such, serum levels of these S100s are often indicative of many inflammatory disorders including cystic fibrosis, chronic bronchitis, Crohn's disease and ulcerative colitis (Manolakis *et al.*, 2011). In addition, other S100s are important components in rheumatoid arthritis and osteoarthritis with increased expression of S100A4 in chondrocytes shown to correlate with MMP-13 expression and thus progressive loss of cartilage (Yammani, 2012).

Increased expression of S100B is also associated with these disorders and S100A11 has been linked with chondrocytes hypertrophy (Marenholz *et al.*, 2004).

As described previously, 16 of the S100 genes are located on chromosome 1q21.3, a site known as the epidermal differentiation complex. This locus is frequently rearranged in cancer including uterine and bladder adenocarcinomas and is the target for translocation in breast adenocarcinoma (Solomon *et al.*, 1991). Accordingly, the altered expression of S100s is frequently observed in cancer and extensive research has sought to characterise their functions in the context of tumour progression as well as their potential use as prognostic markers (reviewed in (Salama *et al.*, 2008).

1.2.1 Cancer

Cancer is a disease where normal cells acquire a number of alterations in cellular processes progressively transforming them from a normal to a neoplastic state. As such, it can be considered a microevolutionary process whereby genetic mutations of key genes provide a selective advantage over those non-cancerous cells leading to clonal expansion. The initial source of these somatic mutations is often caused by DNA damaging agents including chemical carcinogens and radiation in the form of X-rays and UV light. In good agreement with this, is that many agents that provoke cancer (carcinogens) also cause genetic changes in DNA (mutagens). Once these initiating mutations have taken hold, cancer cells are further characterised by their genomic instability thereby increasing the likelihood of generating a mutant population with a selective advantage of their non-cancerous counterparts (reviewed in (Negrini *et al.*, 2010). In 2000, a seminal paper (Hanahan & Weinberg, 2000) provided a framework to understand the extensive diversity of neoplastic disease by proposing six hallmark capabilities that tumour cells often acquire during tumourigenesis:

1. Sustaining proliferative signalling
2. Evading growth suppressors
3. Resisting cell death
4. Enabling replicative potential
5. Inducing angiogenesis
6. Activating invasion and metastasis

To date these hallmarks still remain the foundation for the understanding of tumour development, although two additional capabilities have since been recognised: reprogramming of energy metabolism and evading immune destruction (Hanahan & Weinberg, 2011).

In essence the first five hallmarks enable tumour cells to proliferate uncontrollably by constitutively activating proliferation pathways; evading cell cycle checkpoints or apoptosis when DNA is damaged; escaping replicative-induced senescence and generating a tumour-associated neovasculature to expel waste and acquire nutrients. Notwithstanding, these traits will still only lead to the formation of a benign tumour, that is a collection of tumour cells unable to invade and metastasise (Chaffer & Weinberg, 2011). Indeed, the majority of cancer-related deaths are caused by tumour metastasis with removal of a benign tumour likely to result in eradication of the disease (Valastyan & Weinberg, 2011).

1.2.1.1 The Metastatic cascade

Metastasis is itself a multi-step process, consisting of a number of defined steps known as the metastatic cascade (Chaffer & Weinberg, 2011) (Figure 1.5). It has long been considered the last step in tumorigenesis in which benign, macroscopic tumours progressively transition to a malignant state, although this view has recently been challenged suggesting metastasis can in fact precede the formation of an overt, macroscopic tumour (Klein, 2009).

To initiate metastasis, carcinoma cells must escape their epithelial constraints mediated by tight junctions, desmosomes, hemi-desmosomes and adherens junctions (Sleeman & Thiery, 2011). E-cadherin, a key component of adherens junctions is often down-regulated in numerous cancers via a number of different mechanisms (reviewed in (Van Roy & Berx, 2008)). Subsequent to this, cells pass through the basement membrane by expressing matrix metalloproteinases (MMPs) which physically degrade it. These cells are then able to enter the tissue parenchyma that allows them access to either the lymphatic or haematogenous system through a process known as intravasation (Chaffer & Weinberg, 2011). The tumour-associated neovasculature is often easier to access than traditional vasculature since it is dynamic and therefore often “leaky” (Gupta & Massagué, 2006). Interestingly, the stroma surrounding a tumour is now thought to

play a much more active role in tumorigenesis than previously thought. Indeed, it has recently been shown the intravasation of breast cancer cells is enhanced by perivascular tumour-associated macrophages (TAMs) via a positive feedback loop comprising the reciprocal secretion of EGF and colony-stimulated factor (CSF) by TAMs and carcinoma cells, respectively (Wyckoff *et al.*, 2007).

Once cells have completed intravasation, they must survive in this setting resisting anoikis (apoptosis induced by inadequate cell-matrix contacts), haemodynamic shear stress and predation by innate immune cells, specifically natural killer (NK) cells (Hanahan & Weinberg, 2011). To evade the latter, tumour cells form large emboli via interactions with platelets, a process mediated by the expression of tissue factor and/or L- and P-selectins, protecting them from immune detection (Joyce & Pollard, 2009). Cancer cells are able to survive in the circulation for several hours, allowing time to arrest at the vasculature of distant sites (Meng *et al.*, 2004) although the reason why cells arrest at particular sites is not well-understood (Chaffer & Weinberg, 2011). It is widely known that specific tumours preferentially metastasise to certain sites, for example, prostate cancers almost always metastasise to the bone while colon cancers often metastasise to the liver. In the case of the latter, this is in part due to the physical layout of the vasculature since the portal vein drains the mesenteric circulation directly into the liver (reviewed in (Nguyen *et al.*, 2009).

Additionally, the formation of metastases may be influenced by structural differences in organ-specific capillaries. For example, sinusoid capillaries in bone marrow are formed from single endothelial cells designed to facilitate normal trafficking of haematopoietic cells in and out of the bone marrow. As a consequence, this could represent the path of least resistance and explain why bone marrow is the favoured site of metastasis for many primary tumours (Nguyen *et al.*, 2009). Despite this, it is now considered that the physical structure and layout of the vasculature is in itself insufficient to fully explain organ tropism and, as such, a number of hypotheses have been suggested to explain this. One such idea is that circulating tumour cells (CTCs) have pre-determined predilections to lodge in certain tissues; for example, a recent study suggested that metadherin-expressing breast cancer cells causes homing to the lungs by facilitating binding to the pulmonary vasculature (Brown & Ruoslahti, 2004).

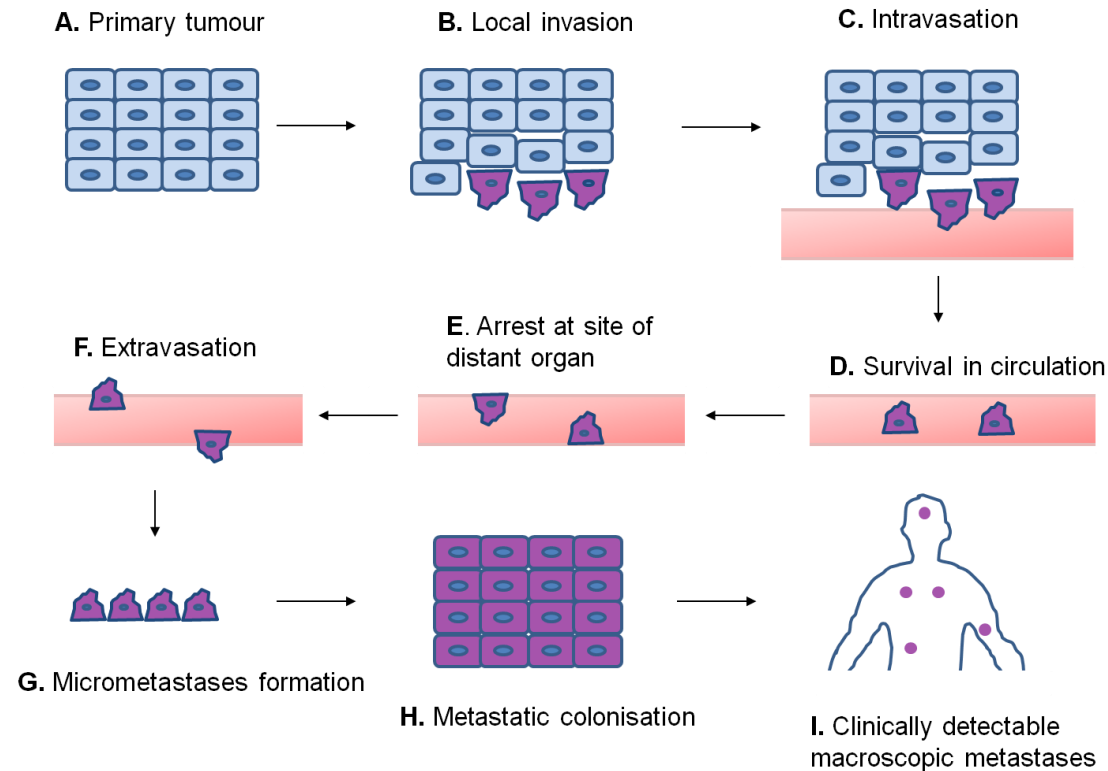


Figure 1.5: The metastatic cascade

A primary tumour forms (A) and a subset of these cells (highlighted in purple) acquire the ability to escape their surroundings (B) and subsequently intravasate into the vasculature (C). Intravasated cells must survive in the circulation (D) and depending on a variety of factors will arrest at the site of a particular organ (E) whereupon they will then extravasate (F). These cells will form micrometastases (G) and once competent to, proliferate extensively to form a metastatic colony (H) and macroscopic metastases (I). (Image drawn by A.F. Irvine)

Additionally, liver metastases from lung carcinomas have been shown to be dependent on a pro-inflammatory cascade that results in Kupffer cells (specialised liver macrophages) secreting chemokines that up-regulate various vascular adhesion receptors facilitating adhesion of CTCs to the liver microvasculature (Auguste *et al.*, 2007).

Following arrest at a distant site, carcinoma cells may extravasate from the lumina of vessels and cross into the tissue parenchyma. To overcome the low intrinsic permeability of the traditional vasculature, tumour cells can secrete factors that increase vascular permeability (Gupta & Massagué, 2006). For example, breast carcinoma cells arrested in the lung vasculature have been shown to secrete angiopoietin-4, as well as EREG, LOX-2 and MMP-1/2 which disrupts pulmonary vascular endothelial cell-cell junctions thus facilitating extravasation (Gupta, 2007; Padua, 2008). Moreover, breast carcinoma cells have also been shown to recruit inflamed monocytes via a CCL2-dependent mechanism promoting lung extravasation by secretion of VEGF (Qian *et al.*, 2011).

Once cells have extravasated, they encounter a foreign environment which they are often poorly adapted to in terms of stromal cells, available growth factors and cytokines (Nguyen *et al.*, 2009). Indeed, it is widely accepted that millions of tumour cells enter the circulation but few are able to form micrometastases (Valastyan & Weinberg, 2011). To account for the few cells that do form micrometastases, the idea of a metastatic niche has been recently established suggesting that certain extracellular matrix (ECM) proteins are able to support the survival and fitness of a sub-population of disseminated tumour cells (DTCs) (Oskarsson & Massagué, 2012). For example, the ECM protein periostin was recently shown to be required for lung metastasis in mammary tumours driven by a polyoma virus middle T antigen (PyMT) transgene (Oskarsson *et al.*, 2011). Interestingly, periostin not only served as a physical cue but also acted via the Wnt pathway to further enhance survival of DTCs (Oskarsson *et al.*, 2011). In addition to this, a separate study identified tenascin C (TNC) as a critical component in the metastatic niche, also necessary for breast cancer metastasis to the lungs (Malanchi *et al.*, 2012).

The final step of metastasis is known as colonisation or the formation of clinically detectable metastases secondary to the primary tumour (macrometastases) (Chaffer & Weinberg, 2011). In the event that DTCs survive the encounter within their new environment, they are not guaranteed to proliferate and form macrometastases. Indeed, colonisation is not strictly coupled with physical dissemination, as evidenced by the presence of multiple micrometastases that have successfully disseminated in patients but never progressed to macroscopic levels (Chaffer & Weinberg, 2011). In part, this may be because DTCs are largely quiescent which in some cases has been attributed to the inability of cells to engage the FAK, integrin $\beta 1$ or Src pathways (Shibue & Weinberg, 2009). The ability to escape dormancy and begin proliferation might also depend on the stromal cells surrounding the DTCs; for instance, carcinoma cells have been shown to recruit bone marrow-derived cells by secreting osteopontin or CXCL-12, supporting the proliferation of DTCs (McAllister *et al.*, 2008; Hiratsuka *et al.*, 2011).

Metastatic colonisation is also likely dependent on the self-renewal capacity of the founding cells with cancer stem cells (CSCs) strongly implicated in this process. Over the last 5 years, significant research has focused on the role of cancer stem cells that are often found to constitute a small, sub-population of the tumour (Hanahan & Weinberg, 2011). The hallmark of CSCs is their ability to seed new tumours at a more efficient rate compared to normal cancer cells when experimentally implanted into animal hosts. Thus, one current hypothesis is that CSCs are required to disseminate during the course of tumourigenesis in order for macroscopic metastases to form (Hanahan & Weinberg, 2011).

1.2.1.2 Cancer cell invasion

Although tumour cells are able to migrate without proteolytic degradation of the cell matrix (Sanz-Moreno *et al.*, 2008), it is still a requirement for many tumour cells when escaping the boundaries of a primary tumour. Indeed, this serves as the central dividing factor between cell migration and cell invasion (Friedl & Alexander, 2011). During tumour invasion there are multiple protease systems upregulated that have overlapping substrate specificities including MMPs, ADAMs, cathepsins, serine protease urokinase plasminogen (uPA) and its receptor uPAR (Wolf & Friedl, 2011). There are three main purposes of ECM breakdown. Firstly, it generates biologically active epitopes of ECM components with adhesion or migrating-promoting effects; for instance, cleavage of

laminin 5 or collagen IV results in exposure of cryptic sites that promotes cell migration (Page-McCaw *et al.*, 2007). Secondly, it structurally remodels tissue to form *de novo* gaps and trails bordered by ECM bundles. Thirdly, MMPs and ADAMs enzymatically process other proteases and cell surface receptors including adhesion and growth receptors regulating their activation, inactivation or degradation (Overall & Blobel, 2007).

Arguably the best characterised protease systems are MMPs that depend on calcium or zinc and cleavage of their pro-domains for their activity (Deryugina & Quigley, 2006). Their expression often correlates with a poor prognosis in many different cancer types and selective inhibitors have already been designed with the view to halt the spread of metastatic dissemination in patients (Deryugina & Quigley, 2006). In general, most MMPs are secreted but MMP-14,-15,-16 and -24 have transmembrane domains and short cytoplasmic tails while MMP-17 and -25 have glycosylphosphatidylinositol (GPI) linkages helping to tether them to the plasma membrane (Page-McCaw *et al.*, 2007). During cancer cell invasion, MMPs are localised towards the leading edge of the cell where they clear a path for the advancing cell; however, actual proteolysis has been shown to occur some distance away from the invading protrusion since it would otherwise leave the cell without an attachment to the ECM (Friedl & Gilmour, 2009).

1.2.1.3 Epithelial-mesenchymal transition (EMT)

The majority of human solid tumours are carcinomas that originate from various epithelial cell types throughout the body (Hanahan & Weinberg, 2011). As previously described, the initial stages of metastasis require these cells to lose their cell-cell contacts, break away from neighbouring cells and invade adjacent layers by acquiring increased migratory and invasive capabilities (Chaffer & Weinberg, 2011). Such a change has long been recognised as crucial during multiple stages of embryogenesis, a process known as the epithelial-mesenchymal transition (EMT). During metazoan gastrulation, cells must undergo EMT for the endoderm and mesoderm to be brought inside of the embryo while ectodermal cells are spread over its surface. Post-gastrulation, the neural crest forms between the boundary of the epidermal and neural territories with neural crest cells also undergoing EMT allowing individual cells to migrate before giving rise to melanocytes, endocrine cells and most of the peripheral nervous system (reviewed in(Thiery *et al.*, 2009).

1.2.1.3.1 EMT and metastasis

Accordingly, it is now considered that certain aspects of EMT are re-activated during carcinoma progression facilitating metastatic dissemination (Thiery, 2002). Indeed, many of the pathways and molecules required during embryogenesis are becoming increasingly important as key players in cancer biology (Sleeman & Thiery, 2011).

Epithelial cells are characterised by their adhesive contacts including adheren junctions, tight junctions and desmosomes with global communication within an epithelial sheet organised by gap junctions (Van Roy & Berx, 2008). They exhibit apical-basal polarity and are separated from adjacent tissues by the basal lamina. In contrast, mesenchymal cells are loosely organised in the ECM and comprise connective tissues adjacent to epithelia. They are characterised by a front-back polarity and a more motile and invasive phenotype (Thiery, 2002). For EMT to occur cells must lose their epithelial characteristics and gain mesenchymal ones. One central event in EMT is therefore the loss of E-cadherin, otherwise known as the “caretaker of the epithelial phenotype” (Thiery, 2002). E-cadherin is a prototypic type I cadherin, key in establishing and maintaining adheren junctions and is composed of a single transmembrane domain, a cytoplasmic domain and an ectodomain comprising 5 extracellular cadherin repeats. It forms adhesive bonds through homophilic interactions between one or more immunoglobulin-like domains in its ectodomain while the cytoplasmic domain forms a complex with α - and β -catenin that links with the actin cytoskeleton via a number of adaptor proteins (reviewed in (Van Roy & Berx, 2008). Due to its central role in EMT, E-cadherin expression often inversely correlates with cancer grade and its expression is tightly controlled in non-pathological settings (Christofori & Semb, 1999).

The main regulation of E-cadherin is co-ordinated by two sets of transcription factors that directly or indirectly repress transcription and are therefore themselves crucial during EMT. The former include the Snail1/2 and Zeb1/2 (Zeb2 or SIP1) family members that bind E-box elements of the *E-cadherin* promoter whereas the latter, consisting of Twist1/2, Goosecoid, E2.2 and FoxC2 repress E-cadherin transcription via alternative mechanisms (Thiery *et al.*, 2009). In agreement with this, knockout mice of these genes results in developmental defects with *SIP1* knockouts displaying a delamination arrest of cranial neural crest cells (De Putte *et al.*, 2003) whilst *Snail*-deficient mouse embryos fail to gastrulate (Carver *et al.*, 2001). Crucially, their

expression is also frequently correlated with a poor prognosis in a variety of cancers (Peinado *et al.*, 2007) and associated with increased invasiveness and aggressive behaviour (Thiery *et al.*, 2009). In spite of their well-characterised role in E-cadherin repression, they also function as “EMT inducers” regulating the expression of a variety of genes controlling epithelial character thereby promoting the mesenchymal state (Peinado *et al.*, 2007).

1.2.1.3.2 EMT and cell invasion

After losing cell-cell contacts, tumour cells must gain migratory and invasive properties to escape their local surrounding and initiate the metastatic cascade (Hanahan & Weinberg, 2011). Accordingly, cells undergoing EMT induce expression of MMPs enabling degradation of the basement membrane and significantly modify their cytoskeleton to increase their migratory potential (Yilmaz & Christofori, 2009). Although EMT is important for cells to break away from contacts and invade neighbouring tissue it has recently been hypothesised that EMT can be modulated to reduce epithelial organisation locally, yet promoting overall cell motility, thus an equilibrium between the epithelialisation and mesenchymalisation of cells is fashioned (Revenu & Gilmour, 2009). Even though EMT directly targets E-cadherin, N-cadherin is in fact often upregulated thereby allowing mesenchymal cells to form putative cell-cell junctions (retention of which is the definition of collective migration) (Sleeman & Thiery, 2011). EMT-derived cells can therefore switch between a single or collective form of cell migration depending on environmental requirements (Revenu & Gilmour, 2009).

1.2.1.3.3 EMT and cancer stem cells

As mentioned previously, CSCs are becoming a central theme in tumour biology and there is now a growing body of research suggesting a link between EMT and CSCs. Indeed, it was initially shown that when embryonic stem cells (ESCs) were grown in a 3D environment, a subpopulation of cells underwent an EMT event characterised by expression of vimentin, Snail and MMPs and a switch from E- to N-cadherin (Eastham *et al.*, 2007). Crucially, these cells retained expression of several totipotent transcription factors including Oct-4 and Nanog, indicating that ESCs can adopt a mesenchymal phenotype without losing their pluripotency (Eastham *et al.*, 2007). Following this, a seminal paper by Mani *et al.*, (2008) showed that over-expression of

Snail or Twist1 in immortalised mammary epithelial cells not only led to an EMT but also resulted in cells with a CD44^{high}/CD24^{low} phenotype consistent with both human breast CSCs and normal epithelial stem cells. Accordingly, it is now considered that normal stem cells and CSCs may share a mesenchymal phenotype that enhances their ability to preserve stemness and to respond to different stimuli during expansion and differentiation (Thiery *et al.*, 2009). Given this, EMT not only provides cells with the ability to invade and survive in the vasculature but ensures tumour cells are more able to revert to an epithelial-like structure through the reverse process, known as mesenchymal-epithelial transition (MET) allowing tumour cells to switch back to a proliferative state and begin the formation of macrometastases (Thiery *et al.*, 2009).

1.2.1.3.4 EMT and other factors

Aside from tumour invasion, EMT has also been implicated in conferring apoptotic resistance to cells (Valesia-Wittmann *et al.*, 2004), (Sayan *et al.*, 2009) promoting cell cycle arrest (Sayan *et al.*, 2009) and increasing resistance to oncogene-induced premature senescence (Ansieau *et al.*, 2008).

1.2.1.3.5 In vitro models of EMT

Many *in vitro* models of EMT exist including those where transcriptional repressors of E-cadherin are over-expressed in epithelial carcinoma cell lines including SIP1 (Mejlvang *et al.*, 2007), Twist (Yang *et al.*, 2004) and Slug (Bolos *et al.*, 2003); as well as growth factors recognizing receptor tyrosine kinases (Thiery, 2003) and the TGF- β receptor (Janda *et al.*, 2002).

1.2.1.4 S100A4 and cancer metastasis

Since the initial cloning and characterisation of S100A4, a significant amount of research has focused on its role in promoting metastases in experimental models and linking its expression with poor prognosis in many different tumour types. Indeed, it has now become known to some in the field as “metastasis-associated protein” S100A4 (Helfman *et al.*, 2005) and amongst the S100 family is most strongly associated with tumour progression and metastatic dissemination (Salama *et al.*, 2008).

1.2.1.4.1 Experimental evidence

S100A4 was initially identified in a screen of genes specifically expressed in metastatic mouse adenocarcinoma cells but not non-metastatic variants, with its expression shown to correlate with the metastatic potential of several tumour cell lines (Ebraldze *et al.*, 1989). Following this, early attention focused on its role in promoting metastasis in rodent models of tumourigenesis. In the first such study, over-expression of S100A4 in the non-metastasising cell line Rama 37 was not only shown to lead to a higher incidence of tumours when implanted into syngenic rats but crucially, led to metastases in the lungs and lymph nodes (Davies *et al.*, 1993). Such an effect was later confirmed when the GRS/A strain of mice, characterised by a high incidence of mammary tumours that rarely metastasise, were crossed with S100A4 transgenic mice leading to 40% of mice developing secondary tumours in the lungs (Ambartsumian *et al.*, 1996). Subsequent to this, crossing S100A4 transgenic mice with a mouse model of mammary tumourigenesis led to tumours that metastasised more frequently and rapidly than tumours in the parental strain (Davies *et al.*, 1996).

Consistent with the over-expression of S100A4, inhibition of S100A4 expression by ribozyme-mediated cleavage in osteosarcoma cells suppressed skeletal metastases when implanted in nude rats (Mælandsmo *et al.*, 1996). Although over-expression of S100A4 in mice does not yield tumours (Ambartsumian *et al.*, 1996; Davies *et al.*, 1996), the accumulated evidence suggests that whilst not being tumorigenic *per se* it is able to promote metastasis in a given tumorigenic background (Helfman *et al.*, 2005). Since these studies, mice carrying null alleles for S100A4 were shown to exhibit significantly fewer metastases when the highly metastatic mouse adenocarcinoma cell line, CMSL100 was implanted (Grum-Schwensen *et al.*, 2005) and when crossed with a mouse model of mammary carcinogenesis (MMTV-PyMT) led to significantly decreased metastasis to the lungs and lymph nodes compared to the parental strain (Grum-Schwensen *et al.*, 2010). In line with these rodent studies, S100A4 expression is often up-regulated at the mRNA and protein level in murine NIH 3T3 fibroblasts or normal rat kidney cells on transformation with oncogenes such as v-K-*ras*, v-Ha-*ras* and v-*src* (De Vouge & Mukherjee, 1992; Takenaga *et al.*, 1994b).

1.2.1.4.2 *Clinical significance*

Given the wealth of experimental data supporting a role for S100A4 in promoting cancer metastasis, numerous studies have focused on its clinical use as a prognostic indicator correlating its expression with disease-free survival, development of metastases and ultimately patient outcome (reviewed in (Salama *et al.*, 2008)). Perhaps the two best studied cancers involving S100A4 include breast and colorectal and are detailed below whilst a correlation with other cancers is summarised in Table 1.1.

The first evidence that S100A4 expression was associated with breast cancer came from a study by Rudland *et al.*, (2000) who with a large cohort of 349 patients identified S100A4 expression as the most significant predictor of patient survival even when compared to well-established markers of disease progression including tumour size, c-erbB2, oestrogen receptor and p53. Strikingly, 80% of S100A4-negative cases were alive 19 years after follow-up compared to just 11% of S100A4-positive cases. This result has since been confirmed in two further studies where S100A4 expression correlated with patient death in one (De Silva Rudland *et al.*, 2006) and served as an independent predictor of disease relapse in another (Lee *et al.*, 2004). In contrast to this data, Pedersen *et al.*, (2002) did not identify an association between S100A4 and survival, despite a correlation between S100A4 and an aggressive tumour phenotype, an effect that the authors later suggested could be due to fixation methods or a shorter observation period (Boye & Mælandsmo, 2010). Interestingly, S100A4 has recently been shown to play a role in normal mammary gland development where it acts in concert with TGF- α and MMP-3 to re-model the ECM during invasion of cells into the fat pad, providing one possible mechanism for its action in breast cancer progression (Andersen *et al.*, 2011).

S100A4 expression has also been strongly associated with colorectal cancer (CRC). In an initial study, it was found to be expressed at high levels in adenocarcinoma compared with normal colonic mucosa and in all carcinoma cells within liver metastases (Takenaga *et al.*, 1997b). Following this, a large cohort of 709 patients with CRC provided a correlation between S100A4 expression and a significant decrease in survival time and also emerged as a highly significant independent factor associated with high grades (pT3/T4) and secondary metastasis (Gongoll *et al.*, 2002). More recently, in a smaller cohort of 36 patients, S100A4 mRNA levels from resected

primary tissue were shown to correlate with those primary tumours that later developed distant metastases and thus a decreased-patient survival (Stein *et al.*, 2006).

Table 1.2: Studies correlating S100A4 over-expression with poor prognosis

Disease	Reference
Breast cancer	(Rudland <i>et al.</i> , 2000; Lee <i>et al.</i> , 2004; Ismail <i>et al.</i> , 2008a)
Colorectal cancer	(Stein <i>et al.</i> , 2006; Takenaga <i>et al.</i> , 1997b; Gongoll <i>et al.</i> , 2002; Boye <i>et al.</i> , 2010; Taylor <i>et al.</i> , 2002)
Pancreatic cancer	(Ai <i>et al.</i> , 2008; Oida <i>et al.</i> , 2006)
Gastric cancer	(Wang <i>et al.</i> , 2010; Kim <i>et al.</i> , 2009; Yoon <i>et al.</i> , 2008; Lee <i>et al.</i> , 2006; Kim <i>et al.</i> , 2008; Cho <i>et al.</i> , 2003; Yonemura <i>et al.</i> , 2000)
Bladder cancer	(Davies <i>et al.</i> , 2002; Matsumoto <i>et al.</i> , 2007)
Ovarian cancer	(Maeldandsmo <i>et al.</i> , 2009; Kikuchi <i>et al.</i> , 2006)
Non-small lung cancer	(Tsuna <i>et al.</i> , 2009; Miyazaki <i>et al.</i> , 2006; Matsubara <i>et al.</i> , 2005; Kimura <i>et al.</i> , 2000)
Liver	(Fabris <i>et al.</i> , 2011)
Brain	(Hernan <i>et al.</i> , 2003; Harris <i>et al.</i> , 2008)

1.2.1.4.3 S100A4 and EMT

The early association of S100A4 with EMT originated from the identification of it being specifically expressed in murine fibroblasts but not isogenic epithelium, and thus a marker of fibroblasts (hence the alternative name, fibroblast-specific protein 1) (Strutz *et al.*, 1995). In addition to cancer metastasis, EMT is now considered to be a central event in the progression of degenerative fibrotic diseases where the conversion of epithelium into mesenchymal/fibroblast-like cells provides a ready source of cells with the increased capacity for excessive deposition of collagen I, a hallmark of fibrosis (Lopez-Novoa & Nieto, 2009). As well as identifying S100A4 expression in fibroblasts, over-expression of S100A4 in the renal proximal tubular epithelial cell line, MCT resulted in an EMT process, as evidenced by an increase in vimentin and decrease

in cytokeratin expression (Strutz *et al.*, 1995). Subsequent to this study, treatment of MCT cells with a combination of TGF- β and EGF was shown to initiate an EMT with concomitant activation of S100A4 whilst surprisingly, knockdown of S100A4 impaired the EMT process (Okada *et al.*, 1997). Although the use of S100A4 as a fibroblast-specific marker has since been categorically disproved (Österreicher *et al.*, 2011; Boye & Mælandsmo, 2010) it is often activated during EMT-induced fibrosis in many organs including the liver, heart, lungs and kidney (Guarino *et al.*, 2009) and considered a marker as such.

In agreement with the role of S100A4 in fibrosis-associated EMT, S100A4 has slowly established itself as a marker of EMT in tumour progression (summarised in Table 1.2), now generally quoted alongside the more established markers of vimentin and MMP-2 (Schneider *et al.*, 2008). Despite this, there have only been two recent studies which have investigated the functional significance of S100A4 expression during EMT. In the first study, Lopez-Lago *et al.*, (2010) developed highly metastatic EMT variants of the renal cell carcinoma cell line, Sn12c by passaging them through a NOD/SCID mouse. Stable knockdown of S100A4 in these highly metastatic cells and subsequent implantation into mice demonstrated a significant reduction in metastatic activity. In contrast, over-expression of S100A4 in the parental, non-metastatic cell line did not significantly increase the metastatic activity, suggesting that S100A4 is required but not sufficient to confer a metastatic phenotype alone. The second study identified a side population of cells in two head-neck squamous carcinoma cell lines (HNSCC) that displayed a higher level of stemness and EMT markers including increased expression of S100A4 (Lo *et al.*, 2011). Intriguingly, stable knockdown of S100A4 reduced the self-renewal capacity of this side population whilst over-expression of S100A4 in the parental cell lines enhanced their stem-cell properties suggesting that S100A4 might be, at least in part, responsible for maintaining stemness in EMT-induced CSCs (Lo *et al.*, 2011). Despite these data, there have been no other functional studies and no mechanistic insight into the action of S100A4 during EMT as yet. Also lacking are histological data from patients linking S100A4 expression with EMT events; however, this is a more general problem with identifying EMT in patient material partly explained by its transient nature and the difficulty to distinguish EMT-induced cells from the tumour stroma (Valastyan & Weinberg, 2011).

Table 1.3: Studies identifying activation of S100A4 during EMT

Cell line	Originating Tumour	EMT Initiator	Reference
PMC42-LA	Breast carcinoma	EGF treatment	(Hugo <i>et al.</i> , 2009)
Mz-ChA-1	Biliary carcinoma	Knockdown of EBP50, a cell junctional-actin cytoskeleton linker protein	(Claperon <i>et al.</i> , 2012)
SN12C	Renal cell carcinoma	Mouse passaging	(Lopez-Lago <i>et al.</i> , 2010)
MDCK	n/a (immortalised epithelial cell line)	Ras transformation	(Mathias <i>et al.</i> , 2009)
MCF7	Breast carcinoma	IL-1 treatment	(Franco-Barraza <i>et al.</i> , 2010)
CCKS-1,TFK-1	Cholangiocarcinoma	TGF- β treatment	(Sato <i>et al.</i> , 2010)
MCF-10	n/a (immortalised breast cell line)	17 β -estradiol treatment	(Huang <i>et al.</i> , 2007)
A431	Epidermoid squamous cell carcinoma	Over-expression of dominant negative E-cadherin (Ec1WVM)	(Andersen <i>et al.</i> , 2005)

1.3 S100 functions

S100s are involved in numerous cellular processes, including but not limited to maintenance of cell shape and motility, modulation of signal transduction pathways and the regulation of calcium homeostasis (reviewed in (Donato, 2003)).

These effects can be mediated either intracellularly or extracellularly. The extracellular effects of S100s are less well-understood since they lack an extracellular signal peptide and their export is not affected by the ER-golgi classical secretion pathway inhibitor, brefeldin A (Donato, 2003). In addition, the receptor for secreted S100 proteins remains controversial although the receptor for advanced glycation endproducts (RAGE) is thought to interact with some S100s (reviewed in (Heizmann *et al.*, 2007)).

1.3.1 S100A4 and cell migration

As previously described, cell migration is a crucial process required for many of the steps occurring during the metastatic cascade (Friedl & Gilmour, 2009). Aside from the experimental and clinical evidence linking S100A4 with metastasis, the main functional aspect of its effect has focused on its role in enhancing cell migration (Donato, 2003). For example, S100A4 was originally shown to correlate with a more motile phenotype in promyelocytic leukaemia cells (Takenaga *et al.* (1994a) while over-expression in the mouse adenocarcinoma cell line, CSML0, also increased cell migration (Ford *et al.*, 1995).

Since these early studies, a wealth of data has been generated showing that S100A4 depletion either by RNA antisense or RNA interference (RNAi) inhibits both cell migration and invasion in Lewis carcinoma cells (Takenaga *et al.*, 1997a); breast carcinoma cells (Jenkinson *et al.*, 2004); colon adenocarcinoma cells (Stein *et al.*, 2006); endometrial adenocarcinoma cells (Xie *et al.*, 2009a); and osteosarcoma cells (Fujiwara *et al.*, 2011) among others (Tarabykina *et al.*, 2007) as summarised in table 1.3. In support of these findings, S100A4 expression in normal cell types is found in highly migratory cells including neutrophils, lymphocytes and macrophages (Cabezón *et al.*, 2007) further establishing a link between S100A4 expression and cell migration.

Table 1.4: Studies correlating S100A4 expression with increased rates of cell migration

Cell line	Originating Tumour	Cell Migration Model	Reference
A11	Lewis lung Carcinoma	Transwell assay coated with Matrigel	(Takenaga <i>et al.</i> , 1997a)
n/a	Mammary gland tumour of transgenic mice	Transwell assay	(Jenkinson <i>et al.</i> , 2004)
HCT116	Colon adenocarcinoma	Transwell assay coated with and without Matrigel	(Stein <i>et al.</i> , 2006)
Hec1A	Endometrial adenocarcinoma	Transwell assay coated with and without Matrigel	(Xie <i>et al.</i> , 2009a)
LM8	Osteosarcoma	Transwell assay	(Fujiwara <i>et al.</i> , 2011)
Bxpc-3	Pancreatic adenocarcinoma	Transwell assay	(Li <i>et al.</i> , 2012)

1.3.1.1 Principles of cell migration

Cell migration is a complex, heterogeneous process that is crucial in a number of physiological settings, including embryogenesis and immune surveillance. However, it also drives disease progression in many pathological conditions, most notably that of cancer metastasis (Ridley *et al.*, 2003). Different cell types migrate in varying ways, in part defined by their microenvironment. For instance, epithelial cells are capable of lateral movement along their basement membrane but not through interstitial tissues, whereas leukocytes are versatile, migrating through any part of the body tissue (Friedl & Wolf, 2010).

Cell migration is most easily organised into two distinct modes: collective or single. The former is defined by the retention of cell-cell contacts, most commonly seen in epithelial cells that are able to migrate as multicellular tubes, strands, sheets or regularly shaped masses, important for remodelling and building of complex tissue (Friedl & Gilmour, 2009). In contrast, single cell migration allows cells to migrate over large distances and integrate within tissues such as during neural crest migration (Friedl & Wolf, 2009). It can be further sub-divided into either amoeboid or mesenchymal modes of migration and is dependent on the microenvironment and cell type (Wolf *et al.*, 2003). Arguably the best studied form of migration is single cell mesenchymal migration where the many pathways and molecules that control it have been delineated leading to what has now become known as the migration cycle (Ridley *et al.*, 2003). It can be usefully conceptualised as a continued process with repeated rounds of polarisation, membrane protrusion, adhesion, translocation and tail retraction allowing cells to migrate efficiently (Ridley *et al.*, 2003) (Figure 1.6).

1.3.1.1.1 Polarisation

Polarisation refers to defining a different set of molecules at the front and back of a cell in response to an external cue. It enables cells to respond directionally to shallow gradients allowing even small differences to be amplified into steeper intracellular gradients facilitating a cellular response (Ridley, 2011). Establishing and maintaining cell polarity in response to extracellular stimuli involves a set of interlinked, positive feedback loops involving Rho GTPases, PI3-kinase, integrins, microtubules, myosin II and vesicular transport (Ridley *et al.*, 2003). The master regulator of polarity is Cdc42 (Fukata *et al.*, 2003), a member of the Rho family of small GTPases. Approximately 20

exist in humans with Rho, Rac and Cdc42 the three-best characterised (Jaffe & Hall, 2005). Rho GTPases operate as molecular switches cycling between an active GTP-bound state and an inactive GDP-bound state. The activity is controlled by three classes of molecules: guanine nucleotide exchange factors (GEFs) which catalyse the exchange of GDP for GTP; GTPase-activating proteins (GAPs) which stimulate the intrinsic GTPase activity to inactivate the switch; and guanosine nucleotide dissociation inhibitors (GDIs) which bind to GDP-bound molecules thus preventing the binding of GTP and their subsequent activation (Jaffe & Hall, 2005) (Figure 1.7).

Cdc42 primarily regulates cell polarity by orientating the centrosome and Golgi anterior to the nucleus. This is thought to facilitate anterograde transport from the Golgi to the leading edge, replenishing material removed by protrusion and retrograde actin flow (Etienne-Manneville, 2004). Mechanistically, it has been shown that Cdc42 acts through one of its downstream effectors, Par6, which exists in a complex with atypical protein kinase C (aPKC) and Par3 (Etienne-Manneville, 2004). In addition, Wnt5a participates alongside the Cdc42-Par6-aPKC-Par3 pathway to also help orientate the centrosome and Golgi with Wnt5a initiating non-canonical Wnt signalling by binding to frizzled and the co-receptor ROR2, causing re-orientation in an APC (Adenomatous Polyposis Coli)-dependent manner (Schlessinger *et al.*, 2007).

Aside from orientating organelles, controlling Rac activity is also crucial for establishing polarity. High levels of Rac are strongly associated with multiple protrusions and lamellipodia (Pankov *et al.*, 2005), thus a cell needs to confine Rac activity to the leading edge otherwise polarity will be lost. Cdc42 has been shown to limit Rac activity to the leading edge (Srinivasan *et al.*, 2003) but it is widely known that myosin II also limits protrusions at the cell rear to help polarise the cell (Vicente-Manzanares *et al.*, (2009). Indeed, myosin IIA activity at the rear of the cell often leads to the loss of GTP-bound Rac because of a failure to recruit Rac-specific GEFs.

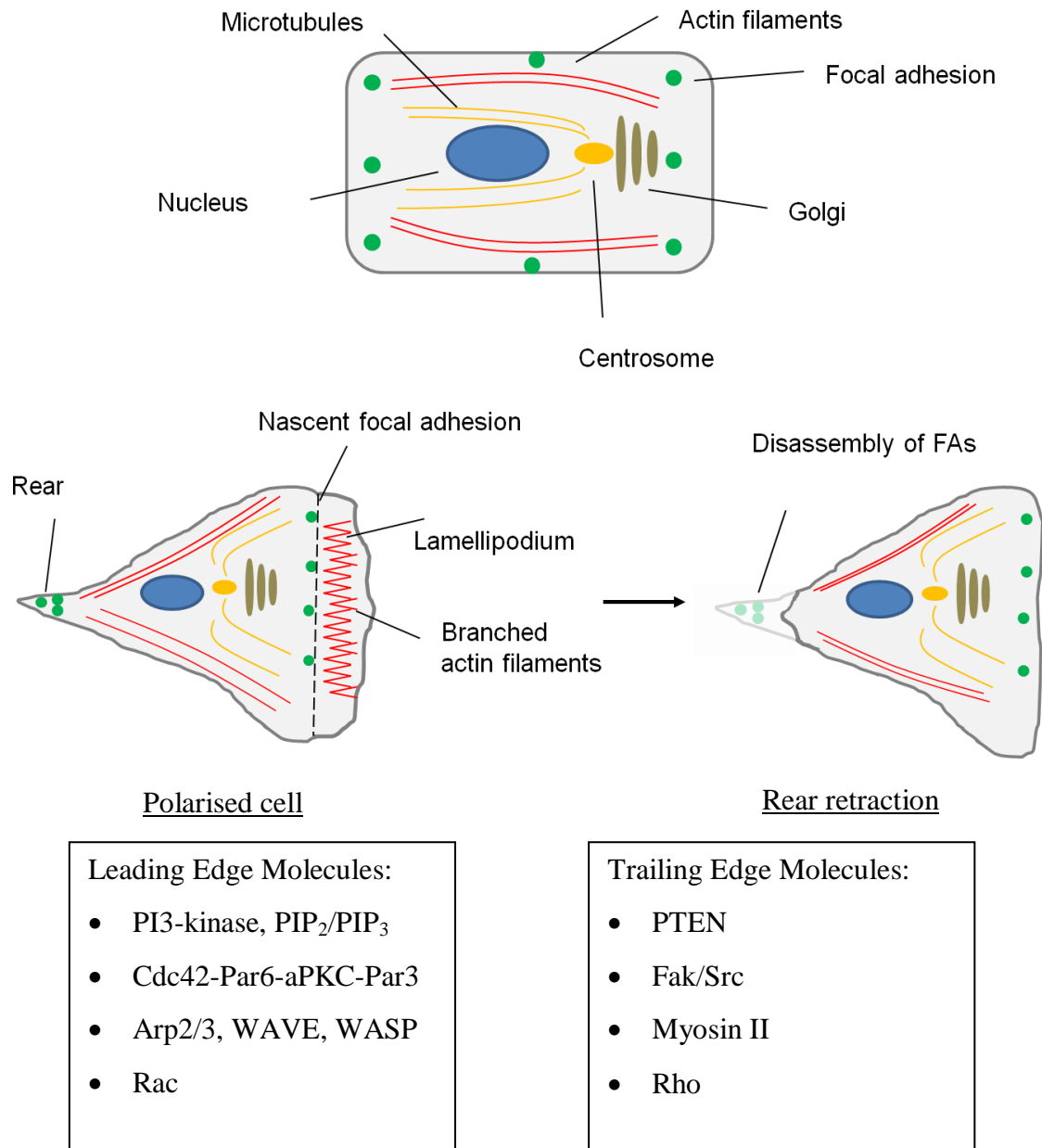


Figure 1.6: Features of the cell migration cycle

A non-polarised cell (top) with an equal distribution of structures e.g. focal adhesions and actin filaments at the front and back. In response to a stimulus a cell will polarise (left) forming a large lamellipodium at the leading edge rich in highly branched actin and associated proteins. Nascent focal adhesions will form posterior to the leading edge, a region whereas the rear of the cell will be rich in mature, stable focal adhesions. To translocate, a cell (right) must disassemble these adhesions, which requires myosin II contractility as well as cleavage of focal adhesion-related proteins talin and vinculin by calcium-regulated proteases. Examples of molecules enriched in the trailing and leading edge are described in each box.

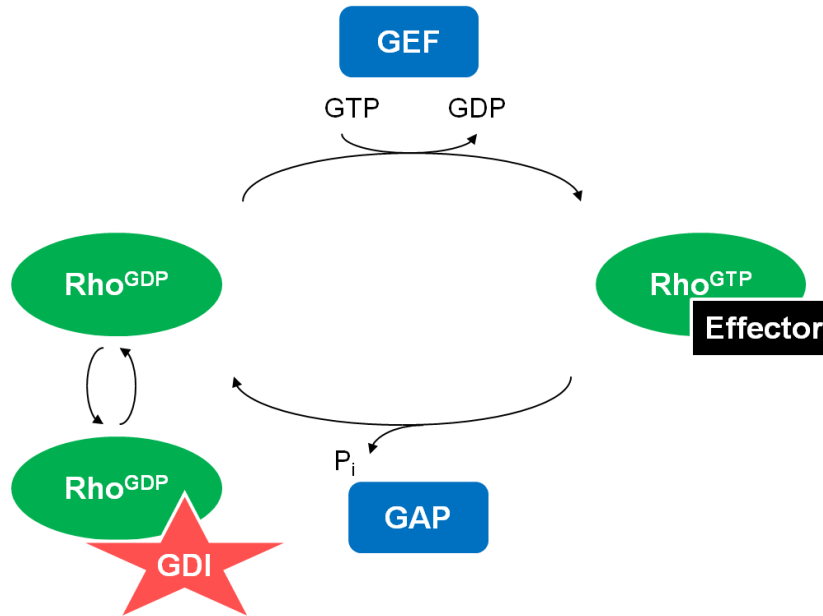


Figure 1.7: Regulation of Rho GTPases

Rho family members cycle between a GTP- (active) and GDP-bound (inactive) form which regulates their ability to bind effector proteins. GEFs stimulate the exchange of GDP for GTP whilst GAPs increase the intrinsic GTPase activity of Rho members to inactivate the switch. GDIs interact with the GDP-bound form of the molecule to prevent binding of GTP and thus subsequent activation.

This was recently shown to be because actomyosin bundling induces hypophosphorylation of focal adhesion proteins, including paxilin and the CrkII-p130 (Cas) which when phosphorylated act as docking sites for Rac-GEFs, β -pix and DOCK180 (Vicente-Manzanares *et al.*, 2011).

Another crucial polarity component is PI3-kinase, a membrane-bound kinase that phosphorylates phosphatidylinositols to generate phosphoinositides of which PI(3,4,5)P₃ and PI(4,5)P₂ are the most important in terms of cell polarisation (Kölsch *et al.*, 2008). In general, they act as docking sites for various intracellular proteins which assemble into signalling complexes that relay a signal into the cell from the cytosolic face of the plasma membrane (Kölsch *et al.*, 2008). During polarisation, PI3-K and PI(3,4,5)P₃ concentrate at the leading edge of a migrating cell whereas the lipid phosphatase, PTEN is localised to the rear and side of the cell (Petrie *et al.*, 2009). Accordingly, knockdown of PI3-K isoforms in the slime mold *Dictyostelium discoideum* prevents cells from efficiently polarising during chemotaxis (Comer & Parent, 2006).

1.3.1.1.2 Protrusion

After polarisation, cells are then able to extend a protrusion outwards which, once stabilised to the substratum, can serve as a traction point. There are a number of cellular protrusions used by cells including filopodia, lamellipodia and pseudopodia; however, the uniting theme is that they are all characterised by rich networks of actin filaments. Filopodia are spindle-like projections that are composed of parallel bundles of unbranched actin whereas lamellipodia are broader and composed of a dense, highly branched network of actin (reviewed in (Ridley, 2011)). Actin filaments are intrinsically polarised with a barbed end (+) and a pointed (-) end that drives membrane protrusion by pushing against the plasma membrane (Pollard & Borisy, 2003). *In vitro*, pure actin monomers polymerise very slowly into filaments. At steady state, growth is approximately 0.04 $\mu\text{m}/\text{min}$ whereas most cells migrate between 0.1-10 $\mu\text{m}/\text{min}$ (Pollard & Borisy, 2003) suggesting there are a number of regulatory proteins that control the assembly and disassembly of actin filaments *in vivo* (Campellone & Welch, 2010). Indeed, one such component is the Arp2/3 complex which is responsible for nucleating actin filaments and initiating new daughter filaments off pre-existing mother filaments, a process known as branching (Goley & Welch, 2006).

Branching is important, especially in the leading edge of lamellipodia (although this notion has recently been challenged (Urban *et al.*, 2010) as it provides the force required to push against the plasma membrane, as well as creating new nucleation sites that are able to polymerise rapidly (Pollard & Borisy, 2003). The Arp2/3 complex itself is essentially inert and requires activation by downstream effectors of Rac1 and Cdc42, namely WAVE and WASP with both sets of proteins localised to the leading edge of a migrating cell (Goley & Welch, 2006).

Profilin is also important in promoting actin filament assembly and does so in a number of ways. Firstly, it acts as a nucleotide exchange factor by binding to ADP-actin thus creating a pool of ATP-actin ready for the incorporation into a growing filament. Secondly, it binds to an actin monomer in such a way that it prevents it from being incorporated into the pointed end of an actin filament, thus enhancing polymerisation at the barbed end at a rate similar to free actin monomers (reviewed in (Dos Remedios *et al.*, 2003).

Despite this, rapid polymerisation of lengthening actin filaments cannot continue for long without exhausting the pool of unpolymerised actin. Indeed, the entire system is poised far from equilibrium with high concentrations of unpolymerised actin maintained by two distinct mechanisms: capping proteins and the family of ADF/cofilin proteins (Pollard & Borisy, 2003). Capping proteins generally bind to the barbed end of actin filaments thus preventing the continued incorporation of actin monomers to the filament. These include gelsolin (Silacci *et al.*, 2004) and the capping protein (CP), the latter of which is a ubiquitous, highly conserved heterodimer (Wear & Cooper, 2004). Aside from shortening filaments at the leading edge, capping proteins also help to spatially regulate where actin filaments push. Only barbed ends in contact with the plasma membrane will generate a propulsive force thus avoiding non-productive consumption of actin subunits elsewhere in the cell (Dos Remedios *et al.*, 2003). The second mechanism of actin disassembly is mediated by the ADF/cofilin family of proteins which disassemble actin filaments in a variety of ways. Firstly, they bind to monomers of ADP-actin preventing their incorporation into filaments, thus altering the equilibrium by the law of mass action; secondly, they change the twist of the actin filament when bound thus inducing severing; and thirdly they enhance phosphate release from ADP-Pi-actin filaments destabilising them (Bernstein & Bamberg, 2010).

Interestingly, aside from exhausting the unpolymerised pool of actin, long filaments are ineffective at pushing against the plasma membrane since thermal energy is taken up by internal bending of the filament (Pollard & Borisy, 2003). Indeed, EM analysis has shown that actin filaments at the leading edge are short, in the region of 30-150 nm, whereas actin filaments posterior to this are significantly longer consistent with this notion (Small *et al.*, 1978). However, some bending in the actin filament is thought to be necessary and consistent with the Brownian ratchet filament mechanism that describes how the bending of an actin filament away from the plasma membrane allows incorporation of an actin monomer, lengthening and restoring the force of the filament abutting the plasma membrane (Ridley *et al.*, 2003). As a result, the length of actin filaments, particularly at the leading edge, is exquisitely controlled to maximise protrusive force (Pollard & Borisy, 2003). For a migrating cell, the net rate of protrusion is dependent on the balance between actin polymerisation and retrograde flow. The latter is mediated by myosin IIA contraction (Cai *et al.*, 2006) or membrane resistance to actin polymerisation and counteracts the protrusive effect of the former. By linking actin filaments to the substratum, these traction points serve to drive retrograde flow to the surface, thereby negating its effects and increasing the protrusive force driven by actin polymerisation, a concept known as the “clutch” hypothesis (Vicente-Manzanares *et al.*, 2009).

1.3.1.1.3 Adhesion, translocation and retraction

Having established a protrusion, this then needs to adhere to the substratum providing traction for the cell body to move forward. Adhesion to the cell surface is largely mediated by integrins, which are heterodimeric transmembrane receptors consisting of an α - and β -subunit (Vicente-Manzanares *et al.*, 2009). They bind ligands with their extracellular domains whilst their cytoplasmic tail is indirectly linked to actin via a number of adaptor proteins including talin, vinculin and α -actinin thus providing a link between the extracellular environment and the cytoskeleton (Vicente-Manzanares *et al.*, 2009). Integrins also nucleate the formation of supramolecular assemblies of structural and signalling proteins known as focal adhesions that aside from providing a physical support are important signalling sites regulating protrusion and adhesion in migrating cells (Harburger & Calderwood, 2009). These structures mature by elongation on a physical template of actin filaments with unbundled actin supporting smaller adhesions, whereas bundled actin, stabilised by α -actinin or myosin II supports larger, elongated

adhesions (Choi *et al.*, 2008). For a migrating cell to move forward, adhesion sites must be disassembled to physically detach the cell from the substratum and for the tail to retract. Both FAK and Src are important in cell adhesion turnover and function via their adaptor proteins Cas and Crk which subsequently activate Rac-specific GEFs as well as ERK1/2 (Ridley *et al.*, 2003). Myosin II is important for many cell types to disassemble their adhesions with myosin II-defective neutrophils displaying multiple protrusions linked to impaired retraction (Xu *et al.*, 2003). In addition, tension generated in migrating cells, especially at the rear of the cell is sufficient to “open” stretch-activated Ca^{2+} -channels. This activates Ca^{2+} -binding proteins such as the phosphatase calcineurin and the protease calpain, the latter of which can cleave adhesion-related proteins including talin, vinculin and integrins (Lee *et al.*, 1999). Interestingly, the rate of migration exhibits a biphasic relationship with cell adhesion (Lauffenburger & Horwitz, 1996) with highly adherent cells unable to detach efficiently from the cell surface whilst poorly adhering cells are incapable of limiting actin retrograde flow thus restricting cell protrusion (Vicente-Manzanares *et al.*, 2009). Having completed one cycle of the migration process, cells will continually iterate this process to efficiently migrate.

1.3.1.2 Plasticity of cell migration

As previously described, cell migration is a heterogeneous process dependent on cell type and the surrounding microenvironment. Indeed, it is becoming increasingly clear that cells are able to adopt different modes of migration depending on a number of extra- and intracellular factors (Friedl & Wolf, 2010). The mechanism discussed above is most applicable for the best-studied mode of migration, that of single cell, mesenchymal migration. This is characterised by high levels of attachment, cytoskeletal contraction and proteolytic degradation required during tumour invasion (Friedl & Gilmour, 2009). Conversely, single cells can also migrate in an amoeboid fashion, a term coined from how the amoeba, *Dictyostelium discoideum* migrates. Amoeboid migration in a 3D environment is characterised by cells squeezing in and out of matrix pores negating the requirement for both ECM breakdown and the formation of focal adhesion contacts (Friedl & Gilmour, 2009). Interestingly, it has also been shown that some melanoma cell lines can interconvert between amoeboid and mesenchymal modes of migration, a process dependent on the switch from Rho signalling for the former and Rac signalling for the latter (Sanz-Moreno *et al.*, 2008)

suggesting migration plasticity could have important implications during metastatic dissemination. In addition, some tumour cell lines have been shown to convert to an amoeboid mode of migration when MMPs are inhibited (Wolf *et al.*, 2003).

1.4 S100 protein targets

As S100s lack catalytic domains, the mechanisms defining their functional roles are dependent on the proteins they interact with. Indeed, over 100 potential targets have been identified for the S100 family to date (reviewed in (Santamaria-Kisiel *et al.*, 2006). Although there are significant sequence differences between S100 proteins (see Figure 1.2), especially within the hinge and tail regions, there are multiple instances of protein target overlap or redundancy. Indeed, S100A1, A2, A4, A6 and S100B have all been shown to bind p53 *in vitro* with varying affinities (van Dieck *et al.*, 2009) whilst S100A1, S100A6 and S100B also interact with annexin A6 *in vitro* (Rintala-Dempsey *et al.*, 2008). Despite this, S100s are expressed in a tissue- and cell-specific manner and proposed to have roles in different functional processes (Donato, 2003). As such, the search for specific or non-redundant protein interactions is vital to establishing the biological role of each S100 protein.

1.4.1 S100A4 protein targets

Since S100A4 was first cloned and characterised, a number of different protein targets have been identified as potential binding-partners. Of particular interest was the interaction between S100A4 and p53, largely due to the importance of p53 in tumour biology (Oren, 2003). This interaction was originally identified in a study by Grigorian *et al.*, (2001) using co-immunoprecipitation and affinity chromatography, with the binding site mapped to the C-terminal negative regulatory domain of p53. In addition, it was also shown that S100A4 binding affects PKC-mediated phosphorylation and *in vivo* expression of S100A4 interferes with p53-DNA binding activity leading to an increase and decrease in Bax and p21 transcription, respectively. In contrast to this, subsequent biophysical characterisation by Fernandez *et al.*, (2005) showed that binding to a peptide corresponding to the Grigorian *et al.*, site only elicited a weak interaction with a reported K_d of $>100 \mu\text{M}$. Following this, an additional study by the same group determined that binding of S100A4 to full-length p53 was almost undetectable by AUC and analytical size-exclusion chromatography (van Dieck *et al.*, 2009) suggesting the interaction between S100A4 and p53 needs to be re-evaluated (Berge & Mælandsmo, 2011). A number of other targets have been identified for S100A4 including liprin $\beta 1$ (Kriajevska *et al.*, 2002) a member of the liprin family of transmembrane tyrosine-phosphatase LAR-interacting proteins and methionine aminopeptidase 2 (Endo *et al.*,

2002) an enzyme that catalyses the co-translational removal of the initiator methionine residue from nascent peptides. More recently, S100A4 was shown to interact with the N-terminal domain of Smad3 (Matsuura *et al.*, 2010), an important mediator in TGF- β signalling as well as a complex of Tag7 and Hsp70, implicating S100A4 in tumour surveillance (Dukhanina *et al.*, 2009). Despite the above targets, the best-characterised interacting partner of S100A4 is the heavy chain of non muscle myosin IIA (hereafter myosin IIA) (Kriajevskaja *et al.*, 1994) and will be the focus of the remaining chapter.

1.4.1.1 Non-muscle myosin IIA

Myosins are a superfamily of proteins with at least 25 different classes known to exist in eukaryotes (Richards & Cavalier-Smith, 2005). All myosins share the ability to walk along, produce tension or propel sliding of actin filaments, a feature that requires both the binding to actin, as well as the conversion of chemical energy to generate directional movement (Vicente-Manzanares *et al.*, 2009). In general, myosins consist of an N-terminal domain that contains the ATPase activity and actin-binding site; a neck region that binds either light chains or calmodulin; and a variable C-terminal tail that allows some myosins to bind to different cargo in a cell or others to self-associate into filaments (Sellers, 2000). Of the 25 or so different classes, myosin IIs [also known as conventional myosins since they were the first to be identified (Sellers, 2000)] are the most abundant and consist of those myosins that form the major contractile elements in smooth, cardiac and skeletal muscle as well as the non-muscle myosin IIs (NMII) (Vicente-Manzanares *et al.*, 2009). Despite the name, NMII are also expressed in muscle cells, where they have distinct functions in muscle development and the maintenance of tension in smooth muscle (Vicente-Manzanares *et al.*, 2009). Similar to their muscle counterparts, NMII are hexameric protein complexes consisting of three pairs of peptides: two myosin heavy chains (MHC); two essential light chains (ELC) and two regulatory light chains (RLC). The N-terminal domain of the NMII heavy chain is followed by the converter domain, a helix that connects movement of the ATP-binding cleft to the rest of the molecule. C-terminal to this is the lever arm containing two IQ motifs that the ELC and RLC bind to very tightly, but non-covalently, in part helping to stabilise the molecule. The C-terminus of the heavy chain consists of a coiled-coil sequence that homodimerises to form the long tail terminating in a short non-helical tail segment (reviewed in Sellers, 2000). NMII can therefore be considered to have two distinct but related functional properties dependent on the N- and C-

terminus respectively: an ability to translocate actin filaments, residing in its globular head domain and lever arm; and a structural function, residing in the ability of the coiled-coil domain of the molecule to form filaments allowing several heads to maintain tension (Conti & Adelstein, 2008). These physical properties confer a multitude of functional abilities to NMII including, but not limited to, a role in cell migration, cytokinesis and generation of cell polarity (Conti & Adelstein, 2008).

There are three different myosin heavy chain genes in mammals: *Myh9*, *Myh10* and *Myh14* that encode three distinct myosin heavy chains known as non-muscle myosin IIA, B and C respectively (hereafter, MIIA, MIIB, MIIC). The pre-mRNA of *Myh10* and *Myh14* are known to undergo alternative splicing with two additional isoforms of each gene having been identified (Itoh & Adelstein, 1995; Golomb *et al.*, 2004; Kim *et al.*, 2005). *In vitro* data also suggests splice forms of *Myh9* exist but there is as yet no evidence these transcripts are translated in cells (Vicente-Manzanares *et al.*, 2009). The essential and regulatory light chains that bind to the IQ motifs in the lever domain are encoded by a different set of genes. The specificity of the light chains for particular MHCs has not been fully characterised but recent evidence suggests that the affinity of the regulatory light chains for MIIA and MIIB are similar (Vicente-Manzanares *et al.*, 2008). Although the three MII isoforms are highly conserved with 89% similarity between MIIA and MIIB and 80% similarity between MIIC and either MIIA or MIIB (Golomb *et al.*, 2004) the isoforms display different localisations in cells and have different functions in cellular processes including migration (Sandquist *et al.*, 2006), adhesion (Vicente-Manzanares *et al.*, 2008) and neurite outgrowth (Wylie & Chantler, 2001; Wylie & Chantler, 2008) to name but a few. Both MIIA and MIIB are ubiquitously expressed in various tissues and are important during vertebrate development as well as maintenance of an adult organism. For instance, ablation of either MIIA or MIIB results in different embryonic defects with a MIIA knockout mouse showing lethality at embryonic day (E) 6.5 caused by defects in cell adhesion and endoderm formation (Conti *et al.*, 2004) whilst MIIB knockout mice show lethality at E14.5 with both heart and brain abnormalities (Takeda *et al.*, 2003; Ma *et al.*, 2004). In contrast, ablation of MIIC does not lead to embryonic lethality with mice surviving to adulthood reflecting the delayed expression of MIIC during development compared with MIIA or MIIB (Ma *et al.*, 2010). Aside from where expression of a single myosin II is restricted to a specific cell type, the different functions and thus roles that each

myosin II plays is likely to reside in the kinetic aspects of each isoform as well as the biochemical properties of the C-terminal tail. For instance, MIIA and MIIB differ in both their actin-activated Mg-ATPase activity and the time they are bound to actin in a force-generating state (duty ratio) with MIIA having a higher rate of ATP hydrolysis whilst also being able to propel actin filaments more rapidly in an *in vitro* motility assay (Wang *et al.*, 2003; Kovács *et al.*, 2003). Conversely, the duty ratio and ADP affinity is significantly higher for MIIB than MIIA (Wang *et al.*, 2003) suggesting that MIIB is more suited to exert tension on actin filaments for longer periods of time and with less expenditure of energy than MIIA (Vicente-Manzanares *et al.*, 2009). Although less well characterised, the kinetic properties of MIIC are more similar to those of MIIB than MIIA (Kim *et al.*, 2005).

Aside from the kinetic differences between isoforms, the C-terminal tail and specifically the non-helical tail piece is also crucial in determining isoform-specific function consistent with the fact that the largest sequence divergence resides in the non-helical tail of the isoforms (Vicente-Manzanares *et al.*, 2009). This hypothesis was tested in an elegant series of experiments where the head domain of MIIA replaced that of MIIB and *vice versa* to generate chimeric proteins. The chimeric proteins displayed isoform-specific localisation in cells dependent on their tail with a MIIA head and MIIB tail chimera able to restore front-back polarisation in MIIB-deficient cells (Vicente-Manzanares *et al.*, 2008). This concept was further refined by Sandquist *et al.*, (2008) who found that swapping the non-helical tail at the very C-terminus of either MIIA or MIIB was sufficient to alter isoform-specific localisation and solubility suggesting this region alone is responsible for some of the different tail-mediated functions observed between myosin IIs.

1.4.1.1.1 Regulation of myosin II

There are two sets of mechanisms regulating the activity of non-muscle myosin II: phosphorylation of the regulatory light chain which is general for myosin II and phosphorylation and protein binding at the C-terminus of the heavy chain which is more isoform-specific (Clark *et al.*, 2007).

1.4.1.1.1 Light chain regulation of myosin II

Light chain regulation depends on the reversible phosphorylation of two key residues on the RLC, Ser19 and Thr18 and affects both the formation of filaments and the binding of actin (Sellers, 2000). The basis for this regulation is thought to depend on the conformation of the molecule, with significant *in vitro* data suggesting that unphosphorylated molecules in the presence of ATP exist in a folded, assembly-incompetent form known as the 10S state while phosphorylation of the RLC leads to an unfolded, assembly-competent form of the molecule known as the 6S state (Conti & Adelstein, 2008) (Figure 1.8). In the 10S conformation, the tail is bent at two specific points to generate three segments of roughly equal length (Jung *et al.*, 2011). 10S and 6S refer to the sedimentation coefficients of each molecule as assessed by ultracentrifugation, a method that provided the first indications of a folded conformer of smooth muscle myosin from gizzard preparations (Suzuki *et al.*, 1978). Since this, a folded conformation has been found for non-muscle myosin II as well as additional myosin isoforms (Sellers & Knight, 2007) and other molecular motors (Dietrich *et al.*, 2008). The 10S form of myosin has been shown to have significantly reduced ATPase activity (Cross *et al.*, 1988) since ADP and Pi products are trapped at the active site. This has led to the hypothesis that the 10S form is physiologically relevant as an inert state of myosin that minimises ATP wastage until myosin filaments are formed at a site where contractile activity is required.

In recent years the structure of the 10S state has been extensively studied using negative staining of 10S myosin molecules. In an important study, Burgess *et al.*, (2007) showed both heads of smooth muscle myosin II interact asymmetrically, with the actin-binding site of one head forming contacts with the converter region of the other thus one head is prevented from binding actin whilst one has blocked ATPase activity. This has since been confirmed with non-muscle myosin II (Hyun *et al.*, 2008) and the mechanism likely to be common for all myosin IIs (Jung *et al.*, 2011). Also important in stabilising the 10S form of the molecule is the head-tail interaction that explains why phosphorylation at Ser19/Thr18 is able to induce unfolding of the molecule, leading to the 6S state. Indeed, a recent study proposed that segment 3 of the tail within a 10S molecule lies across the lever region of the blocked head thus forming contacts with the N-terminal domain of the RLC (Jung *et al.*, 2011) (Figure 1.9).

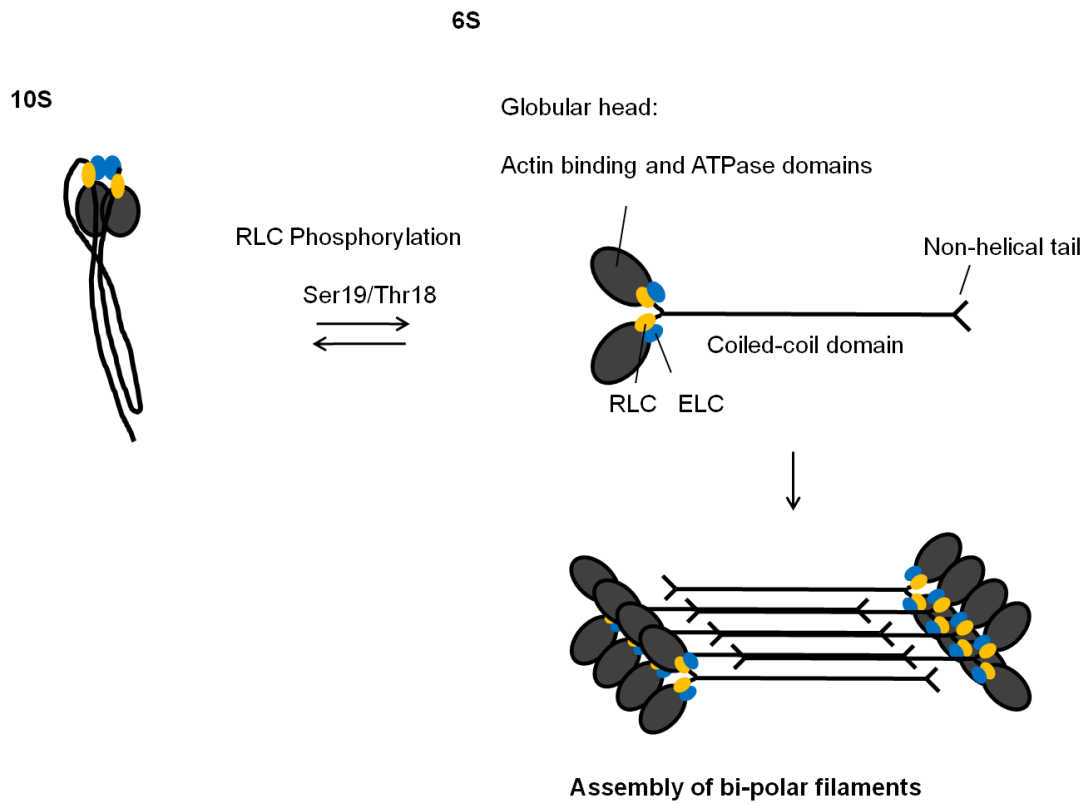


Figure 1.8: Graphic representation of non-muscle myosin II conformers

Unphosphorylated myosin II in the presence of ATP is likely to be in the 10S, assembly-incompetent form (adapted from Jung *et al.*, 2011) whilst phosphorylation at either Ser19 or Thr18 of the RLC by a number of different kinases causes an unfolding of the molecule into an assembly-competent, 6S form. Once phosphorylated 6S myosin II is able to form bipolar filaments mediated by the tail domain of each molecule.

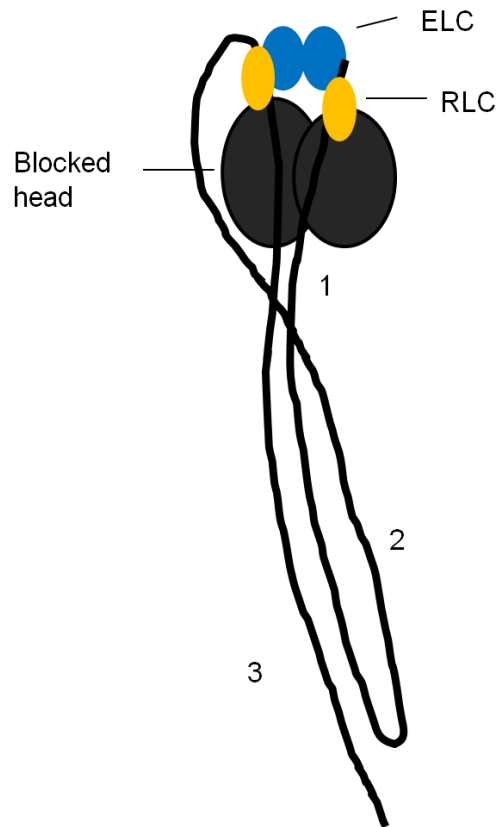


Figure 1.9: Graphical representation of the 10S form of myosin II

The molecule folds at two specific points to generate a tail of approximately three equal lengths, indicated as segment 1, 2, and 3. The two heads interact asymmetrically to block the ATPase activity of one and the actin-binding ability of the other. A head-tail interaction also stabilises the structure with the blocked head (left) forming contacts with the N-terminal domain of the RLC explaining why phosphorylation at either Ser19 or Thr18 is able to disrupt the 10S form. Figure adapted from Jung *et al.*, (2011).

As such, phosphorylation of Ser19 and Thr18 will serve to destabilise the ionic interactions between the blocked head RLC and the tail, causing unfolding of the molecule to the 6S state. Interestingly, sequence comparison shows that the positively charged N-terminus of the RLC and negatively charged region near the start of segment 3 are maintained across phyla suggesting an evolutionary conserved mechanism (Jung *et al.*, 2011). Despite the *in vitro* evidence for 10S myosin, there have only been two studies investigating the presence of 10S myosin *in vivo*. Cremo and colleagues (Milton *et al.*, 2011) designed a peptide corresponding to the area of the lever region of smooth muscle myosin that forms contacts with segment 3 of the tail. The authors hypothesised this would compete with the intermolecular head-tail interaction by binding to segment 3 of the tail thus destabilising the 10S and promoting the 6S form. Accordingly, they used human airway smooth muscle cells permeabilised with alpha-toxin and incubated cells with a 10S-promoting buffer (molar excesses of EGTA and MgATP) which caused disassembly of myosin filaments; however, when cells were incubated in the 10S buffer with the peptide, it induced a prominent stress fibre pattern consistent with there being a population of 10S molecules present in cells. In contrast to this, Horowitz *et al.* (1994) used tail-specific antibodies and found only a minor pool of soluble (potentially 10S) myosin in gizzard smooth muscle.

Once phosphorylated at the RLC and in the 6S form, myosin II molecules are assembly competent and can form bipolar filament assemblies thought to comprise up to 28 molecules (Niederman & Pollard, 1975). Although the sequence of the myosin tail is characteristic of coiled-coil domains with alternating zones of positively and negatively-charged residues, most tail segments are not competent to form filaments (Atkinson & Stewart, 1992). Indeed, a small region near the C-terminus of the tail known as the Assembly Competent Domain (ACD) is recognized to mediate tail assembly across phyla (Cross *et al.*, 1986; O'Halloran *et al.*, 1990). The rationale behind this has recently been explored by Ricketson *et al.*, (2010) who proposed that rather than the ACD forming self-interactions between separate tail domains, it acts as a unique positively charged interaction surface that can stably contact multiple, complementary, negatively charged surfaces thus mediating filament assembly. As such, agents that affect the ACD either by heavy chain phosphorylation (Ronen *et al.*, 2010) or protein binding (see below) perturb filament formation and are thus important regulators of myosin II assembly. A number of different kinases have been reported to

phosphorylate the RLC of non-muscle myosin IIs including myosin light chain kinase (MLCK); Rho-associated, coiled-coil kinase (ROCK); leucine zipper interacting kinase (ZIPK); and myotonic dystrophy kinase-related CDC42-binding kinase (MRCK) (Conti & Adelstein, 2008). These kinases phosphorylate the RLC on Ser19, Thr18 or both and destabilise the 10S form (Vicente-Manzanares *et al.*, 2009) as described above. The major differences between the kinases centre on the upstream signals with MLCK dependent on activation by Ca²⁺-activated calmodulin, whereas ROCK is a downstream effector of RhoA, an important member of the Rho family of small GTPases (Kato *et al.*, 2011). In addition to directly phosphorylating the RLC, ROCK also acts to inhibit the major myosin phosphatase (MP), which is comprised of three subunits: a type 1 protein phosphatase catalytic subunit (PP1), myosin phosphatase target subunit 1 (MYPT1) and a small subunit of unknown function (Matsumura & Hartshorne, 2008). ROCK disrupts this complex by phosphorylating MYPT1 thus inactivating the enzymatic activity of the complex (Matsumura & Hartshorne, 2008) and promoting overall RLC phosphorylation. Interestingly, evidence suggests that MIIA is preferentially phosphorylated by ROCK compared to MIIB (Sandquist *et al.*, 2006).

1.4.1.1.1.2 Heavy chain regulation of myosin IIA

1.4.1.1.1.2.1 Heavy chain phosphorylation

Phosphorylation of the heavy chain of myosin II is known to play an important role in the regulation of *Dictyostelium* myosin II where residues located in the C-terminus are important in driving filament disassembly (Bosgraaf & van Haastert, 2006). Accordingly, a number of residues have also been identified in the heavy chains of myosin IIA, B and C including those phosphorylated by PKC, CK2 and TRPM6 and 7 (Vicente-Manzanares *et al.*, 2009). It was originally shown that myosin IIA was phosphorylated at two serines by PKC and CK2 at the C-terminus (Kelley *et al.*, 1991), residues that were later identified as S1916 and S1943 respectively (Conti *et al.*, 1991). S1916 occurs towards the end of the coiled-coil region whereas S1943 is positioned within the non-helical tailpiece (Figure 1.10). Although S1916/S1943 phosphorylation was first shown not to affect myosin filament assembly (Murakami, 1995; Murakami *et al.*, 1998) additional *in vitro* evidence later provided by Dulyaninova *et al.*, (2005) suggested that phosphorylation by both PKC and CK2 does indeed promote the monomeric state of myosin IIA. In line with the biochemical data, over-expression of full-length myosin IIA constructs harbouring either S1943D or E mutations decreased

levels of filamentous myosin in MDA-MB-231 cells compared to the WT protein (Dulyaninova *et al.*, 2007). Moreover, these cells exhibited elevated rates of cell migration corresponding with severely attenuated levels of phospho-paxilin on Tyr118, a marker of mature focal adhesions. In addition to this study, over-expression of S1943A myosin IIA in HeLa cells caused increased levels of myosin assembly (Breckenridge *et al.*, 2009). Despite evidence suggesting CK2 is the predominant kinase responsible for phosphorylation at S1943 (Dulyaninova *et al.*, 2005; Dulyaninova *et al.*, 2007), a recent study demonstrated that when CK2 expression was attenuated, S1943 was still phosphorylated suggesting there are also other kinases responsible for phosphorylation at this residue (Betapudi *et al.*, 2011).

In recent years, additional phospho sites have also been identified at Ser1800, 1803 and 1808 phosphorylated by TRPM6 and 7 which are bi-functional proteins encoding a TRP cation channel fused to an α -kinase domain. Phosphorylation of these residues has also been shown to increase solubility of myosin IIA both *in vitro* and *in vivo* (Clark *et al.*, 2008a).

1.4.1.1.1.2.2 S100A4-myosin IIA interaction

Myosin II was initially identified as a target for S100A4 when it was immunoprecipitated from radiolabelled mouse adenocarcinoma cells (Kriajevska *et al.*, 1994) and has since been shown to bind myosin IIA with a 9-fold-higher affinity than myosin IIB (Li *et al.*, 2003). Accordingly, a large body of research has focused on the functional effects of S100A4 binding as well as the mechanistic details regarding the binding site, stoichiometry and the effect of heavy chain phosphorylation on the interaction. With regards to the former, S100A4 is now widely accepted to promote the disassembly of myosin IIA filaments (Badyal *et al.*, 2011; Ford *et al.*, 1997) whilst also inhibiting the assembly of monomeric myosin into filaments (Badyal *et al.*, 2011; Li *et al.*, 2003; Murakami *et al.*, 2000); however, there has been some discrepancy in the literature regarding the more mechanistic details of the interaction and only recently have some of them been satisfactorily addressed (Badyal *et al.*, 2011).

The binding site of S100A4 on myosin IIA was originally mapped to a C-terminal region corresponding to residues A1907-G1938 overlapping the end of the coiled-coil and start of the non-helical tail; however, this was disputed by Malashkevich *et al.*,

(2008) who concluded that the binding site represented a shorter peptide consisting of residues A1907-R1923. Despite this, Badyal *et al.*, (2011) recently re-examined the interaction and concluded that A1907-G1938 did indeed represent the minimal binding site and the fluorescein tag used by Malashkevich *et al.*, (2008) had made a significant contribution to the binding energy to the shorter A1907-R1923 peptide. Interestingly, the start of the binding site is proximal to the ACD which could provide a mechanism for myosin-mediated disassembly by S100A4 although this has yet to be proven experimentally. The discrepancy in binding site also had direct implications interpreting the stoichiometry of the interaction since the shorter myosin peptide proposed by Malashkevich *et al.*, (2008) would only occupy a single hydrophobic cleft, typical for an S100-target interaction, whereas the longer peptide would likely occupy both pockets. In line with their binding site data, Malashkevich *et al.*, (2008) proposed that one S100A4 monomer would bind a single myosin peptide leading to a 1:1 stoichiometry; however, Badyal *et al.*, (2011) demonstrated that the stoichiometry is one S100A4 dimer (i.e. two S100A4 monomers) to one myosin peptide, in agreement with their binding site data and representing a novel interaction for an S100-target. Although, Malashkevich *et al.*, (2008) had underestimated the minimal binding site for S100A4, NMR data showed that changes in chemical shift were consistent with a myosin peptide forming contacts within the hydrophobic pocket of S100A4 that is exposed upon calcium binding, in agreement with the majority of S100 proteins that form contacts with target peptides in this region (Zimmer *et al.*, 2003).

Other studies have focused on the S100A4 residues important in the myosin IIA interaction. A truncated form of S100A4 lacking the last 13 amino acids reduced the interaction with myosin IIA, an effect correlating with reduced levels of cell migration in the benign rat mammary carcinoma cell line, Rama37 (Zhang *et al.*, 2005b). This work was later refined when the last two residues of S100A4, -KK, were both mutated to AA reducing the interaction with myosin to levels of the truncated protein (Ismail *et al.*, 2008b). However, it was not shown if these mutations affected dimerisation of the protein, a result that could indirectly affect binding of protein targets. More recently, a screen of pharmacologically active molecules led to the identification of NSC95397, a quinone, which severely reduced the interaction between S100A4 and myosin IIA due to a modification of Cys81 (Dulyaninova *et al.*, 2011). Mutation of Cys81 to C81A/S

replicated this effect suggesting it is an important residue in S100A4 partly mediating the interaction with myosin IIA (Dulyaninova *et al.*, 2011).

1.4.1.1.2.3 S100A4-heavy chain phosphorylation interplay

As described above, there is good evidence suggesting that S100A4 promotes the monomeric form of myosin IIA whilst heavy chain phosphorylation also affects filament formation; however, the effect of S100A4 binding on heavy chain phosphorylation and whether or not S100A4 binding is itself affected by phosphorylation is not well understood. Since the S100A4 binding site was mapped to the C-terminus of myosin IIA where both phospho sites are located (Kriajevska *et al.*, 1998), a number of studies have investigated the interplay between heavy chain phosphorylation and S100A4 binding. Indeed, given the minimal binding site for S100A4, Ser1916 is located within this region whereas Ser1943 is just C-terminal to it (Figure 1.10). It was initially shown by in vitro kinase assay that S100A4 binding attenuated heavy chain phosphorylation at both Ser1916 (Kriajevska *et al.*, 1998) and Ser1943 (Kriajevska *et al.*, 2000) although Ser1943 phosphorylation did not affect

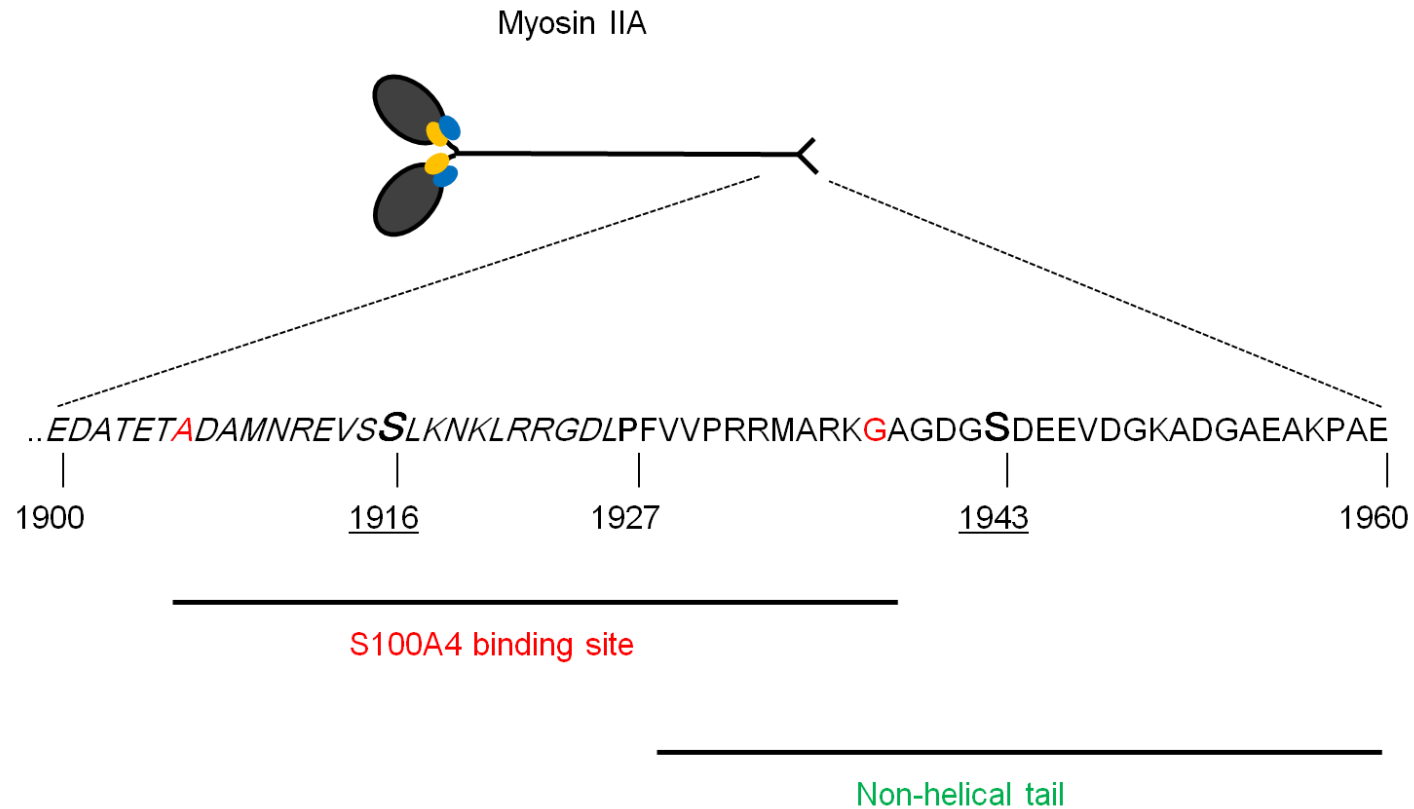


Figure 1.10: Sequence of the C-terminal region of myosin IIA

The sequence of the last 60 amino acids of myosin IIA (1900-1960). The coiled-coil region continues until Pro1927 which also marks the start of the non-helical tail. The S100A4 binding site (according to Badyal *et al.*, 2011) starts at Ala1907 and ends at Gly1938 and overlaps the PKC, S1916 phospho site. The Ser1943 phospho site is outside the S100A4 binding site but within the non-helical tail of the molecule.

S100A4 binding (Kriajevska *et al.*, 2000). More recently, evidence presented in one study partly disputed this by demonstrating that myosin rods phosphorylated by CK2 reduced the S100A4 affinity by approximately 7-fold while phosphorylation at S1916 did not affect S100A4 binding (Dulyaninova *et al.*, 2005). Since Ser1943 is outside the S100A4 binding site, it was proposed that phosphorylation at this residue causes the tail to fold back over itself, preventing S100A4 from binding (Dulyaninova *et al.*, 2005). Despite this more recent evidence, phosphomimetic forms of Ser1943 (S1943D/E), which were able to recapitulate the effect of heavy chain phosphorylation on filament assembly (Dulyaninova *et al.*, 2007), did not reduce the S100A4 affinity for myosin IIA, contrary to the above.

1.4.1.1.2.4 In vivo evidence supporting the S100A4-myosin IIA interaction

Despite the wealth of *in vitro* data supporting a functional complex between S100A4 and myosin IIA, there has been little direct evidence of the interaction *in vivo*, in part due to the intrinsic difficulties associated with validating any genuine protein-protein interaction in cells. In a novel approach, Zhang *et al.*, (2005a) used Fluorescent Lifetime Imaging (FLIM) to provide evidence of an interaction between S100A4 and a C-terminal fragment of myosin IIA in HeLa cells. In a second study, over-expression of S100A4 in the benign rat mammary adenocarcinoma cell line, MTC enhanced rates of forward lamellipodial protrusion in response to a chemoattractant. Microinjection of control cells with an antibody raised against the S100A4 binding site on myosin IIA mimicked this effect, suggesting it is dependent on MIIA (Li & Bresnick, 2006).

Aside from the functions described in the context of cell migration, myosin IIA also plays roles in many other cellular processes including cell-cell adhesion and cytokinesis (Conti & Adelstein, 2008). For the former, myosin II has been shown to colocalise with E-cadherin at cell-cell contacts with local accumulation of cadherins important in supporting cell adhesiveness by establishing and maintaining adheren junctions (Van Roy & Berx, 2008). Inhibition of myosin II activity by RNAi-mediated knockdown or blebbistatin treatment leads to mis-localisation of E-cadherin and subsequent destabilisation of cell-cell contacts (Shewan *et al.*, 2005). This concept was recently developed by showing myosin IIA is important in cadherin clustering whilst IIB supports integrity of the apical ring of actin filaments that are associated with adheren junctions (Smutny *et al.*, 2010). Interestingly, the role of myosin IIA in cell-cell

contacts is consistent with the MIIA knockout mouse which is embryonic lethal due to defects in localising E-cadherin and β -catenin to cell-cell contacts (Conti *et al.*, 2004). For its role in cytokinesis, myosin II has long been regarded as an important component of the contractile ring which acts to segregate a mother and daughter cell after mitosis. This mechanism was thought to depend on the ability of myosin II to translocate actin filaments; however, in a compelling set of experiments the motor function of myosin II was shown to be dispensable for efficient cytokinesis, requiring only myosin II to cross-link actin filaments (Ma *et al.*, 2012).

1.5 Aims and objectives of thesis

Hypothesis 1: Expression of S100A4 is activated in an established model of EMT and contributes to EMT-induced increases in cell migration.

Aims and objectives: Determine if S100A4 expression is increased in an established model of EMT (Mejlvang *et al.*, 2007), and if so, characterise its role.

- Characterise the expression of S100A4 by Western blot and immunofluorescence.
- Determine if S100A4 expression is required for EMT progression.
- Use a transwell assay and RNA interference to assess the effects of cell migration in the presence and absence of S100A4.

Hypothesis 2: The effect of S100A4 on cell migration is dependent on S100A4 interacting with and promoting myosin IIA turnover.

Aims and objectives: Myosin IIA is the best characterised target of S100A4. Does S100A4 interact with myosin IIA *in vivo* and does it promote myosin IIA turnover in cells?

- Confirm S100A4 and myosin IIA interact via immunoprecipitation experiments.
- Analyse co-localisation of S100A4 and myosin IIA using different microscopy methods e.g. light microscopy, transmission electron microscopy.
- Investigate myosin IIA assembly *in vivo* using fluorescent recovery after photobleaching (FRAP) in the presence and absence of S100A4.

Hypothesis 3: Heavy chain phosphorylation at S1916 and S1943 on the myosin heavy chain does not affect the S100A4 interaction. There are important residues that coordinate the S100A4-myosin IIA interaction.

Aims and objectives: Heavy chain phosphorylation at S1943 has been shown to affect the binding of S100A4 to myosin IIA. In collaboration with structural biologists, identify the residues that are important in the S100A4-myosin IIA interaction.

- Clone, express and purify phosphomimetic mutants of a C-terminal fragment of myosin IIA.
- Use this protein to investigate the effects of heavy chain phosphorylation on myosin IIA solubility (turbidity assays) and the interaction with S100A4 (stopped-flow transient kinetics).
- Characterise the interaction of two S100A4 mutants with myosin IIA *in vitro* (stopped-flow transient kinetics) and *in vivo* (cell migration and cell spreading assays).

2 Materials and Methods

2.1 Materials

2.1.1 Chemicals

All chemicals were of analytical or molecular biology grade quality and purchased from Sigma-Aldrich, Dorset, UK or Fisher Scientific, Loughborough, UK unless otherwise stated.

2.1.2 Cell culture

2.1.2.1 Eukaryotic cell line

A431-TETON and A431-SIP1 cell lines were described previously. The parental cell line, A431 was originally purchased from the American Type Tissue Culture Collection (ATCC, Rockville, MD., USA). A431-SIP1 GFP MIIA and A431-SIP1 GFP α -tubulin were generated during this study; see table 2.1 for details of cell lines.

Table 2.1 – Description of cell lines used in this study

Cell Line	Description	Reference
A431	Human epidermoid carcinoma of the vulva (epidermis) derived from 85-year old female.	(Giard <i>et al.</i> , 1973)
A431-TETON	Stable clone of A431 expressing the reverse tetracycline-controlled transactivator (rtTA) protein. Allows the expression of plasmid genes containing the Tetracycline response element (TRE) in the presence of Doxycycline.	(Andersen <i>et al.</i> , 2005)
A431-SIP1	Stable clone of A431-TETON expressing N-terminally-tagged myc-SIP1 (mouse) under Doxycycline-regulated expression.	(Mejlvang <i>et al.</i> , 2007)
A431-SIP1 GFP MIIA	Stable clone of A431-SIP1 expressing constitutively active N-terminally tagged-GFP - myosin IIA (human) under the CMV promoter.	Generated during this study.
A431-SIP1 GFP α-tubulin	Stable clone of A431-SIP1 expressing constitutively active N-terminally tagged-GFP α -tubulin (human) under the CMV promoter.	Generated during this study.

2.1.2.2 Cell culture reagents and supplements

Dulbecco's Modified Eagle's Media (DMEM) with high glucose (4.5 g/l), L-glutamine, sodium pyruvate and phenol red; 100X-penicillin/streptomycin, heat-inactivated foetal bovine serum (FBS), 10X-trypsin-EDTA (TE) were from PAA, Laboratories, Inc., UK. CO₂-independent media was from Invitrogen, Paisley, UK. All routine cell culture plastic-ware including 25 cm², 75 cm², 175 cm² tissue culture flasks and 6, 12 and 24-well plates were also from PAA. 24-well plate transwell inserts (8.0 µm-sized pores), 24-well plate companion plates and rat tail collagen I were from BD Biosciences, USA. All other plastic-ware including 5, 10, and 15 ml pipettes, 15 and 50 ml centrifuge tubes and freezing-cryotubes were from Greiner, USA. Doxycycline (Dox), dimethyl sulfoxide (DMSO) and puromycin were from Sigma-Aldrich, Dorset, UK. ML-7 and Y27632 were from Calbiochem, UK. Buffer V transfection kit (Buffer V and transfection cuvettes) was from Lonza, Slough, UK. Nunc Opticell 1100 chambers were from ThermoScientific, UK. Gurr Rapid staining set and various-sized glass coverslips with thickness No. 1 were from VWR, UK. Disposable Neubauer haemocytometers (C-CHIPs) were from NanoEnTEK Inc. Seoul, South Korea. Micropatterns were custom engineered by Dr. R. Picone, UCL, London, UK.

2.1.2.3 Small-interfering RNA oligonucleotides

RISC-free™ control and Smartpool ON-target Plus™ siRNAs to S100A4 were purchased from Dharmacon, Epsom, UK.

2.1.3 Protein analysis

2.1.3.1 SDS-PAGE and protein quantification

Ammonium persulphate (APS), N,N,N',N'-Tetramethylethylenediamine (TEMED), bovine serum albumin (BSA), bromophenol blue, β-mercaptoethanol (BME) were purchased from Sigma-Aldrich, Dorset, UK. 30% acrylamide/bis-acrylamide was from Geneflow, UK. Pre-stained protein ladder and Commassie stain were from Biorad, UK. Bicinchoninic acid (BCA) Protein Assay Kit was from ThermoScientific, UK. Protein cuvettes were from VWR, UK. SDS-PAGE running buffer, lysis, resolving, stacking buffers and were made from lab stocks.

2.1.3.2 Western blotting

Ponceau-S and tween-20 were purchased from Sigma-Aldrich, Dorset, UK. Immobilon-P polyvinylidene fluoride (PVDF) membrane was purchased from Millipore, Bedford, MA, USA. SuperSignal West Dura Chemiluminescent Substrate for HRP and CL-XPosure Film were purchased from ThermoScientific, UK. 3 mm Whatman Filter paper was purchased from VWR, UK. Transfer, blocking and wash buffers were prepared from lab stocks. Primary antibodies used for Western blotting are described in table 2.2. Goat anti-mouse HRP and Goat-anti rabbit HRP secondary antibodies were from Dako, Ely, UK.

2.1.3.3 Immunoprecipitation

IGEPAL-40 (NP-40 substitute), phenylmethanesulfonylfluoride (PMSF), β -glycerophosphate (BGP), sodium fluoride, leupeptin, aprotinin and sodium orthovanadate were purchased from Sigma-Aldrich, Dorset, UK. Protein G sepharose was purchased from GE Healthcare, Amersham, UK. Coomassie Protein Quantification kit (Bradford Assay) was from ThermoScientific, UK. S100A4 mouse monoclonal antibody was from Prolifa, USA (see table 2.2). Immunoprecipitation buffer was made up from lab stocks.

2.1.4 Immunocytochemistry and microscopy

Paraformaldehyde, 1 mm Whatman filter paper and glass slides were from VWR, UK. Triton X-100, 4',6-diamidino-2-phenylindole (DAPI), normal goat serum were purchased from Sigma-Aldrich, Dorset, UK. Alexa donkey-anti rabbit 488/594 and alexa donkey-anti mouse 488/594 fluorescent secondary-conjugated antibodies were from Invitrogen, UK. Fluoromount-G was from Cambridge Biosciences, UK. Goat anti-rabbit 30 nm gold and goat anti-mouse 15 nm gold secondary antibodies were purchased from British Biocell Inc., UK. Primary antibodies are detailed in table 2.2. Staining and blocking buffers were made from lab stocks.

2.1.5 Cloning and DNA analysis

KOD 2X DNA polymerase buffer was purchased from Calbiochem, UK. DH5- α *E. coli*, Miller's LB Broth Base, Lennox L agar, ampicillin, kanamycin and SOC media were from Invitrogen, UK. XL-1 Blue *E. coli* were from Stratagene, UK. *DpnI* was

from New England Biolabs, USA. Agarose, 100 bp and 1 kbp DNA ladders were from Geneflow, UK. Mini and maxi-prep DNA isolation kits were from Macherey-Nagel, UK. Oligonucleotide primers were purchased desalted from Sigma-Aldrich, Dorset, UK and are described in table 2.3. Plasmids used during this study are detailed in table 2.4.

2.1.6 Protein expression and purification

Isopropyl-1-thio- β -D galactopyranoside (IPTG), hen egg white lysozyme and DNase were purchased from Invitrogen, UK. The BL21 DE3 *E. coli* expression vector cell line was purchased from Stratagene, UK. Nickel (Ni^{2+}) - nitrilotracetic acid (Ni^{2+} - NTA) super flow agarose was purchased from Qiagen, UK and Sephacryl S-75 High Resolution matrix from GE Healthcare, UK.

2.1.7 Kinetics and protein spectrophotometry

Quin-2 was purchased from Sigma-Aldrich, Dorset, UK. M39 peptide (QRELEDATETADAMNREVSSLKNKLRRGNLPPVPPRRMA) was purchased from GL Biochem (Shanghai) Ltd., China.

2.1.8 Antibodies

Table 2.2 – Description of primary antibodies used during this study

Antibody	Immunogen	Species	µg/µl	Dilution		Antigen MW (kDa)	Source
				Western	IC		
S100A4	Full length human S100A4	Rabbit	1.0	1:500	1:300	10	Dako
	Full length human S100A4	Mouse	1.9	N/A	1:300 (IF) 1:25 (EM)	10	Prolifa
GFP	Full length GFP	Rabbit	1.0	1:2000	1:1000 (IF) 1:200 (EM)	30	ImmunoKontakt
Myosin IIA heavy chain	Peptide GKADGAEAKPAE corresponding to the C-terminus of human non-muscle myosin heavy chain isoform A	Rabbit	1.0	1:3000	1:1000	250	Covance
Total myosin light chain	Synthetic peptide corresponding to amino-terminal residues of human Myosin Light Chain 2	Mouse	n/k	1:1000 (BSA)	N/A	18	CST
Di-phospho-	Synthetic phospho-peptide	Rabbit	n/k	1:1000	N/A	18	CST

myosin light chain (Ser19/Thr18)	corresponding to residues surrounding Thr18/Ser19 of human myosin light chain 2			(BSA)			
Vimentin	Purified cow lens vimentin	Mouse	0.5	1:2000	N/A	57	BD transduction labs
α -tubulin	Sarkosyl-resistant filaments from <i>Strongylocentrotus purpuratus</i> (sea urchin) sperm axonemes	Mouse	n/k	1:20,000	N/A	55	Sigma
Myc-tag	Synthetic peptide corresponding to amino acids 408-437 of the Leucine zipper region of human Myc (AEEQKLISEEDLLRKRREQLKHKLE QLRNS)	Mouse	n/k	1:50	1:20	N/A	Hybridoma supernatant (in-house)

Oligonucleotides

CST – Cell signalling Technologies, n/k – not known;

All mouse antibodies are monoclonal and rabbit antibodies polyclonal

2.1.9 Oligonucleotides

Table 2.3 – Description of oligonucleotide primers used during this study

Primer	Sequence (5'-3')	Length (nt)	T _m (°C)	Notes
MIIA.S1916D F	AACCGCGAAGTCAGCGACCT AAAGAACAAGCTCAGG	36	78	Primer set for site-directed mutagenesis of pET28-WT M200 Serine 1916 to Aspartate Mutation (Full-length Myosin IIA; NCBI Reference Sequence: NM_002473.4)
MIIA.S1916D R	CCTGAGCTTGTTCTTTAGGTC GCTGACTTCGCGGTT	36	78	
MIIA.S1943D F	AAAGGCGCCGGGGATGGCG ACGACGAAGAGGTAG	34	79	Primer set for site-directed mutagenesis of pET28-WT M200 Serine 1943 to Aspartate Mutation (Full-length Myosin IIA; NCBI Reference Sequence: NM_002473.4)
MIIA.S1943D R	CTACCTCTTCGTCGTCGCCAT CCCCGGCGCCTTT	34	79	
S100A4.V77D F	ACTTCCAAGAGTACTGTGAC TTCCTGTCCTGCATCG	36	75	Primer set for site-directed mutagenesis of pBI-WT S100A4 Valine 77 to Aspartate Mutation (Full-length S100A4; NCBI Reference Sequence: NM_002961.2)
S100A4.V77D R	CGATGCAGGACAGGAAGTC ACAGTACTCTTGGAAGT	36	75	
S100A4.C81D F	CTGTGTCTTCCTGTCCGACAT CGCCATGATGTGTA	35	79	Primer set for site-directed mutagenesis of pBI-WT S100A4 Cysteine 81 to Aspartate Mutation (Full-length S100A4; NCBI Reference Sequence: NM_002961.2)
S100A4.C81D R	TACACATCATGGCGATGTCTG GACAGGAAGACACAG	35	79	
S100A4.ORF.F	ATGGCGTGCCCTCTGGA	17	62	Forward sequencing primer for S100A4 open reading frame (Full-length S100A4; NCBI Reference Sequence: NM_002961.2)
S100A4.ORF.R	TCATTTCTTCCTGGGCTGC	19	61	Reverse sequencing primer for S100A4 open reading frame (Full-length S100A4; NCBI Reference Sequence: NM_002961.2)

2.1.10 Constructs

Table 2.4 – Description of plasmids used during this study

Plasmid	Vector	Insert	Notes	Source
pBI-S100A4 WT	pBI; eukaryotic expression vector	Full length human S100A4 (NCBI Reference Sequence: NM_002961.2)	S100A4 cloned between <u>Pst</u> I and <u>Sal</u> I. Downstream of tetracycline response element (TRE) and CMV promoter lacking enhancers (P _{Min} CMV). Gene is only transcribed in the presence of rtTA and Doxycycline.	Dr M. Kriajevska (CSMM, University of Leicester)
pET28-M200 WT	pET-28a; prokaryotic expression vector	C-terminal fragment of non-muscle Myosin IIA; residues Q1761-E1960 – “M200” (NCBI Reference Sequence: NM_002473.4)	M200 cloned between <u>Nde</u> I and <u>Xho</u> I. Downstream of T7 promoter and <i>lac</i> operator. Transcription only in the presence of lactose analogs (i.e. IPTG) and T7 RNA polymerase.	Dr J. Basran (Department of Biochemistry, University of Leicester)
pEGFP Myosin IIA	pEGFP-C1; eukaryotic expression vector with N-terminal	Full length non-muscle Myosin IIA (NCBI Reference Sequence: NM_002473.4)	pEGFP-C1 encodes a red-shifted variant of wild-type GFP which has been engineered for brighter fluorescence. (Excitation maximum = 488 nm; emission maximum = 507 nm.). Inserts cloned between the GFP coding sequences and SV40 Poly A will result in N-terminally-tagged GFP fusion proteins.	Prof. Dennis Discher (University of Pennsylvania)
pEGFP α-tubulin	GFP	Full length α -tubulin; (NCBI Reference Sequence: NM_006009.2)		Dr Samantha Loh (MRC Toxicology)
pIRES-puro2	pIRES-puro2; eukaryotic expression vector, encodes the gene for puromycin resistance	n/a	Expresses the gene for puromycin resistance, puromycin-N-acetyl-transferase under the CMV major immediate early promoter/enhancer. Co-transfection with gene of interest will create puromycin-resistant cells.	Dr E. Tulchinsky (CSMM, University of Leicester)

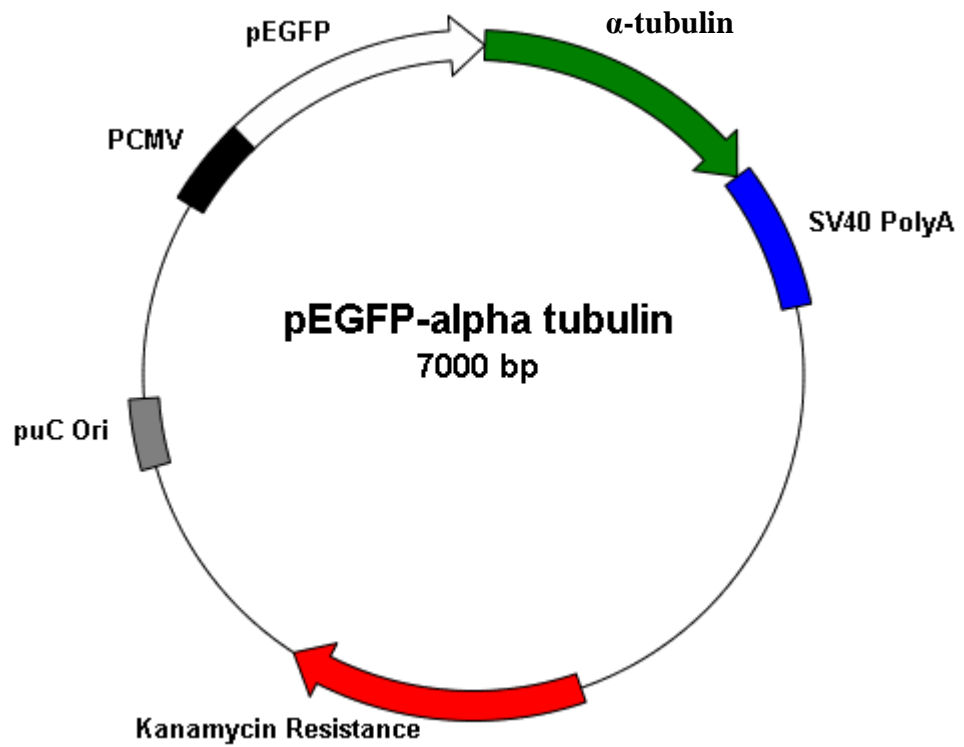


Figure 2.1: Plasmid map for pEGFP- α -tubulin

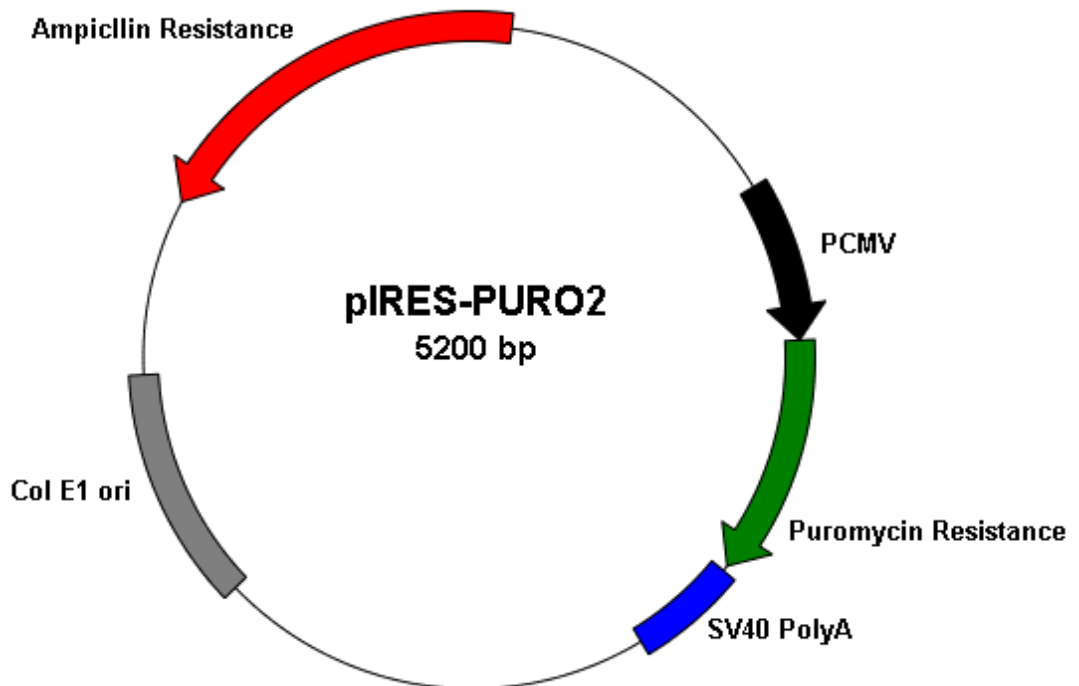


Figure 2.2: Plasmid map for pIRES-PURO2

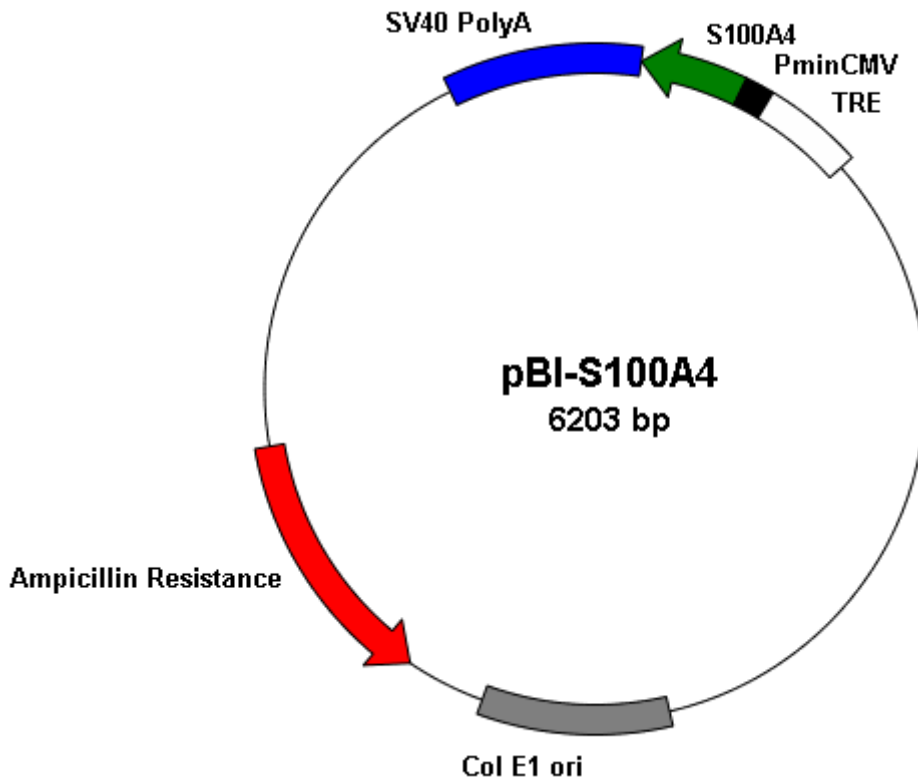


Figure 2.3: Plasmid map for pBI-S100A4

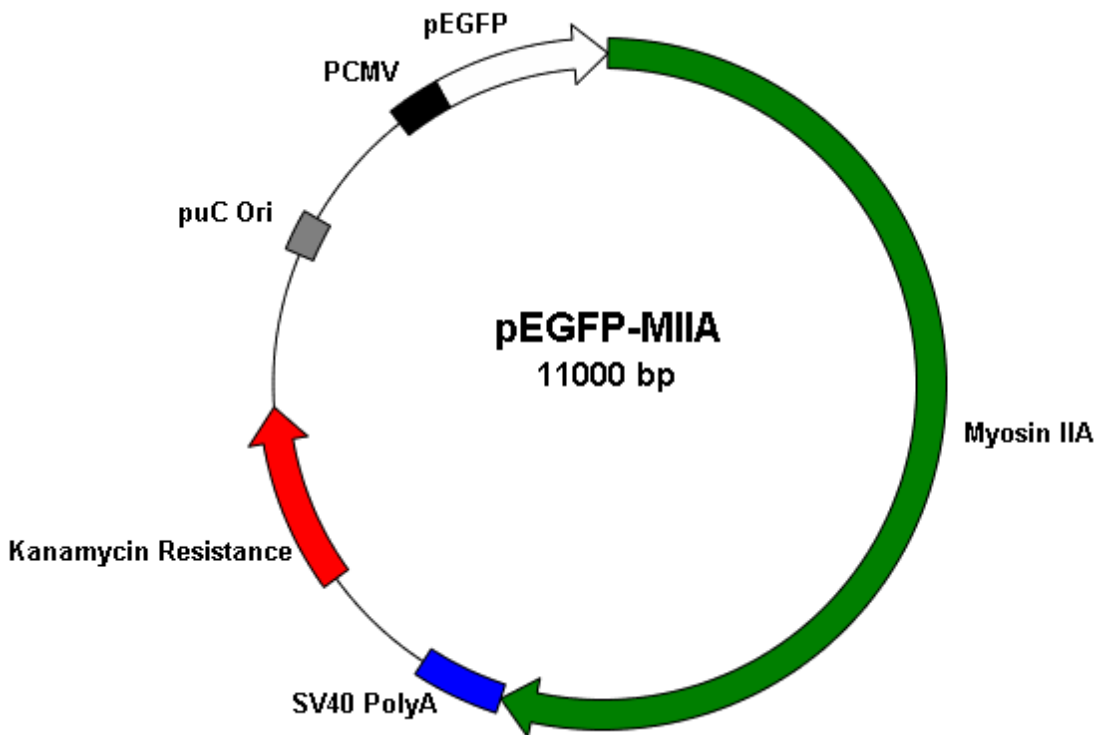


Figure 2.4: Plasmid map for pEGFP-MIIA

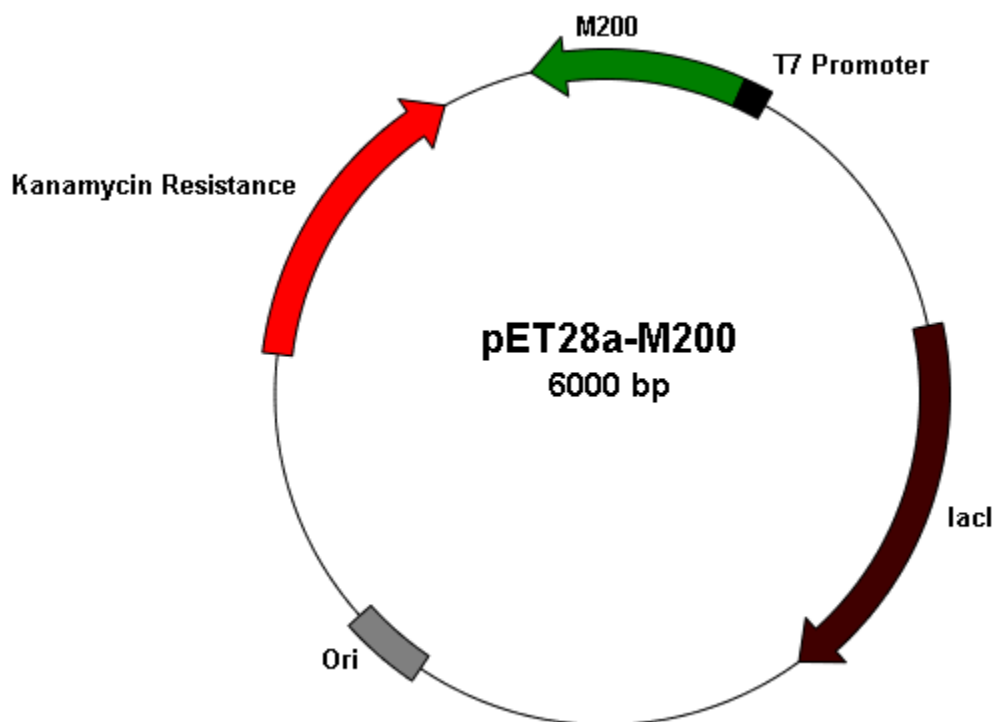


Figure 2.5: Plasmid map for pET28a-M200

Plasmid maps produced using Bio-Log Plasm (Bio-Log, Toulouse, France)

2.2 Mammalian cell culture techniques

2.2.1 Cell culture

Cell culture work was carried out in a Class II laminar flow cabinet. Cell lines were cultured in DMEM, 10% v/v FBS and 1% v/v penicillin/streptomycin (complete DMEM) and maintained in a 37 °C incubator with 5% CO₂ and 100% humidity. Cells were grown in the presence of 2 µg/ml (1.95 µM) Doxycycline (Dox) where indicated. All cell lines tested negative for various forms of *Mycoplasma*.

2.2.2 Passaging and seeding of cells

Cells were routinely passaged at approximately 60-80% confluence and not sub-cultured more than twenty times. Sub-culture of cells was undertaken by washing three-times with PBS (160 mM NaCl, 3 mM KCl, 8 mM Na₂HPO₄, 1m M KH₂PO₄, pH 7.3) and incubating in trypsin/EDTA (0.5 mg/ml Trypsin, 0.22 mg/ml EDTA in PBS, pH 7.5) for 5-10 minutes; flasks were gently tapped to aid detachment and Trypsin/EDTA (TE) neutralised with pre-warmed complete DMEM. Cells were pelleted at 300 g for 5 minutes and resuspended in complete DMEM before seeding at the required density. Volumes of PBS, TE and media required for T25, T75 and T175 cm² flasks are detailed in table 2.5.

Table 2.5: Volumes of PBS, TE and DMEM required for Cell Passaging

Flask (cm ²)	PBS (ml)	Trypsin/EDTA (ml)	Complete DMEM added to neutralise TE (ml)	Total Volume of Media (ml)
T25	2	1	4	5
T75	5	2	5	10
T175	10	3	7	25

2.2.3 Long-term storage and resuscitation of cells

For lab stocks and long-term storage, vials of cell lines were maintained in liquid nitrogen. Cells were detached, pelleted and re-suspended in freezing media (80% complete DMEM, 10% FBS, 10% DMSO) at a concentration of approximately 2-5 x

10^6 /ml cells and 1 ml aliquoted into individual cryotubes. Cells were frozen at rate of 1 °C/min in a -80 °C freezer and then placed in liquid nitrogen. For resuscitation, vials were thawed in a 37 °C waterbath, centrifuged at 300 g and seeded at the appropriate density.

2.2.4 Cell counting

Depending on the assay, harvested cells were re-suspended either in complete DMEM or serum-free DMEM at a concentration of approximately $0.5-2 \times 10^6$ cells/ml. 10 µl of suspension was added to one chamber of a disposable Neubauer haemocytometer (depth = 0.1 mm) and the average number of cells calculated from 4 large squares (1 mm²/square). This was then multiplied by 10,000 (and any dilution factor) to give a final concentration of cells/ml.

2.2.5 Transfection

Cells passaged 48 hours prior to transfection were grown to 60-80% confluence and two hours before transfection, the media replaced. Cells were then washed three times with PBS, trypsinised, centrifuged at 300 g for 5 minutes and re-suspended in complete DMEM. Cells were counted using a haemocytometer and the equivalent of 2.5×10^6 cells added to 1 ml PBS and centrifuged at 300 g for 5 minutes. The pellet was resuspended in 100 µl pre-warmed Buffer V and 2 µl siRNA (of a 100 µM stock) or 2 µg (unless otherwise stated) plasmid DNA added to create a cell suspension. This was transferred to a 4 mm cuvette and transfected using a Nucleofector™ (Lonza, UK) with program T020. The cuvette was then flushed with 900 µl media and cells seeded at the required density. 24 hours post-transfection, cells were washed once with PBS to remove cellular debris and fresh media added.

2.2.6 Invasion assay

For A431-SIP1 invasion assays, 800 µl complete DMEM was dispensed into the required number of wells of a 24-well companion plate and 8.0 µm pore-transwell inserts placed in each well, ensuring no bubbles formed between the media-insert interface. Harvested cells were then resuspended in complete DMEM to a final concentration of 2.5×10^5 /ml and 200 µl of cell suspension seeded in each transwell insert. A431-TETON invasion assays were performed in essentially the same manner,

expect 8.0 μm pore-transwell inserts were first coated with 100 μl of 10 $\mu\text{g}/\text{ml}$ fibronectin in PBS and left at RT for 2 hours, followed by three washes with PBS. Additionally, harvested cells were resuspended in serum-free DMEM (to create a serum gradient) to a concentration of $5 \times 10^5/\text{ml}$ and 200 μl seeded in each collagen-coated insert. In both cases, cells were allowed to migrate for 24 hours.

For processing, inserts were then aspirated, washed in 1 ml PBS and fixed with fixer solution (Gurr Rapid Staining Set) for 2 minutes. Fixer solution was removed, inserts placed in 1 ml staining reagent 1 (eosin-based stain) for 5 minutes and then 1 ml staining reagent 2 (methylene blue-based stain) for 10 minutes and all solution finally aspirated. Inserts were next washed twice in PBS and using a cotton wool bud, the top of each insert was gently wiped, removing non-migratory cells. Six randomly-chosen fields of the bottom of each insert (corresponding to those cells which had migrated) were then imaged using a 20x-objective, manually counted using Image J and averaged.

2.2.7 Micropattern assay

Micropatterns were custom-engineered by Dr. R. Picone (Laboratory for Molecular Cell Biology, UCL, London, UK) using conventional micropatterning techniques (Picone *et al.*, 2010). Essentially, a master was used to generate a polydimethylsiloxane (PDMS) stamp containing patterns of various size and shape. This was then inked in a solution of 100 $\mu\text{g}/\text{ml}$ collagen I for 10 minutes, dried under nitrogen gas and placed in contact with a 15 mm glass coverslip that had been plasma-cleaned and coated with non-adhesive polyethylene glycol (PLL-*g*-PEG). Each coverslip was kept in a sealed, 3 cm^2 dish and stored at 4 $^\circ\text{C}$ until required. Prior to seeding of cells, each micropattern was washed very gently with PBS and incubated in 2 ml serum-free media at 37 $^\circ\text{C}$. For seeding, cells were washed three-times with PBS and detached for 5 minutes using a minimal volume of TE. Dishes were lightly tapped to remove non-adherent cells and an equal volume of complete DMEM added before the suspension was counted. 3×10^5 cells were seeded on each micropattern and cells allowed to adhere; however, to ensure only individual cells occupied each pattern, excess cells were removed after approximately 10 minutes by washing the dish twice with pre-warmed serum-free media. Micropatterns were then placed back in the incubator and attached cells allowed to spread for a further 50 minutes.

2.2.7.1 Micropattern analysis

Individual cells attached to a micropattern that showed negative (vector, vector and Y27632) or positive (WT S100A4, S100A4 C81D) S100A4 expression as appropriate were analysed by confocal microscopy, compiled into image stacks with ImageJ and automatically orientated to ensure the top of each cell overlapped.

2.2.7.1.1 Collapse

The images were thresholded and converted to an 8-bit binary image. Three lines of 37 μm corresponding to each edge of the micropattern boundary were superimposed over all images and the modal pixel value was calculated along the length of each line such that a value of 0 (no cell) or 255 (cell) was recorded for each edge. If 50% or more pixels contained no cell then an edge was considered collapsed. The number of collapsed edges was then divided by the total number of edges for each population and expressed as a percentage.

2.2.7.1.2 Area

The 8-bit binary image stacks were used to calculate the area by using the “Analyze Particles” macro in ImageJ. Average sizes were calculated and expressed as a % of the maximum size of a cell on the micropattern i.e. an equilateral triangle with edges of 37 μm = 592 μm^2 .

2.2.8 Stable integration of plasmid DNA

A431-SIP1 cells were co-transfected with 5 μg of the required plasmid as well as 0.5 μg pIRES-puro2 plasmid (which carries the gene for puromycin resistance) and seeded in 3 96-well plates. 72 hours-post transfection, the media was replaced with selection media (complete DMEM and 0.4 $\mu\text{g}/\text{ml}$ puromycin) and replenished every third day thereafter. After approximately 3 weeks, plates were screened for GFP fluorescence (excitation: 480; emission: 520) using a fluorescence microplate reader (BMG Labtech Ltd., Germany) to identify potential positive colonies and verified using an epifluorescence microscope. Prospective colonies were washed twice with PBS, trypsinised and placed in 48-well plates and further amplified until growing in T25 flasks. Lysates were then collected and analysed for the stable incorporation of the protein of interest.

2.3 Protein analysis techniques

2.3.1 Preparation of protein lysates

Cells gently washed with PBS were lysed in 1X-gel loading buffer (50 mM Tris-HCl pH 6.8, 2 % v/v SDS, 10 % v/v glycerol), scraped into an eppendorf tube and heated at 95 °C for 5 minutes. Lysates were sonicated three times for 15 seconds to disrupt chromosomal DNA and centrifuged at 11,000 g for 1 minute to pellet DNA material. Lysates were then stored at -20 °C or used for protein quantification.

2.3.2 Protein quantification

Cells lysed in gel loading buffer were quantified using a bicinchoninic acid (BCA) assay kit (ThermoScientific) according to the manufacturer's protocol. Briefly, 10 µl unknown protein sample and 10 µl of 5 known bovine serum albumin (BSA) standards (ranging from 2 µg/µl to 0 µg/µl) were added to 1 ml BCA reagent (50 parts BCA reagent A with 1 part reagent B) in individual eppendorfs, vortexed and incubated at 37 °C for 15 minutes. Samples were allowed to cool at RT for 10 minutes and measured at 562 nm using a BioSpectrophotometer (Sanyo, Japan) blanked against water. The absorbance for the blank (0 µg/µl) was subtracted from each sample and a straight line fitted to the graph of absorbance versus concentration to determine the unknowns. Lysates were equilibrated to 1 µg/µl and β-mercaptoethanol and bromophenol blue added to a final concentration of 1% and 0.006% respectively. For quantification of immunoprecipitation lysates, a Bradford assay was used. 10 µl of unknown sample and 10 µl of 5 known BSA standards was added to 1 ml Bradford reagent, vortexed and incubated at RT for 10 minutes. Samples were measured at 595 nm and protein concentration calculated as described above.

2.3.3 SDS-PAGE

To resolve polypeptides on polyacrylamide gels under denaturing conditions, sodium dodecyl sulphate-polyacrylamide gel electrophoresis (SDS-PAGE) was used. Depending on the size of the antigen, resolving gels ranging from 6 to 15% were cast, modifying the relative ratio of acrylamide/bis-acrylamide to water accordingly:

Table 2.6: Volumes of water and acrylamide mix required for SDS-PAGE

% Gel	Water (ml)	Acrylamide Mix (ml)
6	5.3	2.0
8	4.6	2.7
10	4.0	3.3
12	3.3	4.0
15	2.3	5.0

For 10 ml resolving gel 2.5 ml 1.5 M Tris-HCl pH 8.8, 100 μ l 10% SDS, 100 μ l ammonium persulphate (APS) and 6-12 μ l TEMED was also added depending on the percentage gel. To cast a gel, two glass plates were thoroughly cleaned with 100% ethanol and assembled accordingly. The resolving gel was made up by mixing the acrylamide, Tris-HCl, water, SDS and APS before adding TEMED to catalyse the polymerisation reaction. The solution was then transferred to the pre-assembled gel apparatus and approximately 500 μ l of water-saturated butanol overlaid to create a homogenous surface and prevent evaporation; after polymerisation, the butanol was removed and gel washed twice with water. A 4% stacking gel (for 10 ml: 6.8 ml water, 1.7 ml acrylamide mix, 1.25 ml 1M Tris-HCl (pH 6.8), 100 μ l 10% SDS, 100 μ l APS, 10 μ l TEMED) was prepared as above and added on top of the resolving gel before inserting a 14-well comb, while removing excess solution with a pipette. After polymerisation, the gel was placed in a PAGE-running tank, the comb removed and gel lanes gently washed with water before addition of 1X-running buffer (25 mM Tris-HCl, 250 mM glycine, 0.1 % SDS, pH 8.3) to fill the top and bottom reservoirs. Meanwhile, protein lysates were heated for 5 minutes at 95 $^{\circ}$ C and allowed to cool for 10 minutes at RT, after which known concentrations (between 5-25 μ g protein) of samples and 10 μ l protein marker loaded in separate lanes and resolved at 120 V for approximately 1 – 2 hours.

2.3.3.1 Coomassie-blue staining

For visualisation of resolved proteins, the gel was rinsed in water and stained with Coomassie stain (0.1 % Coomassie blue R-250 in 40 % methanol, 10 % acetic acid) while gently rocking for 8-16 hours. The gel was destained with three washes of

destain buffer (40 % methanol, 10 % acetic acid) and imaged using a Canon PowerShot digital camera (Canon UK Ltd.).

2.3.3.2 *Western blotting*

Following SDS-PAGE, resolved gels were rinsed in water and transferred to PVDF membrane using a semi-dry transfer apparatus. For this, six pieces of 3 mm Whatmann filter paper and one piece of 0.2 μm pore polyvinylidene fluoride (PVDF) were cut to match the size of the gel and a sandwich created. Firstly, three pieces of filter paper were soaked in 1X-transfer buffer (25 mM Tris-HCl, 250 mM glycine, 0.1 % v/v SDS, 20 % v/v methanol pH 8.3) and placed in the centre of the transfer apparatus followed by the piece of PVDF, previously activated in methanol, SDS-PAGE gel and finished with the final three pieces of filter paper soaked in transfer buffer. Bubbles were removed by gently rolling a 5 ml pipette across the sandwich and excess solution soaked up with tissue paper. Polypeptides were transferred at a constant rate of 0.2 A per 10 cm^2 gel for 90 minutes. After transfer, membranes were washed in water and placed in Ponceau S solution (0.1% w/v Ponceau S w/v; 5.0% v/v acetic Acid) for 5 minutes to visualise transferred proteins ensuring efficient transfer and a visual estimation of equal loading. Membranes were then washed in water for 15 minutes and once in TBS-T (20mM Tris-HCl pH 8.0, 150 mM NaCl, 0.1% Tween-20) to remove the stain and processed for immunoblotting. To block non-specific sites, membranes were incubated with 1X-blotting buffer (5% w/v dried milk powder in TBS-T), rotated at RT for 30 minutes, washed three times with TBS-T and incubated in primary antibody diluted in either blotting buffer or BSA buffer (5% v/v BSA in TBS-T) for 45 minutes at RT. After several washes in TBS-T, membranes were then incubated for 45 minutes in secondary antibody diluted in blotting buffer and washed three times with TBS-T before application of the enhanced chemiluminescent reagent. For this, excess solution was drained and each membrane placed protein-side down on ECL reagent (1ml /5 cm^2 membrane) for 1 minute. ECL reagent was drained off, membranes placed within a plastic film and then positioned in an autoradiography cassette (GE Healthcare, UK). X-ray film was placed over the membrane for a variety of exposure times and developed using an AGFA curix 60 film developer (AGFA Healthcare, UK). Films were scanned with a Canon LIDE 60 scanner using Arcsoft Photostudio 5 (Arcsoft, Inc., USA) software.

2.3.3.2.1 Re-probing membranes

If further immuno-analysis of Western blots was required, membranes were either stripped to remove the primary-secondary antibody complex or the HRP quenched. Stripping was only used when the secondary antibody was of the same species as the initial probe since the harsh conditions of stripping could also remove antigen. For stripping, membranes were incubated in stripping buffer (62.5 mM Tris pH 6.8, 0.7% v/v β -mercaptoethanol, 2% SDS) for 1 hour at 60 °C with gentle rocking. Quenching of the HRP was carried out by incubating membranes in 15% H_2O_2 for 30 minutes at RT. After stripping or quenching, membranes were washed three times in TBS-T, blocked in blotting buffer for 15 minutes and processed accordingly.

2.3.4 Immunoprecipitation

Cells placed on ice were washed twice with ice-cold PBS and the appropriate volume of IP buffer supplemented with protease and phosphate inhibitors (150 mM NaCl, 0.5% NP-40, 50 mM Tris-HCl pH 8.0, 1 μ M DTT, 10 μ M β -GP, 50 μ M NaF, 0.1 μ M Na_3VO_4 2 μ g/ml aprotinin, 10 μ g/ml leupeptin, 25 μ g/ml PMSF) added for 10 minutes. Cells were then scraped into pre-chilled eppendorf tubes and centrifuged at 11,000 g for 10 minutes at 4 °C. The supernatant was then taken, ensuring to avoid any contact with the pellet, and added to a pre-chilled eppendorf tube. The protein concentration of the lysates was measured using a Bradford Assay (ThermoScientific), diluted to a final concentration of 1 μ g/ μ l and 500 μ l dispensed to another pre-chilled eppendorf tube and 3 μ g specific antibody added. The cell lysate-antibody suspension was rotated on an end-end rotator overnight at 4 °C and the next day 50 μ l protein G sepharose (a 50% slurry diluted in IP buffer) added and incubated at 4 °C for a further three hours. The lysate-antibody-sepharose suspension was then centrifuged at 11,000 g and washed three-times with IP buffer ensuring not to aspirate any of the pellet. 60 μ l of 2X-SDS sample buffer (100 mM Tris-HCl pH 6.8, 4 % SDS, 20 % v/v glycerol, 0.018 % v/v bromophenol blue, 2% v/v β -mercaptoethanol) was then added to the sample, boiled for 5 minutes and centrifuged at 11,000 g for an additional 5 minutes. Equal volumes of eluates were resolved using SDS-PAGE, transferred and stained with specific antibodies depending on application.

2.4 Immunocytochemistry

2.4.1 Immunofluorescence

For fluorescent staining of protein antigens, secondary antibodies conjugated with fluorophores of various excitation and emission spectra were used to bind antigen-specific primary antibodies. Cells washed with PBS were fixed with 4% paraformaldehyde (4% paraformaldehyde in PBS), washed a further three times and permeabilised with 0.5% triton X-100 (0.5 % triton X-100 in PBS) for 5 minutes. Cells were again washed with PBS to remove excess detergent and incubated for 45 minutes at RT with primary antibody diluted in 1X-staining buffer (complete DMEM) before additional washes. Cells were then incubated with 2 µg/ml fluorescent-conjugated secondary antibody for 45 minutes at RT, washed three times and counter-stained using 0.5 µg/ml 4',6-diamidino-2-phenylindole (DAPI) to visualise nuclei. To mount coverslips, excess solution was drained off and a drop of mountant (Fluoromount-G) placed on a glass slide; coverslips were then placed cell-side down and pressure gently applied to spread the mountant and remove air bubbles. Slides were sealed with nail varnish to prevent evaporation and movement of the coverslip and stored at 4 °C. In general samples were initially viewed on an inverted Nikon TE2000S epifluorescence microscope (Nikon, Japan) with the light source from a mercury arc lamp with a Plan Apo VC 60X oil 1.4 NA objective. The following filter sets were used: UV-2E/C DAPI (excitation filter: 325-375 nm; dichroic: 400 nm LP; emission filter: 435-485 nm), GFP-B (excitation filter: 460-500 nm; dichroic: 505 nm LP; emission filter: 510-560 nm) and TRITC (excitation filter: 530-560 nm; dichroic: 570 nm LP; emission filter: 590-650 nm). Images were acquired with a Hamamatsu CCD camera (Hamamatsu Photonics, Germany) attached to a PC using the HCLive software (Version 3.0.1.2, Hamamatsu). For confocal microscopy an inverted Nikon Eclipse Ti microscope connected to a Nikon Eclipse C1 confocal unit was used, also with a Plan Apo VC 60X oil 1.4 NA objective. The following lasers (Melles Griot, New Mexico, USA) and filter sets were used: helium cadmium laser 408 nm, dichroic 480 nm, BA 450-485 nm; argon ion laser 488 nm, dichroic 545 nm, BA 515-545 nm; helium neon laser 561 nm, dichroic 545 nm, BA 650 nm LP. A separate PMT was used for collection of each emission spectra. All image processing was carried out using ImageJ.

2.4.1.1 Co-localisation analysis of light microscopy imaging

The ImageJ plug-in, Intensity Correlation Analysis, was used to calculate Pearson's Correlation Coefficient (PCC) as well as the Intensity Correlation Quotient (ICQ).

2.4.2 Electron microscopy immunolabelling

Cells for transmission electron microscopy (TEM) experiments were processed by the Electron Microscopy Suite, University of Leicester. For preparation of cells for TEM, cells seeded on 9 mm glass coverslips were washed once with PBS and fixed overnight in 4% paraformaldehyde. The next day, they were washed twice with PBS and dehydrated in an ethanol series. Once dehydrated, LR white resin was infiltrated into cells and polymerised under a UV lamp at 4 °C for 24 hours in a nitrogen-atmosphere (oxygen inhibits the polymerisation reaction). Thin sections were then cut using an ultramicrotome and placed on copper grids over a hexagonal mesh to hold the tissue sections in place. For immunolabelling experiments, grids were first floated on drops of buffer A (1% BSA, 1% normal goat serum, 0.1% Tween-20, 1% sodium azide in PBS, pH 7.4) for 30 minutes to block non-specific sites then transferred to drops of primary antibody (diluted in buffer A) for 2 hours. Grids were washed 5 times in buffer A and transferred to 0.5 µg/ml goat anti-rabbit gold 30 nm or goat anti-mouse 15 nm gold secondary antibody for a further 2 hours before three washes in buffer A and 5 washes in ddH₂O. Grids were counterstained with 2% uranyl acetate and observed using a JEOL JEM-1400 transmission electron microscope at an accelerating voltage of 80 kV. Control incubations with only secondary antibodies demonstrated a highly specific signal for each primary antibody with essentially no background labelling from secondary antibodies. Floating of grids ensured sections were only stained on one side; seepage that did occur on grids during labelling were discarded.

2.4.2.1 Spatial Statistics and analysis

To analyse the colocalisation of two antigens over a series of distances a modified version of Diggle's G function was used. The original Diggle's G function states:

$G(y) = P \{ \text{distance from an arbitrary event to the nearest other event is at most } r' \}$ or

$$G(y) = n^{-1} \sum y_i \leq r' \quad \text{Equation 2.1}$$

for n events in a region A , where y_i denotes the distance from the i th event to the nearest other event in A with y_i the nearest-neighbour distances.

This can be modified to analyse a bivariate set of data i.e. for the minimum distance from the i th event in set X to the i th event in set Y [$d(x_i, y_i)$], where x and y are elements of antigen set 1 and antigen set 2, respectively.

$$n^{-1} \sum_{\substack{x \in X_1 \\ y \in X_2}} (d(x_i, y_i) \leq r') \quad \text{Equation}$$

2.2

Calculated for all pooled images,

$$\sum_{j=1}^N n(x, y) \sum_{j=1}^{-1} \sum_{\substack{x \in X_{1,i} \\ y \in X_{2,i}}} (d(x_i, y_i) \leq r') \quad \text{Equation 2.3}$$

where N is the number of pooled images and j is the j th image in the set.

To determine this, the X, Y co-ordinates for every particle were extracted from each image using ImageJ and the nucleus counter plugin and assigned a value of 1 or 2 depending on the size of the gold particle. The exhaustive inter-point distance from each particle in set 1 to set 2 and *vice versa* of one image was then calculated using trigonometry. However, to remove duplicated data points, the distances were ranked in descending order and the minimum distance chosen; the particles corresponding to this distance were then eliminated from the data set and the next minimum distance calculated from each of the remaining particles. This was iterated for each image and all the nearest-neighbour distances pooled and distributed in a histogram from 0-500 nm with 25 nm bins. To generate the statistics, particles equal to the density of antigen 1 and antigen 2 for each image were randomly distributed within the area of one image i.e. $22.55 \mu\text{m}^2$ and nearest neighbour analysis carried out as above. For each image this

process was simulated 100 times (Monte Carlo simulations), thus the 99% confidence intervals for complete spatial randomness could be calculated. All analysis was carried out using Microsoft Excel 2007 with a custom macro written in VBscript (Mr. P. Irvine).

2.5 Live cell imaging

2.5.1 Time-lapse microscopy

Cells seeded on a 6-well plate were grown to the required density and immediately prior to imaging, the media replaced with CO₂-independent media (Invitrogen, UK). Cells were placed in an environmental chamber (equilibrated at 37 °C) housing an inverted Nikon TE2000 (Nikon Instruments Ltd., Japan) microscope and 3-4 positions chosen for each sample. Phase contrast images were automatically acquired with a 20x ELWD Nikon objective every 20 minutes controlled by Micromanager software (Micromanager, Version 1.3). Image stacks were compiled in ImageJ and processed accordingly.

2.5.2 FRAP

Cells were seeded in an optically chamber and imaged using an inverted Nikon Eclipse Ti microscope connected to a Nikon Eclipse C1 confocal unit. After optimisation of the FRAP protocol, cells were imaged for two pre-bleach frames, prior to 3 bleach iterations using 100% (25 mW) of the 488-argon ion laser and recovery measured till steady state conditions had been reached.

2.5.2.1 Analysis

To analyse the recovery, the fluorescent intensity for the bleach area was extracted for each time point; the raw data was then revised for background fluorescence, corrected for photobleaching by adjusting to the total area of the bleached cell and finally the initial fluorescent value normalised to 1 to compare between different experiments. The first three steps of this analysis are represented in Figure 2.6. The experimental data is then fit to a single exponential process to derive the observed rate constant,

$$Fluorescence_{(t)} = A(1 - e^{-k_{obs}t}) + C \quad \text{Equation 2.4}$$

where $\text{Fluorescence}_{(t)}$ is the fluorescence at time t , A is the amplitude, k_{obs} is the observed rate constant and C is an offset value to account for a non-zero baseline.

The observed rate constant, K_{obs} is then used to determine the half-life for a single exponential process,

$$\frac{\ln 2}{K_{obs}}$$

Equation 2.5

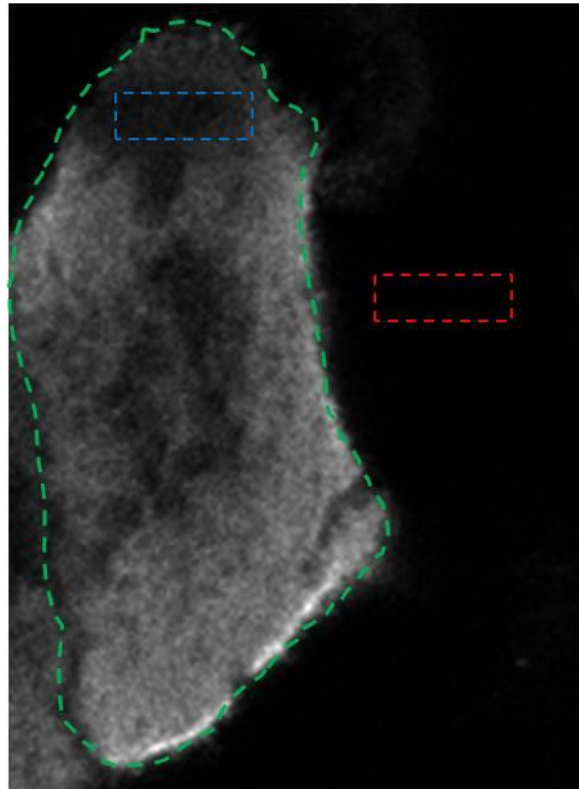
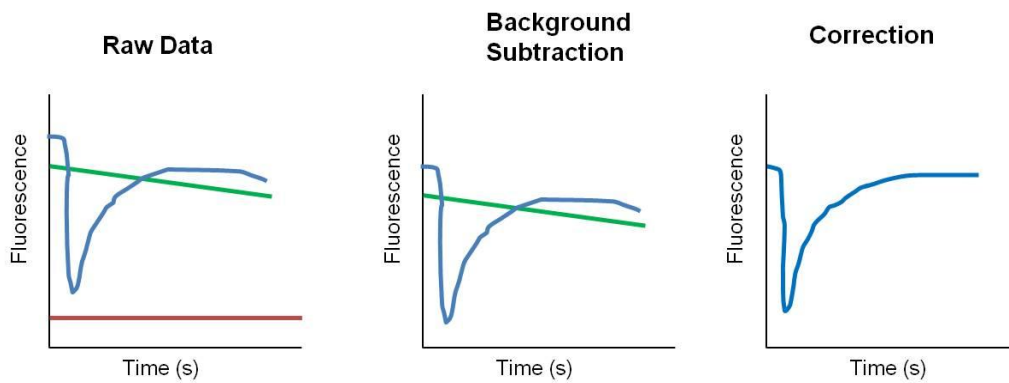
A**B**

Figure 2.6: Graphical Representation of FRAP Data Analysis

(A) Representative image showing a cell immediately post-bleach with the ROI (blue box), area of background fluorescence for subtraction (red box) and total fluorescence of the cell used for photobleaching correction (green line) used for analysis highlighted. (B) Representative graphs showing raw data, background subtraction and correction.

2.6 Molecular biology techniques

2.6.1 Transformation of *E. coli*

DNA was transformed into chemically competent cells according to the manufacturer's instructions. Briefly, aliquots of DH5-a or XL-Blue 1 *E. coli* were thawed on ice for 15 minutes and 25 μ l (per transformation) transferred to pre-chilled eppendorf tubes. 1 μ l of plasmid DNA or 5 μ l PCR product was added, gently mixed with a pipette and incubated on ice for 30 minutes. Cells were then heat-shocked at 42 °C for 30 seconds and placed on ice for 2 minutes. 500 μ l pre-warmed SOC media (2% Tryptone, 0.5% Yeast Extract, 10 mM NaCl, 2.5 mM KCl, 10 mM MgCl₂, 10 mM MgSO₄, 20 mM glucose) was added and cells incubated at 37 °C, 250 rpm shaking for 1 hour to recover. 50 μ l of cell suspension was plated on a selective LB agar plate (10 g/l peptone 140, 5 g/l yeast extract, 5 g/l sodium chloride, 12 g/l agar plus 100 μ g/ml ampicillin or 30 μ g/ml kanamycin as appropriate) with the remaining suspension centrifuged at 11,000 *g* for 1 minute and resulting pellet resuspended in 50 μ l media and plated on a second plate. Plates were incubated at 37 °C for between 12-16 hours.

2.6.2 DNA manipulation

2.6.2.1 Small and large-scale isolation of plasmid DNA

A plasmid DNA mini-prep isolation kit (Nucleobond, Macherey-Nagel, UK) was used for isolation of up to 20 μ g of plasmid DNA according to the manufacturer's instructions. Briefly, a single colony was isolated from a freshly-transformed agar plate and grown in 5 ml LB media (10 g/l peptone 140, 5 g/l yeast Extract, 5 g/l sodium chloride) overnight. The culture was centrifuged for 1 minute at 11,000 *g*, supernatant aspirated and pellet resuspended in 250 μ l re-suspension solution. 250 μ l lysis buffer was added, incubated for 5 minutes at RT and 500 μ l neutralisation buffer then added and the lysate centrifuged for 10 minutes at 11,000 *g* to pellet the flocculent. The supernatant was applied to a DNA-binding column and centrifuged at 11,000 *g* for 1 minute, through-flow discarded and column washed twice with 70% ethanol. Plasmid DNA was eluted in 50 μ l elution buffer (5 mM Tris-HCl pH 6.8) and concentration determined spectrophotometrically with a NanoDrop (ThermoScientific, UK). Additionally, the A₂₆₀/A₂₈₀ ratio was also measured and samples deemed pure if exceeding a value of 1.8. For larger scale isolation of plasmid DNA (approximately 2000 μ g), a plasmid DNA maxi-prep isolation kit (Nucleobond, Macherey-Nagel, UK)

was used. In essence, a similar method was followed as described above but a starting volume of 200 ml overnight culture was used. Additionally, instead of centrifuging the lysate to remove the flocculent after neutralisation, the lysate was filtered. This DNA was then precipitated using isopropanol and concentrated using syringe-based Nucleobond Finalizers™; finally, the DNA was washed twice with 100% ethanol and eluted in elution buffer. To check the relative proportion of nicked, super-coiled or linear plasmid, 0.5 µg DNA was analysed by gel electrophoresis.

2.6.2.2 DNA gel electrophoresis

For analysis of plasmid DNA and DNA fragments, Tris-Acetate-EDTA (TAE) gel electrophoresis was used. 100 ml 1X-TAE buffer (4.8 g/l Tris base, 1 mM EDTA, 1% v/v acetic acid) was mixed with 0.75-2.0 g agarose depending on the size of DNA to be analysed and boiled in a microwave till fully dissolved. The solution was allowed to cool and ethidium bromide added to a final concentration of 1 µg/ml before pouring the solution into a pre-assembled horizontal gel electrophoresis tank with a 20-well comb and allowed to set. The gel comb was then removed and the tank filled with TAE buffer till the gel was fully submerged. Meanwhile, the appropriate concentration of DNA was added to 5X-loading buffer (50% v/v glycerol, 100 mM EDTA, 0.1% v/v bromophenol blue) and made up to a total volume of 15 µl with TAE buffer. Samples were then loaded into wells, together with a DNA marker and electrophoresis carried out at 80 V for 30-60 minutes. Gels were visualised using a UV transilluminator (UVP BioDoc-H System, USA) and images captured using a Sony CCD Chip camera (Sony UK Ltd., UK).

2.6.2.3 Site-directed mutagenesis

Mutation of plasmid DNA was carried out according to the method described by the QuikChange® Site-Directed Mutagenesis kit (Stratagene, USA). Firstly, a Polymerase Chain Reaction (PCR) was performed to amplify template DNA with mutagenic primers (described in table X.Y). Primers were designed to be between 25 and 45 bases in length with a melting temperature (T_m) of ≥ 78 °C, using the following equation:

$$T_m = 81.5 + 0.41(\%GC) 675/N - \% \text{ mismatch} \quad \text{Equation 2.7}$$

where N is the length of the primer and % mismatch is the number of base pairs required for mutation as a percentage of N.

The mutation was placed in the centre of each primer and complementary sequence added either side to anneal to the template DNA. For the PCR, 20 ng template DNA (either pBI-S100A4 WT or pET-28a M200 WT), 10 pmol forward and reverse primer, 10 μ l 2X KOD-DNA polymerase PCR mix and 1 μ l DMSO were added to a PCR tube, made up to a total volume of 20 μ l with DNase-free water and briefly centrifuged. The PCR reaction (GeneAmp PCR system 2400 (Perkin Elmer, USA)) was carried out under the following conditions:

Table 2.7 – PCR cycles for site-directed mutagenesis

Step	Temperature (°C)	Time (s)	Cycles
Initial denaturation	95	120	1
Denaturation	95	20	20
Annealing	55	10	
Extension	70	180 (pBI); 240 (pET28a)	
Final Extension	70	420	1

After amplification, 5 μ l PCR product was analysed by DNA gel electrophoresis to check for the presence of amplified DNA at the correct molecular weight. If successful, 1 μ l *DpnI* (2 units/ μ l) was added to the remaining product and incubated at 37 °C for 1 hour to remove hemi-/methylated-DNA (i.e. parental template). 5 μ l of *DpnI*-treated DNA was then transformed into XL1-Blue *E. coli*, plated on selective-agar plates at several densities and incubated at 37 °C. The next day, two colonies were picked off and grown in 5 ml-selective media overnight and plasmid DNA isolated using a plasmid DNA mini-prep kit.

2.6.3 DNA sequencing

DNA sequencing was carried out by GATC Biotech (GATC Biotech AG, Constance, Germany) on an ABI 3730 XL using the Sanger-Dideoxy method. For sequencing of S100A4 plasmids, forward and reverse primers (see table 2.3) to the open reading frame were used whereas sequencing of phosphomimetic myosin mutants used a T7 terminator primer courtesy of GATC.

2.7 Recombinant protein expression and purification

2.7.1 Protein expression and purification

For small-scale expression trials, bacterial colonies from freshly-transformed plates were picked off and grown overnight in 3 ml LB media at 37 °C. This culture was then diluted 10-times with LB media and once an A_{600} of 0.6 had been reached, half the culture aliquoted into a new tube and a final concentration of 200 μ M Isopropyl-1-thio- β -D galactopyranoside (IPTG) added to one tube. Both cultures were grown for a further 2 hours (with and without IPTG), 100 μ l taken and centrifuged at 11,000 g for 2 minutes. The pellet was resuspended in 20 μ l 8M urea and an equal volume of 2X-sample buffer added before analysis by SDS-PAGE. For large-scale grow-ups, a single colony was grown in 5 ml LB media for approximately 8 hours and used to inoculate 200 ml media and grown for 37 °C with shaking. Eight 1 litre flasks of LB media were then inoculated with 20 ml overnight culture, induced with IPTG at $A_{600} = 0.6$ and grown for 48 hours at 30 °C. Bacteria were harvested by centrifugation at 4000 g for 20 minutes and the pellet frozen at -80 °C overnight. Next day, the pellet was thawed on ice, lysed in a minimal volume of lysis buffer (50 mM KH_2PO_4 pH 8.0, 500 mM NaCl, 10 mM imidazole with 1 mM PMSF and 1 protease cocktail inhibitor tablet (Roche)) and sonicated using a MSE Soniprep 150 (MSE, Lower Sydenham, UK) 6 times for 30 seconds. After sonication, MgCl_2 (to a final concentration of 20 mM) and a spatula of DNase and lysozyme was then added, stirred for 1 hour at 4 °C and centrifuged at 18,000 g for 45 minutes. A column (Pharmacia, UK) previously packed with Ni^{2+} -NTA Nickel agarose was then equilibrated with lysis buffer and cell-free extract loaded on to the column and attached to a peristaltic pump at a flow rate of 1 ml/minute. The column was washed with 150 ml lysis buffer and at least 500 ml wash buffer (50 mM KH_2PO_4 pH 8.0, 500 mM NaCl, 20 mM imidazole) until the absorbance at 280 nm was minimal, indicating that all non-specific proteins had been washed off. A gradient maker with 100 ml wash buffer and 100 ml elution buffer (50mM KH_2PO_4 pH 8.0, 500 mM sodium chloride, 250 mM imidazole) was assembled, connected to the column and used to elute protein (with a linear gradient ranging from 20 mM to 250 mM imidazole) and 2 ml fractions collected by a fraction collector (GE Healthcare, UK). Eluted fractions were analysed spectrophotometrically by measuring the absorbance at 280 nm and fractions with protein assessed by SDS-PAGE. Protein at the correct molecular weight was concentrated using a centrifugal 3000 Dalton molecular weight cut-off filter

unit (Millipore, USA) until a volume of approximately 1 ml had been reached. To further purify the protein and aid buffer exchange, the protein was run on a gel filtration column which separates proteins based on size. A column packed with Sephacryl S-75 High Resolution matrix (GE Healthcare, UK) was pre-equilibrated overnight in myosin buffer (500 mM sodium chloride, 20 mM HEPES pH 7.5) and protein added to the top of the column; after approximately 1 hour, myosin buffer was then applied to the column and fractions collected at 1 ml/min. Fractions were again checked for the presence of protein, pooled and concentrated to yield 1 ml of purified protein.

2.7.2 Quantification of protein and reagent concentration

Protein concentration was calculated using the Beer-Lambert law which describes how the concentration of a substance is related to its absorption of light:

$$A = \varepsilon cl \qquad \text{Equation 2.8}$$

A = absorbance; l = path length (cm); ε = Extinction co-efficient ($\text{L mol}^{-1} \text{cm}^{-1}$); c = mol L^{-1}

The molar co-efficient for S100A4 and M200 fragments (WT, S1916 and S1943D) was $2980 \text{ M}^{-1} \text{cm}^{-1}$ at an absorbance of 280 nm with two tyrosine residues per chain. Concentrations are stated throughout in terms of an S100A4 monomer and single polypeptide chain of myosin fragment. With the concentrations used for kinetic assays S100A4 is predominantly a dimer and myosin forms a stable coiled-coil (Badyal *et al.*, 2011), thus concentrations of these two species are half of those stated in the text. For measuring protein concentration and assessing presence of contaminating species, protein was diluted in either S100A4 or myosin buffer and scanned from 200 to 700 nm using a Cary 50 spectrophotometer (Varian Ltd., Walton-on-Thames, UK) with a path length of 10 mm; corrections were made for the measurement of M200 fragments due to turbidity. The concentration of M39 peptide was determined from its dry weight. Quin-2 was measured with a molar co-efficient of $5000 \text{ M}^{-1} \text{cm}^{-1}$ at 354 nm in $\text{Ca}^{2+}/\text{Mg}^{2+}$ -free PBS plus 1 mM EGTA to chelate contaminating Ca^{2+} .

2.8 Kinetic assays

2.8.1 Measuring myosin turbidity

Myosin turbidity was measured at an apparent absorbance of 300 nm using a spectrophotometer with 10 mm-path length and 0.1 ml microcuvette (105.250-QS; Hellma, Southend-on-Sea, UK). Data was fitted to a sigmoid curve using GraphPad Prism.

2.8.2 Transient kinetics

Transient kinetic studies were performed using a SX18-MV stopped flow spectrophotometer (Applied Photophysics Ltd., Leatherhead, UK) fitted with a circulating water bath. A dead time of 1.5 ms was previously determined (Kovacs *et al.*, 2002). Quin-2 fluorescence was measured by excitation at 336 nm and emission collected with a 455-nm longpass filter.

2.8.2.1 Data Analysis of transient kinetics

All data were collected using Applied Photophysics Pro-Data SX and analysed using non-linear least squares regression analysis with either Applied Photophysics Pro-Data or Grafit 5 (Erithacus Software Ltd.). For biphasic or triphasic kinetic processes, data were fit to either double (Equation 3.1) or triple exponential (Equation 3.2) functions as described in the text,

$$\text{Fluorescence}_{(t)} = A_1 \cdot (1 - e^{-k_{obs1} t}) + A_2 \cdot (1 - e^{-k_{obs2} t}) + C \quad \text{Equation 2.9}$$

$$\text{Fluorescence}_{(t)} = A_1 \cdot (1 - e^{-k_{obs1} t}) + A_2 \cdot (1 - e^{-k_{obs2} t}) + A_3 \cdot (1 - e^{-k_{obs3} t}) + C \quad \text{Equation 2.10}$$

where $\text{Fluorescence}_{(t)}$ is the fluorescence at time t , A_x is the amplitude of phase x , k_{obsx} is the observed rate constant for phase x and C is an offset value to account for a non-zero baseline.

2.8.2.2 Kinetic modelling

Modelling was carried out using Berkeley Madonna software (version 8.3.18).

2.9 Analysis and statistics

2.9.1 Statistics

A student's T-test was used to compare the mean of two groups. For comparison of more than two groups, a one-way ANOVA was used followed by a Dunnett's Multiple Comparison test. All statistics was carried out using GraphPad Prism Version 5. * = $P < 0.05$; ** = $P < 0.01$; *** = $P < 0.001$.

2.9.2 Sequence alignment

Alignment using Clustal W (<http://www.ebi.ac.uk/Tools/msa/clustalw2/>); shading using BOXSHADE 3.3 (<http://www.mobyle.pasteur.fr/cgi-bin/portal.py/>).

3 Characterising the expression of S100A4 in a model of Epithelial-Mesenchymal Transition (EMT)

3.1 Introduction

Epithelial to mesenchymal transition (EMT) is a process whereby cells lose their epithelial characteristics and gain mesenchymal ones. EMT is crucial during several stages of embryogenesis, including gastrulation, somitogenesis and neural cell crest migration. This requires a loss of epithelial cell-cell junctions and a gain in migratory and invasive abilities allowing cells to migrate individually, moving to distant parts of the embryo (Thiery *et al.*, 2009). A similar process is now thought to be reactivated during carcinoma progression allowing cells to become more invasive, contributing to the metastatic cascade (Thiery, 2002). As such, a study of those genes activated during this process could yield important insights into the nature of carcinoma progression and provide potential therapeutic targets (Yang & Weinberg, 2008).

A number of different cell models have been established to study EMT (Yang *et al.*, 2004; Bolos *et al.*, 2003; Janda *et al.*, 2002). Due to its temporal nature, such models generally rely on inducible expression of EMT regulators in epithelial tumour cell lines. Indeed, the model of EMT used in this study is a clone of human epidermoid carcinoma cells, A431, expressing TETON (Dox)-regulated SIP1 (Mejlvang *et al.*, 2007). SIP1 is a transcriptional repressor of *E-cadherin* and is a so-called master regulator of EMT (Browne *et al.*, 2010). Treatment with Dox leads to rapid expression of SIP1 inducing large morphological changes consistent with an EMT. Such changes are reflected in the expression patterns of epithelial and mesenchymal-associated genes with E-cadherin and cytokeratins down-regulated whilst vimentin and fibronectin are up-regulated. The expression of S100A4 has not been investigated in this cell model (Mejlvang *et al.*, 2007).

Among the more established markers of EMT, S100A4 is now widely quoted as an additional factor commonly upregulated during the process although little is known regarding its functional effects during EMT (Schneider *et al.*, 2008). However, since S100A4 is strongly associated with cell migration (Tarabykina *et al.*, 2007) and one hallmark of EMT is the increase in migratory abilities (Thiery, 2003) it is likely that S100A4 promotes EMT-induced migration although this has not been shown experimentally.

One study that did investigate the function of S100A4 during EMT showed S100A4-knockdown was sufficient to attenuate EMT-progression suggesting it is required for the transition from an epithelial to mesenchymal state (Okada *et al.*, 1997) rather than merely playing a causal role.

Accordingly, the aims of the work in this chapter were to characterise the expression of S100A4 in an established model of EMT (Sayan *et al.*, 2009; Mejlvang *et al.*, 2007); determine if S100A4 is required for EMT progression; and finally, assess the effect of S100A4 expression on cell migration.

3.2 Results

3.2.1 S100A4 is activated during SIP1-induced EMT

To examine the expression of S100A4 during EMT, cell lysates were collected at different time points post SIP1-induced expression and analysed by Western blot (Figure 3.1). After 12 hours Dox treatment, SIP1 was detected at low levels and then significantly increased expression remaining stable until 72 hours. Conversely, S100A4 was initially present at low, basal levels but after 48 hours Dox treatment was strongly activated. Expression of vimentin, a mesenchymal-associated gene (Kalluri & Weinberg, 2009), was detected after 24 hours.

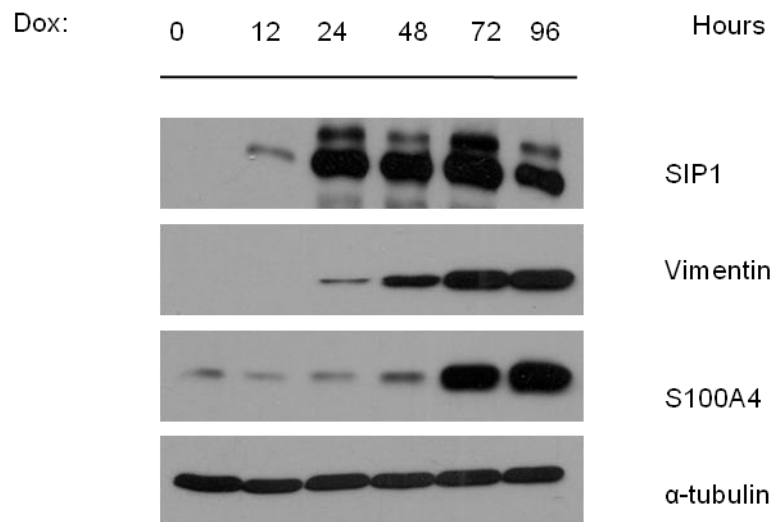


Figure 3.1: Western blot analysis of S100A4 expression during EMT

A431-SIP1 cells maintained in the presence of Dox for indicated times were collected and analysed by Western blot. Membranes were stained for SIP1, S100A4 and vimentin. α -tubulin was used to ensure equal loading. Western blot representative of 3 independent experiments.

To correlate the expression of S100A4 with the phenotypical changes occurring during EMT, time lapse microscopy was used. A431-SIP1 cells maintained either in the

absence or presence of Dox for 72 hours were imaged every 4 hours to acquire a temporal overview of the EMT process (Figure 3.2A). 24 hours post-SIP1 expression, cells had begun to scatter, although still remained within their epithelial boundaries. After 48 hours, cells were less clustered and appeared to migrate more individually compared to the un-induced A431-SIP1 cells and by 72 hours, cells had fully scattered and spread, developing large lamellipodial protrusions (Figure 3.2B). Combining these data, expression of S100A4 occurs after the stages of EMT where cells have fully scattered from their epithelial boundaries but coincides with the formation of lamellipodium required for mesenchymal cell migration (Friedl & Wolf, 2009).

To further characterise the expression of S100A4, the cellular localisation was examined using confocal microscopy. After 72 hours Dox treatment, A431-SIP1 cells were stained for SIP1 and S100A4 using immunofluorescence (Figure 3.3). As previously reported, SIP1 was localised exclusively to the nucleus (Vandewalle *et al.*, 2005) while S100A4 exhibited a cytoplasmic distribution with some nuclear expression, also consistent with previous studies (Kim & Helfman, 2003).

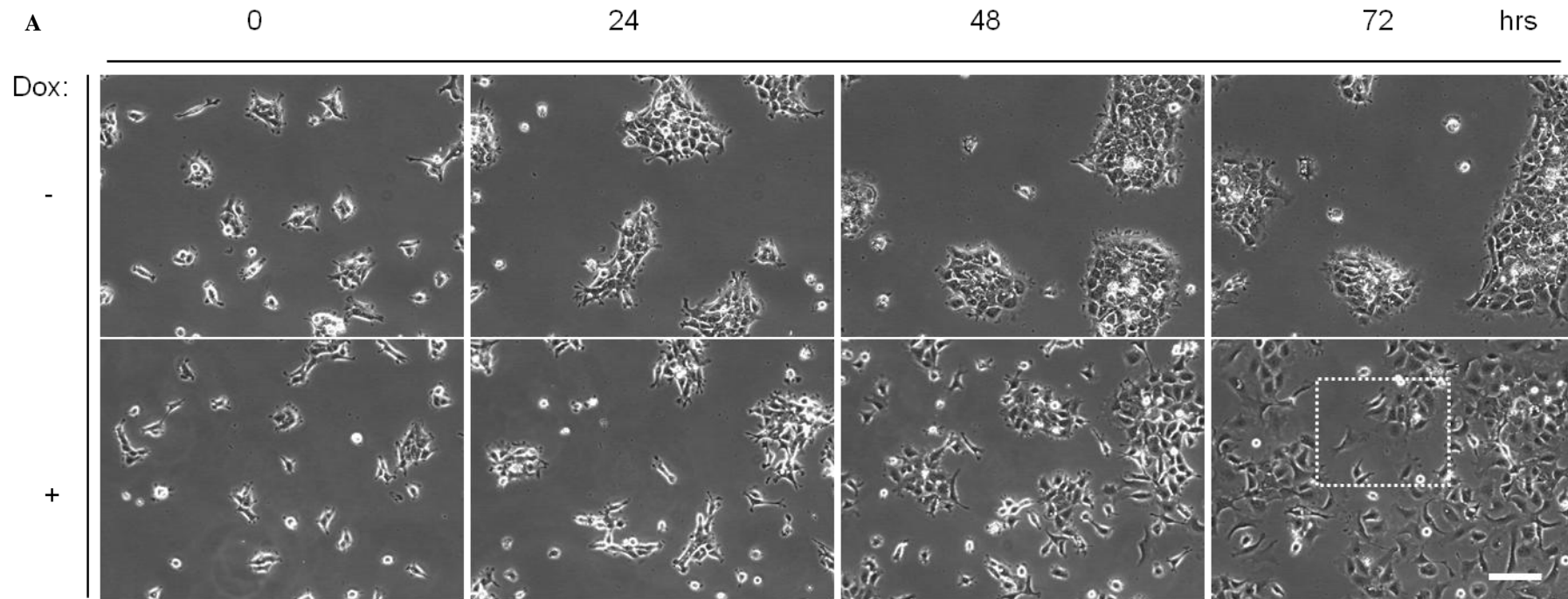


Figure 3.2: Temporal overview of SIP1-induced EMT

A431-SIP1 cells were maintained in the absence or presence of Dox for 72 hours and imaged using a time lapse microscope every 4 hours. (A) Representative phase contrast images are shown. Scale bar = 50 μm . (B) Magnified region of white box in (A). White arrow indicating formation of large lamellipodia, characteristic of mesenchymal cells. Scale bar = 20 μm .

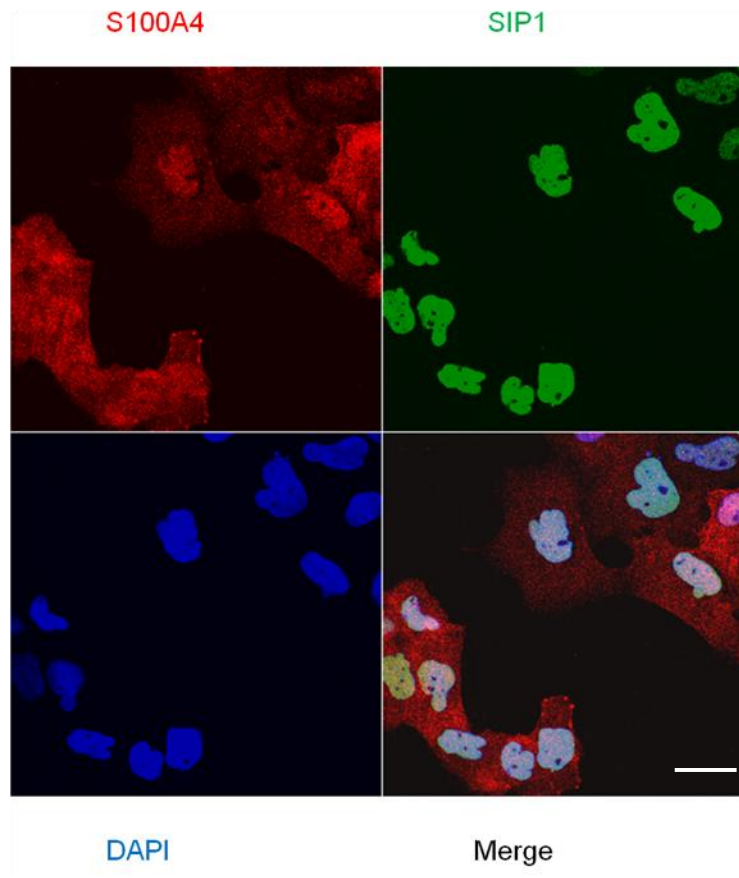


Figure 3.3: Localisation of S100A4 and SIP1 during EMT

A431-SIP1 cells maintained in the presence of Dox for 72 hours were fixed, permeabilised and stained for S100A4, SIP1 and DAPI (to visualise nuclei) using immunofluorescence. Cells were analysed using confocal microscopy. Scale bar = 10 μm . Red = S100A4; Green = SIP1; Blue = DAPI. Control experiments where primary antibodies were omitted yielded no staining indicating a highly specific signal for both primary antibodies.

3.2.2 S100A4 inhibition does not delay or block EMT

In order to determine if S100A4 is required for EMT progression, A431-SIP1 cells were transfected with a non-targeting (control) siRNA or S100A4-targeting siRNA and incubated in the presence of Dox for 0, 24, 48, 72 and 96 hours. Western blot analysis demonstrated a similar expression pattern of SIP1 and S100A4 (Figure 3.4A) in control cells compared to non-transfected cells (cf. Figure 3.1) but those transfected with S100A4-targeting siRNA exhibited a significant reduction in S100A4 levels at all timepoints. The expression pattern of the mesenchymal-associated protein vimentin exhibited no significant changes upon knockdown of S100A4. Furthermore, there were no obvious morphological changes associated with S100A4 knockdown after 72 hours Dox treatment (Figure 3.4B). Taken together these data suggest S100A4 expression is not a requirement for EMT progression.

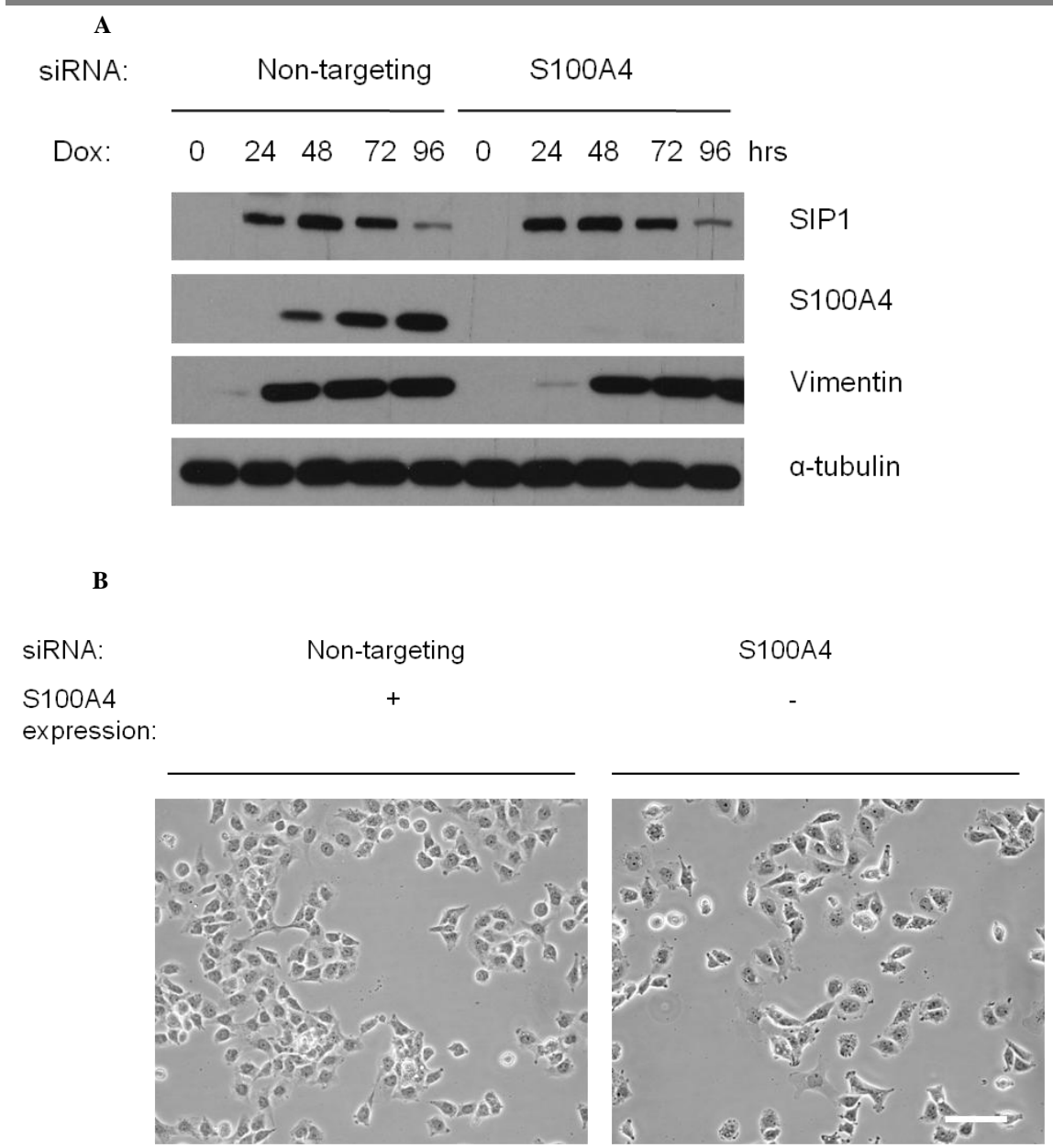


Figure 3.4: Effect of S100A4 knockdown on progression of EMT

(A) A431-SIP1 cells transfected with either a non-targeting (NT) or S100A4-targeting siRNA were maintained in Dox for indicated times. Lysates were collected and membranes probed for S100A4, vimentin, SIP1 and α -tubulin. Western blot representative of three independent experiments. (B) Representative phase contrast images of cells transfected with non-targeting (S100A4-expressing cells) or S100A4-targeting (depleted S100A4 expression) siRNA maintained in the presence of Dox for 72 hours. Scale bar = 30 μ m.

3.2.3 S100A4 promotes cell migration in A431-SIP1 cells

Having established S100A4 expression is not required for EMT, the role of S100A4 in cell migration was next examined. Cells transfected with a non-targeting and S100A4-targeting siRNA were maintained in Dox for 72 hours and then seeded in a transwell insert. After 24 hours incubation, migrated cells were stained, counted and expressed as a factor of the control rate of migration. As hypothesised, knockdown of S100A4 expression reduced the rate of cell migration by approximately 2-fold (Figure 3.5A; $p < 0.01$) with the level of knockdown confirmed by Western blotting (Figure 3.5B).

As a whole, these data suggest S100A4 is activated during a model of EMT and increases the rate of cell migration.

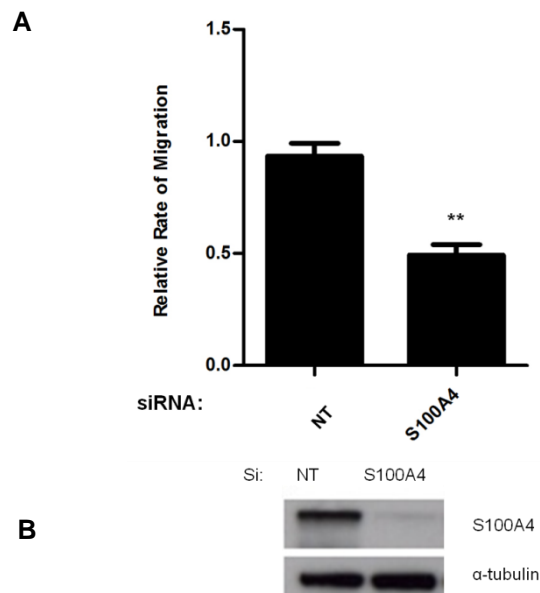


Figure 3.5: RNAi-mediated knockdown of S100A4 reduces the rate of cell migration

(A) A431-SIP1 cells transfected with either a non-targeting or S100A4-targeting siRNA were maintained in Dox for 72 hours and then seeded in uncoated 8.0 μ m transwell inserts. After 24 hours, cells were fixed, stained and non-migratory cells removed from the upper part of the insert. Cells from 6 randomly selected fields were counted using a 20x-objective and rates of migration expressed relative to the control sample. Results represent the average of three independent experiments performed in triplicate. A Student's T-test was used to assess the statistical significance. $** = p < 0.01$. Error bars are SEM. (B) To confirm knockdown, lysates were analysed by Western blot and membranes probed for S100A4 and α -tubulin.

3.3 Discussion

3.3.1 Transcriptional regulation of S100A4 during EMT

S100A4 is now often quoted as a factor commonly activated during EMT and considered a marker as such (Schneider *et al.*, 2008). In agreement with this, SIP1-induced EMT in A431 cells led to a significant increase in S100A4 expression, 48-hours after Dox addition.

In terms of the transcriptional regulation of S100A4, a large number of response elements have been identified within the S100A4 gene, implicating many different cytokines and transcription factors in controlling its expression (Donato, 2003). Notwithstanding, SIP1 has so far not been shown as one of the factors activating S100A4 transcription. In general, SIP1 is characterised as a transcriptional repressor which binds to bipartite E-box elements in target genes containing the sequence CACCT/CACCTG to directly repress transcription (Van Roy & Berx, 2008). Despite this focus, Zeb family members (Zeb1 and Zeb2/SIP1) interact with the transcriptional co-activators, p300 and P/CAF (Vandewalle *et al.*, 2009) suggesting they can also function to activate transcription. Accordingly, there are now a growing number of reports describing activation of genes by Zeb family members with Zeb1 activating transcription of the Vitamin D receptor (VDR) by binding to two sites within its promoter (Lazarova *et al.*, 2001). In the case of SIP1, its expression correlates with vimentin levels in invasive breast cancer cell lines and either transfection or knockdown of SIP1 leads to an increase or decrease vimentin expression, respectively. Intriguingly, this regulation was independent of E-box elements since there are no bipartite elements present in the vimentin promoter, suggesting SIP1 either recognises alternative DNA sequences in the promoter or binds via adaptor proteins (Bindels *et al.*, 2006). More recently, SIP1 was also shown to activate expression of integrin $\alpha 5$ by binding to Sp1 sites in the promoter, forming a complex with the ubiquitously-expressed transcription factor, Sp1, an effect also independent of E-box elements (Nam *et al.*, 2012). Like vimentin, S100A4 does not contain bipartite E-box elements, but three Sp1 sites have been identified in an enhancer region located in the first intron of the gene (Cohn *et al.*, 2001). Moreover, mutation of the most distal Sp1 site was sufficient to reduce S100A4 reporter activity by approximately 80% in the mouse adenocarcinoma cell line, CSML100, suggesting Sp1 in part, regulates S100A4 expression in this cell line (Cohn *et*

al., 2001). Although the role of SIP1 was not investigated in this study, a Sp1-SIP1 complex could represent a novel mechanism for the transcriptional activation of S100A4.

An additional link between S100A4 expression and SIP1 is that S100A4 is commonly activated during TGF- β -induced EMT (Sato *et al.*, 2010; Okada *et al.*, 1997) while SIP1 is strongly implicated in TGF- β signalling. [Zeb proteins bind to receptor-activated Smads, key downstream mediators of TGF- β signalling (Xu *et al.*, 2009)]. Indeed, a study by Xie *et al.*, (2009b) showed S100A4 expression was activated when endometrial carcinoma cells were exposed to TGF- β , an effect dependent on the phosphorylation of Smad2. Despite the evidence linking SIP1 with S100A4 expression, there are many other elements within the S100A4 promoter including FTS-1 or AP-1 sites which could also be responsible for its activation in this cell model and further experiments are required to fully characterise these regions and their associated transcription factors.

Aside from transcriptional regulation, epigenetic regulation and specifically methylation are important factors in controlling S100A4 expression (Leśniak, 2011). Although S100A4 belongs to a group of CpG-poor genes, and does not contain a CpG island, there are a number of CpG sites within the first intron which are important methylation sites (Cohn *et al.*, 2001). Indeed, inactivity of the S100A4 gene in colon, mammary and lymphoma cell lines strongly correlates with DNA methylation (Rosty *et al.*, 2002). Accordingly, a recent study by Lopez-Lago *et al.*, (2010) showed activation of S100A4 in a model of EMT was dependent on de-methylation of all three CpG sites present in the first intron of S100A4. In line with this, treatment of uninduced A431 cells with the methyltransferase inhibitor, 5'azacytadine resulted in activation of S100A4 (our unpublished observations) suggesting S100A4 de-methylation might also be required for its activation during SIP1-induced EMT in A431 cells.

3.3.2 Temporal regulation of S100A4 expression

EMT is a temporal process and although differences exist between models, it can be phenotypically characterised as a distinct number of steps including: (i) loss of cell-cell adhesion, (ii) cell scattering, (iii) cell spreading and (iv) formation of large

lamellipodia, consistent with the conversion to a mesenchymal state (Moreno-Bueno *et al.*, 2009). In this model of EMT, the activation of S100A4 occurred after cells had detached from their cell-cell contacts and scattered but coincided with cell spreading and the formation of lamellipodia-like protrusions raising the possibility that S100A4 might be required for these phenotypical changes to occur. Indeed, a study by Okada *et al.*, (1997) showed S100A4 expression preceded the overt phenotypical changes associated with an EMT in the proximal tubular epithelial cell line, MCT. Moreover, when cells were pre-treated with S100A4 antisense oligomers, EMT was blocked as evidenced by an increase in cytokeratin expression suggesting S100A4 is an early event in EMT and required for its progression. Nonetheless, in A431-SIP1 cells, knockdown of S100A4 did not effect changes in vimentin expression or cell phenotype suggesting it is not essential for the transition from an epithelial to a mesenchymal state. In fact, S100A4 expression in this model can be considered a relatively late event since cells have already completed two of the four phenotypical steps required for an EMT before S100A4 expression is observed on the protein level. In an additional study by Lo *et al.*, (2011) knockdown of S100A4 in two HNSCC cell lines which displayed EMT-like properties reduced their stemness abilities suggesting S100A4 does play a causal role in either promoting or maintain a mesenchymal state in some cell backgrounds.

3.3.3 Cell migration and S100A4

The proposed function of S100A4 has focused on its role in cell migration with its down-regulation reducing the rate of cell migration while its over-expression promotes it (Tarabykina *et al.*, 2007). In agreement with this, S100A4 expression is observed in highly motile cell types including neutrophils, lymphocytes and macrophages (Cabezón *et al.*, 2007). Despite this link and the strong association between S100A4 and EMT, no study had yet examined the effect of S100A4 on cell migration during EMT. In this study, S100A4 promoted cell migration by approximately 2-times in a transwell assay. Although the transwell inserts were not coated with an extracellular matrix component, replicating *in vivo* cell invasion, cells must re-shape their cytoskeleton to squeeze through pores in the insert. As such, this form of migration can be considered a combination of both single cell amoeboid and mesenchymal cell migration and the effect of S100A4 cannot be specifically assigned to one or the other. To determine which form of migration S100A4 contributes to, *in vivo* time-lapse assays would be

required. In addition, to assess which step of cell migration S100A4 is most involved with (cell polarisation, protrusion, translocation or retraction) 2D tracking assays would have to be performed. Interestingly, S100A4 has recently been shown to stabilise cellular protrusions during macrophage chemotaxis (Li *et al.*, 2010) providing a first insight into the specific role S100A4 plays during this form of cell migration.

In conclusion, results from this chapter have confirmed that S100A4 is activated during SIP1-induced EMT in A431 cells but is not required for its progression. Moreover, knockdown of S100A4 expression attenuates cell migration suggesting S100A4 has a function in promoting the rate of cell migration during EMT.

4 Investigating the interaction between S100A4 and myosin IIA in a model of EMT

4.1 Introduction

Since S100s lack catalytic domains, their functional effects are dependent on regulating the activity of other proteins (Santamaria-Kisiel *et al.*, 2006). In the case of S100A4, a number of potential target proteins have been identified including liprin β 1 (Kriajevskaja *et al.*, 2002), Smad3 (Matsuura *et al.*, 2010) and methionine aminopeptidase 2 (Endo *et al.*, 2002); however, the best characterised is non-muscle myosin IIA (Kriajevskaja *et al.*, 1994, Ford *et al.*, 1997, Li *et al.*, 2003, Badyal *et al.*, 2011). This is in part since myosin IIA was the first protein identified as interacting with S100A4 (Kriajevskaja *et al.*, 1994) but also because it has a key role in cell migration (Vicente-Manzanares *et al.*, 2009) thus linking with the central focus of S100A4 function (Tarabykina *et al.*, 2007).

In vitro, S100A4 has been shown to interact with the C-terminal tail of myosin IIA (Badyal *et al.*, 2011; Li *et al.*, 2003) promoting the monomeric state either by inhibiting filament formation (Badyal *et al.*, 2011; Li *et al.*, 2003; Murakami *et al.*, 2000) or promoting filament disassembly (Badyal *et al.*, 2011; Ford *et al.*, 1997). Notwithstanding, there has been relatively little *in vivo* data supporting the interaction between S100A4 and myosin IIA (Zhang *et al.*, 2005a; Li & Bresnick, 2006) and less still correlating the expression of S100A4 with a reduction in the level of filamentous myosin in cells (Li *et al.*, 2010).

Interestingly, *in vitro* evidence suggests non-muscle myosin IIs, like their muscle counterparts can exist in either an assembly-incompetent (10S) or assembly-competent (6S) form (Sellers & Knight, 2007). The former is thought to be physiologically relevant as an inert state of myosin that minimises ATP wastage (Cross *et al.*, 1988; Cross *et al.*, 1986). Despite this, no evidence exists, *in vitro* or *in vivo* indicating which form of myosin S100A4 interacts with and only one study (Milton *et al.*, 2011) has so far provided evidence of the existence of 10S myosin *in vivo*.

With this in mind, the first aim of the chapter was to characterise the level of co-localisation between S100A4 and myosin IIA using confocal and electron microscopy. Intriguingly, given the resolution of electron microscopy, it was hypothesised that the specific monomeric form of myosin that S100A4 interacts with could also be identified.

In addition, the second aim was to compare the dynamics of myosin IIA assembly in the presence or absence of S100A4 in live cells using fluorescent recovery after photobleaching (FRAP).

4.2 Results

4.2.1 Immunoprecipitation of the heavy chain of myosin IIA by S100A4

To investigate the interaction between S100A4 and myosin IIA in this particular cell model, immunoprecipitation experiments were first carried out. A431-SIP1 cells were maintained in the presence or absence of Dox for 72 hours and complexes immunoprecipitated using an S100A4 antibody. Following Western blot analysis (Figure 4.1), S100A4 was successfully precipitated from Dox-induced A431-SIP1 cells with a band corresponding to the heavy chain of myosin IIA also detected, indicating S100A4 is able to interact with myosin IIA in cell lysates.

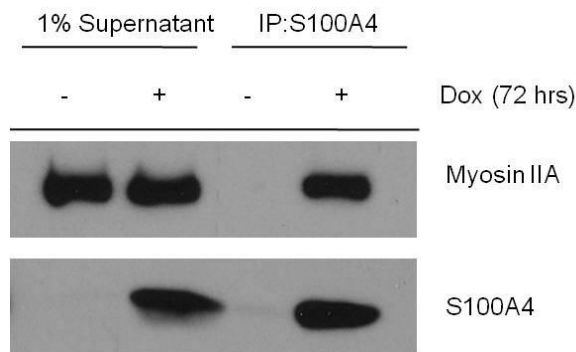


Figure 4.1: Immunoprecipitation of S100A4 from A431-SIP1 cells

A431-SIP1 cells were maintained in the presence or absence of Dox for 72 hours and lysed in IP buffer (See Materials and Methods). S100A4-protein complexes were immunoprecipitated with a monoclonal S100A4 antibody. Lysates were resolved by SDS-PAGE and membranes stained for S100A4 and myosin IIA using Western blotting. 1% of the supernatant input was analysed to ensure equal loading. Result representative of 3 independent experiments.

4.2.2 Co-localisation of S100A4 and myosin IIA *in vivo*

4.2.2.1 Use of quantitative analysis to assess protein-protein co-localisation *in vivo*

To further explore the interaction between S100A4 and myosin IIA, the intracellular distribution of both proteins was examined using confocal microscopy. For two proteins to physically interact, they must be in close enough proximity to do so (Costes *et al.*, 2004). Thus, analysing the co-localisation of two proteins is a necessary part of identifying a genuine protein-protein interaction (Lachmanovich *et al.*, 2003). Co-localisation can be defined as when emitted light from both fluorophores is collected in the same voxel (a 3D pixel) (North, 2006). In the case of where two proteins are stained with a red and green fluorophore, co-localisation is represented by merging of the two to yield a yellow colour, a result that can be readily assessed by visual inspection. Despite this, it is often necessary to quantify the level of co-localisation to provide a non-biased overview (Lachmanovich *et al.*, 2003). A common method to quantitatively assess co-localisation is Pearson's Correlation Coefficient (PCC) which describes the degree of overlap between images stained for two different fluorophores (Manders *et al.*, 1992). The coefficient ranges from -1 to 1 representing a total lack of overlap and a complete co-localisation, respectively. However, one limitation of PCC is that it does not take into account pixel intensity; thus, a bright red pixel co-localising with a faint green pixel is considered equal to a bright red pixel co-localising with a bright green pixel. Intuitively, it would be expected that a red-green pixel pair of similar intensity should be considered "more co-localised" than ones differing in intensity (given a relatively low stoichiometry). Accordingly, Li *et al.*, (2004) suggested a modification of PCC such that the pixel intensities are taken into account when analysing co-localisation. This method known as Intensity Correlation Analysis (ICA) is based on the assumption that if two proteins are part of the same complex then their staining intensities should vary in synchrony; conversely, intensities of proteins not part of the same complex will vary asynchronously. Calculation of the ICA is based on the fact that for any set of random values, the sum of the differences from the mean is zero. However, if a correlation between fluorophores exists this value would exceed 0 whereas a repulsion of fluorophores would lead to a value less than 0. By plotting the intensity of fluorophore A or B versus $(A_i - a)(B_i - b)$ [where a and b represent the mean pixel intensity for each antigen], otherwise known as the Product of the Differences of the Mean (PDM), it is possible to visually assess if two particles are co-localised.

Additionally, the Intensity Correlation Quotient (ICQ) can be derived from this plot providing a quantitative measure of co-localisation by calculating the ratio of positive values to the total number of pixel pairs, with an ICQ value more than 0 indicating a negative correlation and a value less than 0 suggesting repulsion between fluorophores.

4.2.2.2 S100A4 and myosin IIA display partial co-localisation as assessed by confocal microscopy

To analyse co-localisation, cells grown in the presence of Dox were stained for S100A4 and myosin IIA using immunofluorescence and Z-stacks acquired by confocal microscopy at an interplane distance of 500 nm. As seen previously (Figure 3.3), S100A4 demonstrated a diffuse granular staining throughout the cytoplasm and nucleus whereas myosin IIA was enriched in some areas around the edge of cells but also displayed a robust cytoplasmic distribution (Figure 4.2).

To quantitatively analyse this co-localisation, the PCC and ICA for S100A4 and myosin IIA were assessed using the “Intensity Correlation Analysis” plug-in for ImageJ. Both the average PCC and ICQ values exceeded the threshold for a random distribution with values of 0.745 (100% co-localisation = 1) and 0.233 (100% co-localisation = 0.5) respectively, suggesting S100A4 and myosin IIA co-localise (Table 4.1). A representative cell used for quantitative analysis is shown in Figure 4.3A-C. The plots of Product Differences of the Mean (PDM) versus intensity for S100A4 (Figure 4.3E) and myosin IIA (Figure 4.3F) both show a skew toward values above 0 indicative of co-localisation; furthermore, panel D of Figure 4.3 displays the intensity map for the cell showing only positive PDM values, thus highlighting specific areas of co-localisation. The intensity ranges from blue to white indicating a low to high level of fluorescence intensity for pairs of pixels. Interestingly, co-localisation was present throughout the cytoplasm with increased areas of intensity in some perinuclear areas as well as towards the periphery of the cell. In total, these data suggest S100A4 and myosin IIA do exhibit a degree of co-localisation although not throughout the entirety of the cell. Despite this evidence of co-localisation, the resolution limits of light microscopy place a lower estimate of approximately 250 nm on this analysis and as such, it is only possible to conclude that these two proteins are within this distance. To overcome this limitation, the enhanced resolution of transmission electron microscopy (TEM) was employed.

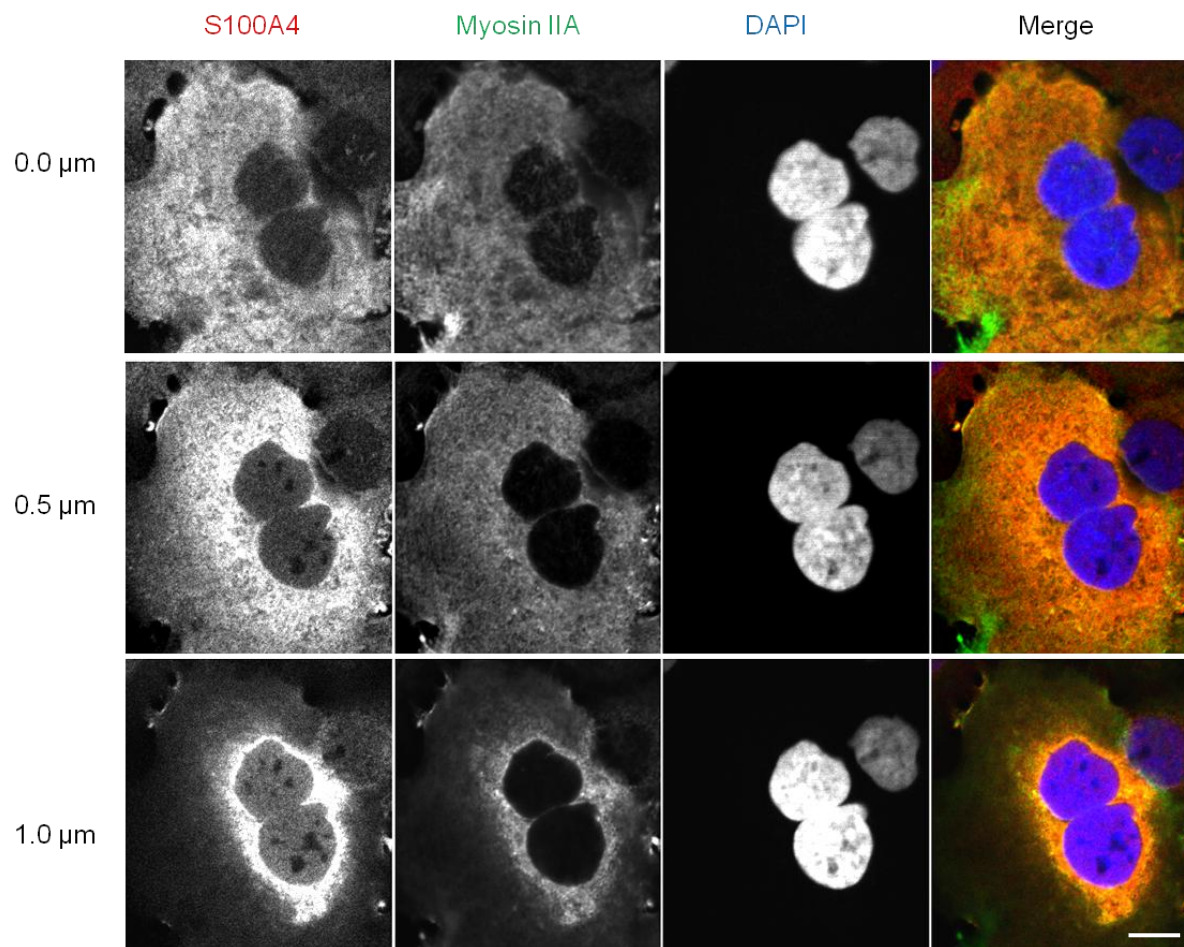


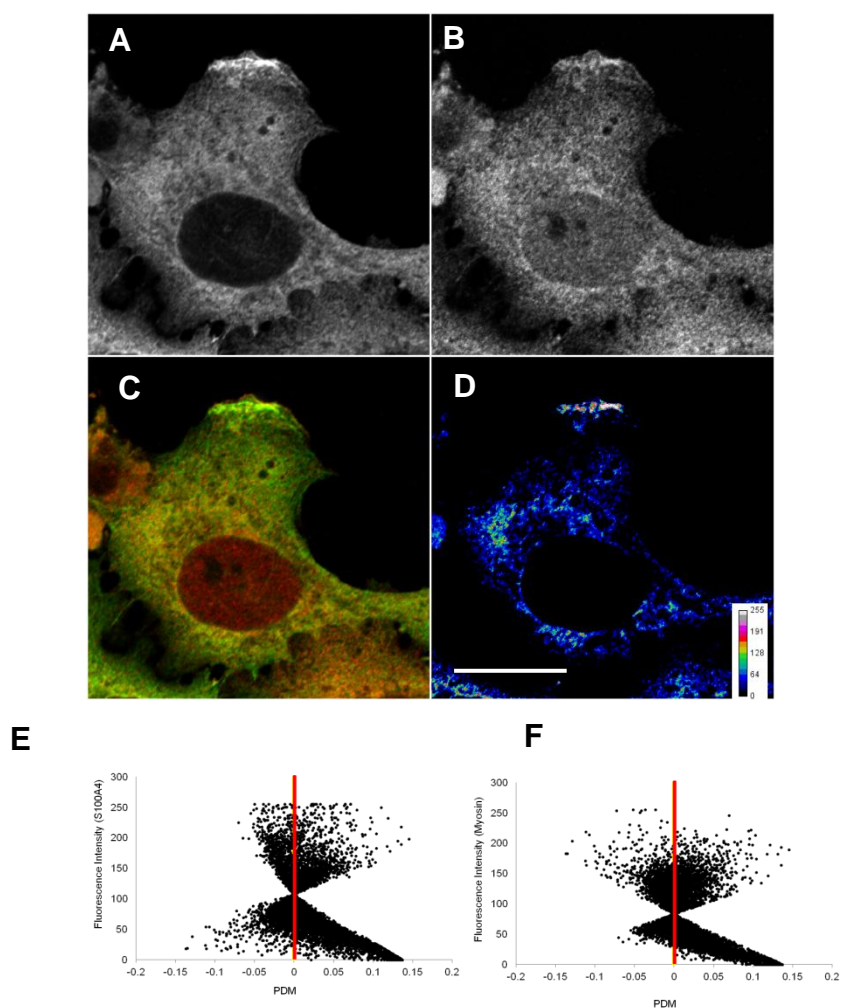
Figure 4.2: Immunofluorescence staining of S100A4 and Myosin IIA in A431-SIP1 cells

A431-SIP1 cells were grown in the presence of Dox for 72 hours and stained for S100A4 (Red), myosin IIA (Green) and DAPI (blue; to visualise DNA) using immunofluorescence. Z-stacks were acquired every 500 nm using a confocal microscope. Scale bar = 10 μm.

Table 4.1: Data summary for quantitative co-localisation analysis of S100A4 and myosin IIA

The average PCC and ICQ values and standard deviations were calculated for 10 cells using the Intensity Correlation Analysis plug-in in ImageJ.

	Average (n=10)	S.D.
PCC	0.745	±0.145
ICQ	0.233	±0.065

**Figure 4.3 Co-localisation analysis for S100A4 and myosin IIA**

An individual cell stained for myosin IIA (A, green) and S100A4 (B, red). The image is merged in (C) demonstrating a yellow colour for areas of co-localisation. Positive PDM values representing co-localisation are shown in (D); the intensity bar ranges from blue to white indicating a low to high level of fluorescence intensity. Scale bar = 10 μ m. Fluorescence intensity vs PDM plots for the above cell are shown for S100A4 (E) and myosin IIA (F); both show a skew towards positive PDM values indicating co-localisation. The red line represents the separation between negative and positive PDM values.

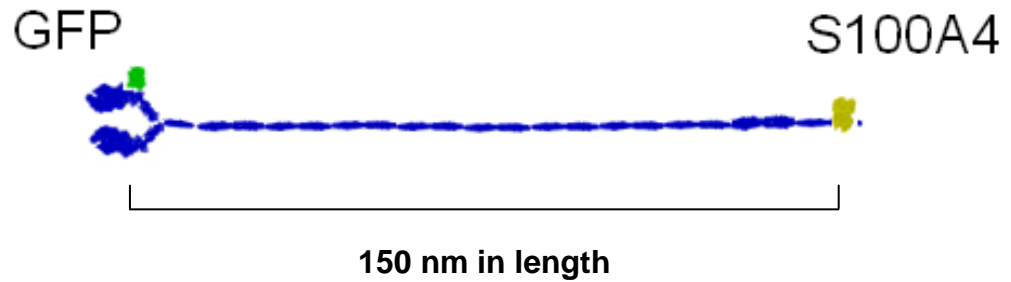
4.2.2.3 *An immunogold approach to assess co-localisation between S100A4 and myosin IIA*

Transmission electron microscopy allows an increase in resolution of at least two orders of magnitude compared to standard light microscopy, with a lower limit for biological material approaching 1 nm (Spector & Goldman, 2006). Additionally, co-localisation experiments can be readily performed by using different-sized gold particles to visualise each antigen as opposed to two different fluorophores (Philimonenko *et al.*, 2000). Combining these factors therefore allows a more precise analysis of co-localisation to be determined.

Given this, it was hypothesised that aside from merely determining co-localisation between S100A4 and myosin IIA, the specific monomeric form of myosin IIA, 10S or 6S could be readily identified too. However, since the myosin IIA antibody used thus far in this study recognises the extreme C-terminus of the non-helical tail (raised against the last 6 amino acids, see Material and Methods for more detail), a combination of this antibody and an S100A4 antibody would be insufficient in differentiating between the two forms. In contrast, an N-terminally-tagged GFP-myosin IIA construct and S100A4 antibody would facilitate staining at the N- and C-terminus of a myosin IIA molecule and thereby differentiating between the 10S and 6S forms of myosin (Figure 4.4).

Although the addition of GFP to myosin IIA could affect its conformation, it has been shown to co-localise with endogenous myosin IIA (Wei & Adelstein, 2000) as well as rescuing aspects of myosin IIB knockout mice (Bao *et al.*, 2007) suggesting the addition of the GFP moiety does not affect any functional characteristic of the protein and therefore its ability to form a 10S or 6S molecule.

6S myosin



10S myosin

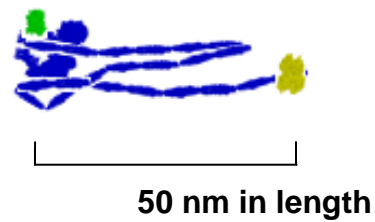


Figure 4.4: Schematic of N-terminally-tagged GFP-myosin IIA and S100A4 bound to the C-terminus

A myosin IIA molecule in the 6S (top) and 10S (bottom) form with a GFP tag (green) at the N-terminus and S100A4 (yellow) bound to the C-terminus. Using this combination of an N- and C-terminal antibody it should be possible to distinguish the 6S form of myosin, 150 nm, from the 10S form of myosin, 50 nm. Scale bar = 50 nm. Image courtesy of Prof. Clive. R. Bagshaw.

4.2.2.3.1 Generation of GFP-myosin IIA stable clones

Since the transfection efficiency of expressing GFP-myosin IIA in A431-SIP1 cells was extremely low (data not shown), a stable clone expressing constitutively active GFP-myosin IIA was generated. Accordingly, A431-SIP1 cells were co-transfected with a plasmid conferring puromycin resistance, pIRES-PURO2 and a plasmid encoding full length, human N-terminally-tagged GFP myosin IIA. Cells were maintained in 2 µg/ml puromycin over a period of 2-3 weeks and resistant colonies expanded based on their GFP fluorescence. One such clone (Cl.M) was further analysed for expression of myosin IIA, GFP and S100A4 in the absence and presence of Dox by Western blot (Figure 4.5). Staining for myosin IIA indicated two bands separated by approximately 25 kDa, consistent with the addition of a GFP moiety. Moreover, GFP staining was only detected in Cl. M, with a band corresponding to the size of the upper band of myosin IIA. The activation of S100A4 in Cl.M was also consistent with the parental cell line, with S100A4 strongly activated after 72 hours incubation with Dox. Furthermore, confocal analysis of Cl.M cells stained for myosin IIA and GFP (Figure 4.6) exhibited a strong co-localisation throughout the entirety of the cell demonstrating the similarity of the GFP-myosin IIA localisation with endogenous myosin IIA.

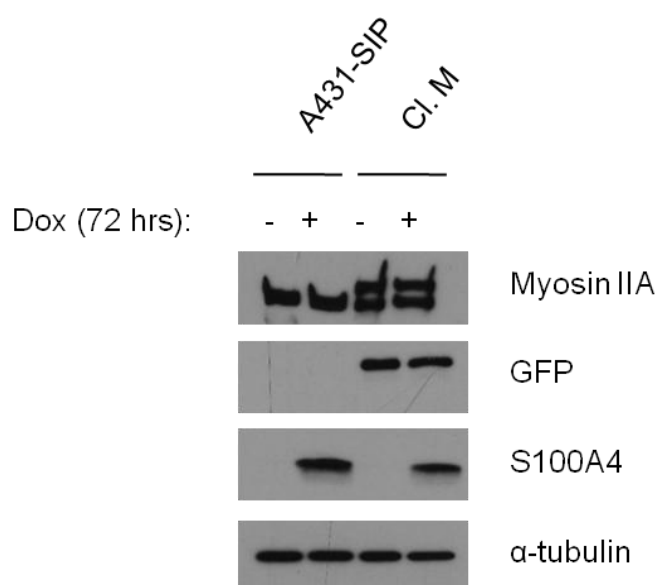


Figure 4.5: Western blot analysis of A431-SIP1 and Cl.M cells

A431-SIP1 and Cl.M cells grown in the absence and presence of Dox for 72 hours were lysed and expression of myosin IIA, GFP, S100A4 and α-tubulin assessed by Western blotting.

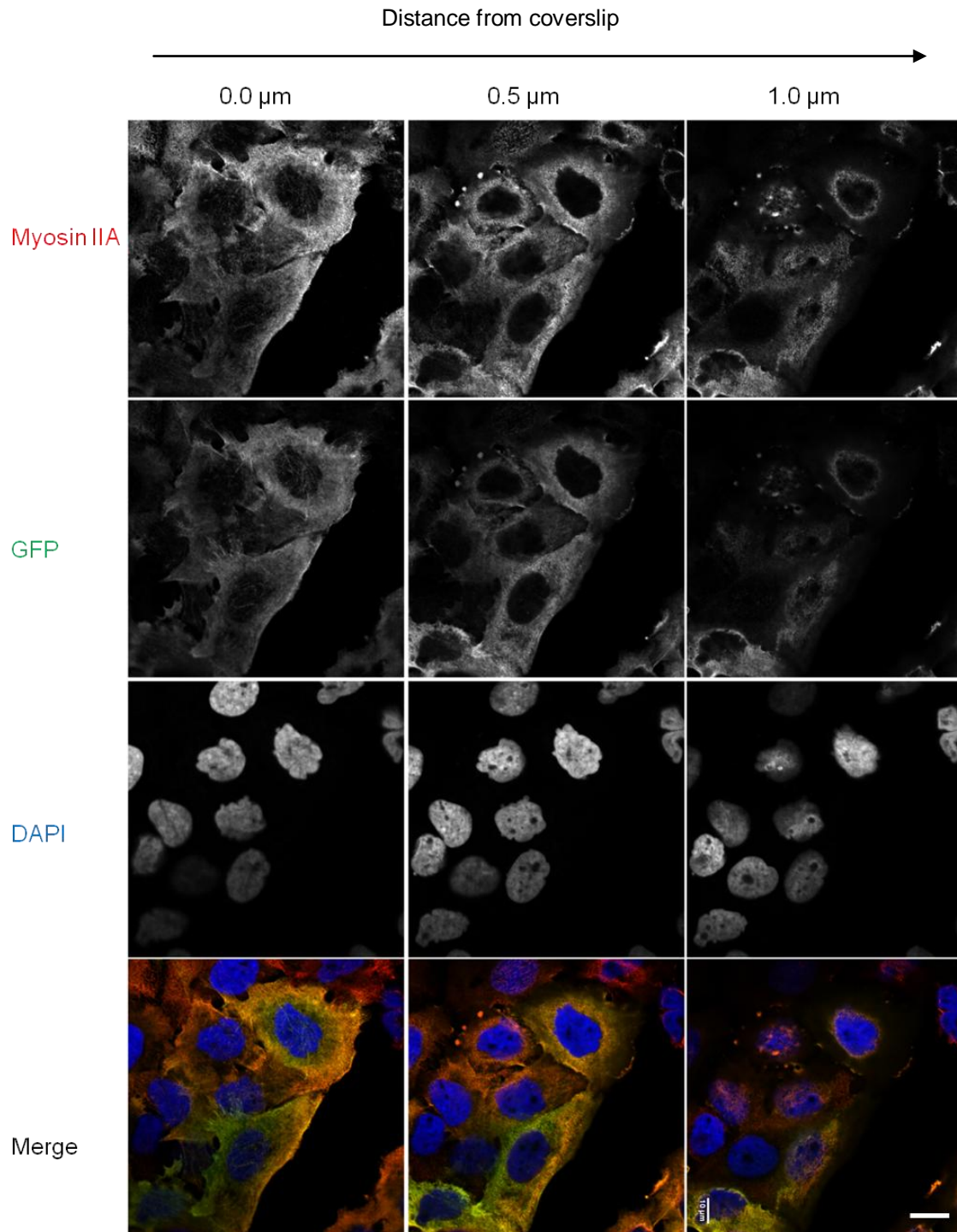


Figure 4.6: Confocal analysis of Cl.M cells

Cl.M cells grown in the presence of Dox for 72 hours were stained for GFP and myosin IIA using immunofluorescence and counterstained with DAPI to visualise nuclei. Images were collected with a confocal microscope at an interplane distance of 500 nm. Scale bar = 10 μm .

4.2.2.3.2 Optimisation of fixation conditions for TEM

Unlike conventional immunocytochemistry, fixation conditions for TEM vary with glutaraldehyde often used for ultrastructure studies because it is a more effective crosslinker than formaldehyde thus helping to preserve cellular structure. However, crosslinking also reduces the antigenicity, severely compromising immunolabelling experiments. Speed of fixation is an additional factor with formaldehyde penetrating tissue faster (owing to its smaller size) than glutaraldehyde, thus helping to ensure a more native state (reviewed in (Griffiths, 1993)). Due to these considerations, both formaldehyde and glutaraldehyde are frequently used in combination to balance preservation of ultrastructure with speed of fixation and retention of antigenicity.

Accordingly, Cl.M cells were grown in the presence of Dox and fixed with formaldehyde with increasing concentrations of glutaraldehyde ranging from 0.005 to 0.5% and processed as for light microscopy. Cells were then stained for S100A4 and GFP using immunofluorescence and analysed by fluorescent microscopy. Whereas GFP-myosin IIA staining was unaffected by any of the fixation conditions (data not shown), S100A4 staining was only detected for cells fixed in formaldehyde, suggesting even low concentrations of glutaraldehyde were sufficient to compromise S100A4 antigenicity (Figure 4.7). Having established this, Cl.M cells were fixed in 4% formaldehyde alone and processed for resin-embedded tissue following standard protocols (EM Lab, University of Leicester, see Materials and Methods for more details).

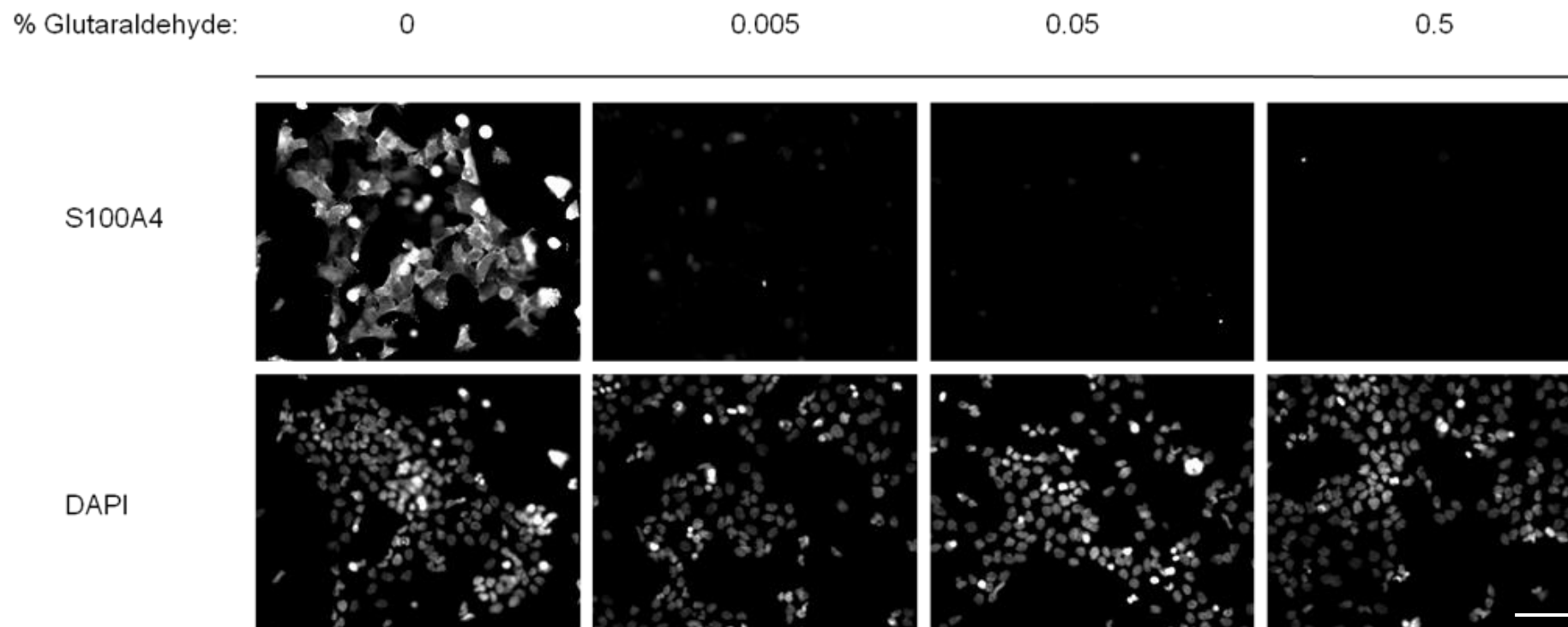


Figure 4.7 Optimisation of fixation conditions for TEM

Cl. M cells grown in the presence of Dox for 72 hours were fixed in 4% formaldehyde with increasing concentrations of glutaraldehyde and stained for S100A4 using immunofluorescence. Cells were counterstained with DAPI. Scale bar = 20 μ m

4.2.2.3.3 Optimisation of labelling conditions for TEM

Before co-localisation experiments were carried out, optimal concentrations of S100A4 and GFP antibodies were empirically determined by staining tissue sections individually. S100A4 staining with a monoclonal antibody at 75 µg/ml yielded labelling throughout the cytoplasm and nucleus (Figure 4.8), whereas GFP staining with a polyclonal antibody at 5 µg/ml demonstrated strong labelling around the edge of the cell and cytoplasm (Figure 4.9), with no nuclear staining. Both these distributions were consistent with light microscopy data.

Since the level of labelling was quite weak, negative controls where primary antibodies were excluded demonstrated no significant gold staining indicating a highly specific signal for both primary antibodies (Figure 4.10). In addition to this control, it was necessary to ensure each secondary antibody would not cross-react with the opposing primary antibody. Accordingly, grids were singly stained with either rabbit GFP or mouse S100A4 primary antibody and then incubated with the opposing secondary antibody i.e. goat anti-mouse or goat anti-rabbit secondary, respectively. These controls yielded no staining indicating a specific interaction of the secondary antibody with the appropriate primary antibody (data not shown).

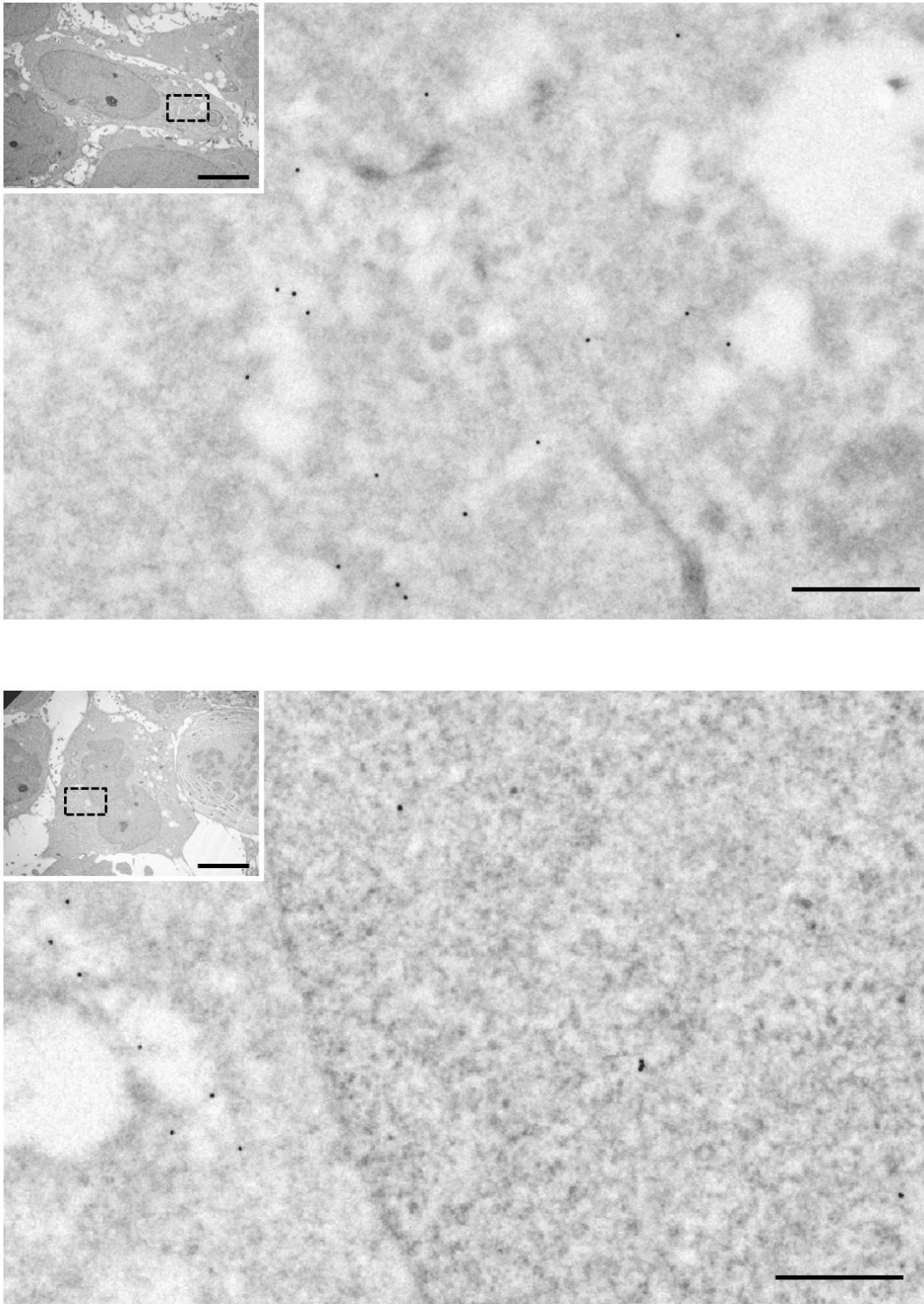


Figure 4.8: Immunogold labelling of Cl. M cells stained for S100A4

Cl. M cells grown in the presence of Dox were stained with an optimised concentration of S100A4 antibody (75 $\mu\text{g/ml}$) and visualised with 15 nm-sized gold particles. Scale bar = 500 nm; inset = 5 μm .

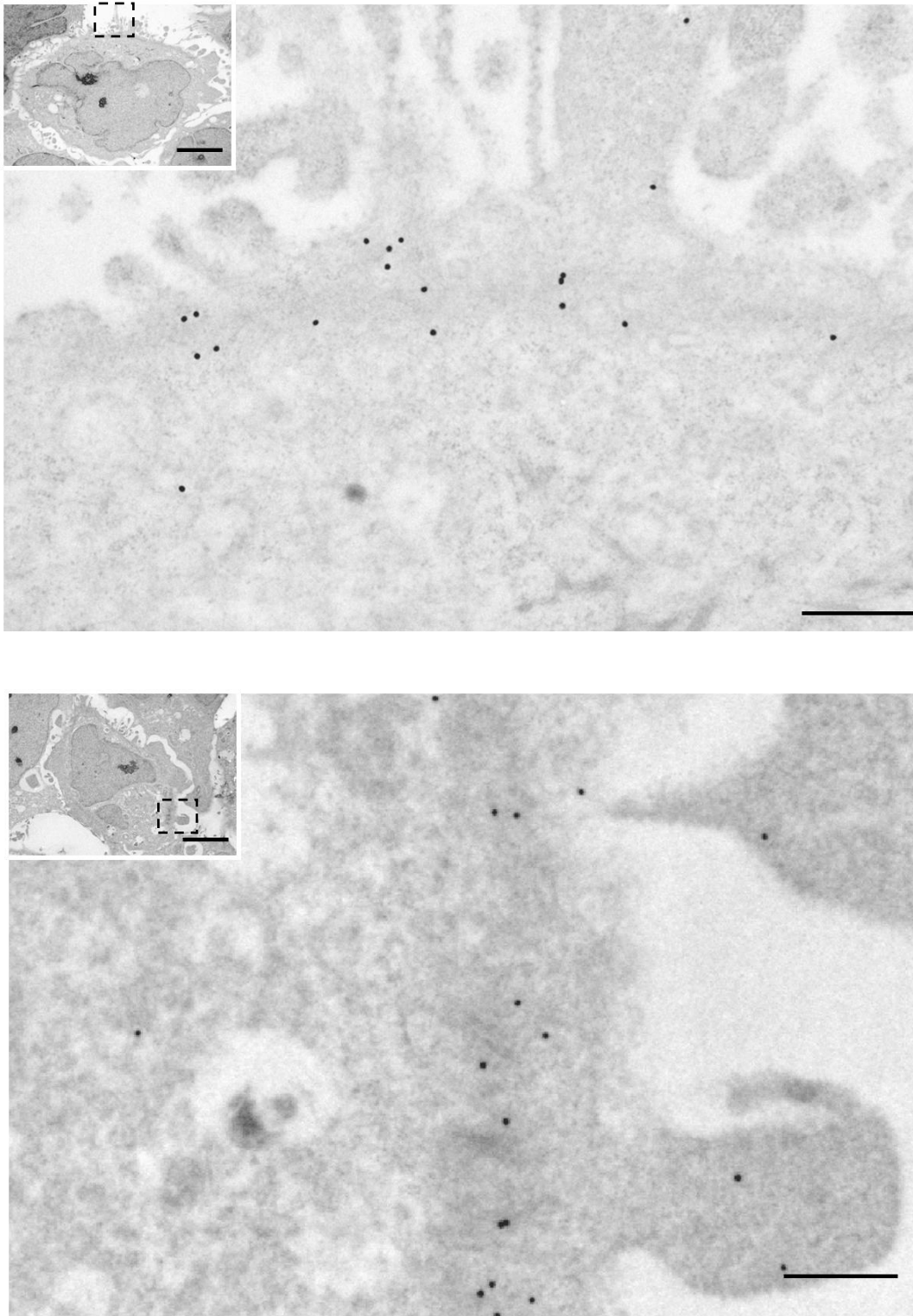


Figure 4.9: Immunogold labelling of Cl.M cells stained for GFP

Cl.M cells grown in the presence of Dox were stained with an optimised concentration of GFP antibody (5 µg/ml) and visualised with 30 nm-sized gold particles. Scale bar = 500 nm; inset = 5 µm.

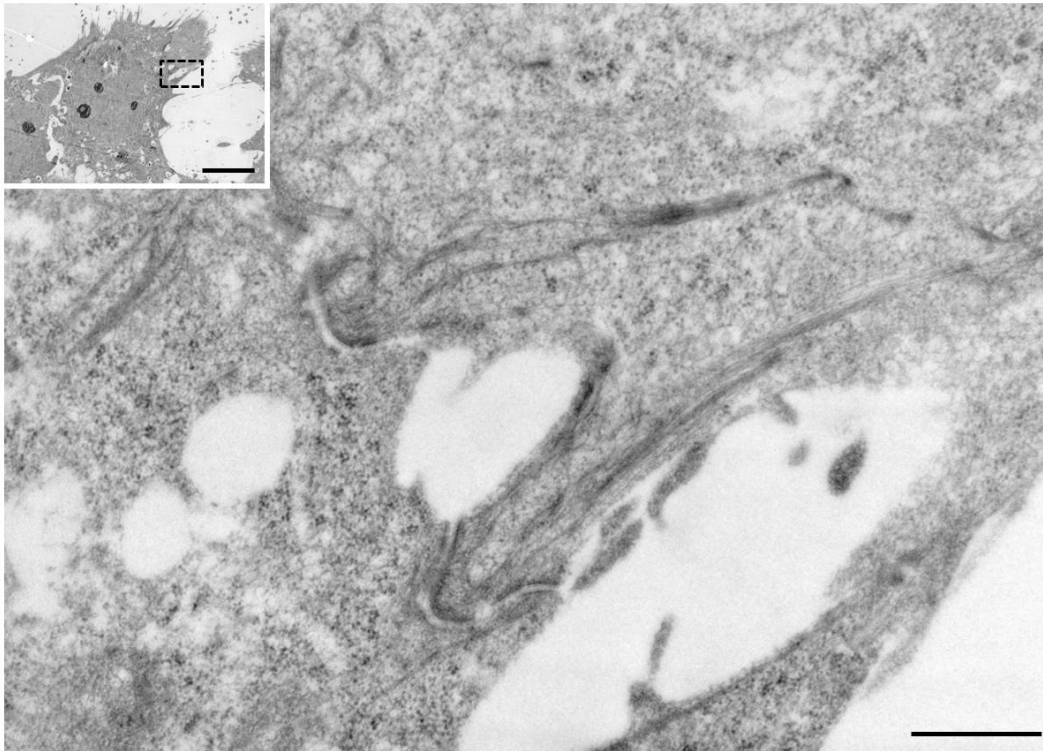
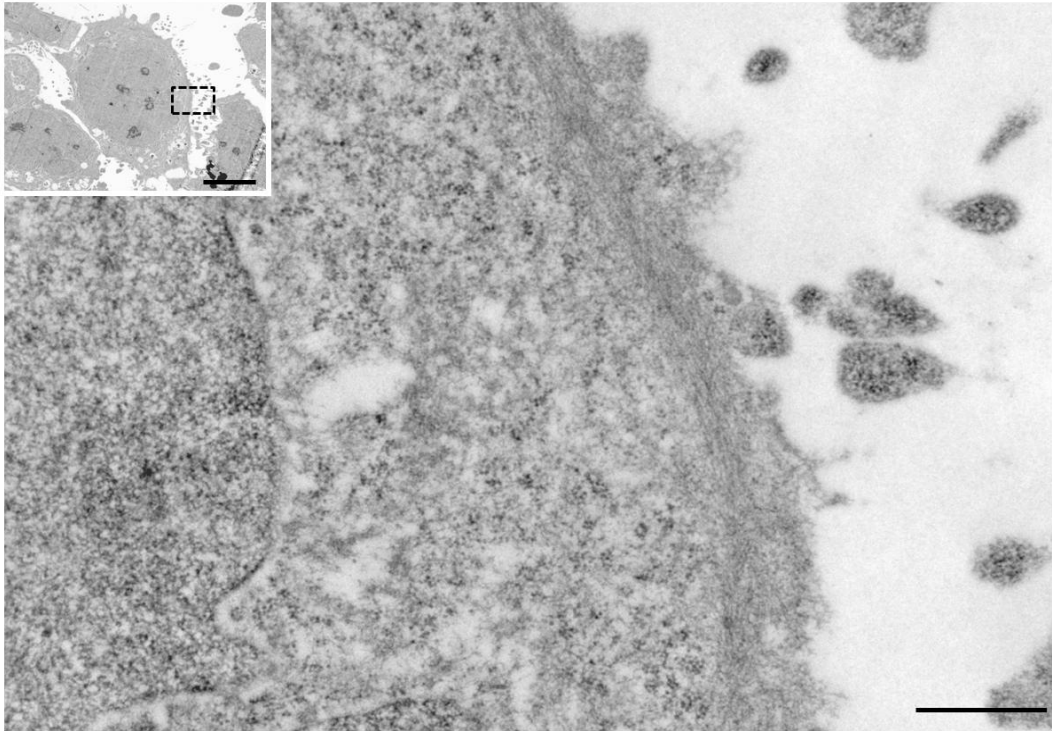


Figure 4.10: Secondary-only control staining of Cl.M cells

Cl.M cells grown in the presence of Dox were stained with secondary antibody only. Scale bar = 500 nm; inset = 5 μ m.

4.2.2.3.4 Statistical methods to quantify co-localisation between S100A4 and GFP-myosin IIA

Following this, cells were double-labelled and each antigen visualised using a different sized-gold particle. Intriguingly, initial observations seemed to demonstrate two specific distances that GFP-myosin IIA and S100A4 particles co-localised; between approximately 50 and 150 nm (Figure 4.11) in agreement with the predicted lengths of 10S and 6S myosin, respectively. To further test this hypothesis, statistical methods for spatial point pattern analysis were used to assess co-localisation between S100A4 and GFP-myosin IIA. Such methods are common in many disciplines of biology and have been used to analyse co-localisation of gold particles in electron microscopy in a number of studies (Rusakov *et al.*, 1995; Prior *et al.*, 2003). They differ from methods for light microscopy co-localisation previously used, since they are capable of discerning the actual distances that objects co-localise at. For this study, a method based on Diggle's G function (Diggle, 1983) was developed with a custom macro written in Excel. Diggle's G function analyses the nearest neighbour distance between pairs of particles from two sets (i.e. antigen A and antigen B), thus providing the co-localisation of two types of particles over a range of distances. Furthermore, the statistical significance of the data can be readily assessed by comparing the distribution to that of complete spatial randomness.

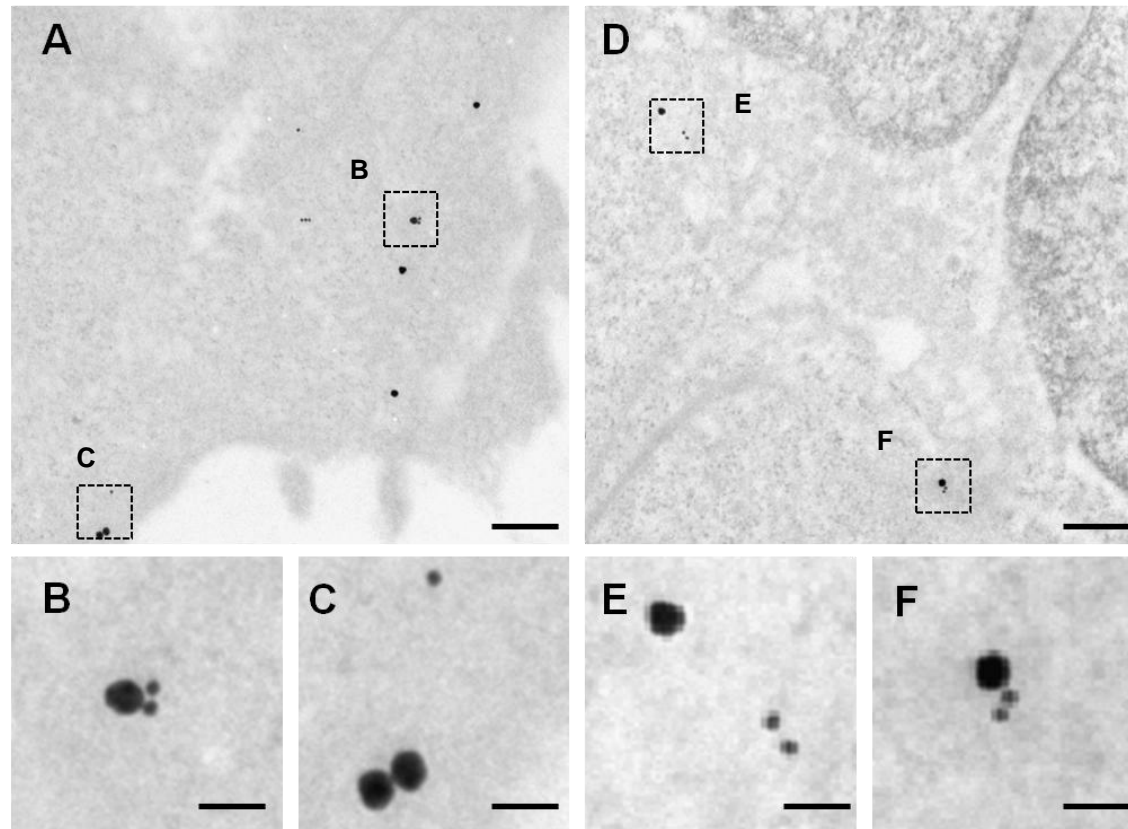


Figure 4.11 Co-localisation of S100A4 and GFP-myosin IIA

Cl.M cells grown in the presence of Dox for 72 hours were stained with antibodies to GFP and S100A4 and visualised using 30 and 15 nm gold-conjugated secondary antibodies respectively. (A) and (D) overviews with images magnified in (B), (C), (E) and (F). Scale bar for overview, 250 nm; magnified images, 50 nm. Distance between S100A4 and GFP-myosin IIA particles are (B) 39 nm; (C) 154 nm; (E) 141 nm; and (F) 46 nm.

Essentially, the analysis process can be described as follows: randomly chosen images were acquired (Figure 4.12A) (with the only criteria being that each image has at least one particle of each type present) and X-Y co-ordinates extracted for each particle and assigned a value of 1 or 2 depending on the size of the gold (Figure 4.12B). The exhaustive map of inter-point distances is then analysed for every particle using trigonometry (Figure 4.12C) and nearest neighbour distances calculated according to a modified version of Diggle's G function (for more details, see Materials and Methods). This analysis is performed for each image in the set and the data pooled together to generate a histogram of co-localisation distances (Figure 4.12E). To assess the statistical significance of the data, the distribution for complete spatial randomness i.e. the frequency of co-localisation between two randomly distributed particles is calculated based on the particle density of both antigens (Figure 4.12D). Accordingly, the appropriate number of particles are uniformly distributed within an area equal to that of one image and the same nearest-neighbour algorithm applied as for the experimental data. This is iterated 100 times (Monte Carlo simulations), enabling the 99% confidence intervals (CI) to be generated. The data are plotted as a histogram with co-localisation distance between particles on the X-axis and the % frequency at that particular distance on the Y-axis (Figure 4.12F). As such, at any point where the experimental data exceeds that of the 99% confidence interval there is a statistically significant co-localisation between particles equal to a P value of <0.01 .

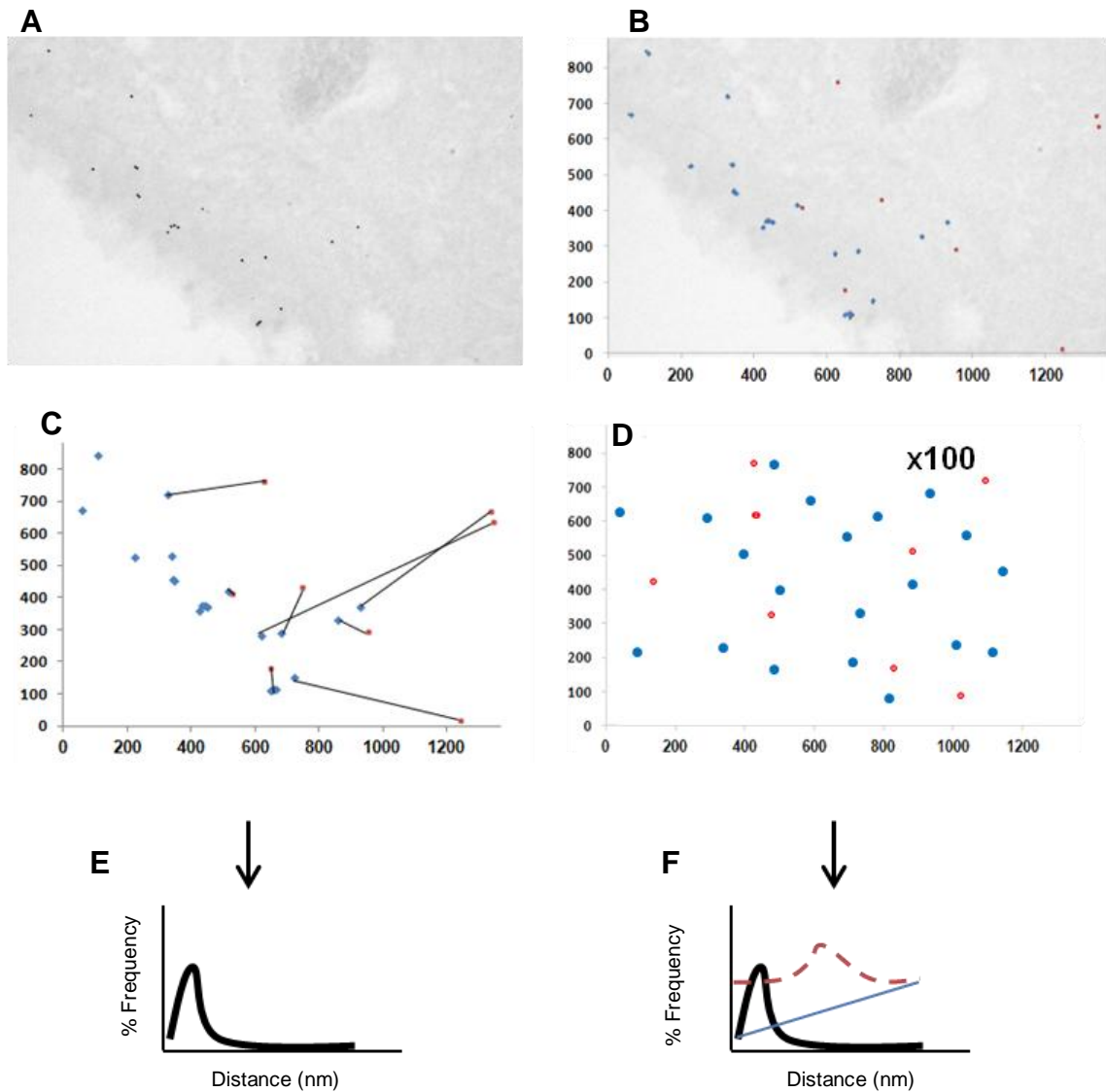


Figure 4.12 Schematic representation of analysis used to assess co-localisation

Randomly chosen images are first acquired (A) and X-Y co-ordinates extracted for each particle (B). A modified version of Diggle's G function is used to calculate the co-localisation between S100A4 and GFP myosin IIA (C) and the data represented as a histogram (E). The statistical significance of the data is based on the random distribution equal to the density of S100A4 and GFP myosin IIA (D). From this, complete spatial randomness (CSR) and the 99% CIs can be generated (F). Accordingly, at any point where the experimental data exceeds that of the 99% CIs, there is a statistically significant co-localisation at that distance. In (E) and (F), the black line represents the experimental data; blue line, CSR; and red dashed line, 99% CIs.

4.2.2.3.5 S100A4 and GFP-myosin IIA co-localise at distances consistent with the 10S and 6S forms of myosin

Confirming the initial observations, nearest-neighbour analysis for GFP-myosin IIA and S100A4 (Figure 4.13) was determined for over 1000 gold particles (N=1012) from three-pooled experiments demonstrating two statistically significant peaks between 25-75 nm and 125-175 nm.

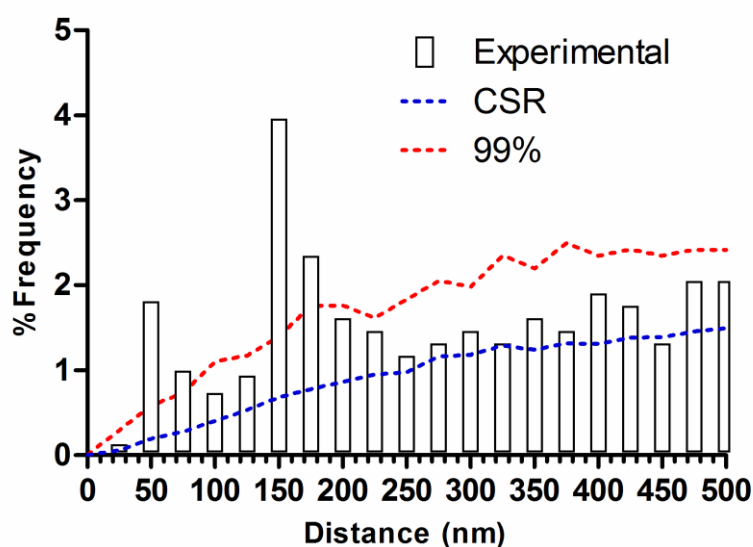


Figure 4.13: S100A4 and GFP-myosin IIA co-localise at two statistically significant distances

Cl.M cells grown in the presence of Dox were stained for S100A4 and GFP. Nearest-neighbour analysis was carried out from three pooled experiments to determine co-localisation (N=1012 particles). The bars equal the experimental data from S100A4 and GFP co-localisation; blue dashed line represents complete spatial randomness calculated from 100 Monte Carlo simulations for each image. Red dashed line indicates the 99% confidence interval calculated from the Monte Carlo simulations; at any point where the experimental data exceeds that of the 99% CIs, there is a statistically significant co-localisation at that specific distance. Statistical significance occurs at two peaks, between 25-75 nm and 125-175 nm. X-axis distances plotted in 25 nm bins.

Although these distances under- and over-estimate the lengths of a 10S and 6S myosin molecule, variation is expected given the extra addition of antibodies and size of gold particles. This introduces approximately ± 40 nm variation from the each antigen to its respective gold particle (Figure 4.14). Indeed, possible scenarios based on different orientations of gold particles and antibodies were modelled (data not shown; personal communication, Prof. C.R. Bagshaw) and demonstrated that there should still be two distinctive peaks consistent with 10S and 6S myosin monomers between 25-75 nm and 125-175 nm respectively, provided the 6S state remains in an extended conformation (See Discussion).

Another factor considered was the penetration of antibody or gold within the tissue, since this would further complicate the analysis; however, it has been shown that colloidal gold particles only stain the very surface of tissue embedded in LR white resin (Newman & Hobot, 1987). Thus, it can be concluded that only molecules on the surface of the tissue are labelled, simplifying co-localisation analysis.

Furthermore, since tissue sections were accessible from both sides of the grid to antibody solution and staining from two sides would again complicate any co-localisation analysis, they were floated on droplets of solution to ensure single-sided staining. Although this method was successfully used in the first double-labelling immunogold experiments (Bendayan, 1982), an initial control was performed to ensure that solution was not “seeping” on to the opposite side of the tissue. For conventional staining, grids were stained on one side such that a single surface, side A was transferred from primary to secondary antibody. To assess the possibility of solution seeping, grids were exposed to primary antibody on side A then inverted prior to floating on secondary antibody on the opposite surface, side B; thus if any solution had seeped to either upper side of the grid during primary or secondary, this would be reflected by the presence of gold particles (represented in Figure 4.15). This control was performed in three independent experiments and yielded no significant staining on any occasion (data not shown).

Taken together, peaks corresponding to 25-75 nm and 125-175 nm are therefore consistent with both 10S and 6S myosin monomers, indicating a co-localisation between S100A4 and GFP-myosin IIA.

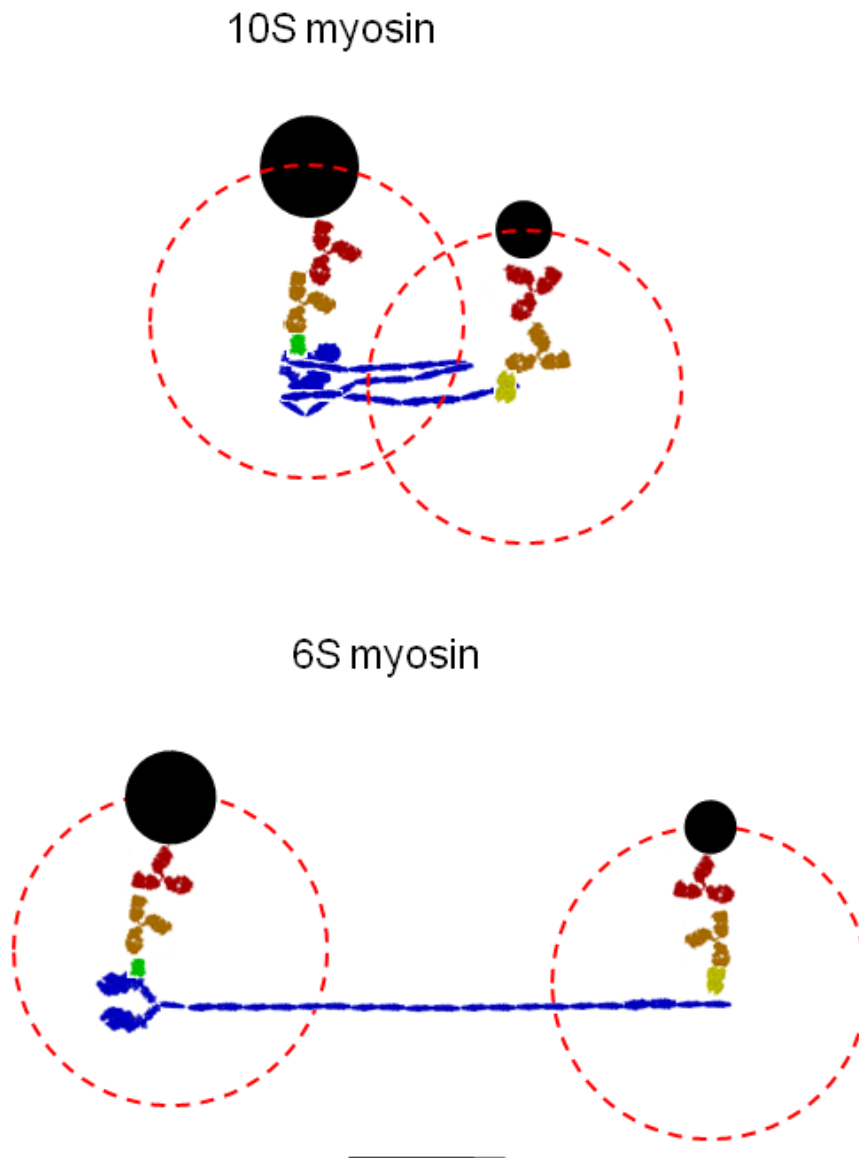


Figure 4.14: Schematic representing the possible variability in measuring the distance between GFP and S100A4 gold particles

Scale drawing of 10S myosin (top) and 6S myosin (bottom) with primary antibodies (orange) attached to either GFP (green) or S100A4 (yellow); secondary antibodies (red) attached to the primary antibody and a gold particle of 30 nm (GFP) or 15 nm (S100A4) attached to secondary antibodies. Given this arrangement there is approximately ± 40 nm variability (indicated by dashed, red circle) in the distance from each antigen to its respective gold particle. Despite this variability, modelling suggests a peak of 25-75 nm and 125-175 nm is consistent with 10S and 6S myosin, respectively. Scale bar = 50 nm. Image courtesy of Prof. Clive. R. Bagshaw.

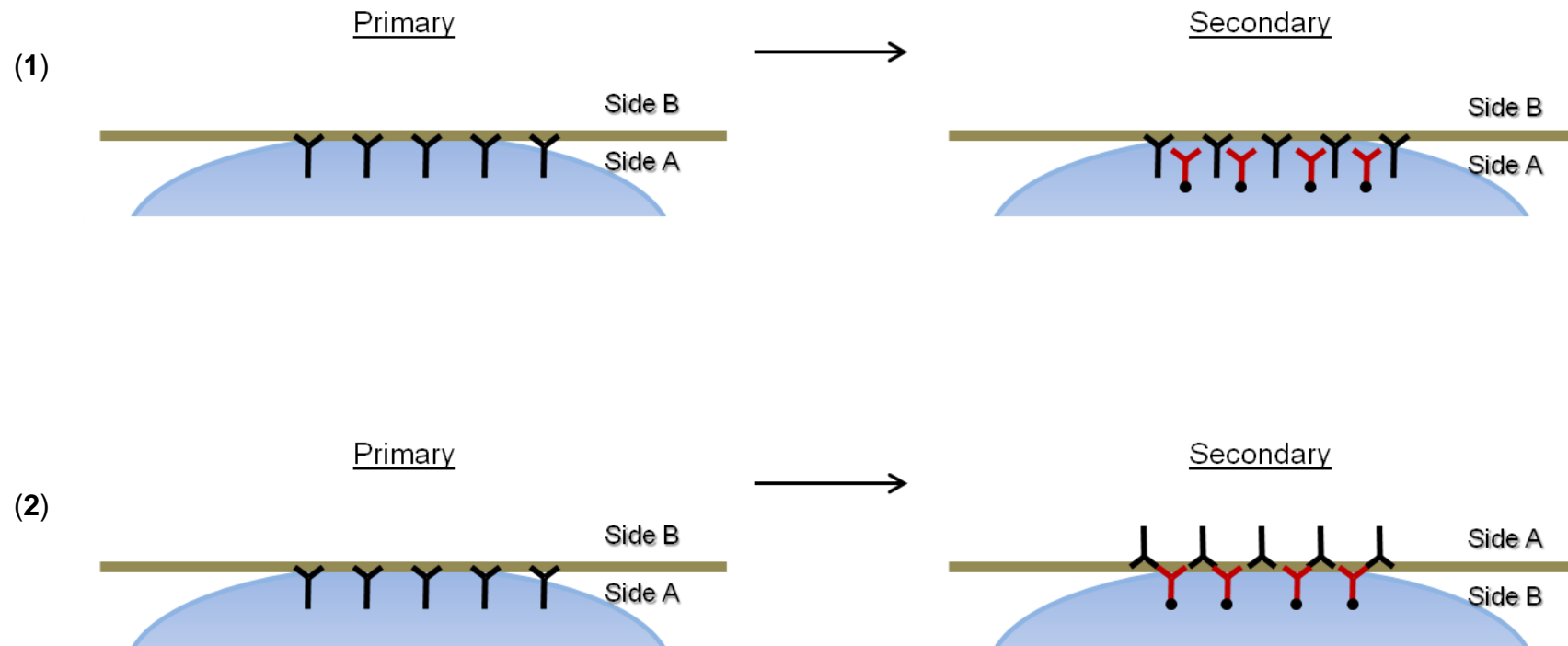


Figure 4.15: Control to assess single-sided immunogold labelling

(1) In conventional single-sided immunogold labelling, a single surface, side A, is exposed to both primary and secondary antibody. (2) To assess the veracity of single-sided staining, a grid containing sections of CLM tissue was floated (Side A) on a drop of primary antibody solution. Prior to secondary antibody staining the grid was then inverted to expose the unstained surface, Side B. If any solution had seeped from Side A to Side B during primary or Side to B to Side A during secondary, gold particles would therefore be present.

4.2.2.3.6 Phosphorylation of the RLC is largely mediated by Rho Kinase

Since phosphorylation of the regulatory light chain of myosin (RLC) is crucial for the switch from a 10S to 6S state (Craig *et al.*, 1983), it was further hypothesised that attenuating RLC phosphorylation should significantly reduce the number of 6S molecules *in vivo* and thus be reflected in the co-localisation analysis. To determine the kinase responsible for phosphorylation of the RLC in this cell model, inhibitors, ML-7 and Y27632 were used to target the two main kinases regulating this phosphorylation: myosin light chain kinase (MLCK) and Rho-associated, coiled coil containing kinase (ROCK) respectively (Conti & Adelstein, 2008). Western blot analysis demonstrated ROCK inhibition led to a significant reduction in the level of phosphorylation on Ser19/Thr18 of the RLC, whereas MLCK inhibition showed no significant changes (Figure 4.16B). Additionally, phenotypical effects of ROCK inhibition were also observed, including formation of long, spindle-like protrusions (Figure 4.16A; indicated by white arrow) consistent with previous reports (Sandquist *et al.*, 2006), thus further confirming the active state of this kinase.

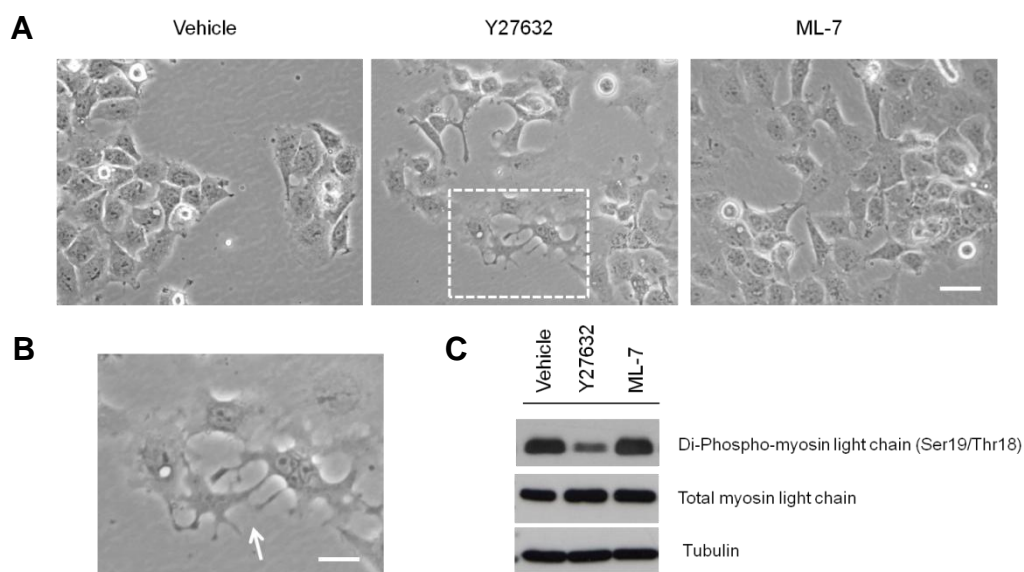


Figure 4.16: ROCK is the major kinase involved in phosphorylation of the RLC

Cl.M cells grown in the presence of Dox for 72 hours were treated with DMSO (vehicle), 10 μ M Y27632 or 10 μ M ML-7 for 1 hour. (A) Representative images of cells prior to lysis, scale bar = 20 μ m. (B) Magnification of dashed, white box in (A) highlighting spindle-like protrusions in the presence of Y27632 (white arrow), scale bar = 10 μ m. (C) Cell lysates were collected and probed for ppRLC (Ser19/Thr18), total myosin light chain and α -tubulin by Western blot.

4.2.2.3.7 Attenuation of RLC phosphorylation abolishes the co-localisation distance between S100A4 and a GFP-myosin IIA consistent with 6S myosin

Subsequent to this, cells were treated with Y27632 and the same nearest-neighbour analysis performed. In contrast to untreated cells, significant co-localisation of GFP-myosin IIA and S100A4 (Figure 4.17) was only present at one peak, corresponding to 25-75 nm (Figure 4.18) consistent with the hypothesis that this distance reflects 10S myosin monomers while the 125-175 nm distance likely reflects the 6S myosin monomer.

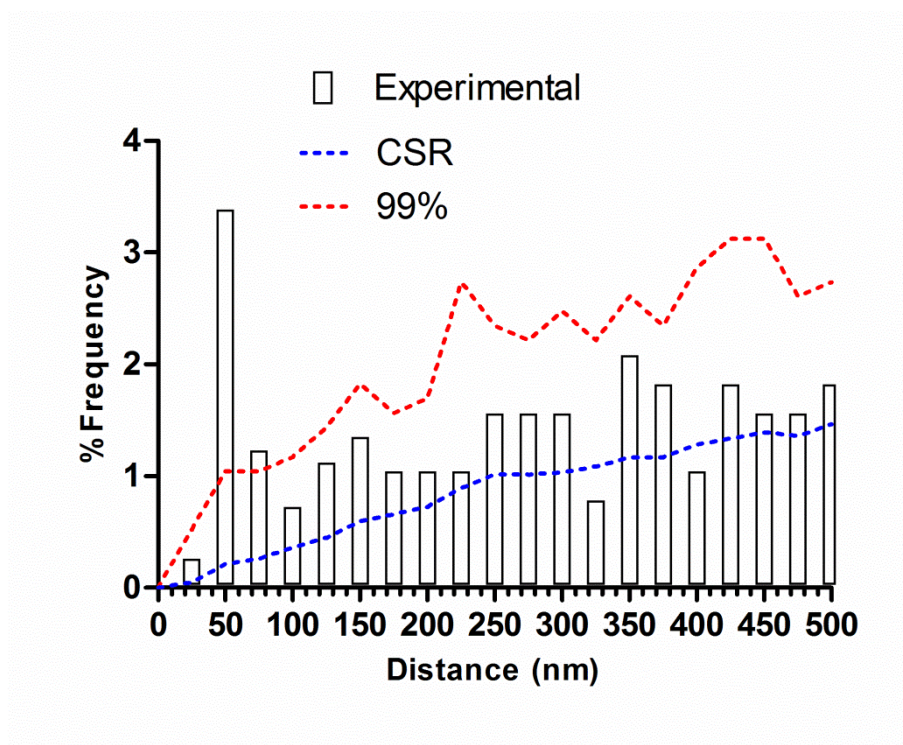


Figure 4.17: Attenuation of RLC phosphorylation leads to co-localisation between GFP and S100A4 at only one specific distance consistent with 10S GFP-myosin IIA

Cl.M cells were grown in the presence of Dox for 72 hours and 1 hour prior to fixation a final concentration of 10 μ M Y27632 was added. Cells were processed as described previously and stained for S100A4 and GFP. Nearest neighbour co-localisation indicates only one specific peak of statistical significance between 25-75 nm. N=850 particles.

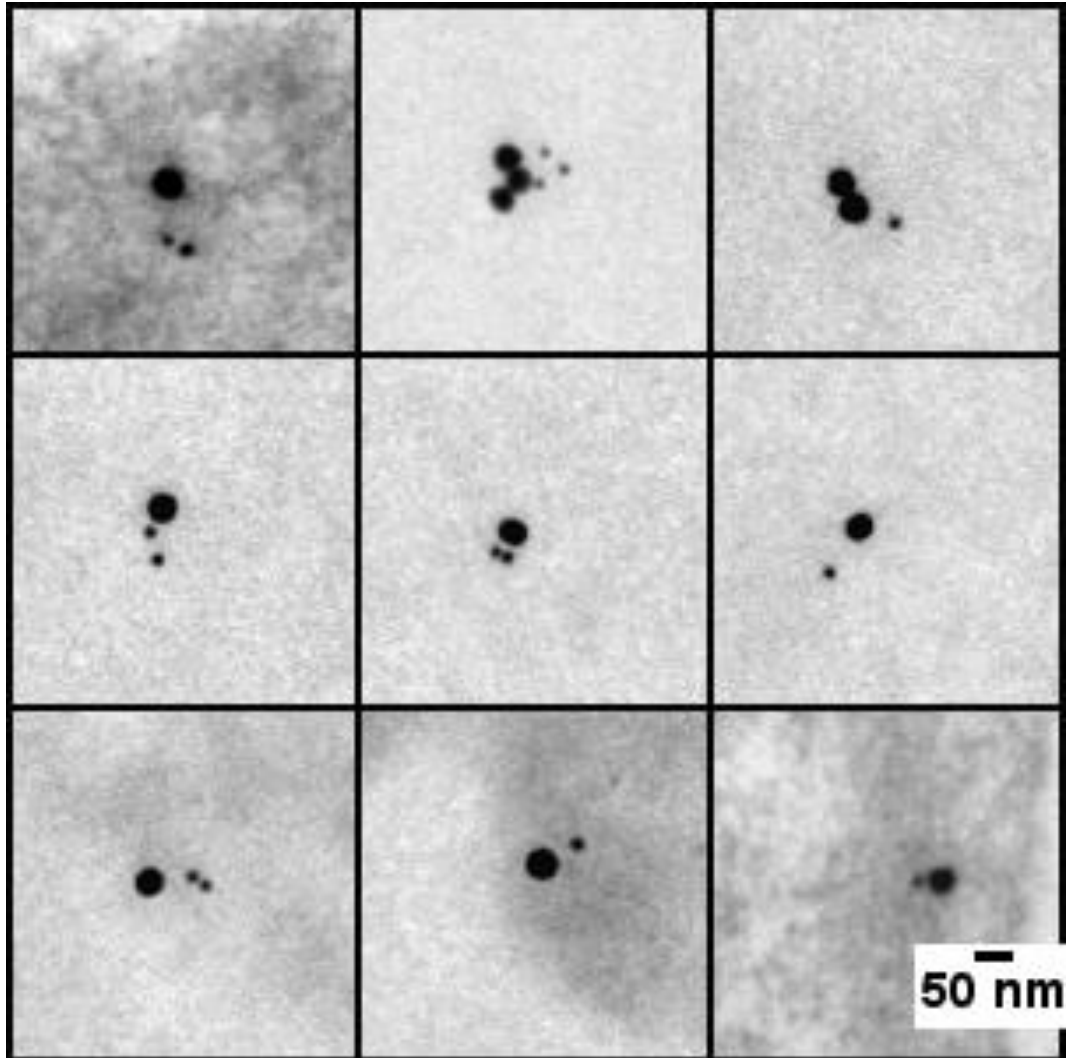


Figure 4.18: Selected images of GFP and S100A4 co-localised at distances consistent with 10S GFP-myosin IIA.

Images of Cl.M cells treated with Y27632 and stained with GFP (30 nm gold) and S100A4 (15 nm gold). Scale bar = 50 nm.

4.2.2.3.8 *S100A4 does not co-localise with GFP α -tubulin*

As an additional biological control, a stable clone of A431-SIP1 constitutively expressing GFP- α -tubulin was generated as described previously for Cl.M. α -tubulin was chosen because like myosin IIA, it is also a cytoskeletal protein but has only been shown to weakly interact with S100A4 (Chen *et al.*, 2001). Furthermore, GFP- α -tubulin constructs were readily available which would allow the same combination of a GFP polyclonal and S100A4 monoclonal antibody to be used for the immunogold labelling. Western blot analysis (Figure 4.19B) of the A431-SIP1 GFP- α -tubulin clone (Cl.T) indicated an equivalent level of S100A4 expression compared to the parental cell line. Expression of GFP- α -tubulin was lower than endogenous α -tubulin as indicated by a long exposure (LE) of the Western blot, but confocal analysis still (Figure 4.19A) demonstrated a significant level of GFP- α -tubulin in interphase cells. Moreover, GFP α -tubulin had a similar localisation to GFP-myosin IIA thus serving as a suitable control for co-localisation analysis.

Having established this, tissue sections of Cl.T were immunolabelled with the same combination of GFP and S100A4 antibody, as for Cl.M. Although the immunolabelling was relatively weak, there was evidence of tubulin-like filaments in some cells and S100A4 localisation in the cytoplasm and nucleus (Figure 4.20). Co-localisation analysis from three independent experiments demonstrated no significant peaks (Figure 4.21) over the distances measured, consistent with there being only a weak interaction between S100A4 and tubulin. As a whole, these data suggest that 6S and 10S forms of myosin IIA exist *in vivo* and S100A4 is able to interact with both.

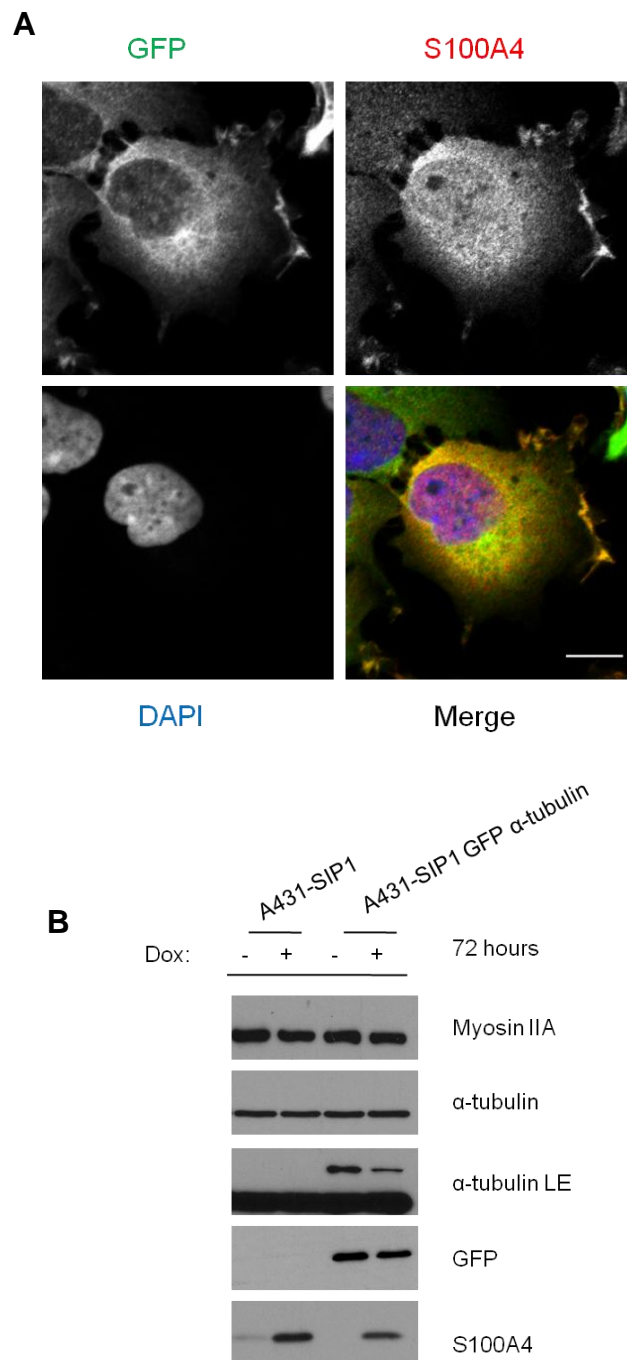


Figure 4.19: Characterisation of A431-SIP1 GFP- α -tubulin (Cl. T) cells

(A) Cl. T cells grown in the presence of Dox were stained for GFP and S100A4 using immunofluorescence. Red= S100A4; Green = GFP; Blue = DAPI. (B) Western blot analysis of A431-SIP1 and Cl.T cells maintained in the absence and presence of Dox for 72 hours. Membranes were probed for GFP, α -tubulin, myosin IIA and S100A4. LE = Long Exposure.

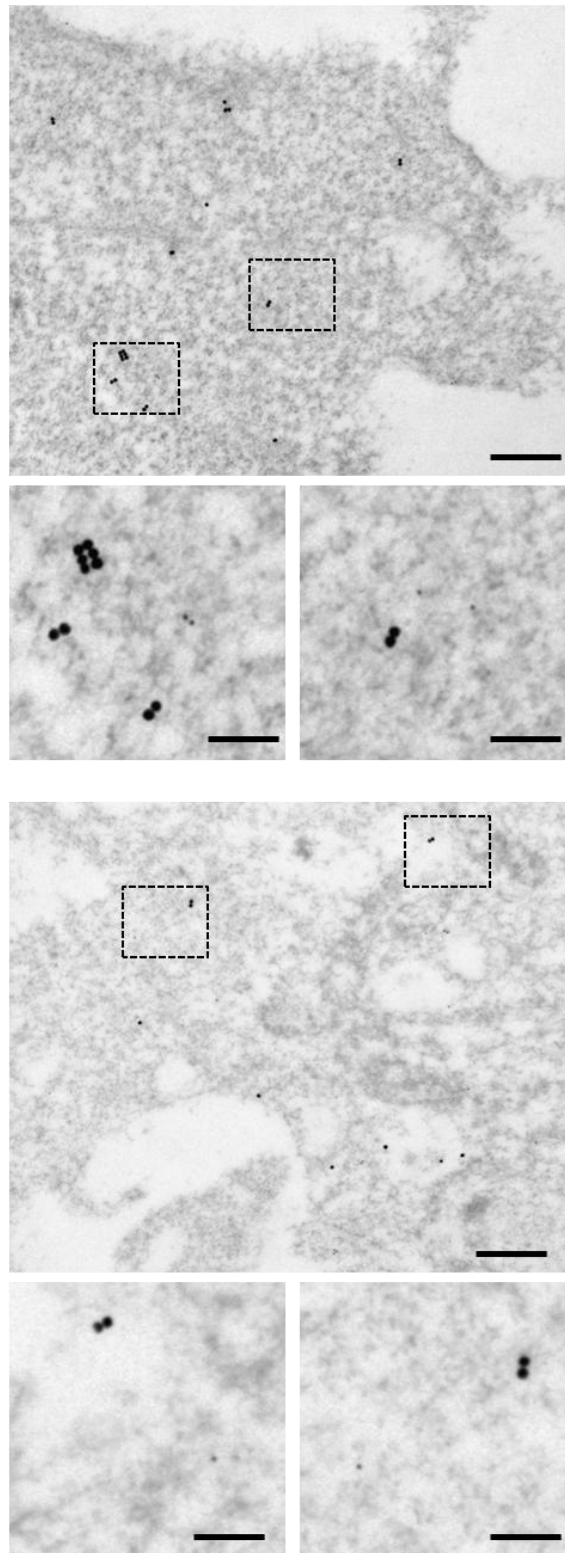


Figure 4.20: Immunogold labelling of GFP-tubulin (Cl.T) Cells stained for S100A4 and GFP

Cl. T cells grown in the presence of Dox were stained for GFP (30 nm gold) and S100A4 (15 nm gold). Upper images, scale bar = 250 nm; lower images, scale bar = 100 nm.

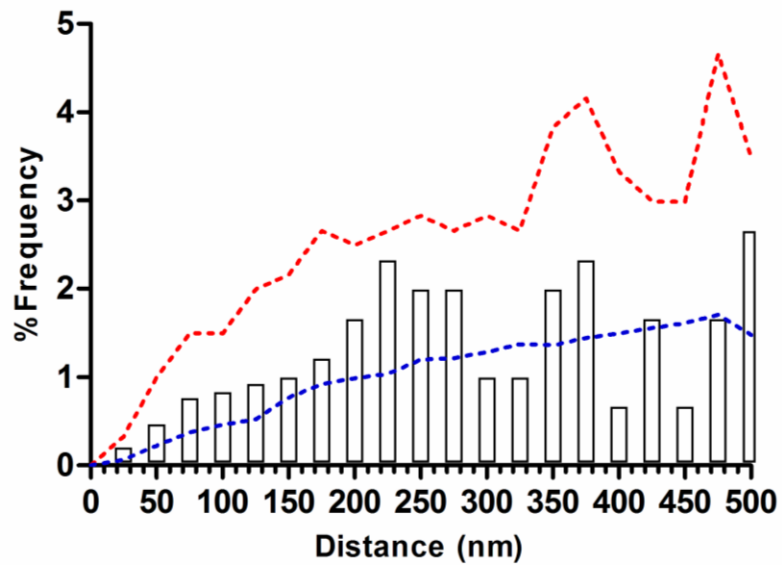


Figure 4.21: GFP- α -tubulin and S100A4 do not co-localise

CI. T cells grown in the presence of Dox were stained for GFP and S100A4. Nearest neighbour co-localisation analysis indicates no statistically significant co-localisation between GFP- α -tubulin and S100A4. N=808.

4.2.3 S100A4 Modulates Myosin IIA Filament Formation *in vivo*

4.2.3.1 RNAi-mediated Knockdown of S100A4 Promotes Myosin IIA Filaments

To explore the functional consequences of the S100A4-myosin IIA interaction, the intracellular distribution of myosin IIA in the presence and absence of S100A4 was next investigated. For imaging purposes, cells were seeded on Opticell which is a 50 cm² chamber consisting of two polystyrene membranes. Although composed of plastic, Opticell allows high quality imaging yet retaining a surface similar to tissue culture plastic. Accordingly, A431-SIP1 cells transfected with a non-targeting- and S100A4-targeting siRNA were seeded on an Opticell, stained for myosin IIA and S100A4 and analysed by confocal microscopy. In general, cells in the absence of S100A4 displayed more myosin filaments compared to cells in its presence with these filaments most prominent on the ventral layer where they extended the entire width of the cell (Figure 4.22).

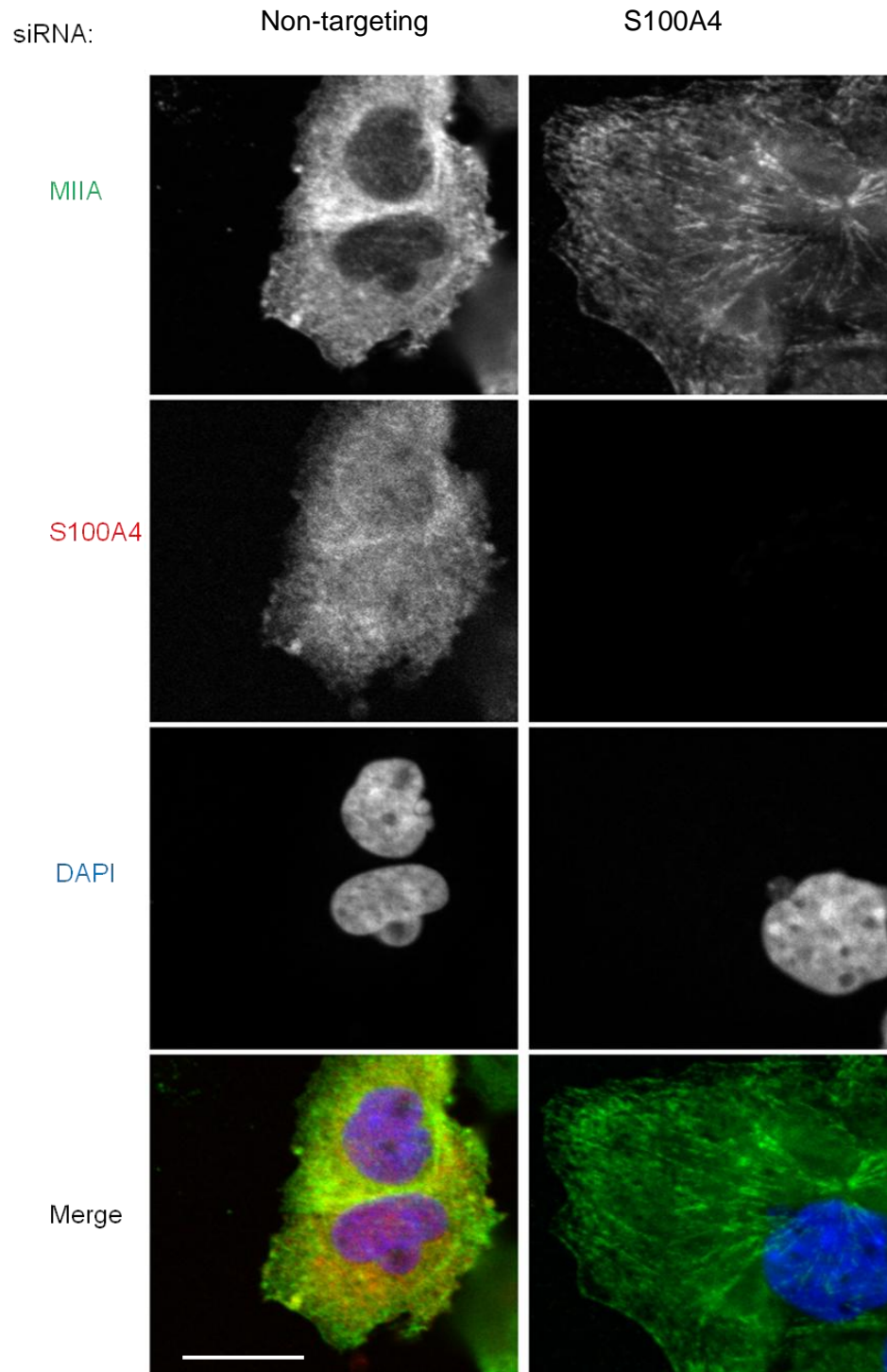


Figure 4.22: Knockdown of S100A4 causes an increase in myosin IIA filaments

A431-SIP1 cells transfected with either a non-targeting- or S100A4-targeting siRNA and seeded in an optically chamber. Cells maintained in Dox for 72 hours were stained for S100A4 and myosin IIA using immunofluorescence. S100A4 = Red; MIIA = Green; DAPI = Blue. Images acquired using confocal microscopy. Scale bar = 10 μ m.

4.2.3.2 Use of Fluorescence Recovery After Photobleaching (FRAP) to quantify the effect of S100A4 on myosin IIA recovery

To quantify these effects, Fluorescence Recovery After Photobleaching (FRAP) was used. FRAP is a commonly-used technique to study the mobility of molecules *in vivo* (Sprague & McNally, 2005). In essence, a small region of a cell expressing a fluorophore-tagged protein is irreversibly bleached by application of a short but intense burst of laser, otherwise known as a bleach. As fluorescent molecules from outside of this area move into replace the bleached molecules, the fluorescence recovery is measured (Figure 4.23); this mobility is determined both by the diffusion and transport of fluorescent molecules through the cellular milieu and exchange kinetics in the case of myosin filaments.

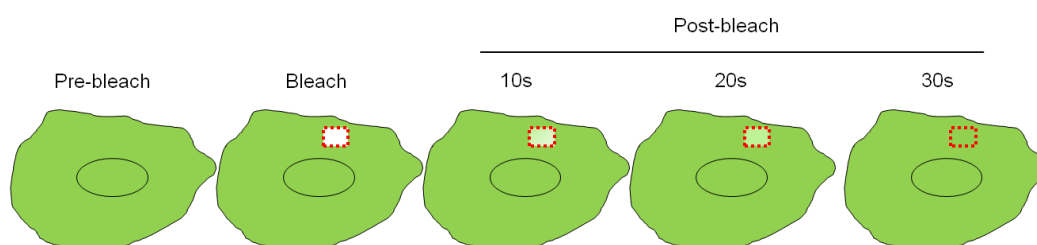


Figure 4.23: A graphical overview of the FRAP process

Pre-bleach images are initially collected to capture steady state. Part of the cell is then irreversibly bleached (red, dashed box) and the fluorescence intensity is measured as a function of time till steady state has been reached again.

Given the above observations, it would be expected that cells with less myosin filaments would recover more quickly since there would be a larger pool of diffusible myosin to replace the bleached molecules; conversely, more myosin filaments would result in less diffusible myosin and thus a slower rate of recovery.

4.2.3.2.1 *Optimisation of the FRAP Protocol*

Before FRAP experiments could be conducted, a number of conditions had to be first optimised. FRAP experiments were performed on a Nikon confocal Eclipse microscope using software EZ-C1 and a macro add-on, “Zoom FRAP” which allows the specification of a number of variables necessary for an optimised FRAP experiment. According to Rabut and Ellenberg (2005), there are three main factors to consider when optimising a FRAP experiment:

1. An efficient bleach;
2. Balance between temporal and spatial resolution;
3. Limiting sample bleaching during recovery.

The optimum bleach would be both instantaneous and complete although these are often incompatible goals. Complete depletion of fluorescent molecules yields better contrast between bleached and unbleached regions and thus allows more precise measurement of the exchange between molecules. Moreover, the bleaching time should be as short as possible since a significant fraction of molecules will otherwise have exchanged out of the region of interest (ROI) before the bleach is over.

To optimise this, the laser intensity, bleach size and number of iterations were determined empirically. The size of the ROI is a compromise between a large enough area to efficiently measure recovery but small enough so bleaching can be carried out rapidly. In this case, a 7x2 μm -sized rectangle was chosen. Having established this, the 488 Argon-ion laser used to bleach was set to a maximum intensity of 25mW (100%) and a region of cytoplasm chosen; however, a single iteration proved to be insufficient for a complete bleach and the number of iterations was increased to three yielding a more total depletion of fluorescent molecules.

Following this, the balance between the temporal and spatial resolution had to be determined. The higher the pixel number, the greater the spatial resolution, but the slower the image acquisition time between each frame. Since preliminary data demonstrated that some recoveries would be over in tens of seconds, the image acquisition had to be quick enough to resolve these shorter recoveries. As a result, a pixel size of 256x256 was chosen instead of the more conventional 512x512. This

would ensure scanning was fast enough but still provide suitable spatial resolution to effectively measure the recovery rate of the bleached area. Reducing the number of pixels would also limit photobleaching of the sample during the recovery stage which was the third condition to optimise. Finally, images were acquired every 2.0 seconds which would limit photobleaching but ensure enough data points were collected to effectively resolve the fluorescence recovery.

4.2.3.2.2 S100A4 knockdown slows the recovery of myosin IIA

After optimising these parameters, A431-SIP1 GFP-myosin IIA cells transfected with non-targeting- and S100A4-targeting siRNA were seeded in an Opticell™ as previously described and FRAP experiments carried out according to the conditions above. Cells were chosen at random, although apoptotic or mitotic cells were discounted. Prior to each bleach, two images were acquired to reach steady state at which point a representative area of cell cytoplasm was bleached and the fluorescence recovery measured every 2.0 s till steady state conditions had been established. An example of a bleached cell from each condition is shown in Figure 4.24 (Non-targeting siRNA) and 4.25 (Si S100A4) with the field of view in (A); specific cell bleached in (B) and magnification of bleach spot in (C). Kinetic traces for the cells seen in Figure 4.2.4 and 4.25 are represented in Figure 4.26; the convention of assessing FRAP experiments is to calculate the half-life, or the time it takes for 50% of the fluorescence to recover.

In each experiment, ten cells were analysed for both conditions and three independent experiments performed. On average, cells in the presence of S100A4 recovered nearly twice as quickly (10 s) as those in the absence (19 s) ($p < 0.01$) validating the initial observations (Figure 4.27A). The knockdown of S100A4 was confirmed by Western blotting (Figure 4.27B).

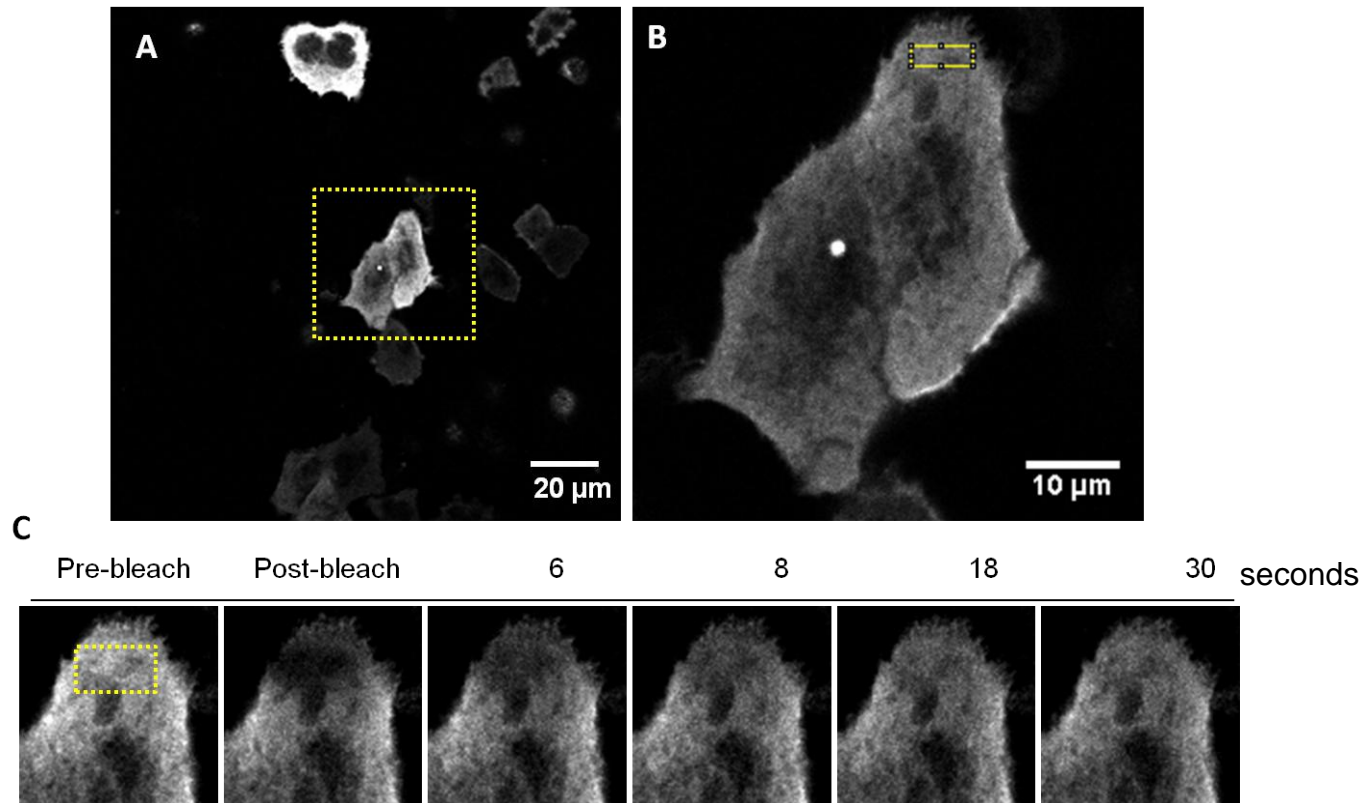


Figure 4.24: Representative cell transfected with a non-targeting siRNA used for FRAP experiments

CI.M cells transfected with a non-targeting siRNA were seeded in Opticell and maintained in the presence of Dox for 72 hours. Large field of view (A) indicates cell selected for FRAP and dashed yellow box enlarged in (B). Yellow box indicates bleach spot; area of cell including bleach spot is magnified in (C). Time series of FRAP experiments represented in (C); text above each image indicates seconds after bleach. Scale bar as indicated on image.

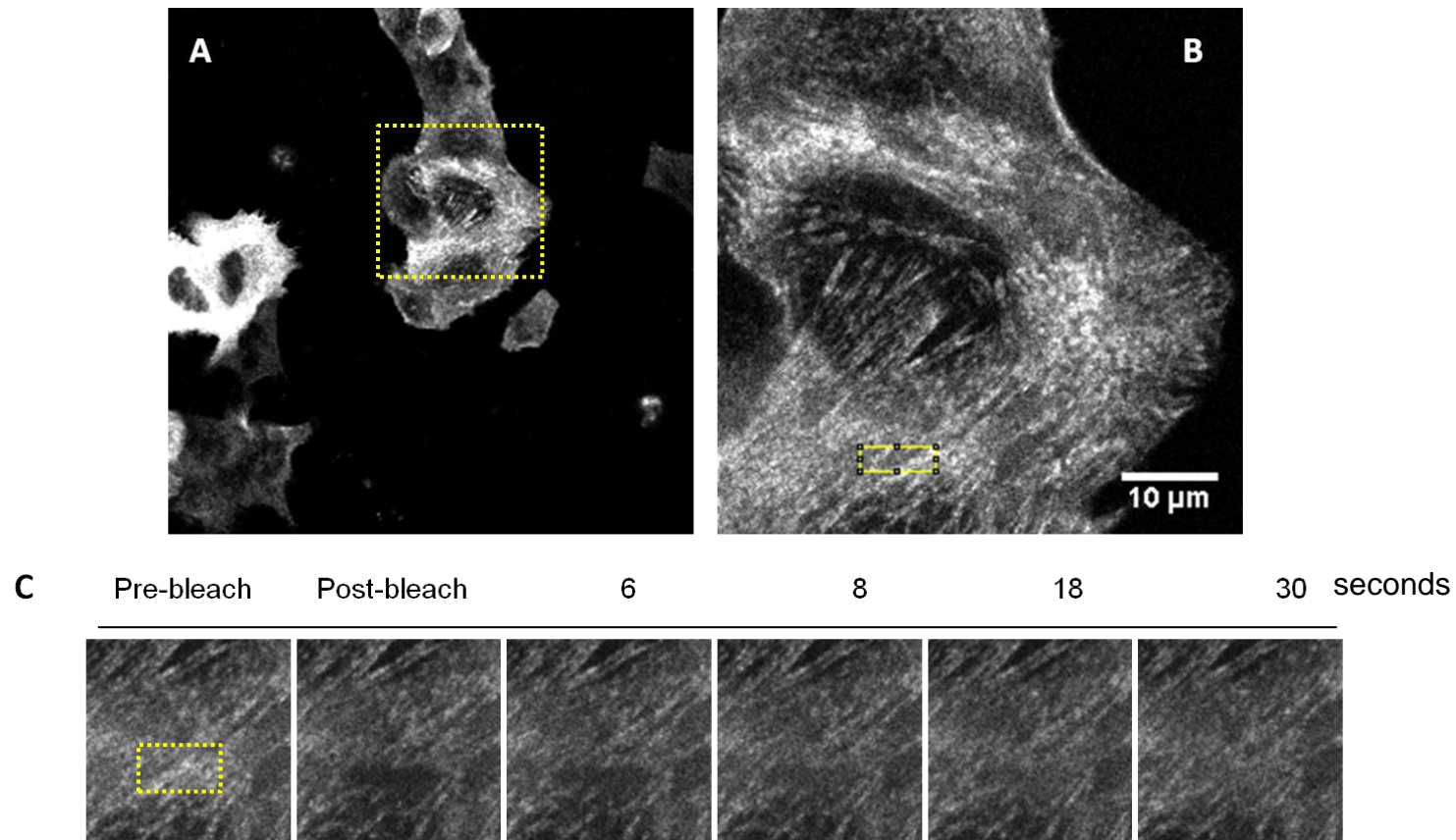


Figure 4.25: Representative cell transfected with siS100A4 used for FRAP experiments

CI.M cells transfected with Si S100A4 were seeded in Opticell and maintained in the presence of Dox for 72 hours. Large field of view (A) indicates cell selected for FRAP and dashed yellow box enlarged in (B). Yellow box indicates bleach spot; area of cell including bleach spot is magnified in (C). Time series of FRAP experiments represented in (C); text above each image indicates seconds after bleach. Scale bar as indicated on image.

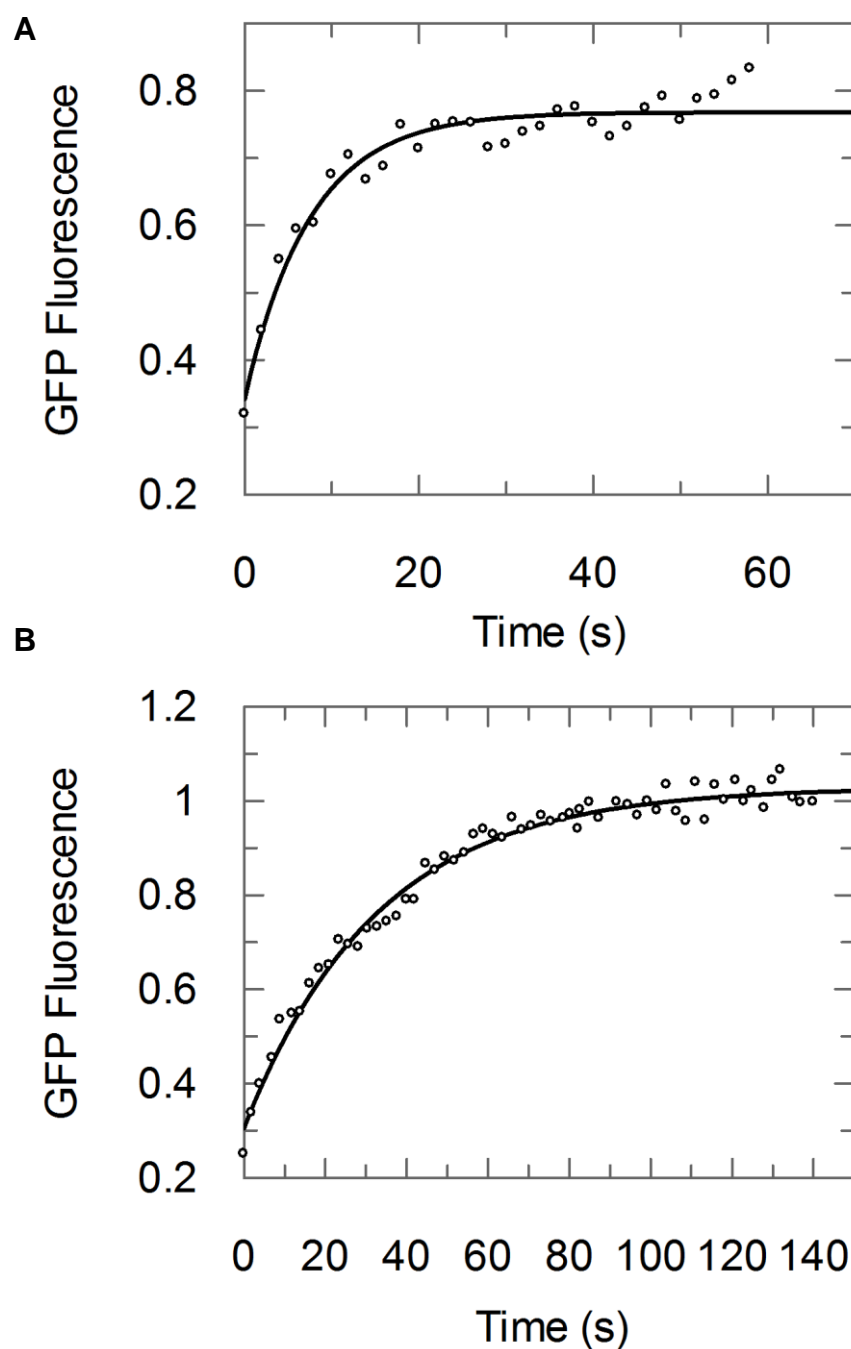


Figure 4.26: Kinetic traces from selected cells in the presence and absence of S100A4

Fluorescence intensity for the bleach area is extracted for each time point, corrected for background fluorescence and normalised to a non-bleached area of the cell. Kinetic traces are plotted as a function of fluorescence over time and fitted to a single exponential to derive k_{obs} . Kinetic trace of non-targeting siRNA (A) and Si S100A4 (B) cells from Figure 4.24 and 4.25, respectively.

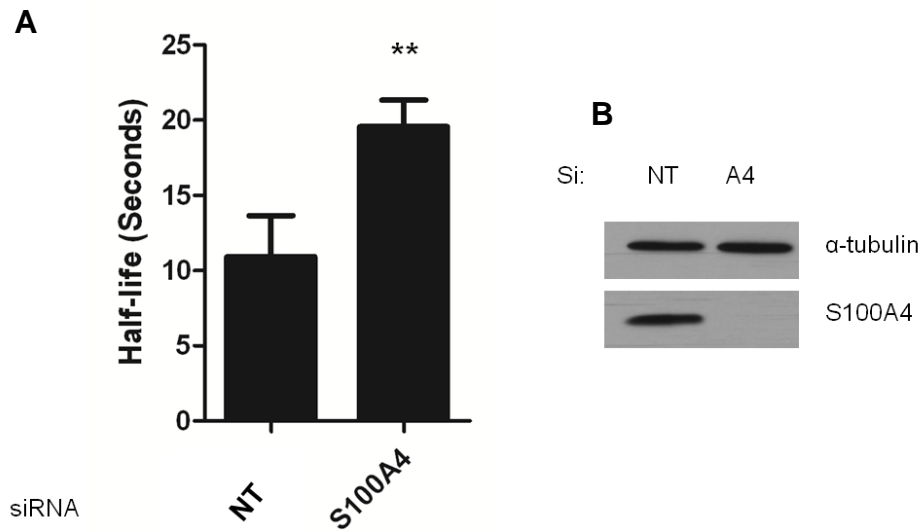


Figure 4.27: Knockdown of S100A4 significantly slows GFP-myosin IIA recovery

Summary of half-lives from CLM cells transfected with non-targeting (NT) siRNA and Si S100A4 (**A**). Cells in the presence of S100A4 have an average recovery rate of 10 s whereas cells in the absence have a recovery rate of 19s. 10 cells per experiment. Error bars represent SEM for average half-life from three separate experiments. Level of knockdown confirmed by western blot (**B**). P value < 0.01; calculated with a Student's T-test.

4.3 Discussion

S100A4 is a known regulator of cell migration in a number of cellular contexts including colon adenocarcinoma cells, osteosarcoma cells, promyelocytic leukaemia cells, macrophages (Tarabykina *et al.*, 2007) and cells which have undergone an epithelial-mesenchymal transition (this study). Despite this, little is known regarding the mechanisms controlling S100A4-induced migration. As S100 proteins lack catalytic domains, their functions are dependent on regulating the activity of interacting partners (Santamaria-Kisiel *et al.*, 2006). In the case of S100A4, a number of proteins have been identified including liprin β 1 (Kriajevska *et al.*, 2002), Smad3 (Matsuura *et al.*, 2010) and methionine aminopeptidase 2 (Endo *et al.*, 2002); however, the interaction with non-muscle myosin IIA has been the focus of its role in cell migration (Helfman *et al.*, 2005). Myosin IIA plays important roles in this process by regulating cell polarity, controlling cellular protrusions and mediating adhesion and translocation at the rear (Vicente-Manzanares *et al.*, 2009). It has been hypothesised that by promoting the monomeric state of myosin IIA, S100A4 allows cells to more efficiently cycle through the co-ordinated steps required during cell migration (Li & Bresnick, 2006) [See General Discussion].

There is significant *in vitro* data to support the interaction between myosin IIA and S100A4 but few studies have provided evidence for this interaction *in vivo* and less still have correlated the expression of S100A4 with a reduction in the level of filamentous myosin in cells. Zhang *et al.*, (2005a) used FLIM to demonstrate an interaction between S100A4 and a C-terminal fragment of myosin IIA in HeLa cells while Kim *et al.*, (2003) showed co-localisation of S100A4 and myosin IIA in MDA-MB-231 cells at the level of light microscopy. However, to validate the hypothesis that S100A4 directly promotes the monomeric state of myosin in cells, further evidence is required to prove that S100A4 and myosin IIA interact *in vivo*.

4.3.1 Co-localisation of S100A4 and myosin IIA A431-SIP1 cells

Accordingly, a number of approaches were taken to examine the interaction between S100A4 and myosin IIA in A431-SIP1 cells. Using immunoprecipitation, S100A4 interacted with myosin IIA in cell lysates and the two proteins co-localised at the level of light microscopy with PCC and ICQ values of 0.745 and 0.233, respectively. Given

the maximum values for both PCC and ICQ of 1.0 and 0.5, this represents a relatively high degree of co-localisation. The difference between the PCC and ICQ is that when a broadly expressed protein is distributed across the whole cell a second protein will “co-localise” according to the PCC even if its distribution is essentially random. In contrast, the ICQ value is based on signals that vary in synchrony, so a bright-coloured green pixel co-localised with a bright-coloured red pixel will score highly compared with pixels which exhibit asynchronous staining. The ICQ approach is therefore a more robust way of determining co-localisation. Notwithstanding, when both proteins display a cytoplasmic distribution, as myosin IIA and S100A4 do in these cells, co-localisation analysis is severely restricted due to the diffraction limitation of light. This places a limit of approximately 250 nm on two “co-localised” proteins, a value too large to say if they categorically interact or not. Given this physical limit, transmission electron microscopy was used providing an increase in resolution by around two orders of magnitude which would allow a more accurate level of co-localisation to be determined.

Analysis of S100A4 and myosin IIA distribution using TEM suggested both proteins co-localised. Although immunolabelled cells exhibited a relatively low frequency of co-localisation (between 2-4%), a combination of Diggle’s nearest neighbour function and Monte Carlo simulations showed S100A4 interacts with myosin IIA at two statistically significant distances, 25-75 nm and 125-175 nm consistent with 10S (50 nm) and 6S myosin (150 nm), respectively. These data therefore represents the first evidence that 6S and 10S forms of myosin exist in non-muscle cells.

The low level of co-localisation is to be expected for a molecule like myosin since it would have to be essentially horizontal to the plane of the section for both the N- and C-terminus to be successfully labelled. In addition, the extra uncertainty can be explained due to the two antibodies and gold particle which add a combined distance of approximately ± 40 nm between the epitope and gold particle. Despite this, modelling of distances for 10S and 6S myosin taking into account this variation, demonstrates that there should still be two distinctive peaks consistent with 10S and 6S forms of myosin.

A further consideration is the exact conformation of 6S myosin since it is widely known to display a degree of flexibility at the heavy meromyosin-light meromyosin junction

(Figure 4.28A) (Trybus *et al.*, 1982). Indeed, EM data has shown isolated 6S myosin can adopt a variety of conformers with the HMM region even folding back over itself, which would give significantly shorter distances between the N- and C-terminus of myosin (Elliott & Offer, 1978). However, electron microscopy might introduce artefacts into the myosin molecule due to solvent conditions or how it lands and dries on the grid. Solution-based studies using ultracentrifugation have shown that the flexibility of myosin is likely to be more constrained with an average bend of the rod approximately 60° (Iniesta *et al.*, 1988). Given this value, the distance between the N- and C-terminus would only differ by approximately 20 nm compared to a non-bent molecule (Figure 4.28B). Regardless of the exact conformation of the molecules which represent the 125-175 nm peak, attenuation of RLC phosphorylation abolishes it, strongly suggesting it is composed of myosin with a phosphorylated RLC.

Another consideration was that close co-localisation between epitopes could arise from myosin in the filamentous state with one molecule of GFP-myosin IIA stained for GFP and a neighbouring, nearby molecule stained for S100A4. While this may arise, the affinity of S100A4 to filamentous myosin is weaker when compared to monomeric myosin (Badyal *et al.*, 2011) suggesting that the bulk of S100A4-bound myosin is likely to be monomeric. Moreover, when cells were treated with Y27632, which further reduced the level of myosin filaments in cells, the 25-75 nm peak was still present. Taken together, it is therefore unlikely that a close localisation of two gold particles represents S100A4 and GFP antibodies bound to separate molecules.

The question of which myosin conformer S100A4 interacts with has not been previously addressed in the literature. Notwithstanding, there have been a number of studies investigating the effect of monoclonal antibodies recognising the C-terminus of myosin which are highly relevant. Although these antibodies were raised against chicken intestinal epithelial brush border myosin, this is a very close homolog of human non-muscle myosin IIA (92% sequence identity). One such antibody, BM4 recognises the C-terminus of myosin in a position approximately analogous to the binding site of S100A4 and prevents assembly of myosin *in vitro* (Citi & Kendrick-Jones, 1987). Intriguingly, BM4 significantly reduced the actin-activated MgATPase activity of phosphorylated myosin (Citi & Kendrick-Jones, 1988). An effect consistent with the conversion of myosin filaments to the ATPase-limited, 10S state (Cross *et al.*, 1986).

Interestingly, a study by Ford *et al.*, (1997) also showed that S100A4 significantly reduced the MgATPase activity of platelet myosin suggesting S100A4, like BM4, is able to interact with 10S myosin. Given this, does S100A4 affect the equilibrium between a 6S and a 10S myosin monomer? The structural data on the 10S state suggests the S100A4 binding site would extend past the first bend (Burgess *et al.*, 2007), thus it would seem unlikely that S100A4 could affect this equilibrium directly, either by stabilising or destabilising the 10S state. In agreement with this, EM data from Citi *et al.*, (1988) showed BM4 did not affect folding of 10S myosin or unfold previously folded molecules, consistent with S100A4 binding to the 10S state. To quantitatively test this hypothesis though, AUC studies with full-length myosin in the absence and presence of S100A4 would be required. In addition, EM studies characterising the effect of BM4/S100A4 on myosin in the presence of high ionic buffer would be useful since this would promote 6S monomeric myosin (conditions used by Citi *et al.*, (1988) meant myosin was predominantly in the 10S state; low ionic strength and high ATP).

What is less clear is how the S100A4-6S myosin complex originates. In general, the 6S state is considered a more transient species acting as an intermediary between the 10S state and the polymerisation of myosin into filaments (Kendrick-Jones *et al.*, 1987). If S100A4 interacts with monomeric 6S myosin, this could either represent (i) S100A4 initially bound to 10S myosin which is then phosphorylated and unfolds into the 6S; (ii) S100A4 binding to 6S (phosphorylated) myosin; (iii) or S100A4 having disassembled a phosphorylated myosin monomer from a filament (Figure 4.29). Possibly the least likely of these scenarios is S100A4 binding to a pre-phosphorylated 6S monomer since this would rapidly assemble into filamentous myosin if above the critical concentration for assembly; however, without additional experimentation, it is not possible to speculate further as to which of the remaining two scenarios represents the more likely origin of the S100A4-6S myosin complex.

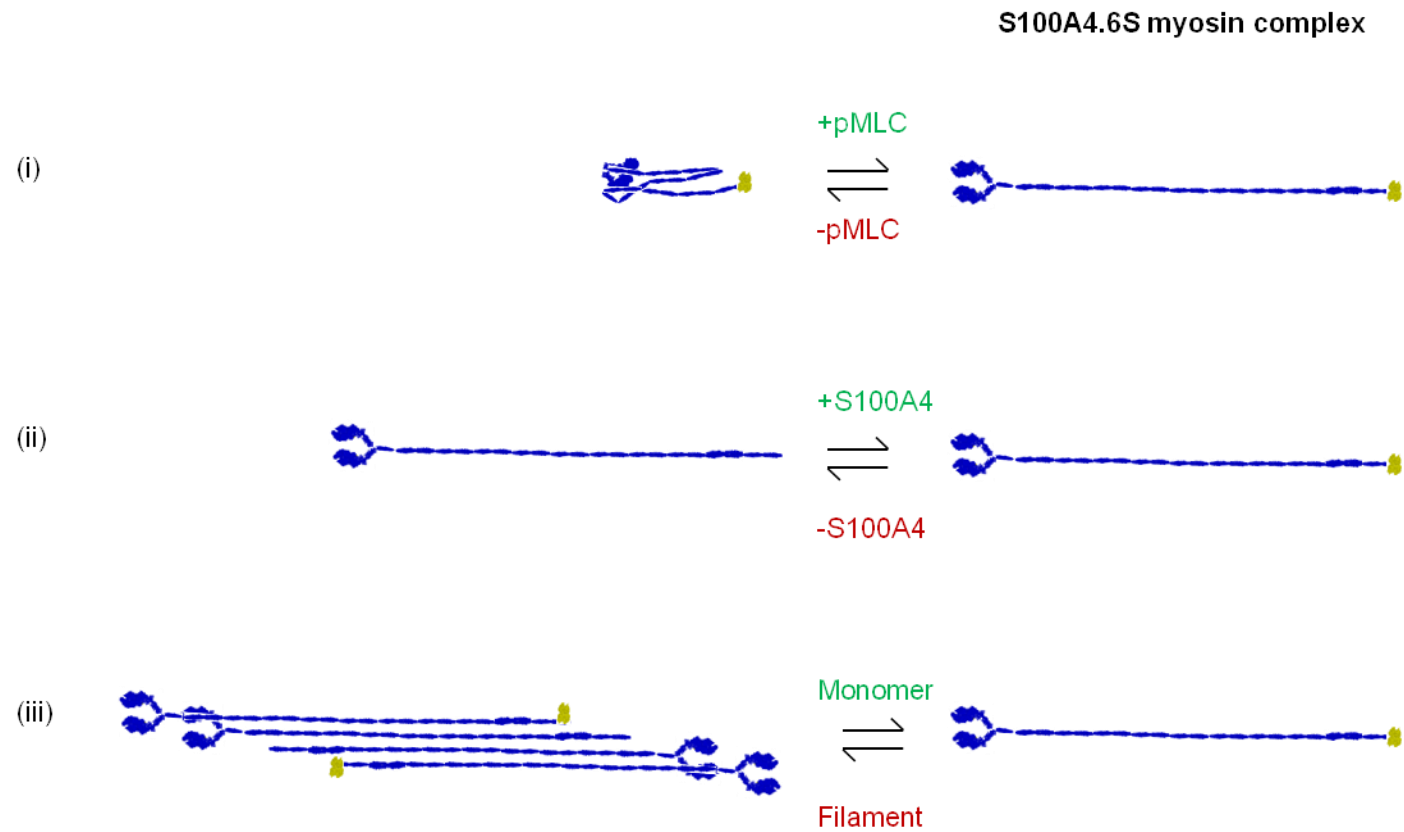


Figure 4.29: Schematic representing possible origins of the S100A4.6S myosin state

(i) S100A4 initially bound to 10S myosin which is then phosphorylated and unfolds into the 6S ; (ii) S100A4 binding to 6S (phosphorylated) myosin; (iii) S100A4 having disassembled a phosphorylated myosin monomer from a filament

4.3.2 The effect of S100A4 on myosin IIA turnover *in vivo*

A large number of studies have demonstrated that S100A4 promotes the monomeric state of myosin *in vitro* but there is very little evidence of this *in vivo*. Li *et al.*, (2006) demonstrated that a myosin IIA antibody raised against the S100A4 binding site mimicked the effect of over-expressing S100A4 in MTC cells. More recently, a study by Li *et al.*, (2010) showed increases of myosin in triton-insoluble fractions of S100A4-knockout macrophages. In A431-SIP1, cells in the presence of S100A4 generally displayed fewer stress fibres than cells in the absence. This effect was most evident when cells were seeded on an Opticell, a chamber composed of tissue-culture like plastic. The effect was also observed on glass, although was less obvious because cells seeded on this surface were a more heterogeneous population. Depending on the confluence of the culture, cells seeded on glass did not progress through a full EMT, as the case with cells seeded on tissue-culture plastic (our unpublished observations). EMT is widely known to be sensitive to cell density and cell-substrate interactions (De Rooij *et al.*, 2005) which could explain why EMT progression in some cells was disrupted, creating a heterogeneous population of cells.

Quantitative analysis of this effect using FRAP indicated cells transfected with a non-targeting siRNA recovered twice as quickly as those with an S100A4-targeting siRNA (Figure 4.27; Si Neg :10 s cf. Si A4: 19 s). Rates of recovery for FRAP are determined by diffusion of molecules through the cytoplasm as well as active transport, and in the case of myosin filaments, exchange kinetics. Given that most cells transfected with non-targeting siRNA exhibited a non-filamentous distribution of myosin, recovery is likely to be dominated by diffusion of soluble myosin to replace the bleached molecules. In contrast, fluorescence recovery for S100A4-siRNA cells, which displayed more prominent myosin fibres, would be dominated by the exchange of fluorescent molecules within these filaments, thus explaining the longer recovery time. Although the average half-life for recovery from three independent experiments was 10 s in non-targeting-siRNA cells, the shortest half-life was as low as 4 s. This rate is in fact very close to what would be expected for pure-diffusion based kinetics, with a recovery half-life of approximately 3 s and 2.1 s for 6S and 10S myosin, respectively. Equally in S100A4-siRNA transfected cells, recoveries of over 50 s were recorded with a strong correlation between levels of filamentous myosin and slower rates of recovery.

This heterogeneity can be explained as experiments were being performed with live cells, and there was no indication of S100A4 expression. Indeed the criteria for choosing cells for FRAP cells were based solely on discounting those which were either mitotic or apoptotic. Based on immunofluorescence data (our unpublished observations), S100A4 expression does vary within a population of cells which would therefore account for these differences. In addition, although the knockdown of S100A4 was highly efficient according to the Western blot data, this might represent a complete knockdown in some cells but a rather more modest decrease in others which could also explain faster recoveries in the S100A4-siRNA samples.

In the absence of S100A4, the increase in myosin filaments could alter other aspects of the cytoskeleton including the extent of filamentous actin, indirectly affecting the recovery of myosin in the absence of S100A4. Whilst this is a possibility, the hypothesis would be that S100A4 knockdown directly affects myosin polymerization which, in addition, may affect other properties of the cytoskeleton further slowing down myosin recovery. Indeed, it would be interest to further characterize the changes in the cell cytoskeleton in the absence of S100A4 including actin polymerisation and cell-matrix adhesion to determine what other properties are affected by S100A4-induced depolymerisation of myosin IIA.

In conclusion, data in this chapter has provided both indirect and direct evidence that S100A4 and myosin IIA interact in A431-SIP1 cells. Direct evidence is provided by immunoelectron TEM which suggests that not only does myosin IIA exist in both a 10S and 6S state but S100A4 is able to interact with both. From a mechanistic point of view, this raises further questions about how S100A4 regulates myosin polymerisation which will be of future importance to the field. Indirect evidence of an interaction between S100A4 and myosin IIA is also provided from functional studies. It is widely acknowledged that S100A4 promotes the monomeric state of myosin *in vitro* but *in vivo* evidence is more limited. FRAP analysis indicates that in the presence of S100A4, A431-SIP1 cells turnover myosin as quickly than in the absence, a result supported by the significant increase in filamentous myosin. Together this is strong evidence that S100A4 promotes the monomeric state of myosin in cells and is in agreement with the effect of S100A4 *in vivo*.

5 Mechanism of the S100A4-myosin II α interaction

5.1 Introduction

As previously described, S100A4 is widely acknowledged to promote the monomeric state of myosin IIA *in vitro* and some evidences suggests it affects myosin polymerisation *in vivo* (this study); however, the mechanistic details have been more elusive leading to several discrepancies in the literature. These include how heavy chain phosphorylation of myosin IIA, particularly at Ser1943 affects the interaction with S100A4 (Dulyaninova *et al.*, 2005; Kriajevska *et al.*, 2000) and the minimal binding site of myosin IIA that S100A4 interacts with (Badyal *et al.*, 2011; Malashkevich *et al.*, 2008).

Two phosphorylation sites are present at the very C-terminus of myosin IIA: Ser1916 and Ser1943 (Vicente-Manzanares *et al.*, 2009); with phosphorylation of either shown to reduce the formation of myosin IIA filaments (Dulyaninova *et al.*, 2005). Since the S100A4 binding site (as determined by (Badyal *et al.*, 2011) overlaps the Ser1916 site and is just N-terminal to Ser1943, the interplay between the two has been investigated in a number of studies. Indeed, phosphorylation at Ser1943 was originally shown not to affect the interaction with S100A4 (Kriajevska *et al.*, 2000) although this was later disputed by Dulyaninova *et al.*, (2005) who showed a 7-fold reduction in the binding affinity between S100A4 and *in vitro* phosphorylated myosin IIA rods. In contrast, phosphomimetic mutants of myosin IIA replacing Ser1943 with either Asp or Glu that recapitulated the effects of Ser1943 phosphorylation on myosin IIA solubility did not affect the interaction with S100A4 (Dulyaninova *et al.*, 2007) contrary to the effect seen with *in vitro* phosphorylated myosin IIA rods. Despite overlapping with the S100A4 binding site, phosphorylation at S1916 has been shown not to affect the interaction with S100A4 (Dulyaninova *et al.*, 2005).

As such, one aim of the work in this chapter was to re-address this question by creating phosphomimetic mutants of a C-terminal fragment of myosin IIA (M200) by replacing the appropriate serine residue with a negatively charged amino acid, aspartate. Our group has previously used this fragment as a model system to investigate the interaction and effect of S100A4 on myosin IIA using kinetic and other biochemical methods (Badyal *et al.*, 2011).

Aside from heavy chain phosphorylation, the minimal binding site of S100A4 on myosin IIA has also been under question. Although the site was originally mapped to residues A1907-G1938 (Kriajevska *et al.*, 1998), this was again disputed by Malashkevich *et al.*, (2008) who claimed the minimal site was shorter, consisting of residues A1907-R1923. However, our group re-examined this showing the minimal binding site represents at least residues A1907-G1938 (Badyal *et al.*, 2011). To further characterise the binding site, we have collaborated with structural biologists who recently resolved the structure of the S100A4-myosin IIA interaction using NMR spectroscopy (Elliott *et al.*, 2012) and concluded the minimal binding site represents a peptide consisting of residues Q1897-A1935 (M39) in agreement with our earlier studies. Given these structural data, it would therefore be possible to rationally design myosin IIA-specific mutants of S100A4 that could be used to probe the effect of S100A4 *in vivo*.

Accordingly, the second part of this work was to characterise the interaction of M39 with WT S100A4 and design single-residue mutants of S100A4 that would abolish the interaction with myosin IIA *in vitro*. These same mutants would then be used *in vivo* to explore myosin IIA-dependent effects of S100A4 on cell migration and cell spreading.

5.2 Results

5.2.1 Cloning of phosphomimetic M200 mutants

To explore the effect of heavy chain phosphorylation on the interaction with S100A4, phosphomimetic mutants of Ser1916 and Ser1943 were cloned. The starting template for PCR was the pre-existing M200 cDNA cloned into the T7 inducible prokaryotic expression vector, pET28a. M200 corresponds to the last 200 amino acids of myosin IIA (Figure 5.1). This vector contains a T7 promoter and when transformed into T7 bacterial strains, recombinant protein can be expressed using IPTG. In addition, inserts cloned into the multiple cloning site have an N-terminal 6X-Histidine tag to facilitate protein purification.

Since only single mutations had to be made for each construct, a site-directed mutagenesis cloning strategy was used. Forward primers were first designed containing mutations in the middle of each primer to mutate the serine to an aspartate (See Materials and Methods) and either side of the mutation, 13-15 bases of complementary sequence was added. The reverse primer was complementary to the forward primer, thereby enabling whole-scale amplification of the plasmid excluding the need for addition of restriction sites or ligation.

DNA amplified by KOD polymerase was digested with DpnI to remove methylated (i.e. parental) DNA and then transformed into XL-1 Blue *E.coli* cells. Two single colonies for each mutant were grown and plasmid DNA isolated. Analysis of plasmid DNA by gel electrophoresis (Figure 5.2) demonstrated single bands at approximately 6 kb consistent with the predicted size of the plasmid. The insert of each plasmid was then sequenced to ensure the correct mutation had been introduced and no spurious mutations had arisen from the PCR amplification. Following this, one plasmid for each mutant was transformed into the T7 expression strain, BL21 DE3.

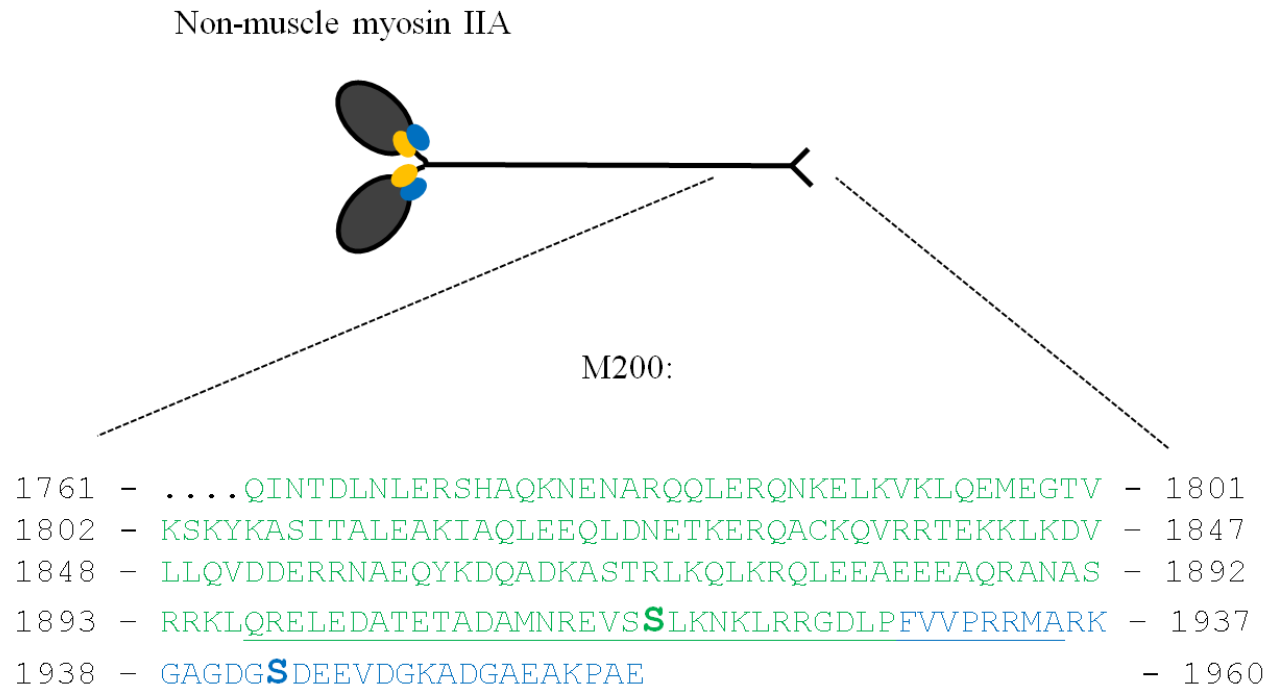


Figure 5.1: Schematic representation of a M200, a C-terminal fragment of non-muscle myosin IIA

M200 represents the last 200 amino acids (Q1761-E1960) of non-muscle myosin IIA incorporating the end of the coiled-coil (green residues) and the non-helical tail (blue residues). The residues representing the S100A4 binding site (as determined by Elliott et al., (2012)) are underlined. Two serine residues, S1916 and S1943 which can be phosphorylated are highlighted in bold.

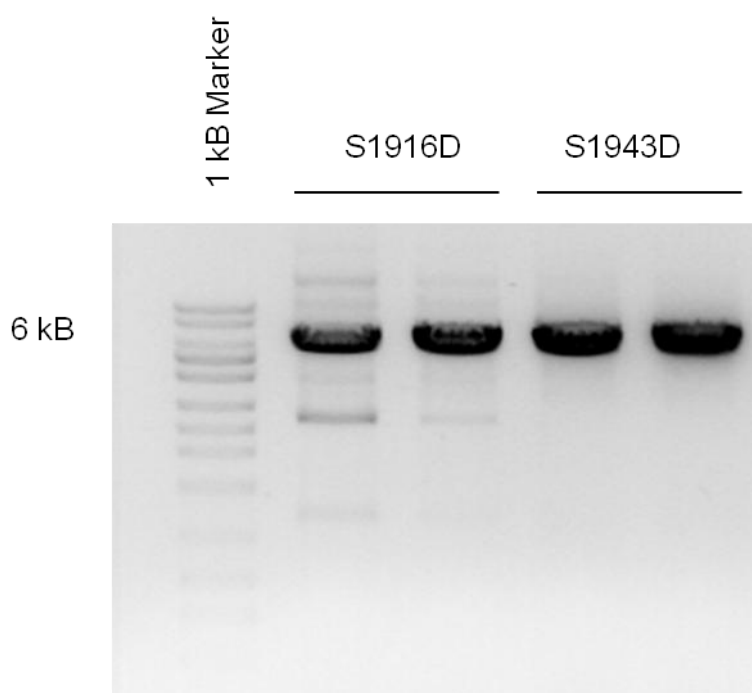


Figure 5.2: Analysis of S1916D and S1943D plasmid DNA by gel electrophoresis

Plasmid DNA from two separate colonies was isolated for each S1916D and S1943D mutant. 0.5 μg DNA was loaded on to a 1% TAE agarose gel and visualised using ethidium bromide. The major band represents the plasmid migrating at approximately 6 kb, consistent with the predicted size of the plasmid.

5.2.2 Protein expression trials

Small-scale expression trials were first conducted to confirm that these constructs yielded protein at the correct molecular weight. Single colonies grown overnight were diluted 10-times and then grown in the presence and absence (to ensure integrity of the inducible system) of IPTG for 2 hours. Lysates were collected and analysed by SDS-PAGE (Figure 5.3) indicating bands of correct molecular weight only in the presence of IPTG for both mutants.

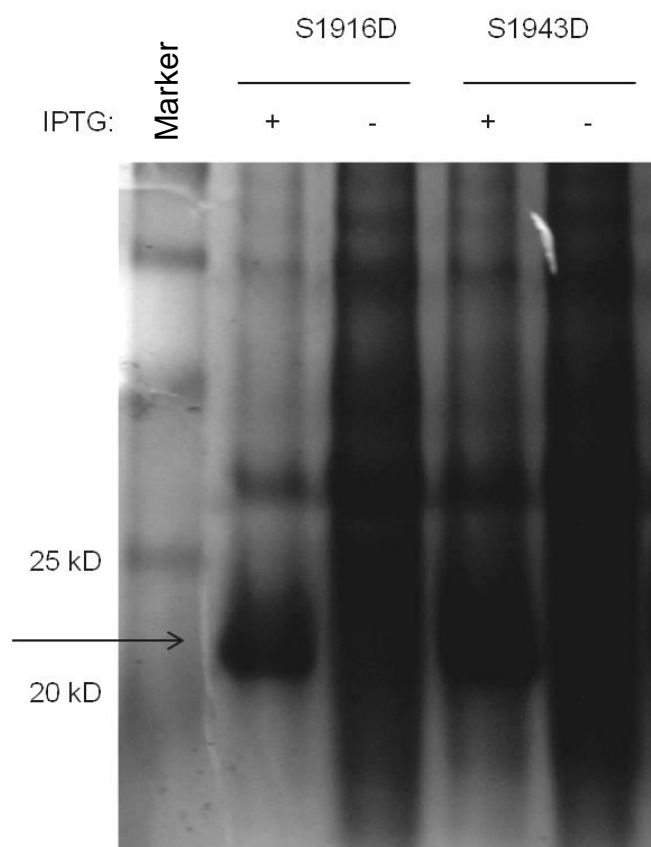


Figure 5.3: Expression of S1916D and S1943D protein in the presence or absence of IPTG

S1916D and S1943D colonies grown overnight were diluted 10-times and then incubated in the presence (+) or absence (-) of 200 μ M IPTG for 2 hours. Bacterial lysates were resolved on a 15% gel and stained with coomassie dye. The arrow indicates a major band present only in the induced samples at approximately 23 kD, consistent with the calculated size of S1916D and S1943D.

5.2.3 Large-scale expression and purification

Having confirmed the protein expression of each mutant, large-scale grow-ups were undertaken to produce enough protein for biochemical assays. In total, 8 litres of bacteria were prepared for both mutants and after inducing with IPTG, cultures were grown for 48 hours at 30°C before harvesting by centrifugation. Bacterial pellets were resuspended in lysis buffer and soluble protein applied to a Ni-NTA agarose column before washes to remove non-specific proteins and elution with imidazole. Eluted protein was collected in 2 ml aliquots and every third fraction assessed by UV spectroscopy (Figure 5.4).

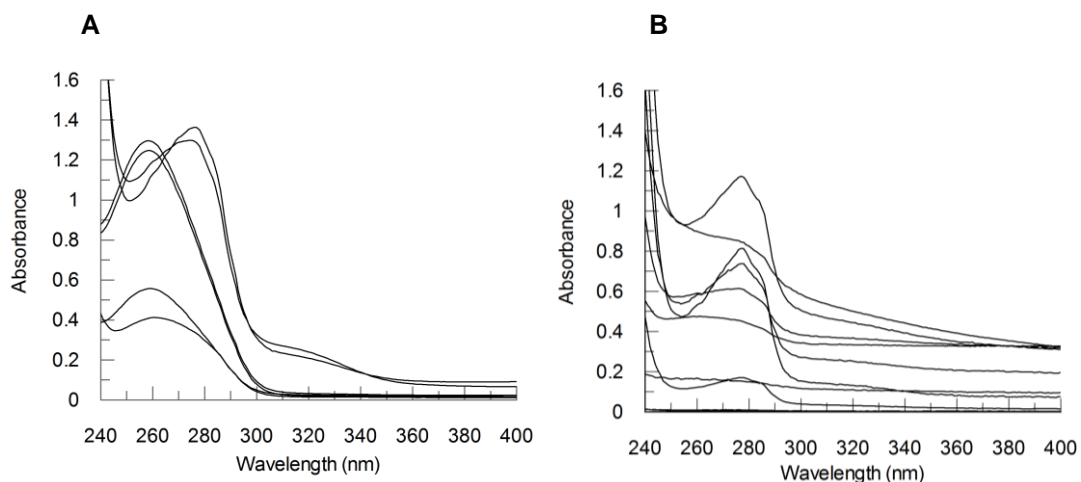


Figure 5.4: UV Spectroscopy of eluted fractions to assess the presence of S1916D or S1943D protein

Fractions eluted from the Ni-NTA agarose column using imidazole were analysed by UV spectroscopy between 240 and 400 nm to assess the presence of protein (peaks at 280 nm). Representative scans of S1916D (A) and S1943D (B). Each trace represents a separate fraction.

Fractions that contained a major peak at 280 nm were then analysed by SDS-PAGE (Figure 5.5) which showed large bands at the correct molecular weight.

To further purify the protein and aid buffer exchange, a gel filtration column was used which separates proteins based on size. After gel filtration, pooled protein fractions were concentrated and the final protein analysed by SDS-PAGE showing single bands for both S1916D and S1943D mutant proteins at the correct molecular weight, consistent with the wild-type M200 protein (Figure 5.6). The concentration of S1916D and S1943D was determined at physiological pH using an absorption co-efficient (determined from amino acid composition [Gasteiger *et al.*, 2005]) of $2980 \text{ M}^{-1} \text{ cm}^{-1}$ at 280 nm. In total, over 100 milligrams of soluble protein was recovered for both mutants.

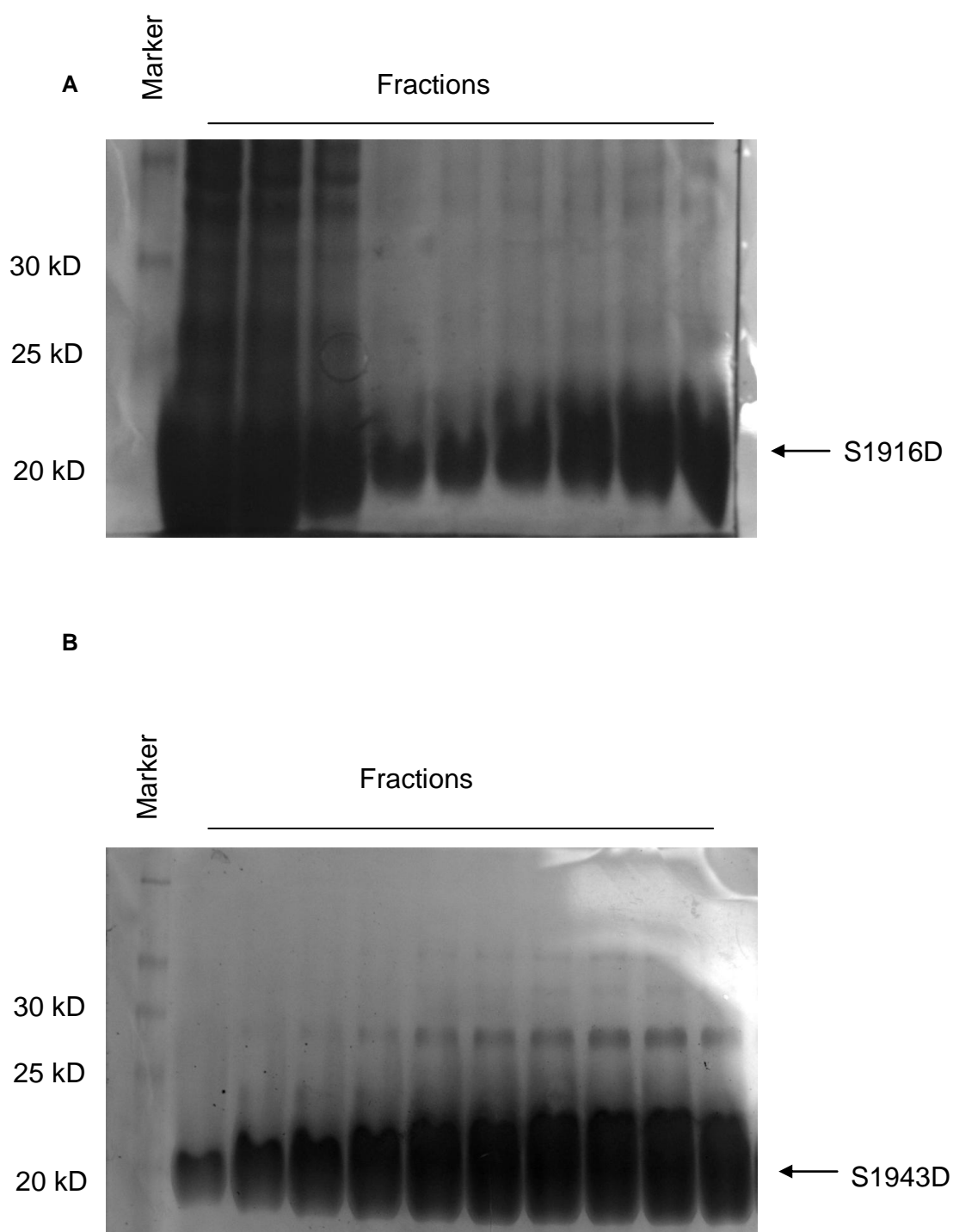


Figure 5.5: SDS-PAGE analysis of fractions containing S1916D and S1943D as identified by UV

Fractions containing significant peaks at 280 nm were resolved on 15% SDS-PAGE gels to assess purity. (A) S1916D, (B) S1943D. Major bands were present for all fractions at approximately 23 kD.

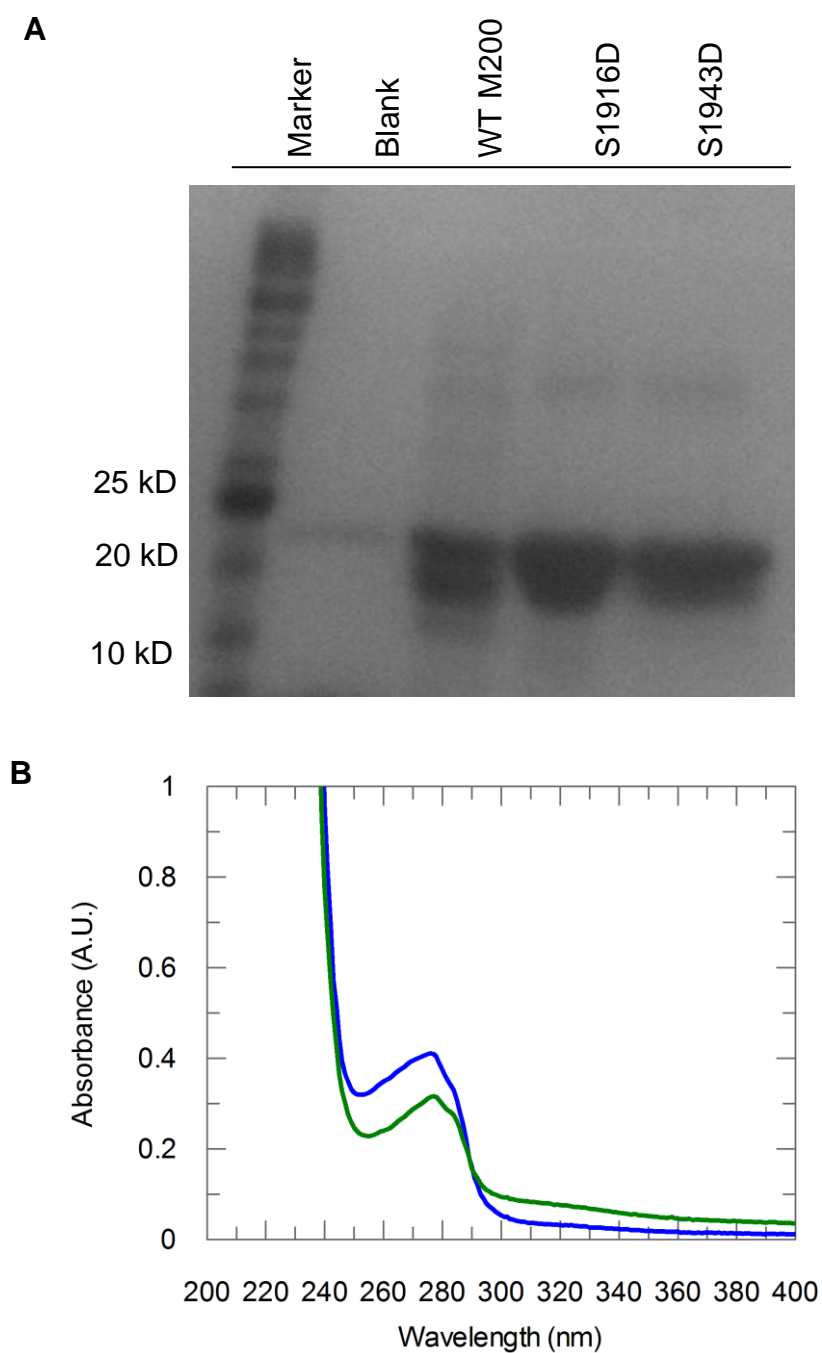


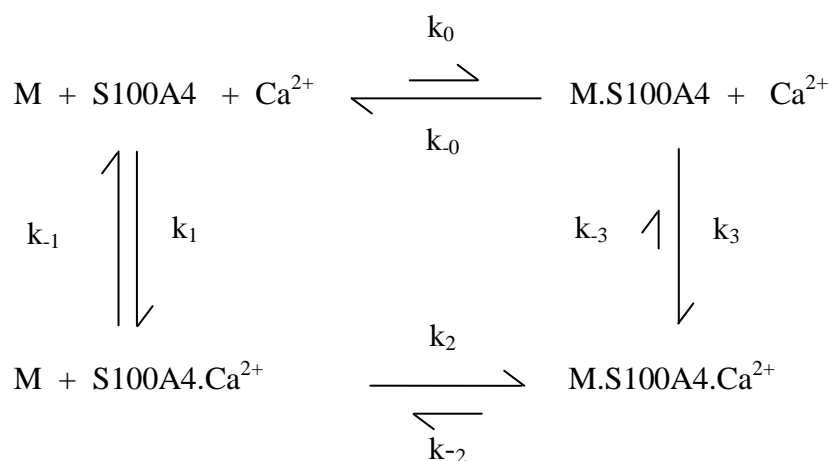
Figure 5.6: UV Spectropic and SDS-PAGE Analysis of Purified S1916D and S1943D

Following gel filtration and concentration, S1916D and S1943D protein was analysed by (A) SDS-PAGE and (B) UV spectroscopy. Both confirm the presence of highly purified protein consistent with WT M200 (A).

5.2.4 Characterising the interaction between S100A4 and phosphomimetic Forms of M200

To assess the interaction between S100A4 and the two phosphomimetic forms of M200, S1916D and S1943D, transient kinetic methods based on stopped flow spectroscopy were carried out. These assays were previously developed by our group to characterise the interaction between S100A4 and tail fragments of wild-type non-muscle myosin IIA (Badyal *et al.*, 2011). They are based on the high-affinity calcium chelator and fluorescent indicator, Quin-2 which when bound to calcium has an emission profile at 452 nm when excited with light at 336 nm. Since thermodynamic linkage (Badyal *et al.*, 2011) requires the target-bound form of S100A4 to bind calcium more tightly than in the absence, it is a convenient measure to assess the interaction between S100A4 and interacting proteins or peptides. The minimal pathway describing the interaction between myosin, S100A4 and Ca^{2+} is presented in Scheme 5.1 as defined by Badyal *et al.*, (2011).

Scheme 5.1: Ca^{2+} and myosin (M) binding to S100A4



5.2.4.1 Effect of Ca^{2+} -dissociation from the $\text{S100A4.Ca}^{2+}\text{.M200}$ complex

To first test the conditions for the assay, S100A4 and Ca^{2+} were preloaded in one syringe and pushed against an excess of Quin-2 to derive an observed profile, as seen in Figure 5.7A. When fitted to a double exponential, the major phase yielded a k_{obs} of 15.4 s^{-1} (89% amplitude) and a minor phase (11% amplitude) of 3.6 s^{-1} defining the rate constant of k_1 (Scheme 5.1). The former represents calcium dissociation from the dimer, whereas the latter, slower phase likely corresponds to higher order S100A4 structures (tetramers, oligomers) that have a greater affinity for Ca^{2+} and thus a reduced dissociation rate constant (Badyal *et al.*, 2011). This was important to account for during analysis since it could otherwise affect interpretation of rate constants in the presence of interacting protein.

When stoichiometric concentrations of wild type (WT) M200 were added to the S100A4/ Ca^{2+} syringe, the dissociation rate constant of Ca^{2+} from the S100A4. $\text{Ca}^{2+}\text{.WT}$ M200 complex reduced to 0.33 s^{-1} (Figure 5.7B) corresponding to k_3 of Scheme 5.1. This was derived from a fit to triple exponential to account for three possible species: S100A4 dimer, S100A4 higher order structure and S100A4 bound to interacting protein. These results were consistent with those reported for WT M200 by Badyal *et al.*, (2011). Having established this, the dissociation rate constants for Ca^{2+} release from S1916D (Figure 5.7C) and S1943D (Figure 5.7D) complexed with S100A4 were measured by the same methods and yielded values similar to WT M200 of 0.29 and 0.39 s^{-1} , respectively (summarised in Table 5.1). Taken together, these data suggest the substitution of negatively charged residues at S1916 or S1943 does not significantly affect the interaction between M200 and S100A4.

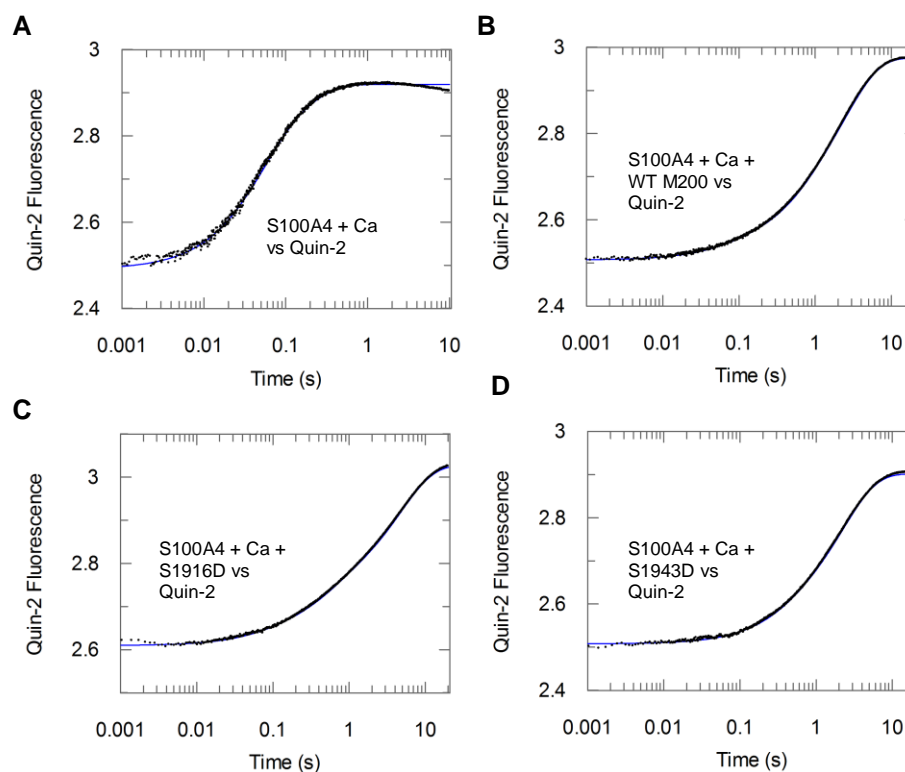


Figure 5.7: Dissociation of Ca^{2+} from S100A4 Monitored Using Quin-2 Fluorescence in the Presence and Absence of Myosin Proteins.

(A) Solution containing 13 μM S100A4 and 50 μM Ca^{2+} was pushed against 100 μM Quin-2 (stopped flow reaction chamber concentrations). A fit to a double exponential yielded rate constants of 15.4 s^{-1} ($A=89\%$) and 3.6 s^{-1} ($A=11\%$). (B), (C), (D) As in (A) but with 13 μM WT M200 (B), 13 μM S1916D (C) and 13 μM S1943D (D) premixed with S100A4. (B), (C) and (D) were fit to triple exponentials; the rate constants and associated amplitudes are summarised in Table 5.1. All experiments were carried out in 500 mM NaCl, 20 mM HEPES, 1 mM MgCl_2 at pH 7.5 and 20 °C. Each exponential was the average of 3-4 individual traces. Fits to exponentials are represented by the solid, blue line.

Table 5.1: Summary of rate constants and associated amplitudes from Figure 5.7

Fits to triple exponentials. Associated error from all fits was less than 1% for each condition.

	WT M200	S1916D	S1943D
k_1 (s^{-1})	15.39	15.42	14.38
A_1	0.01	0.01	0.01
k_2 (s^{-1})	0.33	0.20	0.38
A_2	0.36	0.29	0.33
k_3 (s^{-1})	1.75	2.17	2.98
A_3	0.04	0.02	0.03

5.2.4.2 Ionic dependence of S1916D and S1943D on filament formation

Since phosphorylation of S1916 and S1943 residues has been shown to affect filament formation (Dulyaninova *et al.*, 2005; Dulyaninova *et al.*, 2007), the ionic dependence of S1916D and S1943D solubility was investigated. WT M200 has previously been used as a model system to study the solubilisation of myosin by S100A4 (Badyal *et al.*, 2011). It forms filaments at low ionic strength that can be measured at an apparent absorbance of 300 nm due to an increase in turbidity of the solution. Formation of these filaments is dependent on ionic strength with the midpoint for WT M200 approximately 120 mM NaCl at 5 μ M (Badyal *et al.*, 2011).

Accordingly, 5 μ M of either S1916D or S1943D was added to buffer containing 20 mM NaCl to give a final concentration of approximately 40 mM NaCl and the absorbance measured after reaching equilibrium (Badyal *et al.*, 2011). The ionic strength was steadily increased with aliquots of NaCl and the absorbance measured after each addition until a background level of absorbance had been reached. Plotting the absorbance versus the NaCl concentration gave rise to a sigmoid curve and midpoint values of 72 mM and 100 mM for S1916D and S1943D respectively (Figure 5.8).

Both these values were significantly lower than the midpoint value reported for WT M200 suggesting that phosphomimetic forms of M200 are more soluble at physiological ionic strength, consistent with previous reports. Despite this, it is still of interest whether or not S100A4 is able to further promote the solubility of S1916D and S1943D and as such the effect of filament solubilisation by S100A4 was next investigated.

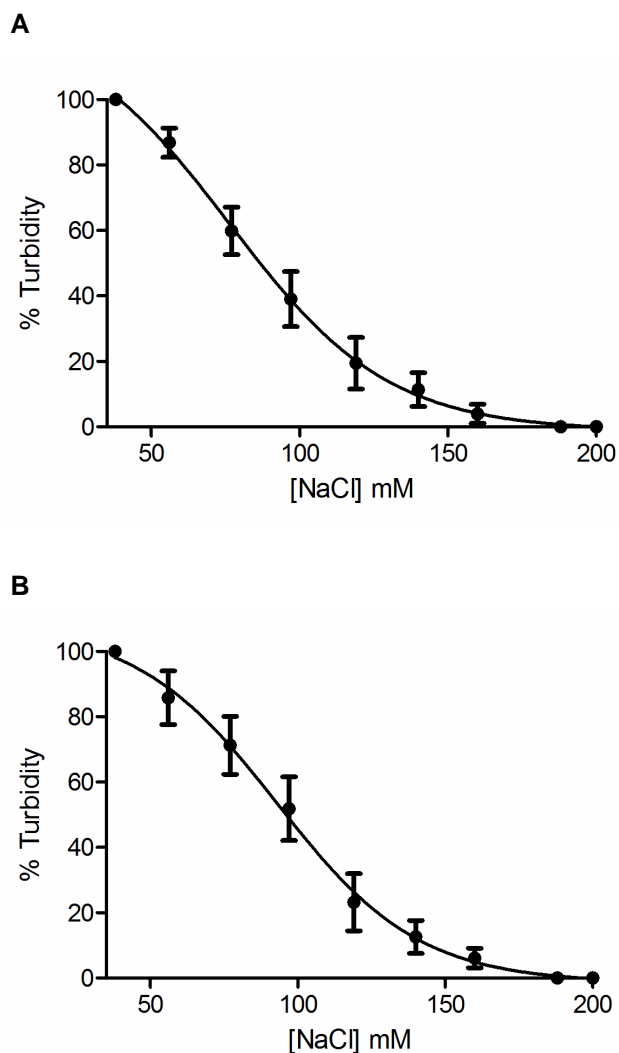


Figure 5.8: Turbidity of S1916D and S1943 as a function of [NaCl]

5 μM of S1916D (A) or S1943D (B) was added to buffer containing 20 mM NaCl, 10 mM HEPES, 0.1 mM Ca^{2+} at pH 7.5 and the turbidity measured at an absorbance of A_{300} . Aliquots of 500 mM NaCl were added and the absorbance measured until a background level had been achieved (approximately 200 mM NaCl). % turbidity values (absorbance value/maximal absorbance (%)) were plotted as a function of NaCl concentration and fit to a sigmoid curve to yield midpoint values for S1916D and S1943D of 72 mM and 100 mM respectively. Absorbance values were corrected for the dilution (by addition of NaCl aliquots) of S1916D or S1943D. Values represent means from two independent experiments and error bars are standard deviations.

5.2.4.3 *Disassembly of filaments by S100A4*

According to the stopped flow experiments, S100A4 was able to interact with both S1916D and S1943D to a similar extent to WT M200; as a result, it would be expected that S100A4 would solubilise S1916D and S1943D filaments in a similar manner. Since S1916D and S1943D have different ionic dependencies, the midpoint value for each protein was taken as the final concentration of NaCl used for the turbidity assay buffer. Addition of 5 μM S1916D or S1943D gave a rise in turbidity that was fully solubilised with 10 μM S100A4 (i.e. twice stoichiometric) in the presence of calcium. Addition of 0.5 mM EGTA was sufficient to increase the turbidity to initial levels while excess Ca^{2+} reversed the process to cause re-solubilisation (Figure 5.9). These profiles were similar to that obtained for WT M200 (Badyal *et al.*, 2011) suggesting that S100A4 is able to significantly interact with phosphomimetic forms of M200 in the conditions used in this assay, thus effecting filament solubilisation.

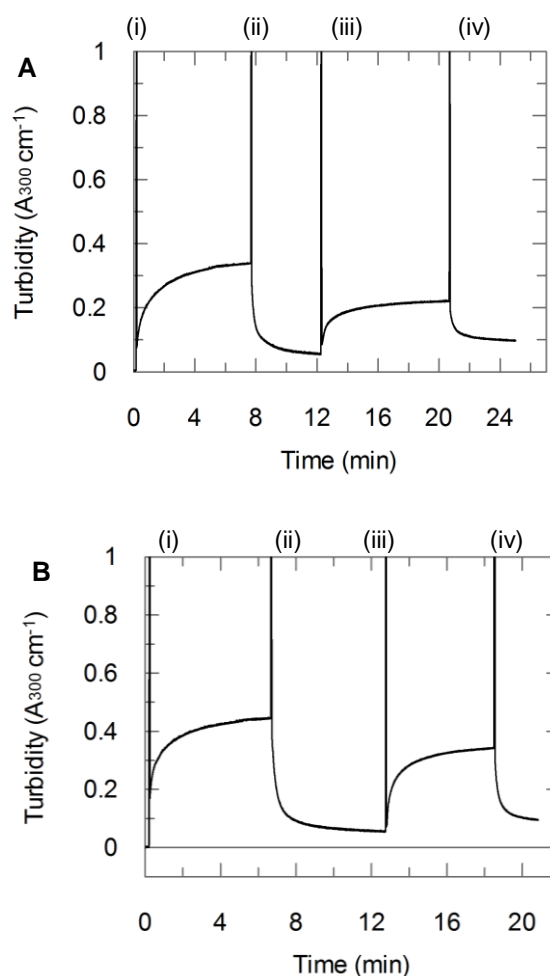


Figure 5.9: Dissociation of S1916D or S1943D filaments by S100A4

(i) 5 μM of S1916D (**A**) or S1943D (**B**) was added to a buffer containing 10 mM HEPES, 0.1 mM Ca^{2+} at pH 7.5 to give a final concentration of NaCl of 72 mM (A) or 100 mM (B). A rise in turbidity was recorded for 420 s. (ii) 10 μM S100A4 was added to disassemble myosin filaments; (iii) 0.5 mM EGTA was added to chelate Ca^{2+} ; (iv) 2 mM Ca^{2+} was added to resolubilise myosin. Results are representative of experiments performed on two separate occasions.

5.2.5 Characterising the interaction of S100A4 with a minimal binding peptide of myosin IIA

As stated in the introduction, our collaboration with structural biologists has recently resulted in the structure of the S100A4-myosin IIA complex being determined by NMR spectroscopy (Elliott *et al.*, 2012). Extending our previous work (Badyal *et al.*, 2011), the minimal binding site of myosin IIA represents a peptide of 39 residues (M39), overlapping the end of the coiled-coil and start of the non-helical tail (Figure 5.10).

Structurally, the M39 peptide forms a helix positioned across the EF hands of both S100A4 monomers, linking each hydrophobic binding pocket. Interestingly, this results in each S100A4 subunit interacting with opposite ends of M39, leading to an asymmetric binding mode, a unique form of interaction for S100 proteins (Figure 5.11).

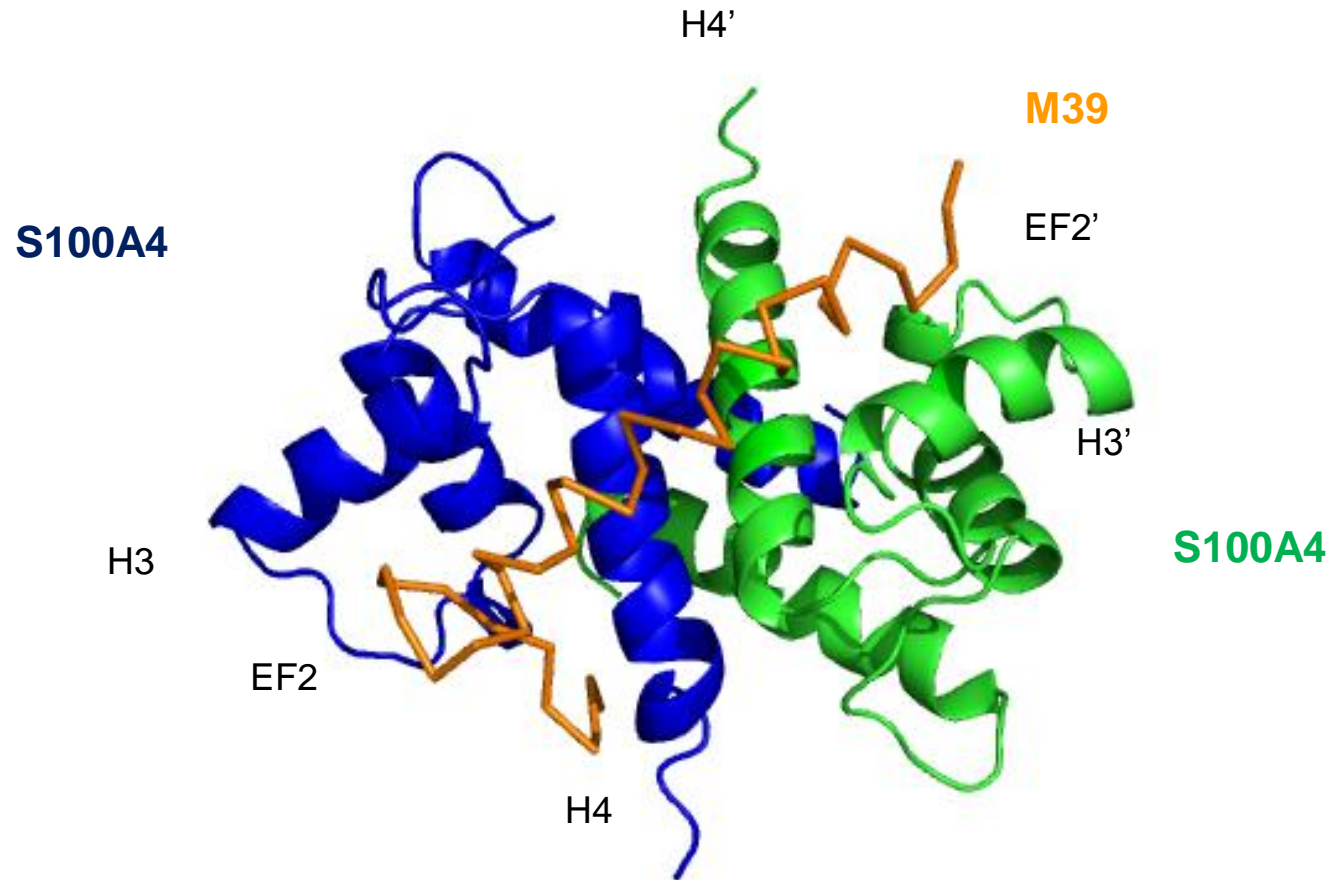


Figure 5.11: Structure of S100A4 complexed with a C-terminal fragment of myosin IIA(M39)

An S100A4 dimer (monomer 1, blue; monomer 2, green) is shown complexed with M39 which forms a helix positioned across EF hands of both monomers. The myosin helix forms extensive contacts with the surface residues of S100A4, particularly at the hydrophobic pockets between helix 3 (H3), helix 4 (H4) and EF hand 2 (EF2) of each S100A4 monomer. This leads to an asymmetric interaction, where each hydrophobic cleft is interacting with opposite ends of the myosin helix. PDB = 2LNK; image constructed using Pymol (Version 1.3)

5.2.5.1 Kinetic characterisation of S100A4 and M39

To first characterise the interaction between S100A4 and M39, stopped flow techniques were used as previously described. M39, a 39 amino acid-long peptide was chemically synthesised corresponding to residues Q1897 to A1935 of the heavy chain of myosin IIA.

5.2.5.1.1 Ca^{2+} -dissociation from the S100A4. Ca^{2+} .M39 complex

Calcium dissociation was measured with stoichiometric concentrations of M39 and S100A4 yielding a rate constant of 0.06 s^{-1} (81% A) representing calcium dissociation from the S100A4. Ca^{2+} .M39 complex (Scheme 5.1; k_{-3}) (Figure 5.12). This is approximately similar to the dissociation rate constant for S100A4 complexed with M200 ($k_{\text{off}} = 0.3\text{ s}^{-1}$; Figure 5.6) suggesting M39 represents the S100A4 binding site. Furthermore, comparison of this value with a shorter myosin peptide of the same region, M32, which has a k_{off} two orders of magnitude greater ($k_{\text{off}} = 6\text{ s}^{-1}$) (Badyal *et al.*, 2011) further suggests that the additional residues that make up M39 are critical in the S100A4-myosin IIA interaction.

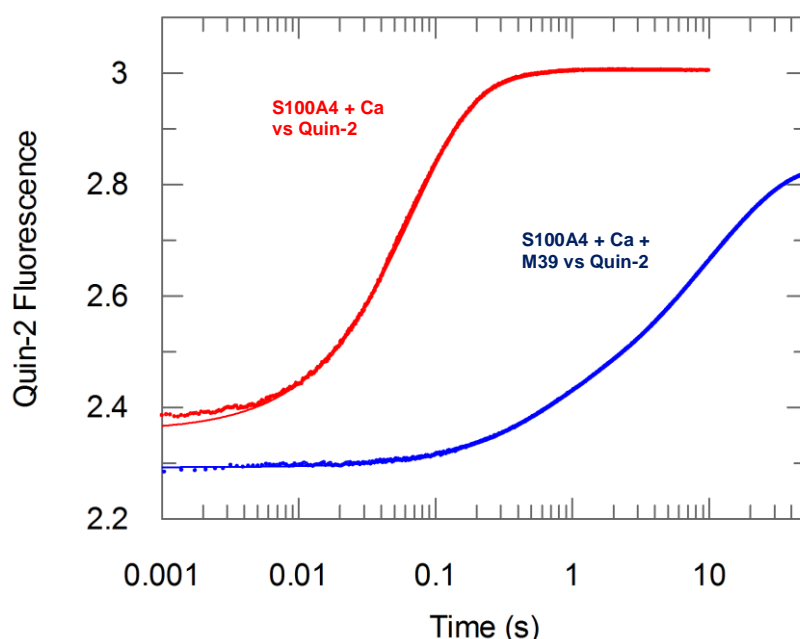


Figure 5.12. Dissociation of Ca^{2+} from S100A4 monitored using quin-2 fluorescence in the presence and absence of M39

Solution containing $13\text{ }\mu\text{M}$ S100A4 in the absence (red trace) or presence of $13\text{ }\mu\text{M}$ M39 (blue trace) was pushed against $100\text{ }\mu\text{M}$ Quin-2 (stopped flowed reaction chamber concentrations). A triple exponential for S100A4 in the presence of M39 yielded rate constants of 0.06 s^{-1} (A=81%), 1.4 s^{-1} (A=17%) and 14.7 s^{-1} (A=2%). All experiments were carried out in 10 mM HEPES, 20 mM NaCl, $100\text{ }\mu\text{M}$ Ca^{2+} , 1 mM $MgCl_2$, pH 7.5 at $20\text{ }^\circ\text{C}$.

5.2.5.1.2 Calculation of the equilibrium dissociation constant for Ca²⁺-bound S100A4 interacting with M39

Although measuring the calcium dissociation from the S100A4.Ca²⁺.M39 complex provides an indirect estimate of the binding affinity between S100A4.Ca²⁺ and M39, it is of interest to directly calculate the K_d between these two species as this represents the most likely thermodynamic route for formation of the S100A4.Ca²⁺.M39 complex (Scheme 5.1; k₂ and k₋₂). To determine the K_d for Ca²⁺-bound S100A4 binding to M39, the association and dissociation rate constant for this interaction were calculated individually. For the association rate constant a competition assay was used. In essence, this was based on the stopped flow measurements to calculate the Ca²⁺ dissociation of S100A4 from the S100A4.Ca²⁺.M39 complex; however, instead of including M39 in the same syringe as S100A4 it was added to the syringe containing Quin-2. Thus conditions were established whereby M39 and Quin-2 would compete for the S100A4.Ca²⁺ complex, either slowing Ca²⁺ dissociation to approximately 0.1 s⁻¹ (M39 binding followed by Quin-2 dissociation) or dissociating the S100A4.Ca²⁺ complex (initial Quin-2 binding) at 15 s⁻¹. When the amplitudes of these two phases are equal, it suggests that the apparent association rate constant (k_{on} apparent) of S100A4.Ca²⁺ and M39 is equal to the dissociation rate constant of the S100A4.Ca²⁺ complex i.e. 15 s⁻¹. Since this is the time it takes for Quin-2 to dissociate 2 sets of calcium ions from the S100A4 dimer, the M39 k_{on} apparent should be twice as large, 15 x 2 or 30 s⁻¹. Consequently, the association rate constant can be calculated by dividing the k_{on} apparent by the concentration of M39 when amplitudes of the slow and fast phases are equal.

Accordingly, the concentration of M39 added to the syringe containing Quin-2 was varied between 0 and 30 μM and plotted as a function of the relative amplitude of the fast phase and fit to a kinetic model derived from the modelling software Berkeley Madonna (Figure 5.13). This yielded a 50% value (where the slow and fast phases are equal) of approximately 2.5 μM and thus an association rate constant of approximately 12 μM⁻¹ s⁻¹ (=30 s⁻¹/2.5 μM). Combining this value with the dissociation rate constant (k₋₂) of 0.001 s⁻¹ calculated from an anisotropy assay (Elliott *et al.*, 2012), the equilibrium dissociation constant for calcium-bound S100A4 interacting with M39 is 0.001 s⁻¹/12 μM⁻¹ s⁻¹ (k₋₂/k₂) or ~0.1 nM which represents an extremely tight binding interaction for a protein-protein complex.

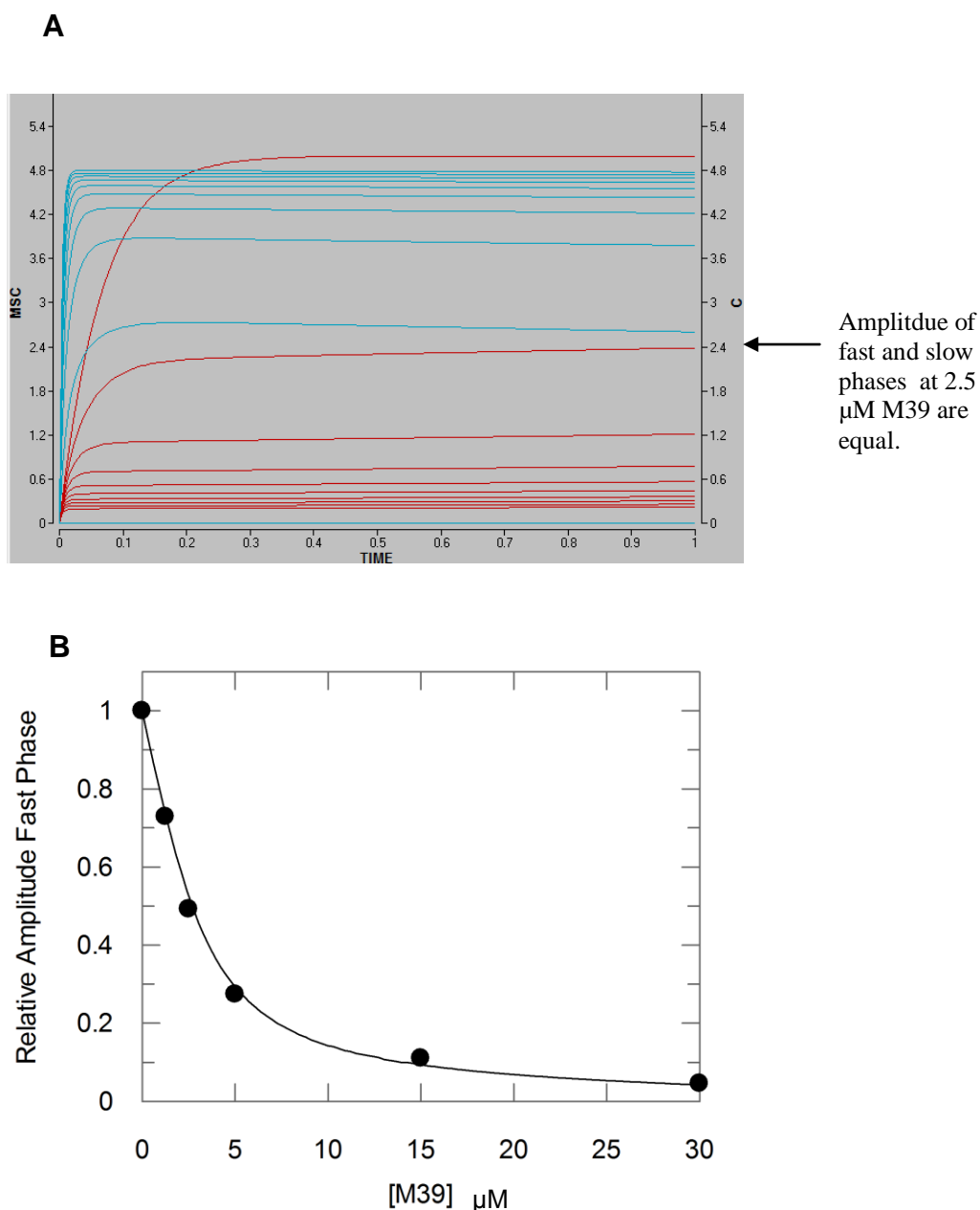


Figure 5.13 Competition assay to determine the association rate constant for M39 binding to the S100A4.Ca²⁺ Complex

(A) Kinetic simulations of Quin-2 and M39 competing for the S100A4.Ca²⁺ complex at increasing concentrations of M39 modelled using Berkeley Madonna software. Red and blue traces represent the amplitude of the slow and fast phase, respectively. When the end-points of the red and blue traces are approximately equal, this indicates the concentration of M39 required for a k_{on} apparent of 30 s⁻¹ (15 s⁻¹ x2 since there are two sets of calcium ions on the dimer). (B) Solution containing 13 μM S100A4 and 50 μM Ca²⁺ was pushed against 100 μM Quin-2 and concentrations of M39 varying from 0 to 30 μM (stopped flow cell concentrations). Fits to triple exponentials yielded rate constants and associated amplitudes of the fast (Quin-2 binding) and slow (M39 binding) phases of the reaction. The relative amplitude of the fast phase was plotted against the concentration of M39 added and fitted to a kinetic model derived from the Berkeley Madonna software yielding a 50% value of approximately 2.5 μM . All experiments were carried out in 20 mM NaCl, 10 mM HEPES, 1 mM MgCl₂ at pH 7.5 and 20 °C. Each exponential was the average of 3-4 individual traces.

5.2.6 Rational design of S100A4 mutants to perturb the S100A4-myosin IIA interaction

Since the structure of S100A4 and M39 has been resolved, it was possible to rationally design mutants of S100A4 to perturb the interaction with myosin IIA. As many of the S100A4-M39 contacts occur within the hydrophobic pocket (Figure 5.11) that are partially buried in the apo form of the molecule (Gingras *et al.*, 2008), mutation of these residues could lead to instability and thus severely affect calcium binding properties. As a result, residues outside of this region were chosen, V77 and C81, both of which are positioned in helix 4 of each S100A4 monomer contacting the middle of the M39 helix (Figure 5.14A). Furthermore, mutating V77 and C81 would enhance the effect of mutation as each residue from the monomer is involved compared to residues within the hydrophobic pocket which would have a lesser effect due to the asymmetric binding mode. Conversion of these residues to aspartate (V77D and C81D) would be highly unfavourable as it would cause burying of negative charges within the hydrophobic environment of the complex with additional disruption caused by the nearby glutamate of M39, E1913 (Figure 5.14B).

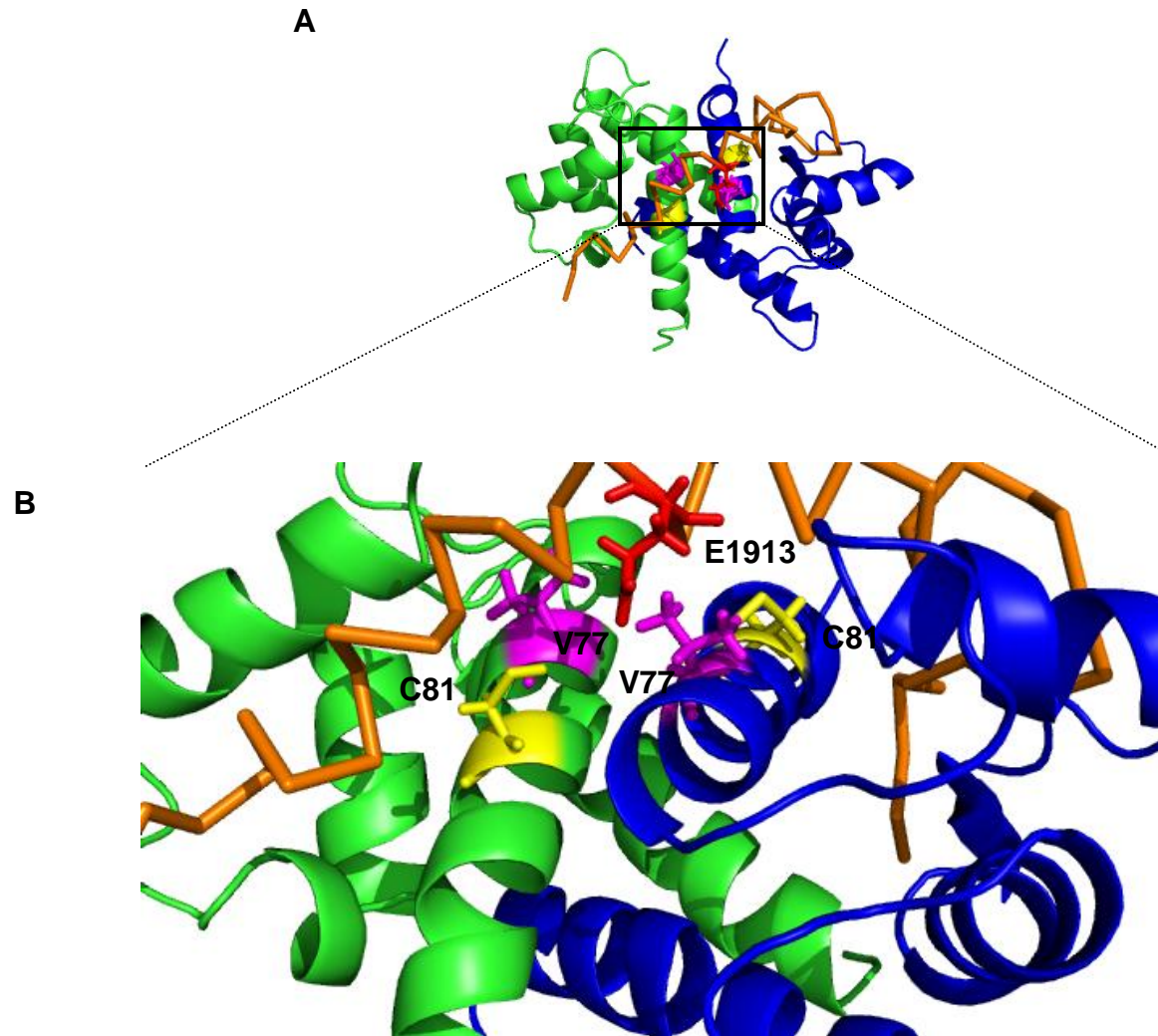


Figure 5.14: Schematic representation of the M39/S100A4 complex and mutated residues

(A) Structure of S100A4 complexed with M39, as in Figure 5.1. (B) Magnification of region containing the S100A4 myosin IIA mutants, V77 (pink) and C81 (yellow). Mutation of these residues to aspartate would be highly unfavourable for complex formation, in part due to the presence of E1913 (red) in M39. PDB = 2LNK; image constructed using Pymol (Version 1.3).

5.2.6.1 Kinetic Characterisation of S100A4 mutants and M39

The effect of V77D and C81D mutants on the myosin interaction was first characterised by stopped flow methods using Quin-2 to measure calcium dissociation from the S100A4.Ca²⁺.myosin complex as previously described. V77D and C81D recombinant protein was kindly provided by Drs. Badyal and Basran (University of Leicester).

In the absence of M39, V77D and C81D both had similar Ca²⁺ dissociation rate constants of 13 s⁻¹ and 8 s⁻¹ respectively, compared to 15 s⁻¹ for the wild-type S100A4, thus confirming that the choice of mutation had not significantly affected the Ca²⁺ binding (Figure 5.15). However, in the presence of stoichiometric concentrations of M39, there was no effect on Ca²⁺-dissociation from V77D or C81D (Figure 5.15) compared with a reduction of the rate constant in the presence of WT S100A4 to 0.06 s⁻¹.

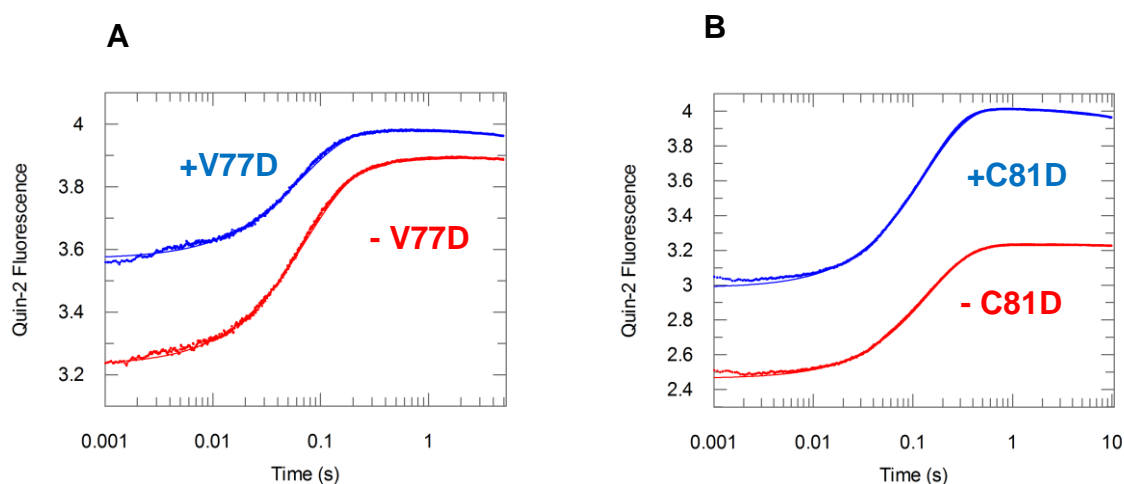


Figure 5.15: Dissociation of Ca²⁺ from V77D and C81D monitored using quin-2 fluorescence in the presence or absence of M39

Solution containing 13 μM V77D (A) and C81D (B) in the absence (red line) or presence of 13 μM M39 (blue line) was pushed against 100 μM Quin-2 (stopped flowed reaction chamber concentrations). Traces were fit to single exponentials to yield rate constants of 13 s⁻¹ and 8 s⁻¹, respectively, in the absence or presence of M39. All experiments were carried out in 10 mM HEPES, 20 mM NaCl, 100 μM Ca²⁺, 1 mM MgCl₂, pH 7.5 at 20 °C. Fits are represented by solid lines.

In addition, concentrations of up to 30 μM M39 (Figure 5.16) also failed to alter Ca^{2+} -dissociation suggesting a reduction in the affinity of V77D and C81D for M39 by several orders of magnitude thus indicating these residues are important in the S100A4-myosin IIA interaction.

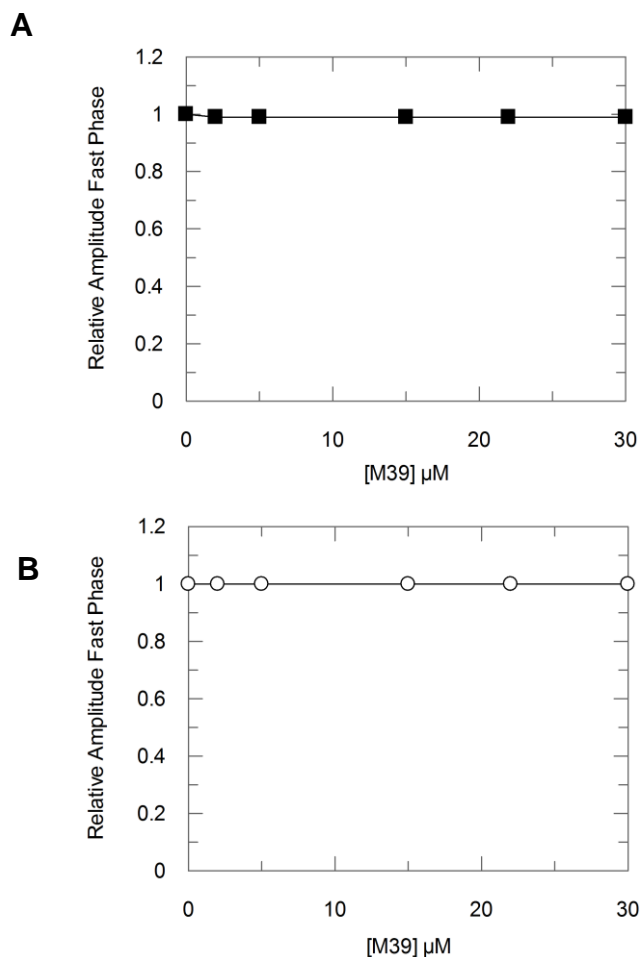


Figure 5.16: Effect of increasing M39 Concentration on Ca^{2+} Dissociation from V77D and C81D

Solution containing 13 μM V77D (A) or C81D (B) and concentrations varying from 0 to 30 μM of M39, were pushed against 100 μM Quin-2 (stopped flow cell concentrations). The relative amplitude of the fast phase (i.e. S100A4. Ca^{2+} .complex) was plotted against the concentration of M39 added indicating no change in the Ca^{2+} dissociation in the presence of peptide. All experiments were carried out in 20 mM NaCl, 10 mM HEPES, 100 μM Ca^{2+} 1 mM MgCl_2 at pH 7.5 and 20 $^\circ\text{C}$. Each exponential was the average of 3-4 individual traces.

5.2.6.2 Investigating the interaction of S100A4 mutants in cells

5.2.6.2.1 Cloning of V77D and C81D S100A4 mutants

Having established the effects of these mutants *in vitro*, the same mutants were examined in A431-teton cells. A431-SIP1 was not used because induction of SIP1 in these cells leads to endogenous expression of S100A4, which would otherwise compete with any mutant protein and potentially mask any effects.

To generate V77D and C81D mutants of S100A4, a pre-existing eukaryotic expression vector was used, pBI-S100A4. pBI is a teton-inducible vector which, in the presence of the reverse tetracycline controlled-transactivator (rtTA) protein, permits Doxycycline-regulated gene transcription. V77D and C81D mutants were engineered using a site-directed mutagenesis approach previously described for phosphomimetic mutants of M200. Oligonucleotides were designed to incorporate valine to aspartate and cysteine to aspartate amino acid substitutions within the middle of each primer pair for V77D and C81D mutants, respectively. pBI-S100A4 WT was used as the starting template and PCR performed with each set of mutant primers. Resulting DNA was transformed into XL-1 Blue *E.coli* and plasmid DNA isolated from two separate colonies for both V77D and C81D. Analysis by DNA gel electrophoresis indicated that mutants 1 and 2 for V77D and mutant 1 for C81D were of the size consistent with the predicted size of the plasmid (Figure 5.17). DNA sequencing confirmed the presence and correct sequence for both pBI-S100A4 V77D mutant 1 and pBI-S100A4 C81D mutant 1.

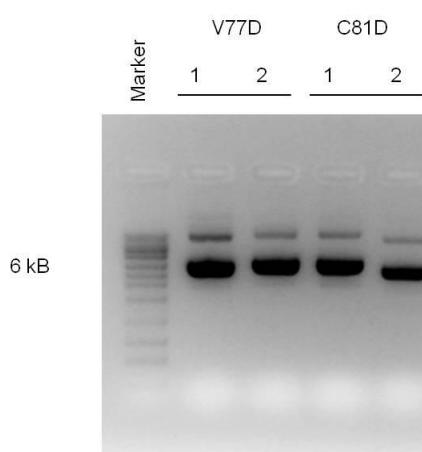


Figure 5.17: Analysis of V77D and C81D plasmid DNA by gel electrophoresis

Plasmid DNA from two separate colonies was isolated for each V77D and C81D mutant. 0.5 µg was loaded on to a 1% TAE agarose gel and visualised using ethidium bromide. The major band represents the plasmid migrating at approximately 6 kB, consistent with the predicted size of the plasmid.

5.2.6.2.2 Effect of S100A4 mutation on the S100A4-myosin IIA interaction

To test the interaction of each mutant with myosin IIA, immunoprecipitation experiments were first carried out. Accordingly, A431-teton cells were transiently transfected with control vector (pBI), pBI-S100A4 WT, V77D and C81D and maintained in the presence of DOX for 48 hours. Cells were lysed in IP buffer and S100A4-protein complexes immunoprecipitated using a S100A4 antibody. Analysis of input lysates by Western blotting indicated similar levels of expression for WT S100A4, V77D and C81D; however, only the antibody to WT S100A4 was able to precipitate significant quantities of myosin IIA with no readily detectable bands present for either V77D or C81D (Figure 5.18). These data therefore support the *in vitro* data, suggesting that V77 and C81 are crucial residues for the interaction between S100A4 and myosin IIA.

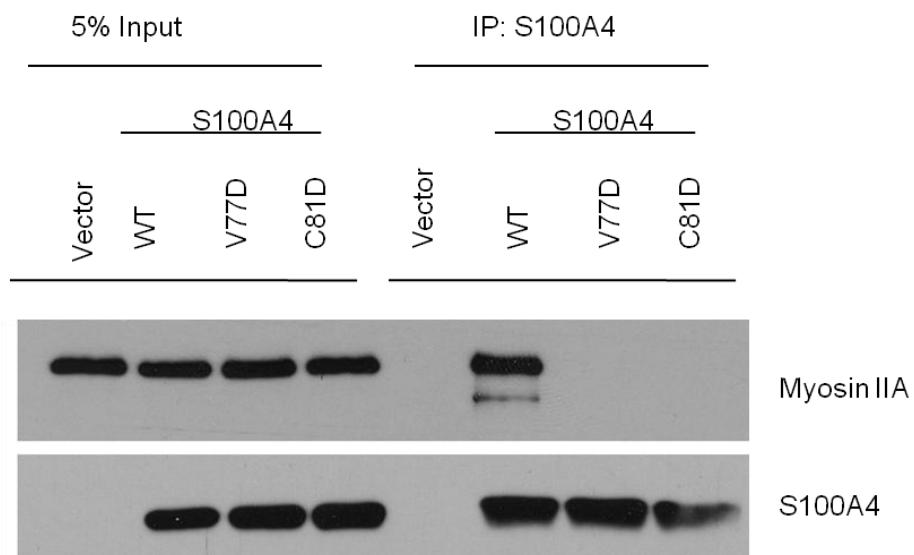


Figure 5.18: Immunoprecipitation analysis of WT S100A4, V77D and C81D

A431-teton cells transfected with control vector, WT S100A4, V77D and C81D were maintained in the presence of Dox for 48 hours. Cells were lysed in IP buffer and S100A4-protein complexes immunoprecipitated with a S100A4 antibody. Lysates were resolved by SDS-PAGE and membranes stained for S100A4 and myosin IIA using Western blotting. 5% input lysate was also analysed as a loading/expression control.

5.2.6.2.3 Intracellular Distribution of S100A4 mutants in vivo

Although the *in vitro* evidence suggested that the V77D and C81D mutant proteins behaved similarly to WT S100A4 with similar Ca²⁺ dissociation rate constants (Figure 5.15), the intracellular distribution of V77D and C81D was next examined to assess the effect of these mutations on localisation or aggregation. Accordingly, transfected cells were stained for S100A4 and myosin IIA using immunofluorescence. Confocal analysis displayed a granular distribution with some nuclear expression for WT S100A4, as well as for mutant V77D and C81D (Figure 5.19). Thus, V77D and C81D were expressed normally, and exhibited no sign of mis-localisation or aggregation.

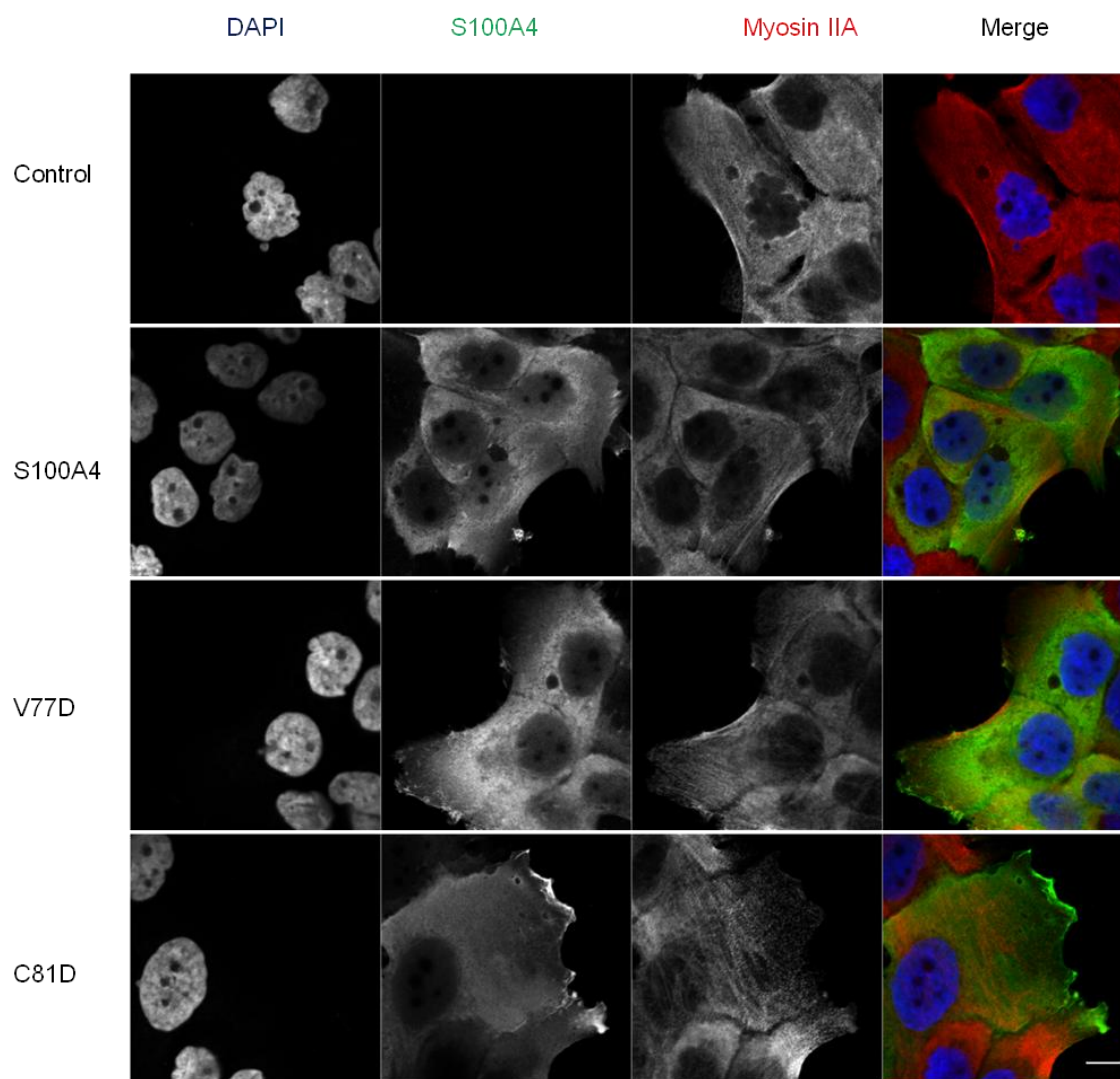


Figure 5.19: Immunofluorescence analysis of WT S100A4, V77D and C81D

A431-teton cells transfected with control vector, WT S100A4, V77D and C81D were maintained in the presence of Dox for 48 hours. Cells were stained with for S100A4 (red) and myosin IIA (green) using immunofluorescence; cell nuclei were visualised with DAPI. Scale bar = 10 μ m.

5.2.6.2.4 Effect of S100A4 mutants on cell migration

Since S100A4 has been strongly implicated in cell migration in a number of cell models (Tarabykina *et al.*, 2007), the effect of WT and S100A4 mutants were next investigated. Because V77D and C81D significantly decrease the interaction with myosin IIA, it would be expected that they would also have a reduced effect on cell migration compared to WT S100A4. To investigate this, a transwell assay was used as previously described. Transiently-transfected A431-teton cells were maintained in the presence of Dox and after 48 hours resuspended in media without serum and cells seeded in transwell inserts. After 24 hours, the number of migrated cells was counted and the relative rates of migration calculated. Cells transfected with WT S100A4 increased migration by approximately 1.8-times compared to the control vector, a result that was statistically significant ($p = <0.001$). Conversely, V77D and C81D had only minor effects on cell migration, neither of which were statistically significant ($p = >0.05$) (Figure 5.20). Therefore, S100A4 mutants that are unable to interact with myosin IIA abolish the WT effect of S100A4 suggesting that myosin IIA is critical to the S100A4-induced increase in cell migration.

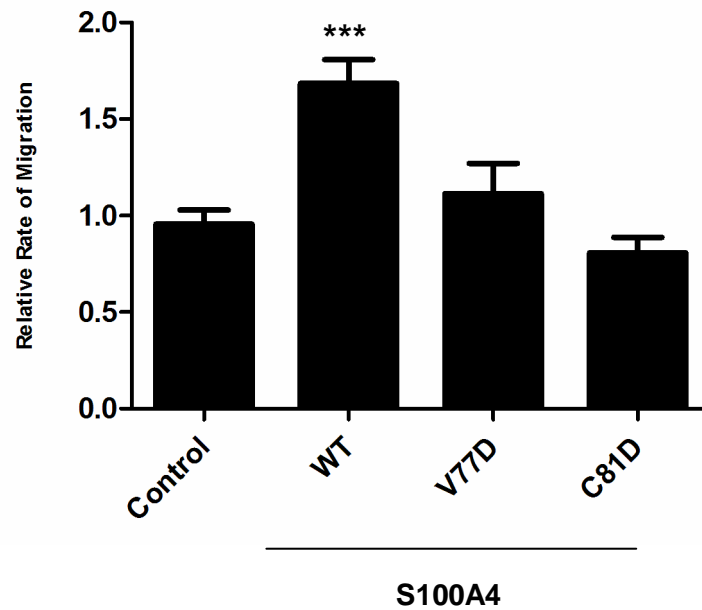


Figure 5.20: Effect of WT S100A4, V77D and C81D on cell migration

A431-teton cells transfected with control vector, WT S100A4, V77D and C81D were maintained in the presence of Dox for 48 hours. 1×10^5 cells were seeded in the upper chamber of fibronectin-coated (5 $\mu\text{g/ml}$) transwell inserts in the absence of serum. Media with 10% serum was placed in the bottom of the chamber to stimulate cell migration and cells allowed to migrate for 24 hours. Migration rates are expressed as the ratio of cells migrated relative to the control vector. Values represent averages of three independent experiments each performed in triplicate. Error bars are SEMs. P values were determined by a one-way ANOVA followed by a Dunnett's Multiple Comparison Test. *** = p value <0.001 , extremely significant.

5.2.6.2.5 Use of cell ECM micropatterns to study the effect of S100A4 on the cytoskeleton

To assess the effects of S100A4 on myosin IIA filaments more directly, a micropattern approach was employed. Micropatterns are a culture substrate with microscopic features that confine cell geometry. In general, they consist of glass coverslips stamped with ECM-proteins (usually fibronectin or collagen) of various shapes and sizes depending on application. They have been used to study many aspects of cellular function including the cytoskeleton, cell polarity and cell adhesion (They, 2010). They have two main advantages over seeding cells on unpatterned substrates (They, 2010). Firstly, by co-ordinating cell geometry, they prevent cells from moving and impose a reproducible shape thus any differences affecting the cytoskeleton become more evident. Secondly, shapes cells adopt in culture are transitory as they permanently disassemble and reassemble their cytoskeleton during translocation but on micropatterns, a so-called steady-state is reached, facilitating cell cytoskeleton analysis and creating more *in vivo*-like conditions.

After initial optimisation, collagen-coated equilateral triangles of $592 \mu\text{m}^2$ were chosen to investigate the effect of S100A4 on the cell cytoskeleton. An equilateral triangle was used since preliminary data demonstrated strong myosin IIA filaments formed along each edge of the micropattern consistent with previous reports (They *et al.*, 2006). Thus it was hypothesised that over-expression of WT S100A4 would act to destabilise the formation of these filaments and that this would be reflected by changes in cell shape. Additionally, the size of the micropattern was selected as $592 \mu\text{m}^2$ with each edge of the triangle $37 \mu\text{m}$ in length. This ensured cells assumed the shape of the micropattern, compared with larger-sized micropatterns that cells were not able to efficiently spread to, preventing formation of steady-state conditions (data not shown).

Having established conditions, A431-teton cells were transfected with plasmids (due to the limited availability of micropatterns, V77D was excluded from this experiment) and seeded on micropatterns. After approximately one hour of attachment, cells were fixed and stained for S100A4 and myosin IIA using immunofluorescence. As shown in Figure 5.21, controls cells adopted the shape of the equilateral triangle imposed by the micropattern, with myosin IIA filaments enriched along the three edges of the triangle indicative of acto-myosin stress fibres (first row). On the contrary, cells over-

expressing S100A4 did not conform to one particular phenotype; however, in general, a curved edge along at least one length of the micropattern was observed, suggesting a collapse of the defined cell borders (second row). Over-expression of C81D displayed a phenotype typical of the control cells with enriched areas of myosin IIA concentrated along the edges of the cell with no sign of border collapse (third row). As an indicator of impaired-cytoskeletal assembly, control cells treated with the Rho kinase inhibitor, Y27632 were also assessed by micropatterns. Rho kinase is an important downstream effector of RhoA and is known to phosphorylate the regulatory myosin light chains at Ser19 and Thr18 (Vicente-Manzanares *et al.*, 2009). Consistent with the effect of S100A4, Y27632-treated cells displayed significant curvature of cell borders (fourth row). To quantitatively analyse this effect, over 100 cells for each condition from two independent experiments were imaged (Figure 5.22A) and a custom macro in ImageJ used to analyse cell collapse, as illustrated in Figure 5.22B. In essence, a collapsed cell edge was defined as one that deviates by more than 50% from the micropattern boundary. For this, the micropattern shape was super-imposed over each cell (Figure 5.22B, middle panel) and the modal pixel value calculated along each cell edge of a thresholded cell (Figure 5.22, right panel). If this deviated by more than 50%, the cell edge was scored as collapsed. Quantitative analysis (Figure 5.22C) indicated a significant increase in cell edge collapse for WT S100A4 compared to control cells (an increase from 12 to 36%) while there was no significant effect observed for C81D-expressing cells. Additionally, cell border collapse increased to 46% for Y27632-treated cells, in line with effect of S100A4.

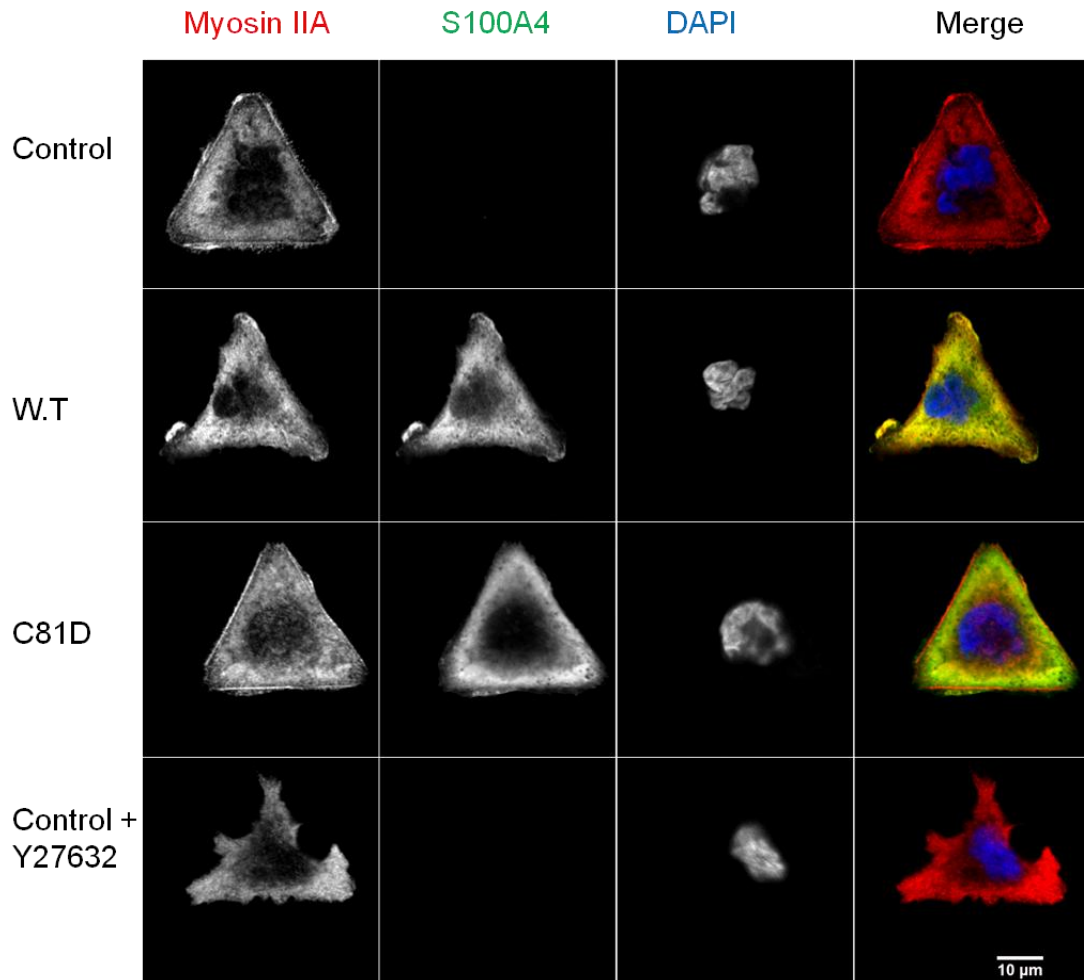


Figure 5.21: Representative images of transfected cells seeded on micropatterns

A431-tet on cells transfected with control vector, WT S100A4 and C81D were maintained in the presence of Dox for 48 hours and then seeded on micropatterns. Cells were fixed after 1 hour (for Y27632-treated cells, the drug was added 15 mins prior to fixation) stained for S100A4, myosin IIA and DAPI. Scale bar = 10 μm.

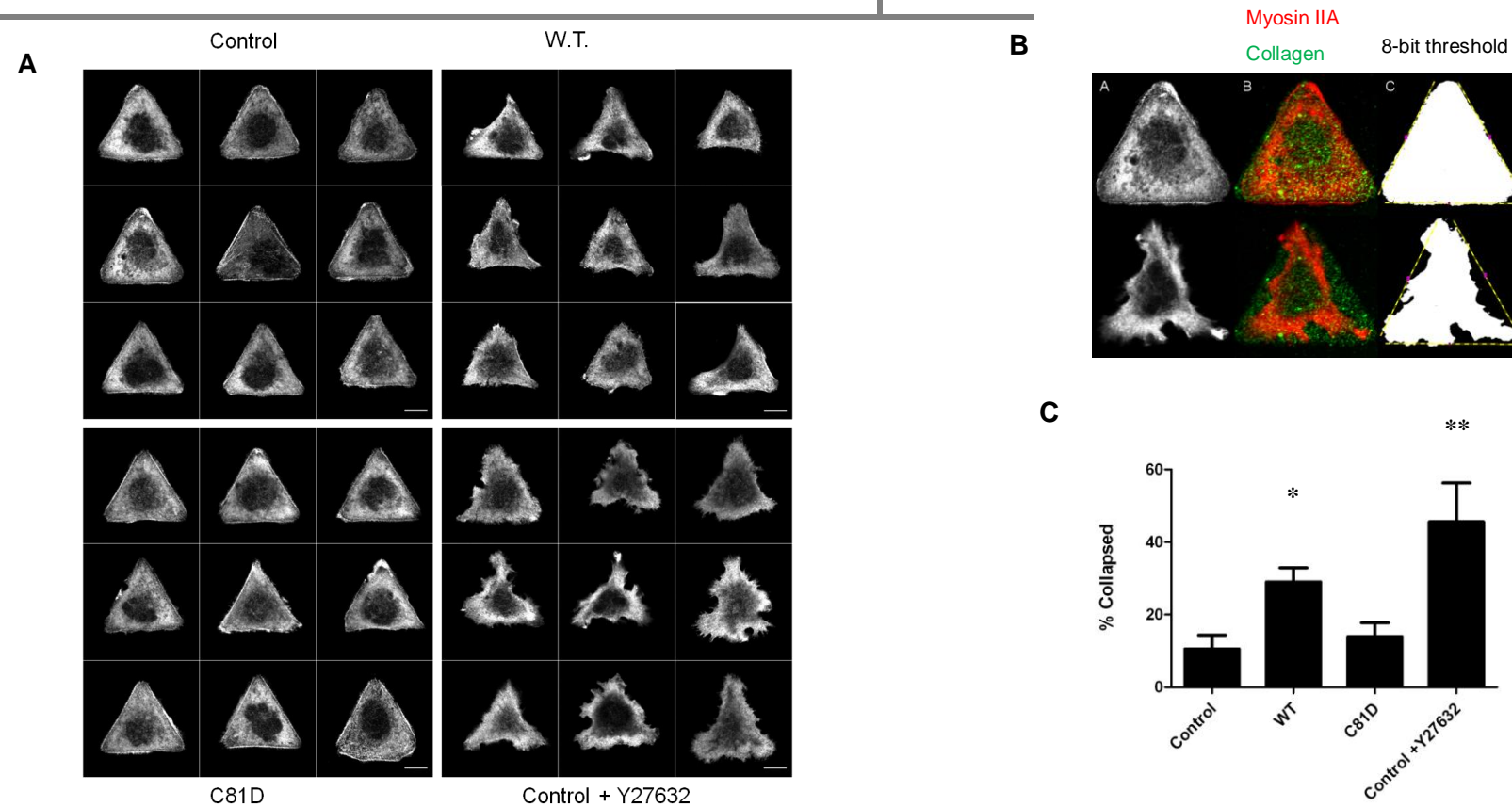


Figure 5.22: S100A4 Induces a collapsed-like phenotype on cells

(A) Selected cells taken from experiment described in Figure 5.22. In the case of WT S100A4 and C81D, cells were selected based on their expression of S100A4. Notice deviation of cell edges from micropattern boundary in the presence of S100A4 and control cells treated with Y27632. Scale bar = 10 μ m. A collapsed edge is defined as one that deviates by more than 50% from the micropattern boundary. (B) To calculate this, images were thresholded and an 8-bit binary image created (see Materials and Methods). The collagen micropattern boundary (yellow lines) was superimposed over the binary image and the modal pixel value (0 – no cell; 255 – cell) calculated along this length. If 50% or more of the pixels contained no cell i.e. 0, this was scored as collapsed. (C) Graph summarising collapsed phenotype. Values represent averages of two independent experiments. Error bars represent SEMs. P values were determined by a one-way ANOVA followed by a Dunnett's Multiple Comparison Test. * = p value <0.05, significant; **=p value <0.01 very significant.

Consistent with an increase in cell border collapse, quantitative analysis of cell area indicated a statistically significant reduction in the presence of WT S100A4 compared to C81D whilst there was also a significant reduction in cell area due to Y27632 (Figure 5.23). As a whole, these data suggest that S100A4 destabilises the cytoskeleton, promoting the cell border collapse; an effect which is abolished with a myosin IIA-deficient mutant of S100A4.

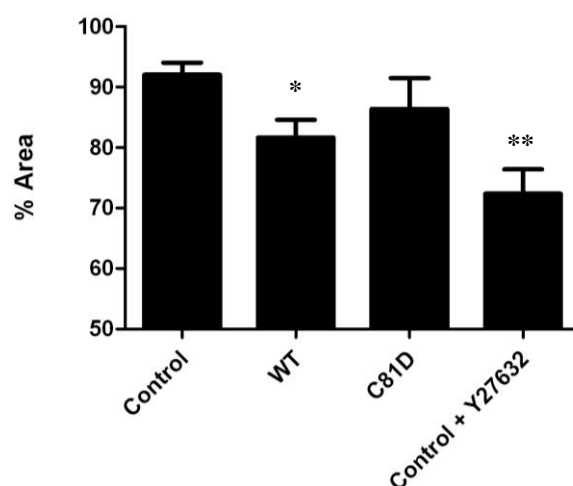


Figure 5.23: Effect of S100A4 on size of cells seeded on micropatterns

In the case of WT S100A4 and C81D, cells are selected based on their expression of S100A4. % area calculated by dividing the average area of cells by the maximum area imposed by a triangle-shaped micropattern i.e. $750 \mu\text{m}^2$. Values represent the average from two independent experiments. Error bars represent SEMs. P values were determined by a one-way ANOVA followed by a Dunnett's Multiple Comparison Test. * = p value <0.05 , significant; **=p value <0.01 very significant.

5.3 Discussion

5.3.1 Heavy chain phosphorylation of myosin IIA and S100A4

The mechanistic details of the interaction between S100A4 and myosin IIA have been the subject of some dispute over the last decade or so. These primarily include the effect of myosin IIA heavy chain phosphorylation on S100A4 binding and the minimal region of myosin IIA that comprises the S100A4 interaction site. Two phospho sites exist on myosin IIA, Ser1916 and Ser1943 which are phosphorylated by PKC and CK2 respectively. Despite evidence to the contrary (Murakami *et al.*, 1998; Murakami *et al.*, 2000) phosphorylation at either of these residues is now acknowledged to promote the monomeric state of myosin (Ronen *et al.*, 2010; Dulyaninova *et al.*, 2005; Dulyaninova *et al.*, 2007). In addition, the general consensus is that PKC phosphorylation at Ser1916 does not affect S100A4-binding, (Dulyaninova *et al.*, 2005; Kriajevska *et al.*, 1998) while the effect of S1943-phosphorylation is less well understood. It was originally shown that a C-terminal fragment of myosin IIA (equivalent to WT M200) phosphorylated by CK2 did not affect S100A4 binding (Kriajevska *et al.*, 2000) although this was later disputed by Dulyaninova *et al.*, (2005) who showed CK2-phosphorylated myosin rods (residues 1339-1961) reduced the S100A4 affinity by 7-fold. In contrast, Dulyaninova *et al.*, (2007) later demonstrated that phosphomimetic forms of Ser1943 did not affect the interaction with S100A4, although were able to recapitulate the effects observed on solubility. Given this, phosphomimetic forms of S1916 and S1943 of the C-terminal fragment previously used by Kriajevska *et al.*, (2000) were generated and the effect of S100A4 binding investigated.

Stopped flow assays indicated essentially no difference in Ca^{2+} dissociation with either S1916D or S1943D compared to WT myosin. Consistent with this, S100A4 was also able to solubilise S1916 and S1943 filaments suggesting substitution of negatively-charged residues at these two sites does not affect the interaction with S100A4. Despite this, the ionic dependence of S1916D and S1943D was significantly increased with midpoint values determined as 72 and 100 mM, respectively, compared to 120 mM for WT M200 (Badyal *et al.*, 2011). As a whole these data are therefore in agreement with Dulyaninova *et al.*, (2007) who showed phosphomimetic forms of S1943 do not affect S100A4 binding but do increase myosin solubility. Assuming phosphorylation of S1943 does affect the interaction with S100A4 (Dulyaninova *et al.*, 2007), the simplest

explanation of this result is that the single negative charge of the aspartate side chain is sufficient to disrupt filament formation of S1943 but two negative charges (i.e. a phosphoryl group) are required to attenuate S100A4 binding. However, due to the discrepancy between phosphomimetic and *in vitro* phosphorylated forms of myosin, chemically-synthesised phospho-peptides would be a useful starting point to further explore whether or not phosphorylation of myosin at S1943 affects binding. Although phosphomimetic forms of M200 might not fully recapitulate phosphorylation, from a structural point of view, the addition of a phosphoryl group at S1916 is unlikely to affect the interaction with S100A4. This region of myosin binds S100A4 as a helix and only one face makes contacts with S100A4, with S1916 pointing out into solution. In addition, a nearby negatively-charged residue, E1913 also points into solution (Figure 5.24) suggesting negative charges on this side of the helix do not affect the interaction between S100A4 and myosin. Conversely, phosphorylation of S1916 is consistent with increased levels of solubility since it is embedded in a site of positive charge and would therefore destabilise the electrostatic interactions which are important in the formation of bipolar filaments (Ricketson *et al.*, 2010). Although S1943 is located within the non-helical tailpiece, outside the S100A4 binding site, it has been proposed that phosphorylation might induce the tail to fold back over itself, preventing S100A4 from forming stable contacts with myosin. This has yet to be proven experimentally but cross-linking studies (using glutaraldehyde or dimethyl suberimidate) linking the non-helical tailpiece with the S100A4-binding site would be of interest in determining if such a mechanism would indeed perturb the myosin-S100A4 interaction.

5.3.2 Nanomolar affinity of the S100A4 and M39

As well as heavy chain phosphorylation, the minimal region of myosin IIA that S100A4 binds to has also been under debate. It was initially mapped to residues A1907-G1938 (Kriajevska *et al.*, 1998) but this was disputed and Malashkevich *et al.*, (2008) claimed the site was significantly shorter, corresponding to D1908-R1923. Notwithstanding, the recent structure of S100A4 and myosin IIA (Elliott *et al.*, 2012) is in agreement with the original mapping data, with the minimal region of myosin representing a peptide of 39 amino acids (M39) extending across both hydrophobic pockets of a S100A4 dimer. This leads to an asymmetric binding mode where each S100A4 monomer interacts with a different end of the myosin peptide, a unique interaction for a S100 protein. Calcium

dissociation from this complex was measured at 0.06 s^{-1} , several orders of magnitude lower than a peptide corresponding to the Malashkevich *et al.*, site (Badyal *et al.*, 2011) suggesting a 16-mer peptide severely underestimates the minimal binding site of

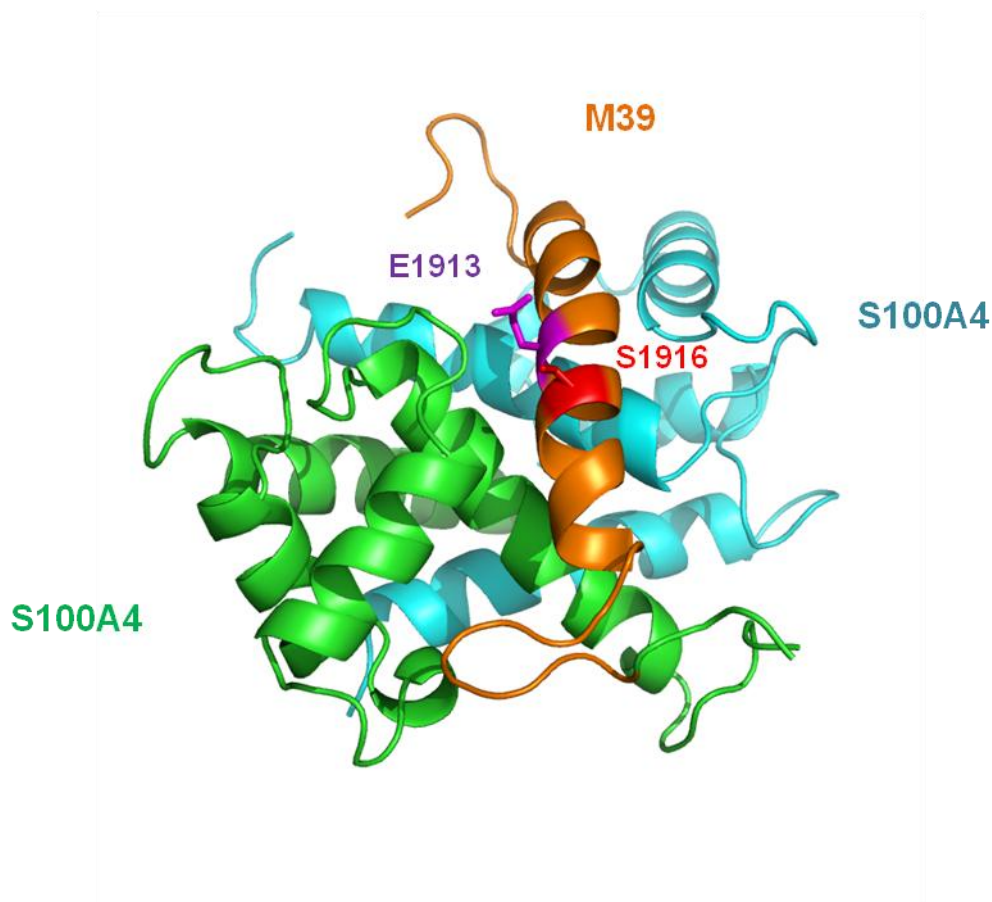


Figure 5.24: Acidic residues point out into solution from the S100A4-M39 complex

Image courtesy of Dr. I. L. Barsukov

myosin. This is also slower than the off rate constant recorded for WT M200 ($\sim 0.3 \text{ s}^{-1}$) indicating M39 likely represents the full binding surface required for complex formation with S100A4. Moreover, it suggests the myosin coiled-coil might be an additional binding energy that must be overcome by S100A4 (M39 is monomeric whilst M200 forms a coiled-coil structure). Indeed, the K_d for calcium-bound S100A4 interacting with M39 is sub-nanomolar whereas the binding constant previously measured for myosin rod fragments is in the micromolar region (Ford *et al.*, 1997; Li *et al.*, 2003) further supporting this notion.

5.3.3 Rational design of S100A4 mutants to abolish the interaction with myosin IIA

With the structure of S100A4 and M39 resolved, it was possible to rationally design S100A4 mutants which would specifically abolish the interaction with myosin IIA without affecting other wild-type functions. Although residues within the hydrophobic pocket of S100A4 would be the most obvious for mutation, such alterations could affect the stability of the protein as they are buried in the calcium-free state. Accordingly, V77 and C81, both located within helix 4 of each S100A4 monomer were mutated to aspartate. Mutation of these sites would have an additive effect as both sets (in each monomer) contribute to the interaction with myosin compared to residues within the hydrophobic pocket which interact with different ends of the myosin helix. Consistent with this, calcium dissociation from V77D and C81D was unaffected even in the presence of $30 \mu\text{M}$ M39 whilst the off rate constants in the absence of peptide were similar to the WT protein, an effect also supported by immunoprecipitation experiments in A431 cells. In addition, the intracellular localisation of these proteins was unchanged, suggesting these mutations had significantly reduced the interaction with myosin while otherwise retaining WT-like properties. Interestingly, chemical modification of C81 by the quinone, NSC95397 has recently been shown to significantly decrease the affinity between S100A4 and myosin IIA inhibiting its function with respect to myosin IIA disassembly (Dulyaninova *et al.*, 2011), validating the findings in this study.

5.3.4 Myosin IIA-deficient mutants abolish the effect of WT S100A4 on cell migration and spreading

Over-expression of these mutants in A431 cells did not alter rates of cell migration compared to control cells while WT S100A4 stimulated migration by 1.8-times. This level of increase is in accordance with previous studies where S100A4 has been over-expressed (Ford, 1995; House, 2011). Although these mutants were designed based on the structure of S100A4 and myosin IIA, it is possible that these mutations might affect the interactions with other S100A4 targets. However, the structure of myosin IIA and S100A4 is unique for an S100 protein, with the myosin ligand forming contacts across both hydrophobic pockets in an S100A4 dimer. Mutation of either V77 or C81 disrupts the simultaneous engagement of both hydrophobic pockets, which likely contributes to the high affinity interaction (Elliott, 2012). As a result, S100A4 ligands which do not display this unique structure would not be affected to the same extent by these mutations although it remains to be seen if other S100A4 targets display this mechanism of interaction or not. Other studies have also correlated a reduced interaction of MIIA-deficient S100A4 mutants with cell migration. For instance, a truncated form of S100A4 lacking the last 13 amino acids abolished the interaction with myosin IIA which was also unable to efficiently migrate (Zhang *et al.*, 2005b). However, data from our study represents the first rational design of S100A4 mutants based on structural information.

To further establish that this effect was myosin IIA-dependent, spreading assays were performed. Myosin IIA has important roles in this process by promoting the retrograde flow of actin, limiting cell protrusion (Cai *et al.*, 2006), as well as providing the contractile force for the cell cytoskeleton (Vicente-Manzanares *et al.*, 2009). Although differences were observed when cells were seeded on conventional collagen (our unpublished observations), these effects were most notable when cells were seeded on triangle-shaped micropatterns. Indeed, cells expressing WT S100A4 did not conform to one particular shape when seeded on micropatterns and displayed a statistically significant increase in cell collapse consistent with treatment of control cells with Y27632. In contrast, control and C81D-expressing cells fully adopted the shape of an equilateral triangle and had significantly lower levels of cell collapse. The reason these effects were more evident on micropatterns is that filamentous myosin IIA is integral

for a cell to adopt and maintain the shape of a triangle-micropattern compared to unpatterned substrate. This was evidenced by the enrichment of myosin IIA around the cell edge of a micropatterned cell compared to those seeded on standard collagen, an effect consistent with that noted by They *et al.*, (2006). This phenotype can therefore be interpreted as S100A4 promoting the monomeric state of myosin which affects the integrity of myosin filaments required for the cell to correctly adopt the shape of a micropattern. Together, these data implicate myosin IIA as an effector of S100A4-mediated migration.

In conclusion, data from this chapter has failed to categorically determine if heavy chain phosphorylation of myosin IIA affects S10A4 binding although it is likely that it does affect solubility. Rational design of single amino acid mutants of S100A4 deficient in myosin IIA binding significantly reduced the effect of S100A4 on cell migration. Although not direct evidence that this is a myosin-dependent effect, spreading assays revealed diminished levels of filamentous myosin, consistent with changes in cell shape. Together, this represents strong evidence that myosin IIA is a target for S100A4 in cells and is important for the S100A4-induced effect on cell migration.

6 General Discussion

6.1 Cancer, EMT and S100A4

An increase in S100A4 protein expression correlates with a poor prognosis in a number of different cancers including breast, gastric, pancreatic, colorectal, liver and bladder (Salama *et al.*, 2008). In addition to this, there is experimental evidence demonstrating S100A4 promotes tumour metastasis in rodent models (Ambartsumian *et al.*, 1996; Davies *et al.*, 1996). As a result, a significant amount of research has sought to address the role of S100A4 in tumour metastasis. Although S100A4 does not induce neoplastic transformation in cells (Helfman *et al.*, 2005), it promotes metastasis in a given tumorigenic background suggesting it is required but not sufficient for the cancer progression.

Tumour formation and metastasis are extremely complex processes which involve the switching on or off of specific signalling pathways, leading to changes in the expression of hundreds of genes (Chaffer & Weinberg, 2011). Indeed, re-activation of signalling pathways controlling EMT, a highly conserved developmental program, are now considered key steps in cancer metastasis (Thiery *et al.*, 2009). A common factor often up-regulated during this process is S100A4. Several key questions arise from this: at what stage of EMT is S100A4 activated and how; is it required for EMT progression; what other functional roles does it play and are these specific within the context of EMT.

In the majority of studies which correlated S100A4 expression with a poor prognosis, primary tumour samples were analysed. Given the link between S100A4 and EMT, do these cells therefore represent epithelial tumours undergoing a mesenchymal transition or carcinoma cells simply over-expressing S100A4? It has long been considered that metastasis and EMT are the last steps in cancer progression (Thiery, 2002) which would therefore reason against the first hypothesis but evidence now suggests that metastasis can occur before the formation of a macroscopic primary tumour (Klein, 2009). For instance, using a mouse model of pancreatic ductal adenocarcinoma (PDAC) it was shown that cells undergoing EMT metastasised into the liver at very early stages of the disease, previously thought to be pre-invasive based on standard histological examination (Rhim *et al.*, 2012). As a consequence, S100A4 expression in these tumours could indeed represent early EMT. In future studies, it would be of interest to

correlate the expression of S100A4 with other mesenchymal markers to test this hypothesis. If the second hypothesis was also proved valid, it would suggest S100A4 can also be activated and contribute to tumourigenesis independently of an EMT program.

Activation of S100A4 expression is commonly observed during cell stress events including inflammation, osmotic shock and hypoxia (Schneider *et al.*, 2008). All three of these processes have been shown to induce EMT in pathological settings resulting in fibrosis or tumourigenesis depending on cellular context (Lopez-Novoa & Nieto, 2009). Accordingly, S100A4 is downstream of many pathways which activate EMT. For example, both TGF- β and HIF-1 α act as potent inducers of EMT in an inflammatory microenvironment (Guarino *et al.*, 2009) but are also strongly linked with activation of S100A4 expression (Xie *et al.*, 2009a). These signalling cascades often converge on the activation of NF- κ B, the main inflammatory response pathway, which activates S100A4 expression, creating a feedback loop linking EMT and inflammation (Lopez-Novoa & Nieto, 2009). Furthermore, S100A4 is a downstream target of the Wnt pathway which itself is often activated during EMT (Stein *et al.*, 2006). Down-regulation of E-cadherin by EMT inducers abolishes the cytoplasmic sequestering of β -catenin facilitating its nuclear translocation (Kim *et al.*, 2002). β -catenin can then bind to TCF/LEF family members activating gene transcription including that of S100A4 which has a TCF binding site in its promoter. Although it is unclear how S100A4 expression is controlled in A431-SIP1 cells, S100A4 is often upregulated during EMT because it is downstream of many pathways which are themselves activated during this process.

Data from this study indicates S100A4 expression is a fairly late event during EMT and is not required for cells to fully adopt a mesenchymal phenotype. This is in contrast to the findings of Okada *et al.*, (1997) who showed S100A4 expression preceded the overt phenotypical changes associated with EMT in MCT cells whilst antisense treatment of S100A4 attenuated this transition. Although the authors did not provide a mechanism for this result, it would be dependent on the target proteins S100A4 associates with. However, such a mechanism is clearly not active in A431-SIP1 cells suggesting there are other factors present in MCT cells which implicate S100A4 in promoting EMT in this cell model.

If S100A4 is not required for EMT progression, what is its functional role during this process? A hallmark feature of EMT is the increase in migratory and invasive abilities which allow cells to degrade the basement membrane, migrate through the surrounding tissue and intravasate into the vasculature or lymphatic system (Hanahan & Weinberg, 2011). Since S100A4 is strongly associated with cell migration in other cellular contexts it would seem likely that S100A4 contributes to the increases in EMT-induced migration. In line with this, data from this study demonstrated S100A4 promotes cell migration representing direct evidence supporting this hypothesis.

Despite this, does S100A4 contribute to additional functions during EMT? Although cell migration is important during EMT and metastasis, it is arguably not the rate limiting step with millions of tumour cells believed to enter the vasculature during the metastatic cascade (Nguyen *et al.*, 2009). However, only a small minority of these cells will go on to colonise distant sites and it is this process which is considered most challenging for the formation of secondary tumours (Chaffer & Weinberg, 2011). Indeed, EMT is now thought to directly contribute to this process by endowing a sub-population of tumour cells with stem-cell like properties (Malanchi *et al.*, 2012). Interestingly, S100A4 has been shown in two separate studies to be important in maintaining the stemness properties of CSCs in cells which have undergone an EMT (Harris *et al.*, 2008; Lo *et al.*, 2011). Although the mechanism behind this effect was not explored, it offers a new insight into how S100A4 promotes tumour metastasis.

6.2 Evidence for S100A4 interaction with myosin IIA *in vivo*

In this study, several lines of evidence have been presented which suggest S100A4 interacts with myosin IIA in epidermoid carcinoma cells (A431) and cells undergoing an epithelial-mesenchymal transition (A431-SIP1). The most direct evidence is provided by statistical analysis of colocalisation in A431-SIP1 cells using TEM. Such methods have previously been used to characterise the colocalisation between biological molecules (Philimonenko *et al.*, 2000; Rusakov *et al.*, 1995; Prior *et al.*, 2003) but are rarely used. This analysis has not only identified a statistically significant colocalisation between S100A4 and myosin IIA but also indicates that 10S and 6S forms of myosin exist in cells and S100A4 interacts with both. The only other evidence of myosin IIA 10S in cells came from a study by Milton *et al.*, (2010) who used a

peptide corresponding to the MHC immediately N-terminal of the head-tail junction which shifted the balance of myosin from a monomeric to a filamentous state suggesting there is a significant proportion of 10S myosin in smooth muscle cells. The data presented in this study therefore represents the first evidence of either 10S or 6S myosin in non-muscle cells. The colocalisation of S100A4 and myosin IIA using TEM is also in agreement with the evidence that these two proteins co-localise according to the quantitative confocal analysis. Light microscopy places a lower limit of 250 nm on any co-localisation analysis but the TEM analysis demonstrates these proteins co-localise at distances less than 200 nm, consistent with the light microscopy data. Interestingly, with advances in super resolution microscopy (Patterson *et al.*, 2010), in future work it might be possible to confirm the TEM findings with light microscopy techniques, further validating the data presented in this study.

Additional evidence for an interaction between these two proteins is also provided by myosin IIA-deficient mutants of S100A4 and is based on the functional consequence of S100A4 binding. A wealth of data suggests S100A4 promotes the monomeric state of myosin *in vitro* although this has been harder to prove *in vivo*. V77D and C81D mutants were rationally designed based on the S100A4-myosin IIA structure and significantly reduced binding affinity to myosin *in vitro* and *in vivo* without affecting other WT properties of the protein. Cells expressing these mutants migrated at control levels and unlike WT cells fully adopted the shape of a triangle micropattern, consistent with the formation of robust myosin filaments along the edges of each micropatterned cell. Although not direct evidence of an interaction with myosin IIA, these phenotypes are consistent with S100A4 promoting the monomeric state of myosin *in vivo*.

Since the original hypothesis was that S100A4 promotes myosin turnover in cells, a more direct way of analysing this was by measuring the recovery of GFP-tagged myosin IIA molecules expressed in A431-SIP1 cells. FRAP analysis unequivocally demonstrated that cells expressing S100A4 displayed a faster rate of fluorescent recovery than those not expressing S100A4. This effect strongly correlated with the extent of filamentous myosin in cells, with cells displaying a more extensive network of myosin filaments recovering more slowly. Taken together, this represents good evidence that not only does S100A4 interact with myosin IIA in A431-SIP1 cells but the interaction is functional and in agreement with the *in vitro* data.

6.2.1 Mechanism of the S100A4-myosin IIA interaction

The FRAP data has implications for whether or not S100A4 promotes the monomeric state by simply sequestering the monomer or actively disassembling myosin from filaments and leads to the general question of how S100A4 promotes the monomeric state of myosin. In the case of the former, monomer sequestration would reduce the effective free concentration of myosin required for polymerisation and therefore not affect the intrinsic rate of depolymerisation *per se* (although this would reduce the size and extent of myosin filaments thus increasing the rate of depolymerisation). In contrast, if S100A4 actively depolymerised myosin filaments, this rate would be expected to increase. Although it is difficult to estimate from the FRAP data which mechanism S100A4 proceeds via, *in vitro* evidence suggests S100A4 can indeed actively depolymerise myosin filaments (Badyal *et al.*, 2011). From a structural point of view, disassembly of myosin filaments would require an agent that can bind a region of myosin that is accessible in the filamentous state. The non-helical tail is reported to be unstructured and should therefore be accessible for agents to induce filament disassembly (Elliott *et al.*, 2012). In accordance with this, part of the S100A4 binding site is located within this region, consistent with S100A4 actively disassembling myosin filaments. The structure of S100A4 and myosin also suggests that S100A4 binding to a filament is likely a two-step binding mode where S100A4 first engages the non-helical tail, which then destabilises the coiled-coil, allowing S100A4 access to the rest of the myosin binding site (Elliott *et al.*, 2012). If S100A4 is indeed able to engage the full myosin binding site in the filamentous state, the N-terminal boundary of the interaction would be proximal to the assembly competent domain (ACD) of myosin which is a region crucial in stabilising bipolar filaments of myosin (Ricketson *et al.*, 2010). This would likely aid more efficient disassembly of filamentous myosin. Notwithstanding, S100A4 binds more tightly to monomeric than filamentous myosin and as such this might represent a less favourable route for the S100A4-myosin interaction (Badyal *et al.*, 2011).

6.2.2 Functional consequence of the S100A4-myosin IIA interaction

The hypothesis that S100A4 increases the turnover of myosin can also be seen as a two step process. S100A4 first promotes the monomeric state by either reducing the effective concentration of free myosin by monomer sequestration or actively disassembling filaments (as discussed above). Secondly, S100A4 is then released from myosin, creating a large pool of assembly-competent myosin which would lead to rapid assembly and increased rates of myosin turnover. This second step is essential since all myosin would otherwise effectively remain bound to S100A4 in an inactive state. Interestingly, such a mechanism is similar to that of the ADF/cofilin family of proteins which promote the monomeric state of actin, therefore increasing turnover (Bernstein & Bamburg, 2010). Although there are fundamental differences between actin and myosin assembly, they both represent the formation of higher order polymer structures which need to assemble and disassemble *in vivo* on a seconds timescale. ADF/cofilin proteins act by both sequestering ADP-G-actin and binding to ADP-F-actin actively destabilising the actin helix by inducing a twist into its structure thus creating a pool of actin monomers. The binding of ADF/cofilin proteins is dependent on the nucleotide state of actin but they are also negatively regulated by LIM kinases which phosphorylate the N-terminus blocking their interaction with ADP-actin filaments or monomers. This regulation therefore creates a large pool of free G-actin, required for rapid assembly of actin filaments. Analogous to this, S100A4 would need to be active when promoting the monomeric state of myosin but then release myosin and allow it to polymerise again suggesting there are mechanisms, like with ADF/cofilin, which control the activity of the S100A4-myosin IIA interaction (Figure 6.1).

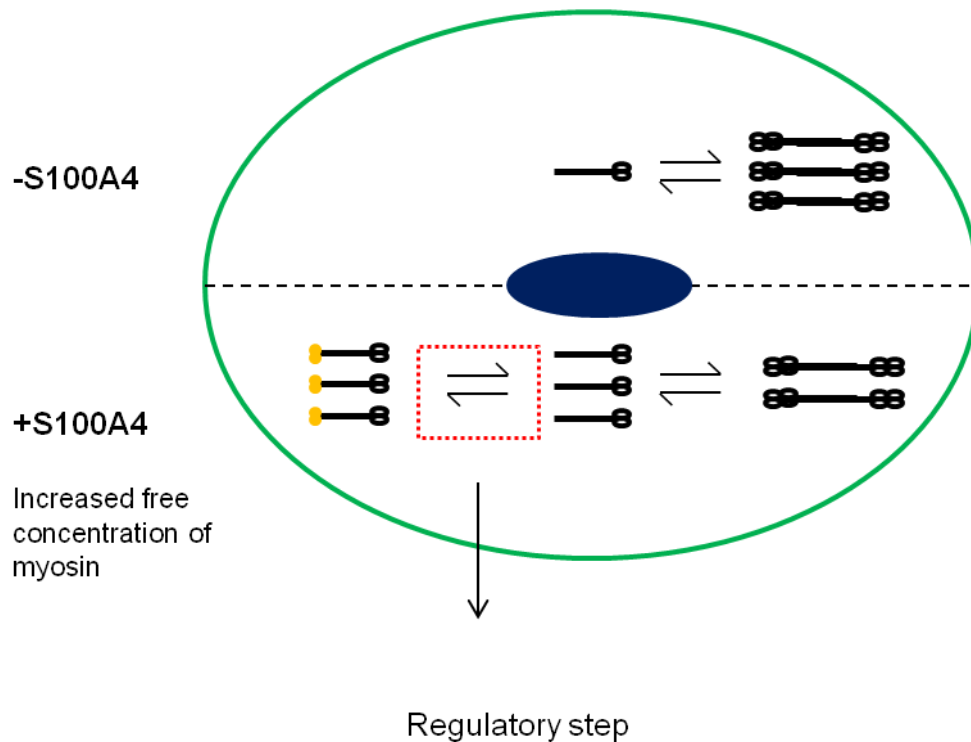


Figure 6.1: Mechanism for S100A4 promoting the turnover of myosin IIA *in vivo*

Monomeric and filamentous myosin will be in equilibrium with each other depending on a number of factors, including S100A4. In the absence of S100A4, myosin is likely to form more extensive filaments. In the presence of S100A4, the equilibrium will be towards the monomeric state (either by monomer sequestration or active filament disassembly) with an increase in the free concentration of myosin which should be reflected in a decrease in myosin filaments. However, for S100A4 to promote myosin turnover, there should be a regulatory step which “inactivates” the S100A4-myosin IIA complex, freeing a large pool of monomeric myosin to re-polymerise again. Such a mechanism is akin to the family of ADF/cofilin proteins which promote turnover of actin filaments in cells.

6.2.3 Regulation of the S100A4-myosin IIA interaction

As described above, regulation of the S100A4-myosin IIA interaction is likely important for its proposed function. This regulation can take one of two forms: either promoting the formation of the complex or inactivating a pre-existing interaction with separate mechanisms potentially responsible for each form. Calcium levels in the cell are exquisitely controlled through a balance of calcium import and export, and are important in regulating a number of cellular processes (Berridge *et al.*, 2003). Given this, the activity of calcium-binding proteins such as S100A4 will be controlled by the level of intracellular calcium. Indeed, the interaction between S100A4 and myosin IIA has been shown to be calcium-dependent in a number of studies (Badyal *et al.*, 2011; Li *et al.*, 2003; Kriajevska *et al.*, 2000). In the case of S100s, this regulation is dependent on a change in the tertiary structure which opens up a hydrophobic cleft crucial in mediating target binding (Donato, 2003). Despite this, there is often a large discrepancy between the calcium-binding affinity of S100s and the intracellular levels of calcium as most S100s binding calcium with a K_d between 10 – 50 μM , an order of magnitude greater than signalling levels (Badyal *et al.*, 2011). However, it is now clear that target-bound forms of S100s bind calcium more tightly than in the absence of interacting ligand. In fact, this principle was the basis for the calcium dissociation assays with higher affinity target interactions displaying slower calcium off rates. Consistent with this notion, quantitative modelling by Badyal *et al.*, (2011) showed that even at resting levels of calcium (~ 100 nM), there is significant interaction between S100A4 and myosin to the extent a proportion of myosin is likely to be monomeric when both proteins are present a micromolar levels. However, for a sustained level of S100A4-mediated depolymerisation, calcium levels would need to remain high for tens of seconds. As such, calcium levels will be integral to regulating both the binding of S100A4 to myosin IIA and for disassembling the complex. Although the intracellular levels of calcium were not addressed in this study, the levels are presumably high enough to explain the functional effects observed in both A431-SIP1 and A431 cells. Interestingly, it was recently shown that engineering of a permanently active mutant of S100P based on S100A10 [this is the only S100 protein which is constitutively active in terms of calcium binding (Donato, 2001)] bound one of its protein targets ezrin even in the absence of calcium (Austermann *et al.*, 2009). Engineering of a calcium-insensitive

S100A4 (i.e. permanently active) would serve as a good control to further explore the role calcium plays in regulating the interaction with myosin.

An additional method of regulation which has been directly addressed in this study is that of myosin heavy chain phosphorylation at S1916 and S1943. Although further studies are required to answer if phosphorylation at these two residues does indeed compromise the interaction with S100A4, the consensus view, also supported by this study is that phosphorylation promotes the monomeric state of myosin (Dulyaninova *et al.*, 2005; Dulyaninova *et al.*, 2007; Clark *et al.*, 2008b). Consequently, these processes might represent two distinct, but functionally equivalent mechanisms to solubilise myosin. For instance, both mechanisms could be differentially regulated either temporally or spatially in the same cell or only activated in specific cell types.

A further regulatory mechanism that is known to control the activity of S100 proteins is oligomerisation with tetrameric forms of S100A4 binding targets with sufficiently reduced affinity (Badyal *et al.*, 2011). From a crystal structure of S100A4, this was shown to be because one of the hydrophobic pockets in each S100A4 dimer interacts with the C-terminal tail of another, thus disrupting peptide interactions (Gingras *et al.*, 2008). Interestingly, the drug trifluoperazine (TFP) was shown to severely compromise the interaction between S100A4 and myosin IIA (Malashkevich *et al.*, 2010) suggesting if biological agents exist in cells and act by similar mechanisms they could control the binding of S100A4 to myosin IIA. However, this mechanism is likely to be only important in controlling the binding of S100A4 to myosin IIA and not disassembly of the complex.

Although there is relatively little data regarding post-translational modifications of S100A4, such a mechanism would represent an effective method of regulating the activity of the S100A4-myosin IIA interaction. As described previously, modification of S100A4 Cys81 by the quinone, NSC95397 was sufficient to inhibit S100A4 function with respect to myosin IIA binding and depolymerisation (Dulyaninova *et al.*, 2011). As cysteine residues are modified by post-translational modifications including S-glutathionylation and S-nitrosylation (Winterbourn & Hampton, 2008) this could therefore represent a method of inactivating S100A4. In support of this, S100A4 was

detected in glutathionylated and cysteineylated forms in cells exposed with ionizing radiation suggesting such modifications can be found *in vivo* (Orre *et al.*, 2007).

An additional factor which would indirectly affect the S100A4-myosin IIA interaction is redundancy in both the S100 and myosin II families. There are a number of instances where multiple S100 proteins bind to the same target; for example, S100A1, A2, A4, A6 and S100B all bind p53 with varying affinities (van Dieck *et al.*, 2009) while S100B and S100A6 both interact with annexin A6 (Santamaria-Kisiel *et al.*, 2006). Interestingly, a recent study has shown that S100P also interacts with the C-terminus of myosin IIA suggesting other S100s can compete with S100A4 for interaction with myosin IIA (Du *et al.*, 2012). Although S100A4 binds myosin IIA with a 9-times higher affinity than myosin IIB (Li *et al.*, 2003), myosin IIA and IIC share a high degree of sequence similarity in the C-terminal tail (Golomb *et al.*, 2004) suggesting myosin IIC might also represent a valid target for S100A4 binding.

6.3 S100A4 and cell migration

A large body of research has shown that S100A4 promotes cell migration in a number of different cell types (Tarabykina *et al.*, 2007) with data from this study also supporting these observations. The mechanism controlling this has focused on the interaction between S100A4 and myosin IIA. *In vitro* data clearly demonstrates that S100A4 promotes the monomeric state of myosin either by sequestering monomers or actively disassembling myosin filaments; thus, it is hypothesised that by promoting the monomeric state of myosin in cells, S100A4 increases myosin turnover leading to more efficient cell migration (Li & Bresnick, 2006). Recent evidence (Li *et al.*, 2010) and data from this study is in agreement with this hypothesis. However, what is the role of myosin in cells with relation to cell migration and why do elevated levels of myosin turnover promote cell migration? Myosin plays important roles at many stages of the cell migration cycle including focal adhesion maturation, cell protrusion and polarisation with the formation of filamentous myosin critical in all these processes (Vicente-Manzanares *et al.*, 2009). As such, agents that regulate the assembly of myosin are likely to be important players in cell migration.

For a cell to efficiently migrate, focal adhesions must be disassembled allowing the cell to move forward (Ridley *et al.*, 2003). Myosin IIA supports focal adhesion maturation by bundling actin allowing these structures to elongate (Choi *et al.*, 2008). As such, mature focal adhesions will take longer to disassemble and therefore reduce the rate of cell migration (Gupton & Waterman-Storer, 2006). However, myosin II contractility is also required for disassembly of these complexes, especially at the rear of the cell (Conti & Adelstein, 2008). Indeed, myosin IIA-deficient cells often have defects in tail retraction leading to impaired cell migration (Xu *et al.*, 2003). Accordingly, the extent of filamentous myosin has to be controlled both spatially and temporally to control the balance of focal adhesion maturation and myosin IIA-mediated disassembly. Interestingly, it has recently been shown that over-expression of S100A4 in Rama37 cells limited focal adhesion maturation without inducing large-scale retraction defects in cells (Goh Then Sin *et al.*, 2011), consistent with this hypothesis.

Myosin IIA contractility is also important in controlling the retrograde flow of actin from the leading edge (Cai *et al.*, 2006). This limits cell protrusion and therefore negatively regulates cell migration. Although myosin IIA is not localised to the leading lamellipodium, its localisation at the lamellum is sufficient to control this effect. It is widely acknowledged that the intracellular calcium signal displays a rear-front gradient with the lowest concentrations at the front of a migrating cell (Carafoli, 2002). This would therefore limit the activity of S100A4 at the leading edge, reducing its ability to regulate myosin assembly. However, it is now thought that calcium flickers or hot-spots are present at the leading edge of migrating cells which would enable localised activation of Ca^{2+} signalling cascades amidst a low-calcium background (Wei *et al.*, 2009). Given this, it is thus feasible that S100A4 could act towards the leading edge of the cell to reduce retrograde flow in cells, increasing protrusion and therefore overall cell motility.

Controlling the extent and turnover of myosin filaments is therefore important for cell migration. However, S100A4 likely operates in concert with light and heavy chain phosphorylation to regulate this process (Figure 6.2). Myosin assembly is initiated by phosphorylation of 10S state which then unfolds in to the 6S form. If above the critical concentration for myosin assembly, 6S myosin would then rapidly polymerise into filamentous myosin and provide the contractile force in the cell by bundling actin

filaments. Once in this state, S100A4, myosin heavy chain phosphorylation and dephosphorylation of the light chain will all promote disassembly either directly or indirectly via a 10S or 6S monomer. For instance, S100A4 or MHC phosphorylation could actively disassemble filamentous myosin which even when phosphorylated could destabilise the molecule leading to a 10S monomer. Alternatively, S100A4 binding or heavy chain phosphorylation could disassemble a myosin filament and molecules could remain in 6S state. Taken together, a combination of those factors which promote or attenuate myosin assembly, including S100A4, are likely to be crucial in fine-tuning the activity of myosin IIA, both temporally and spatially, which in turn will enable cells to more efficiently cycle through the co-ordinated stages of cell migration.

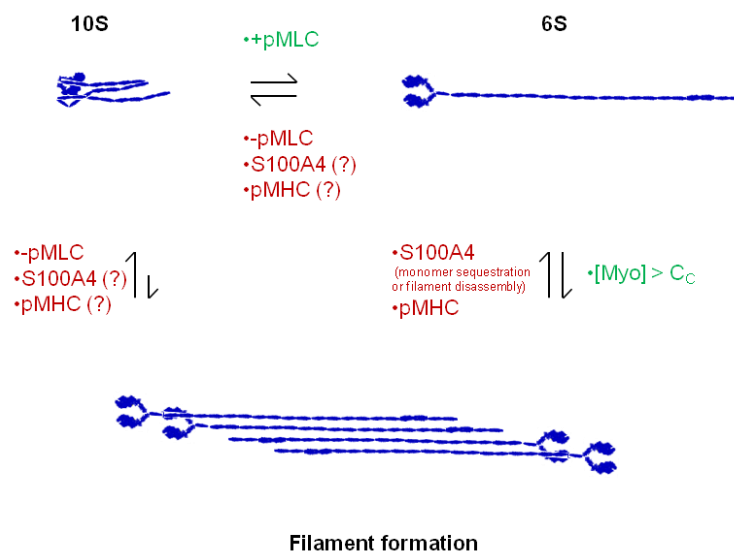


Figure 6.2: Regulation of myosin IIA assembly/disassembly: The role of RLC/MHC phosphorylation and S100A4-binding

The assembly/disassembly of myosin IIA will be controlled by a number of factors including RLC phosphorylation, heavy chain phosphorylation and S100A4 binding. The state of myosin polymerisation will depend on the relative equilibrium between these factors.

In conclusion, this thesis has addressed several issues relating to the interaction between S100A4 and myosin IIA *in vivo* and *in vitro*. Evidence of an interaction in cells is

supported by co-localisation methods and functional studies. Nearest-neighbour analysis based on TEM immunogold microscopy demonstrated that myosin IIA is present in a 10S and 6S monomeric state in A431-SIP1 cells, and S100A4 interacts with both. This is the first evidence that either form of myosin exists in non-muscle cells but also represents an important step forward in understanding the mechanism of the S100A4-myosin IIA interaction. Further evidence of an interaction between both proteins is provided by functional data, correlating the ability of S100A4 to promote the monomeric state of myosin *in vitro* with this effect *in vivo*. Indeed, RNAi-mediated knockdown of S100A4 in A431-SIP1 cells significantly increases the level of filamentous myosin. Moreover, over-expression of S100A4 in A431 cells leads to an increase in monomeric myosin as determined by spreading assays, an effect which is abolished when expressing S100A4 mutants that do not interact with myosin. Together, these data confirm that S100A4 promotes the monomeric state of myosin, suggesting a functional interaction between both proteins exists in A431-SIP1 and A431 cells. *In vitro* evidence from this study confirmed that heavy chain phosphorylation of myosin IIA increases its solubility although the effect it has on S100A4 binding is still unclear. This question will be of future importance for the field as it could represent an important mechanism to regulate the interaction between S100A4 and myosin IIA. In addition to this, kinetic methods validated a peptide of myosin IIA, M39, as the S100A4 binding site, a result in agreement with the structural data. Taken together, this data suggests myosin IIA is an important binding partner of S100A4 and could at least partly explain the mechanism of S100A4-induced cell migration. Importantly, this interaction could therefore serve as a future target for small molecule inhibitors and be of therapeutic potential in the treatment of tumour metastasis.

Appendices

Appendix I: Publications arising from this thesis

The following publications from work conducted for this thesis are either in print or in submission:

Badyal, S.K., Basran, J., Bhanji, N., Kim, J.H., Chavda, A.P., Jung, H.S., Craig, R., Elliott, P.R., **Irvine, A.F.**, Barsukov, I.L., Kriajevska, M., Bagshaw, C.R., 2011. Mechanism of the Ca²⁺-dependent interaction between S100A4 and tail fragments of nonmuscle myosin heavy chain IIA. *Journal of Molecular Biology*. **405**, 1004-1026.

Elliott, P.R*., **Irvine, A.F***., Jung, H.S*., Tozawa, K., Pastok, M.W., Picone, R., Badyal, S.K., Basran, J., Rudland, P.S., Barraclough, R., Lian, L.Y., Bagshaw, C.R., Kriajevska, M., Barsukov, I.L., 2012. Asymmetric Mode of Ca(2+)-S100A4 Interaction with Nonmuscle Myosin IIA Generates Nanomolar Affinity Required for Filament Remodeling. *Structure* (London, England : 1993). **20**, 654-666.

Irvine, A.F., Park, S.O., Allcock, N.S., Badyal, S.K., Basran, J., Chaban, Y., Barsukov, I.L., Jung, H.S., Bagshaw, C.R., Kriajevska, M. S100A4 binds to the extended and compact forms of non-muscle myosin IIA in A431 cells undergoing epithelial-mesenchymal transition (*in submission*)

* These authors contributed equally to this work.

References

- Ai, K.-., Lu, L.-., Huang, X.-., Chen, W., Zhang, H.-., 2008. Prognostic significance of S100A4 and vascular endothelial growth factor expression in pancreatic cancer. *World Journal of Gastroenterology*. **14**, 1931-1935.
- Ambartsumian, N.S., Grigorian, M.S., Larsen, I.F., Karlstrøm, O., Sidenius, N., Rygaard, J., Georgiev, G., Lukanidin, E., 1996. Metastasis of mammary carcinomas in GRS/A hybrid mice transgenic for the mts1 gene. *Oncogene*. **13**, 1621-1630.
- Andersen, H., Mejlvang, J., Mahmood, S., Gromova, I., Gromov, P., Lukanidin, E., Kriajevskaja, M., Mellon, J.K., Tulchinsky, E., 2005. Immediate and delayed effects of E-cadherin inhibition on gene regulation and cell motility in human epidermoid carcinoma cells. *Molecular and Cellular Biology*. **25**, 9138-9150.
- Andersen, K., Mori, H., Fata, J., Bascom, J., Øyjord, T., Mælandsmo, G.M., Bissell, M., 2011. The metastasis-promoting protein S100A4 regulates mammary branching morphogenesis. *Developmental Biology*. **352**, 181-190.
- Ansieau, S., Bastid, J., Doreau, A., Morel, A.-., Bouchet, B.P., Thomas, C., Fauvet, F., Puisieux, I., Doglioni, C., Piccinin, S., Maestro, R., Voeltzel, T., Selmi, A., Valsesia-Wittmann, S., Caron de Fromentel, C., Puisieux, A., 2008. Induction of EMT by Twist Proteins as a Collateral Effect of Tumor-Promoting Inactivation of Premature Senescence. *Cancer Cell*. **14**, 79-89.
- Atkinson, S.J. & Stewart, M., 1992. Molecular interactions in myosin assembly. Role of the 28-residue charge repeat in the rod. *Journal of Molecular Biology*. **226**, 7-13.
- Auguste, P., Fallavollita, L., Wang, N., Burnier, J., Bikfalvi, A., Brodt, P., 2007. The host inflammatory response promotes liver metastasis by increasing tumor cell arrest and extravasation. *The American Journal of Pathology*. **170**, 1781-1792.
- Austermann, J., Nazmi, A.R., Heil, A., Fritz, G., Kolinski, M., Filipek, S., Gerke, V., 2009. Generation and characterization of a novel, permanently active S100P mutant. *Biochimica Et Biophysica Acta*. **1793**, 1078-1085.
- Badyal, S.K., Basran, J., Bhanji, N., Kim, J.H., Chavda, A.P., Jung, H.S., Craig, R., Elliott, P.R., Irvine, A.F., Barsukov, I.L., Kriajevskaja, M., Bagshaw, C.R., 2011. Mechanism of the Ca²⁺-dependent interaction between S100A4 and tail fragments of nonmuscle myosin heavy chain IIA. *Journal of Molecular Biology*. **405**, 1004-1026.
- Bao, J., Ma, X., Liu, C., Adelstein, R.S., 2007. Replacement of nonmuscle myosin II-B with II-A rescues brain but not cardiac defects in mice. *The Journal of Biological Chemistry*. **282**, 22102-22111.
- Bendayan, M., 1982. Double immunocytochemical labeling applying the protein A-gold technique. *Journal of Histochemistry & Cytochemistry*. **30**, 81-85.
- Berge, G. & Mælandsmo, G.M., 2011. Evaluation of potential interactions between the metastasis-associated protein S100A4 and the tumor suppressor protein p53. *Amino Acids*. **41**, 863-873.

- Bernstein, B.W. & Bamburg, J.R., 2010. ADF/Cofilin: A functional node in cell biology. *Trends in Cell Biology*. **20**, 187-195.
- Berridge, M.J., Bootman, M.D., Roderick, H.L., 2003. Calcium signalling: Dynamics, homeostasis and remodelling. *Nature Reviews Molecular Cell Biology*. **4**, 517-529.
- Berridge, M.J., Lipp, P., Bootman, M.D., 2000. The versatility and universality of calcium signalling. *Nature Reviews Molecular Cell Biology*. **1**, 11-21.
- Betapudi, V., Gokulrangan, G., Chance, M.R., Egelhoff, T.T., 2011. A proteomic study of myosin II motor proteins during tumor cell migration. *Journal of Molecular Biology*. **407**, 673-686.
- Bindels, S., Mestdagt, M., Vandewalle, C., Jacobs, N., Volders, L., Noel, A., van Roy, F., Berx, G., Foidart, J.M., Gilles, C., 2006. Regulation of vimentin by SIP1 in human epithelial breast tumor cells. *Oncogene*. **25**, 4975-4985.
- Bolos, V., Peinado, H., Perez-Moreno, M.A., Fraga, M.F., Esteller, M., Cano, A., 2003. The transcription factor Slug represses E-cadherin expression and induces epithelial to mesenchymal transitions: a comparison with Snail and E47 repressors. *Journal of Cell Science*. **116**, 499-511.
- Bosgraaf, L. & van Haastert, P.J.M., 2006. The regulation of myosin II in Dictyostelium. *European Journal of Cell Biology*. **85**, 969-979.
- Boye, K. & Mælandsmo, G.M., 2010. S100A4 and metastasis: A small actor playing many roles. *American Journal of Pathology*. **176**, 528-535.
- Boye, K., Nesland, J.M., Sandstad, B., Mælandsmo, G.M., Flatmark, K., 2010. Nuclear S100A4 is a novel prognostic marker in colorectal cancer. *European Journal of Cancer*. **46**, 2919-2925.
- Breckenridge, M.T., Dulyaninova, N.G., Egelhoff, T.T., 2009. Multiple regulatory steps control mammalian nonmuscle myosin II assembly in live cells. *Molecular Biology of the Cell*. **20**, 338-347.
- Brown, D.M. & Ruoslahti, E., 2004. Metadherin, a cell surface protein in breast tumors that mediates lung metastasis. *Cancer Cell*. **5**, 365-374.
- Browne, G., Sayan, A.E., Tulchinsky, E., 2010. ZEB proteins link cell motility with cell cycle control and cell survival in cancer. *Cell Cycle*. **9**, 886-891.
- Burgess, S.A., Yu, S., Walker, M.L., Hawkins, R.J., Chalovich, J.M., Knight, P.J., 2007. Structures of Smooth Muscle Myosin and Heavy Meromyosin in the Folded, Shutdown State. *Journal of Molecular Biology*. **372**, 1165-1178.
- Cabezón, T., Celis, J.E., Skibshøj, I., Klingelhöfer, J., Grigorian, M., Gromov, P., Rank, F., Myklebust, J.H., Mælandsmo, G.M., Lukanidin, E., Ambartsumian, N., 2007. Expression of S100A4 by a variety of cell types present in the tumor microenvironment of human breast cancer. *International Journal of Cancer*. **121**, 1433-1444.

- Cai, Y., Biais, N., Giannone, G., Tanase, M., Jiang, G., Hofman, J.M., Wiggins, C.H., Silberzan, P., Buguin, A., Ladoux, B., Sheetz, M.P., 2006. Nonmuscle myosin IIA-dependent force inhibits cell spreading and drives F-actin flow. *Biophysical Journal*. **91**, 3907-3920.
- Campellone, K.G. & Welch, M.D., 2010. A nucleator arms race: Cellular control of actin assembly. *Nature Reviews Molecular Cell Biology*. **11**, 237-251.
- Carafoli, E., 2002. Calcium signaling: a tale for all seasons. *Proceedings of the National Academy of Sciences of the United States of America*. **99**, 1115-1122.
- Carver, E.A., Jiang, R., Lan, Y., Oram, K.F., Gridley, T., 2001. The mouse Snail gene encodes a key regulator of the epithelial-mesenchymal transition. *Molecular and Cellular Biology*. **21**, 8184-8188.
- Chaffer, C.L. & Weinberg, R.A., 2011. A perspective on cancer cell metastasis. *Science*. **331**, 1559-1564.
- Chen, H.-., Fernig, D.G., Rudland, P.S., Sparks, A., Wilkinson, M.C., Barraclough, R., 2001. Binding to intracellular targets of the metastasis-inducing protein, S100A4 (p9Ka). *Biochemical and Biophysical Research Communications*. **286**, 1212-1217.
- Chen, M., Sastry, S.K., O'Connor, K.L., 2011. Src kinase pathway is involved in NFAT5-mediated S100A4 induction by hyperosmotic stress in colon cancer cells. *American Journal of Physiology - Cell Physiology*. **300**, C1155-C1163.
- Chen, M., Sinha, M., Luxon, B.A., Bresnick, A.R., O'Connor, K.L., 2009. Integrin $\alpha 6\beta 4$ controls the expression of genes associated with cell motility, invasion, and metastasis, including S100A4/metastasin. *Journal of Biological Chemistry*. **284**, 1484-1494.
- Cho, Y.G., Nam, S.W., Kim, T.Y., Kim, Y.S., Kim, C.J., Park, J.Y., Lee, J.H., Kim, H.S., Lee, J.W., Park, C.H., Song, Y.H., Lee, S.H., Yoo, N.J., Lee, J.Y., Park, W.S., 2003. Overexpression of S100A4 is closely related to the aggressiveness of gastric cancer. *APMIS : Acta Pathologica, Microbiologica, Et Immunologica Scandinavica*. **111**, 539-545.
- Choi, C.K., Vicente-Manzanares, M., Zareno, J., Whitmore, L.A., Mogilner, A., Horwitz, A.R., 2008. Actin and α -actinin orchestrate the assembly and maturation of nascent adhesions in a myosin II motor-independent manner. *Nature Cell Biology*. **10**, 1039-1050.
- Christofori, G. & Semb, H., 1999. The role of the cell-adhesion molecule E-cadherin as a tumour-suppressor gene. *Trends in Biochemical Sciences*. **24**, 73-76.
- Citi, S. & Kendrick-Jones, J., 1988. Brush border myosin filament assembly and interaction with actin investigated with monoclonal antibodies. *Journal of Muscle Research and Cell Motility*. **9**, 306-319.

- Citi, S. & Kendrick-Jones, J., 1987. Studies on the structure and conformation of brush border myosin using monoclonal antibodies. *European Journal of Biochemistry / FEBS*. **165**, 315-325.
- Claperon, A., Guedj, N., Mergey, M., Vignjevic, D., Desbois-Mouthon, C., Boissan, M., Saubamea, B., Paradis, V., Housset, C., Fouassier, L., 2012. Loss of EBP50 stimulates EGFR activity to induce EMT phenotypic features in biliary cancer cells. *Oncogene*. **31**, 1376-1388.
- Clark, K., Langeslag, M., Figdor, C.G., van Leeuwen, F.N., 2007. Myosin II and mechanotransduction: a balancing act. *Trends in Cell Biology*. **17**, 178-186.
- Clark, K., Middelbeek, J., Dorovkov, M.V., Figdor, C.G., Ryazanov, A.G., Lasonder, E., van Leeuwen, F.N., 2008a. The α -kinases TRPM6 and TRPM7, but not eEF-2 kinase, phosphorylate the assembly domain of myosin IIA, IIB and IIC. *FEBS Letters*. **582**, 2993-2997.
- Clark, K., Middelbeek, J., Lasonder, E., Dulyaninova, N.G., Morrice, N.A., Ryazanov, A.G., Bresnick, A.R., Figdor, C.G., van Leeuwen, F.N., 2008b. TRPM7 Regulates Myosin IIA Filament Stability and Protein Localization by Heavy Chain Phosphorylation. *Journal of Molecular Biology*. **378**, 788-801.
- Cohn, M.A., Hjelmsø, I., Wu, L.-., Guldborg, P., Lukanidin, E.M., Tulchinsky, E.M., 2001. Characterization of Sp1, AP-1, CBF and KRC binding sites and minisatellite DNA as functional elements of the metastasis-associated mts1/S100A4 gene intronic enhancer. *Nucleic Acids Research*. **29**, 3335-3346.
- Comer, F.I. & Parent, C.A., 2006. Phosphoinositide 3-kinase activity controls the chemoattractant-mediated activation and adaptation of adenylyl cyclase. *Molecular Biology of the Cell*. **17**, 357-366.
- Conti, M.A. & Adelstein, R.S., 2008. Nonmuscle myosin II moves in new directions. *Journal of Cell Science*. **121**, 11-18.
- Conti, M.A., Even-Ram, S., Liu, C., Yamada, K.M., Adelstein, R.S., 2004. Defects in cell adhesion and the visceral endoderm following ablation of nonmuscle myosin heavy chain II-A in mice. *Journal of Biological Chemistry*. **279**, 41263-41266.
- Conti, M.A., Sellers, J.R., Adelstein, R.S., 1991. Identification of the serine residue phosphorylated by protein kinase C in vertebrate nonmuscle myosin heavy chains. *Biochemistry*. **30**, 966-970.
- Costes, S.V., Daelemans, D., Cho, E.H., Dobbin, Z., Pavlakis, G., Lockett, S., 2004. Automatic and Quantitative Measurement of Protein-Protein Colocalization in Live Cells. *Biophysical Journal*. **86**, 3993-4003.
- Craig, R., Smith, R., Kendrick-Jones, J., 1983. Light-chain phosphorylation controls the conformation of vertebrate non-muscle and smooth muscle myosin molecules. *Nature*. **302**, 436-439.

- Cross, R.A., Cross, K.E., Sobieszek, A., 1986. ATP-linked monomer-polymer equilibrium of smooth muscle myosin: the free folded monomer traps ADP.Pi. *EMBO Journal*. **5**, 2637-2641.
- Cross, R.A., Jackson, A.P., Citi, S., Kendrick-Jones, J., Bagshaw, C.R., 1988. Active site trapping of nucleotide by smooth and non-muscle myosins. *Journal of Molecular Biology*. **203**, 173-181.
- Davies, B.R., Davies, M.P.A., Gibbs, F.E.M., Barraclough, R., Rudland, P.S., 1993. Induction of the metastatic phenotype by transfection of a benign rat mammary epithelial cell line with the gene for p9Ka, a rat calcium-binding protein, but not with the oncogene EJ-ras-1. *Oncogene*. **8**, 999-1008.
- Davies, B.R., O'Donnell, M., Durkan, G.C., Rudland, P.S., Barraclough, R., Neal, D.E., Mellon, J.K., 2002. Expression of S100A4 protein is associated with metastasis and reduced survival in human bladder cancer. *Journal of Pathology*. **196**, 292-299.
- Davies, M.P., Rudland, P.S., Robertson, L., Parry, E.W., Jolicoeur, P., Barraclough, R., 1996. Expression of the calcium-binding protein S100A4 (p9Ka) in MMTV-neu transgenic mice induces metastasis of mammary tumours. *Oncogene*. **13**, 1631-1637.
- De Putte, T.V., Maruhashi, M., Francis, A., Nelles, L., Kondoh, H., Huylebroeck, D., Higashi, Y., 2003. Mice lacking Zfhx1b, the gene that codes for Smad-interacting protein-1, reveal a role for multiple neural crest cell defects in the etiology of hirschsprung disease-mental retardation syndrome. *American Journal of Human Genetics*. **72**, 465-470.
- De Rooij, J., Kerstens, A., Danuser, G., Schwartz, M.A., Waterman-Storer, C.M., 2005. Integrin-dependent actomyosin contraction regulates epithelial cell scattering. *Journal of Cell Biology*. **171**, 153-164.
- De Silva Rudland, S., Martin, L., Roshanlall, C., Winstanley, J., Leinster, S., Platt-Higgins, A., Carroll, J., West, C., Barraclough, R., Rudland, P., 2006. Association of S100A4 and osteopontin with specific prognostic factors and survival of patients with minimally invasive breast cancer. *Clinical Cancer Research*. **12**, 1192-1200.
- De Vouge, M.W. & Mukherjee, B.B., 1992. Transformation of normal rat kidney cells by v-K-ras enhances expression of transin 2 and an S-100-related calcium-binding protein. *Oncogene*. **7**, 109-119.
- Deloulme, J.C., Gentil, B.J., Baudier, J., 2003. Monitoring of S100 homodimerization and heterodimeric interactions by the yeast two-hybrid system. *Microscopy Research and Technique*. **60**, 560-568.
- Deryugina, E.I. & Quigley, J.P., 2006. Matrix metalloproteinases and tumor metastasis. *Cancer and Metastasis Reviews*. **25**, 9-34.
- Dietrich, K.A., Sindelar, C.V., Brewer, P.D., Downing, K.H., Cremo, C.R., Rice, S.E., 2008. The kinesin-1 motor protein is regulated by a direct interaction of its head and

tail. *Proceedings of the National Academy of Sciences of the United States of America*. **105**, 8938-8943.

Diggle, P.J., 1983. *Statistical Analysis of Spatial Point Patterns*. Academic Press.

Donato, R., 2003. Intracellular and extracellular roles of S100 proteins. *Microscopy Research and Technique*. **60**, 540-551.

Donato, R., 2001. S100: A multigenic family of calcium-modulated proteins of the EF-hand type with intracellular and extracellular functional roles. *International Journal of Biochemistry and Cell Biology*. **33**, 637-668.

Donato, R., 1999. Functional roles of S100 proteins, calcium-binding proteins of the EF-hand type. *Biochimica Et Biophysica Acta - Molecular Cell Research*. **1450**, 191-231.

Dos Remedios, C.G., Chhabra, D., Kekic, M., Dedova, I.V., Tsubakihara, M., Berry, D.A., Nosworthy, N.J., 2003. Actin binding proteins: Regulation of cytoskeletal microfilaments. *Physiological Reviews*. **83**, 433-473.

Du, M., Wang, G., Ismail, T.M., Gross, S., Fernig, D.G., Barraclough, R., Rudland, P.S., 2012. S100P dissociates myosin IIA filaments and focal adhesion sites to reduce cell adhesion and enhance cell migration. *The Journal of Biological Chemistry*. **287**, 15330-15344.

Dukhanina, E.A., Kabanova, O.D., Lukyanova, T.I., Shatalov, Y.V., Yashin, D.V., Romanova, E.A., Gnuchev, N.V., Galkin, A.V., Georgiev, G.P., Sashchenko, L.P., 2009. Opposite roles of metastasin (S100A4) in two potentially tumoricidal mechanisms involving human lymphocyte protein Tag7 and Hsp70. *Proceedings of the National Academy of Sciences of the United States of America*. **106**, 13963-13967.

Dulyaninova, N.G., Hite, K.M., Zencheck, W.D., Scudiero, D.A., Almo, S.C., Shoemaker, R.H., Bresnick, A.R., 2011. Cysteine 81 is critical for the interaction of s100a4 and myosin-IIA. *Biochemistry*. **50**, 7218-7227.

Dulyaninova, N.G., House, R.P., Betapudi, V., Bresnick, A.R., 2007. Myosin-IIA heavy-chain phosphorylation regulates the motility of MDA-MB-231 carcinoma cells. *Molecular Biology of the Cell*. **18**, 3144-3155.

Dulyaninova, N.G., Malashkevich, V.N., Almo, S.C., Bresnick, A.R., 2005. Regulation of myosin-IIA assembly and Mts1 binding by heavy chain phosphorylation. *Biochemistry*. **44**, 6867-6876.

Dutta, K., Cox, C.J., Huang, H., Basavappa, R., Pascal, S.M., 2002. Calcium coordination studies of the metastatic Mts1 protein. *Biochemistry*. **41**, 4239-4245.

Eastham, A.M., Spencer, H., Soncin, F., Ritson, S., Merry, C.L.R., Stern, P.L., Ward, C.M., 2007. Epithelial-mesenchymal transition events during human embryonic stem cell differentiation. *Cancer Research*. **67**, 11254-11262.

- Ebralidze, A., Tulchinsky, E., Grigorian, M., Afanasyeva, A., Senin, V., Revazova, E., Lukanidin, E., 1989. Isolation and characterization of a gene specifically expressed in different metastatic cells and whose deduced gene product has a high degree of homology to a Ca²⁺-binding protein family. *Genes & Development*. **3**, 1086-1093.
- Elliott, A. & Offer, G., 1978. Shape and flexibility of the myosin molecule. *Journal of Molecular Biology*. **123**, 505-519.
- Elliott, P.R., Irvine, A.F., Jung, H.S., Tozawa, K., Pastok, M.W., Picone, R., Badyal, S.K., Basran, J., Rudland, P.S., Barraclough, R., Lian, L.Y., Bagshaw, C.R., Kriajevska, M., Barsukov, I.L., 2012. Asymmetric Mode of Ca(2+)-S100A4 Interaction with Nonmuscle Myosin IIA Generates Nanomolar Affinity Required for Filament Remodeling. *Structure (London, England : 1993)*. **20**, 654-666.
- Endo, H., Takenaga, K., Kanno, T., Satoh, H., Mori, S., 2002. Methionine aminopeptidase 2 is a new target for the metastasis-associated protein, S100A4. *Journal of Biological Chemistry*. **277**, 26396-26402.
- Etienne-Manneville, S., 2004. Cdc42 - The centre of polarity. *Journal of Cell Science*. **117**, 1291-1300.
- Fabris, L., Cadamuro, M., Moserle, L., Dziura, J., Cong, X., Sambado, L., Nardo, G., Sonzogni, A., Colledan, M., Furlanetto, A., Bassi, N., Massani, M., Cillo, U., Mescoli, C., Indraccolo, S., Rugge, M., Okolicsanyi, L., Strazzabosco, M., 2011. Nuclear expression of S100A4 calcium-binding protein increases cholangiocarcinoma invasiveness and metastasization. *Hepatology*. **54**, 890-899.
- Fernandez-Fernandez, M.R., Veprintsev, D.B., Fersht, A.R., 2005. Proteins of the S100 family the regulate the oligomerization of p53 tumor suppressor. *Proceedings of the National Academy of Sciences of the United States of America*. **102**, 4735-4740.
- Ford, H.L., Salim, M.M., Chakravarty, R., Aluiddin, V., Zain, S.B., 1995. Expression of Mts1, a metastasis-associated gene, increases motility but not invasion of a nonmetastatic mouse mammary adenocarcinoma cell line. *Oncogene*. **11**, 2067-2075.
- Ford, H.L., Silver, D.L., Kachar, B., Sellers, J.R., Zain, S.B., 1997. Effect of Mts1 on the structure and activity of nonmuscle myosin II. *Biochemistry*. **36**, 16321-16327.
- Franco-Barraza, J., Valdivia-Silva, J.E., Zamudio-Meza, H., Castillo, A., Garcia-Zepeda, E.A., Benitez-Bribiesca, L., Meza, I., 2010. Actin cytoskeleton participation in the onset of IL-1beta induction of an invasive mesenchymal-like phenotype in epithelial MCF-7 cells. *Archives of Medical Research*. **41**, 170-181.
- Friedl, P. & Alexander, S., 2011. Cancer invasion and the microenvironment: Plasticity and reciprocity. *Cell*. **147**, 992-1009.
- Friedl, P. & Gilmour, D., 2009. Collective cell migration in morphogenesis, regeneration and cancer. *Nature Reviews Molecular Cell Biology*. **10**, 445-457.

- Friedl, P. & Wolf, K., 2010. Plasticity of cell migration: A multiscale tuning model. *Journal of Cell Biology*. **188**, 11-19.
- Friedl, P. & Wolf, K., 2009. Proteolytic interstitial cell migration: A five-step process. *Cancer and Metastasis Reviews*. **28**, 129-135.
- Fujiwara, M., Kashima, T.G., Kunita, A., Kii, I., Komura, D., Grigoriadis, A.E., Kudo, A., Aburatani, H., Fukayama, M., 2011. Stable knockdown of S100A4 suppresses cell migration and metastasis of osteosarcoma. *Tumour Biology : The Journal of the International Society for Oncodevelopmental Biology and Medicine*. **32**, 611-622.
- Fukata, M., Nakagawa, M., Kaibuchi, K., 2003. Roles of Rho-family GTPases in cell polarisation and directional migration. *Current Opinion in Cell Biology*. **15**, 590-597.
- Garrett, S.C., Hodgson, L., Rybin, A., Touthkine, A., Hahn, K.M., Lawrence, D.S., Bresnick, A.R., 2008. A biosensor of S100A4 metastasis factor activation: Inhibitor screening and cellular activation dynamics. *Biochemistry*. **47**, 986-996.
- Gasteiger E., Hoogland C., Gattiker A., Duvaud S., Wilkins M.R., Appel R.D., Bairoch A., 2005. The Proteomics Protocols Handbook, Humana Press
- Giard, D.J., Aaronson, S.A., Todaro, G.J., Arnstein, P., Kersey, J.H., Dosik, H., Parks, W.P., 1973. In vitro cultivation of human tumors: establishment of cell lines derived from a series of solid tumors. *Journal of the National Cancer Institute*. **51**, 1417-1423.
- Gingras, A.R., Basran, J., Prescott, A., Krijajevska, M., Bagshaw, C.R., Barsukov, I.L., 2008. Crystal structure of the Ca(2+)-form and Ca(2+)-binding kinetics of metastasis-associated protein, S100A4. *FEBS Letters*. **582**, 1651-1656.
- Goch, G., Vdovenko, S., Kozłowska, H., Bierzyński, A., 2005. Affinity of S100A1 protein for calcium increases dramatically upon glutathionylation. *FEBS Journal*. **272**, 2557-2565.
- Goh Then Sin, C., Hersch, N., Rudland, P.S., Barraclough, R., Hoffmann, B., Gross, S.R., 2011. S100A4 downregulates filopodia formation through increased dynamic instability. *Cell Adhesion & Migration*. **5**, 439-447.
- Goley, E.D. & Welch, M.D., 2006. The ARP2/3 complex: An actin nucleator comes of age. *Nature Reviews Molecular Cell Biology*. **7**, 713-726.
- Golomb, E., Ma, X., Jana, S.S., Preston, Y.A., Kawamoto, S., Shoham, N.G., Goldin, E., Conti, M.A., Sellers, J.R., Adelstein, R.S., 2004. Identification and Characterization of Nonmuscle Myosin II-C, a New Member of the Myosin II Family. *Journal of Biological Chemistry*. **279**, 2800-2808.
- Gongoll, S., Peters, G., Mengel, M., Piso, P., Klempnauer, J., Kreipe, H., von Wasielewski, R., 2002. Prognostic significance of calcium-binding protein S100A4 in colorectal cancer. *Gastroenterology*. **123**, 1478-1484.

- Goyette, J. & Geczy, C.L., 2011. Inflammation-associated S100 proteins: New mechanisms that regulate function. *Amino Acids*. **41**, 821-842.
- Griffiths, G., 1993. *Fine Structure Immuno-cytochemistry*. Springer-Verlag.
- Grigorian, M., Andresen, S., Tulchinsky, E., Kriajevskaja, M., Carlberg, C., Kruse, C., Cohn, M., Ambartsumian, N., Christensen, A., Selivanova, G., Lukanidin, E., 2001. Tumor suppressor p53 protein is a new target for the metastasis-associated Mts1/S100A4 protein. Functional consequences of their interaction. *Journal of Biological Chemistry*. **276**, 22699-22708.
- Grum-Schwensen, B., Klingelhofer, J., Berg, C.H., El-Naaman, C., Grigorian, M., Lukanidin, E., Ambartsumian, N., 2005. Suppression of tumor development and metastasis formation in mice lacking the S100A4(mts1) gene. *Cancer Research*. **65**, 3772-3780.
- Grum-Schwensen, B., Klingelhofer, J., Grigorian, M., Almholt, K., Nielsen, B.S., Lukanidin, E., Ambartsumian, N., 2010. Lung metastasis fails in MMTV-PyMT oncomice lacking S100A4 due to a T-cell deficiency in primary tumors. *Cancer Research*. **70**, 936-947.
- Guarino, M., Tosoni, A., Nebuloni, M., 2009. Direct contribution of epithelium to organ fibrosis: epithelial-mesenchymal transition. *Human Pathology*. **40**, 1365-1376.
- Gupta, G.P. & Massagué, J., 2006. Cancer Metastasis: Building a Framework. *Cell*. **127**, 679-695.
- Gupton, S.L. & Waterman-Storer, C.M., 2006. Spatiotemporal feedback between actomyosin and focal-adhesion systems optimizes rapid cell migration. *Cell*. **125**, 1361-1374.
- Hanahan, D. & Weinberg, R.A., 2011. Hallmarks of cancer: The next generation. *Cell*. **144**, 646-674.
- Hanahan, D. & Weinberg, R.A., 2000. The Hallmarks of Cancer. *Cell*. **100**, 57-70.
- Harburger, D.S. & Calderwood, D.A., 2009. Integrin signalling at a glance. *Journal of Cell Science*. **122**, 159-163.
- Harris, M.A., Yang, H., Low, B.E., Mukherjee, J., Guha, A., Bronson, R.T., Shultz, L.D., Israel, M.A., Yun, K., 2008. Cancer stem cells are enriched in the side population cells in a mouse model of glioma. *Cancer Research*. **68**, 10051-10059.
- Haugen, M.H., Flatmark, K., Mikalsen, S.-., Malandsmo, G.M., 2008. The metastasis-associated protein S100A4 exists in several charged variants suggesting the presence of posttranslational modifications. *BMC Cancer*. **8**, .
- Heizmann, C.W., Ackermann, G.E., Galichet, A., 2007. Pathologies involving the S100 proteins and RAGE. *Sub-Cellular Biochemistry*. **45**, 93-138.

- Helfman, D.M., Kim, E.J., Lukanidin, E., Grigorian, M., 2005. The metastasis associated protein S100A4: Role in tumour progression and metastasis. *British Journal of Cancer*. **92**, 1955-1958.
- Hernan, R., Fasheh, R., Calabrese, C., Frank, A.J., Maclean, K.H., Allard, D., Barraclough, R., Gilbertson, R.J., 2003. ERBB2 up-regulates S100A4 and several other prometastatic genes in medulloblastoma. *Cancer Research*. **63**, 140-148.
- Hiratsuka, S., Duda, D.G., Huang, Y., Goel, S., Sugiyama, T., Nagasawa, T., Fukumura, D., Jain, R.K., 2011. C-X-C receptor type 4 promotes metastasis by activating p38 mitogen-activated protein kinase in myeloid differentiation antigen (Gr-1)-positive cells. *Proceedings of the National Academy of Sciences of the United States of America*. **108**, 302-307.
- Horiuchi, A., Hayashi, T., Kikuchi, N., Hayashi, A., Fuseya, C., Shiozawa, T., Konishi, I., 2012. Hypoxia upregulates ovarian cancer invasiveness via the binding of HIF-1 α to a hypoxia-induced, methylation-free hypoxia response element of S100A4 gene. *International Journal of Cancer*.
- Horowitz, A., Trybus, K.M., Bowman, D.S., Fay, F.S., 1994. Antibodies probe for folded monomeric myosin in relaxed and contracted smooth muscle. *The Journal of Cell Biology*. **126**, 1195-1200.
- Huang, Y., Fernandez, S.V., Goodwin, S., Russo, P.A., Russo, I.H., Sutter, T.R., Russo, J., 2007. Epithelial to mesenchymal transition in human breast epithelial cells transformed by 17 β -estradiol. *Cancer Research*. **67**, 11147-11157.
- Hugo, H.J., Wafai, R., Blick, T., Thompson, E.W., Newgreen, D.F., 2009. Staurosporine augments EGF-mediated EMT in PMC42-LA cells through actin depolymerisation, focal contact size reduction and Snail1 induction - a model for cross-modulation. *BMC Cancer*. **9**, 235.
- Hyun, S.J., Komatsu, S., Ikebe, M., Craig, R., 2008. Head-head and head-tail interaction: A general mechanism for switching off myosin II activity in cells. *Molecular Biology of the Cell*. **19**, 3234-3242.
- Iniesta, A., Diaz, F.G., Garcia de la Torre, J., 1988. Transport properties of rigid bent-rod macromolecules and of semiflexible broken rods in the rigid-body treatment. Analysis of the flexibility of myosin rod. *Biophysical Journal*. **54**, 269-275.
- Ismail, N.I., Kaur, G., Hashim, H., Hassan, M.S., 2008a. S100A4 overexpression proves to be independent marker for breast cancer progression. *Cancer Cell International*. **8**, .
- Ismail, T.M., Fernig, D.G., Rudland, P.S., Terry, C.J., Wang, G., Barraclough, R., 2008b. The basic C-terminal amino acids of calcium-binding protein S100A4 promote metastasis. *Carcinogenesis*. **29**, 2259-2266.

- Itoh, K. & Adelstein, R.S., 1995. Neuronal cell expression of inserted isoforms of vertebrate nonmuscle myosin heavy chain II-B. *Journal of Biological Chemistry*. **270**, 14533-14540.
- Jaffe, A.B. and Hall, A., 2005. Rho GTPases: Biochemistry and biology.
- Janda, E., Lehmann, K., Killisch, I., Jechlinger, M., Herzig, M., Downward, J., Beug, H., Grunert, S., 2002. Ras and TGF[beta] cooperatively regulate epithelial cell plasticity and metastasis: dissection of Ras signaling pathways. *The Journal of Cell Biology*. **156**, 299-313.
- Jenkinson, S.R., Barraclough, R., West, C.R., Rudland, P.S., 2004. S100A4 regulates cell motility and invasion in an in vitro model for breast cancer metastasis. *British Journal of Cancer*. **90**, 253-262.
- Joyce, J.A. & Pollard, J.W., 2009. Microenvironmental regulation of metastasis. *Nature Reviews Cancer*. **9**, 239-252.
- Jung, H.S., Billington, N., Thirumurugan, K., Salzameda, B., Cremo, C.R., Chalovich, J.M., Chantler, P.D., Knight, P.J., 2011. Role of the tail in the regulated state of myosin 2. *Journal of Molecular Biology*. **408**, 863-878.
- Kalluri, R. and Weinberg, R.A., 2009. The basics of epithelial-mesenchymal transition.(Review series)(Report).
- Katoh, K., Kano, Y., Noda, Y., 2011. Rho-associated kinase-dependent contraction of stress fibres and the organization of focal adhesions. *Journal of the Royal Society Interface*. **8**, 305-311.
- Kelley, C.A., Kawamoto, S., Conti, M.A., Adelstein, R.S., 1991. Phosphorylation of vertebrate smooth muscle and nonmuscle myosin heavy chains in vitro and in intact cells. *Journal of Cell Science*. **98**, 49-54.
- Kendrick-Jones, J., Smith, R.C., Craig, R., Citi, S., 1987. Polymerization of vertebrate non-muscle and smooth muscle myosins. *Journal of Molecular Biology*. **198**, 241-252.
- Kikuchi, N., Horiuchi, A., Osada, R., Imai, T., Wang, C., Chen, X., Konishi, I., 2006. Nuclear expression of S100A4 is associated with aggressive behavior of epithelial ovarian carcinoma: an important autocrine/paracrine factor in tumor progression. *Cancer Science*. **97**, 1061-1069.
- Kim, E.J. & Helfman, D.M., 2003. Characterization of the metastasis-associated protein, S100A4: Roles of calcium binding and dimerization in cellular localization and interaction with myosin. *Journal of Biological Chemistry*. **278**, 30063-30073.
- Kim, K., Lu, Z., Hay, E.D., 2002. Direct evidence for a role of beta-catenin/LEF-1 signaling pathway in induction of EMT. *Cell Biology International*. **26**, 463-476.

- Kim, K.-., Kovács, M., Kawamoto, S., Sellers, J.R., Adelstein, R.S., 2005. Disease-associated mutations and alternative splicing alter the enzymatic and motile activity of nonmuscle myosins II-B and II-C. *Journal of Biological Chemistry*. **280**, 22769-22775.
- Kim, M.A., Lee, H.S., Lee, H.E., Kim, J.H., Yang, H.K., Kim, W.H., 2009. Prognostic importance of epithelial-mesenchymal transition-related protein expression in gastric carcinoma. *Histopathology*. **54**, 442-451.
- Kim, Y.J., Kim, M.A., Im, S.A., Kim, T.M., Kim, D.W., Yang, H.K., Heo, D.S., Lee, K.U., Choe, K.J., Kim, N.K., Kim, T.Y., Kim, W.H., Bang, Y.J., 2008. Metastasis-associated protein S100A4 and p53 predict relapse in curatively resected stage III and IV (M0) gastric cancer. *Cancer Investigation*. **26**, 152-158.
- Kimura, K., Endo, Y., Yonemura, Y., Heizmann, C.W., Schafer, B.W., Watanabe, Y., Sasaki, T., 2000. Clinical significance of S100A4 and E-cadherin-related adhesion molecules in non-small cell lung cancer. *International Journal of Oncology*. **16**, 1125-1131.
- Klein, C.A., 2009. Parallel progression of primary tumours and metastases. *Nature Reviews Cancer*. **9**, 302-312.
- Kölsch, V., Charest, P.G., Firtel, R.A., 2008. The regulation of cell motility and chemotaxis by phospholipid signaling. *Journal of Cell Science*. **121**, 551-559.
- Kovacs, M., Malnasi-Csizmadia, A., Woolley, R.J., Bagshaw, C.R., 2002. Analysis of nucleotide binding to Dictyostelium myosin II motor domains containing a single tryptophan near the active site. *The Journal of Biological Chemistry*. **277**, 28459-28467.
- Kovács, M., Wang, F., Hu, A., Zhang, Y., Sellers, J.R., 2003. Functional divergence of human cytoplasmic myosin II. Kinetic characterization of the non-muscle IIA isoform. *Journal of Biological Chemistry*. **278**, 38132-38140.
- Kriajevska, M., Bronstein, I.B., Scott, D.J., Tarabykina, S., Fischer-Larsen, M., Issinger, O.-., Lukanidin, E., 2000. Metastasis-associated protein Mts1 (S100A4) inhibits CK2-mediated phosphorylation and self-assembly of the heavy chain of nonmuscle myosin. *Biochimica Et Biophysica Acta - Molecular Cell Research*. **1498**, 252-263.
- Kriajevska, M., Fischer-Larsen, M., Moertz, E., Vorm, O., Tulchinsky, E., Grigorian, M., Ambartsumian, N., Lukanidin, E., 2002. Liprin beta 1, a member of the family of LAR transmembrane tyrosine phosphatase-interacting proteins, is a new target for the metastasis-associated protein S100A4 (Mts1). *The Journal of Biological Chemistry*. **277**, 5229-5235.
- Kriajevska, M., Tarabykina, S., Bronstein, I., Maitland, N., Lomonosov, M., Hansen, K., Georgiev, G., Lukanidin, E., 1998. Metastasis-associated Mts1 (S100A4) protein modulates protein kinase C phosphorylation of the heavy chain of nonmuscle myosin. *Journal of Biological Chemistry*. **273**, 9852-9856.

- Kriajevska, M.V., Cardenas, M.N., Grigorian, M.S., Ambartsumian, N.S., Georgiev, G.P., Lukanidin, E.M., 1994. Non-muscle myosin heavy chain as a possible target for protein encoded by metastasis-related mts-1 gene. *Journal of Biological Chemistry*. **269**, 19679-19682.
- Lachmanovich, E., Shvartsman, D.E., Malka, Y., Botvin, C., Henis, Y.I., Weiss, A.M., 2003. Co-localization analysis of complex formation among membrane proteins by computerized fluorescence microscopy: application to immunofluorescence co-patching studies. *Journal of Microscopy*. **212**, 122-131.
- Lauffenburger, D.A. & Horwitz, A.F., 1996. Cell migration: a physically integrated molecular process. *Cell*. **84**, 359-369.
- Lazarova, D.L., Bordonaro, M., Sartorelli, A.C., 2001. Transcriptional regulation of the vitamin D(3) receptor gene by ZEB. *Cell Growth & Differentiation : The Molecular Biology Journal of the American Association for Cancer Research*. **12**, 319-326.
- Lee, J., Ishihara, A., Oxford, G., Johnson, B., Jacobson, K., 1999. Regulation of cell movement is mediated by stretch-activated calcium channels. *Nature*. **400**, 382-386.
- Lee, O.J., Hong, S.M., Razvi, M.H., Peng, D., Powell, S.M., Smoklin, M., Moskaluk, C.A., El-Rifai, W., 2006. Expression of calcium-binding proteins S100A2 and S100A4 in Barrett's adenocarcinomas. *Neoplasia (New York, N.Y.)*. **8**, 843-850.
- Lee, W.-., Su, W.-., Lin, P.-., Guo, H.-., Chang, T.-., Chen, H.H.W., 2004. Expression of S100A4 and Met: Potential Predictors for Metastasis and Survival in Early-Stage Breast Cancer. *Oncology*. **66**, 429-438.
- Leśniak, W., 2011. Epigenetic regulation of S100 protein expression. *Clinical Epigenetics*. **2**, 77-83.
- Li, N., Song, M.M., Chen, X.H., Liu, L.H., Li, F.S., 2012. S100A4 siRNA inhibits human pancreatic cancer cell invasion in vitro. *Biomedical and Environmental Sciences : BES*. **25**, 465-470.
- Li, Q., Lau, A., Morris, T.J., Guo, L., Fordyce, C.B., Stanley, E.F., 2004. A syntaxin 1, Galpha(o), and N-type calcium channel complex at a presynaptic nerve terminal: analysis by quantitative immunocolocalization. *The Journal of Neuroscience : The Official Journal of the Society for Neuroscience*. **24**, 4070-4081.
- Li, Z.-. & Bresnick, A.R., 2006. The S100A4 metastasis factor regulates cellular motility via a direct interaction with myosin-IIA. *Cancer Research*. **66**, 5173-5180.
- Li, Z.-., Dulyaninova, N.G., House, R.P., Almo, S.C., Bresnick, A.R., 2010. S100A4 regulates macrophage chemotaxis. *Molecular Biology of the Cell*. **21**, 2598-2610.
- Li, Z.H., Spektor, A., Varlamova, O., Bresnick, A.R., 2003. Mts1 regulates the assembly of nonmuscle myosin-IIA. *Biochemistry*. **42**, 14258-14266.

- Lim, S.Y., Raftery, M., Cai, H., Hsu, K., Yan, W.X., Hsieh, H.-., Watts, R.N., Richardson, D., Thomas, S., Perry, M., Geczy, C.L., 2008. S-nitrosylated S100A8: Novel anti-inflammatory properties. *Journal of Immunology*. **181**, 5627-5636.
- Lindsey, J.C., Lusher, M.E., Anderton, J.A., Gilbertson, R.J., Ellison, D.W., Clifford, S.C., 2007. Epigenetic deregulation of multiple S100 gene family members by differential hypomethylation and hypermethylation events in medulloblastoma. *British Journal of Cancer*. **97**, 267-274.
- Lo, J.F., Yu, C.C., Chiou, S.H., Huang, C.Y., Jan, C.I., Lin, S.C., Liu, C.J., Hu, W.Y., Yu, Y.H., 2011. The epithelial-mesenchymal transition mediator S100A4 maintains cancer-initiating cells in head and neck cancers. *Cancer Research*. **71**, 1912-1923.
- Lopez-Lago, M.A., Thodima, V.J., Guttapalli, A., Chan, T., Heguy, A., Molina, A.M., Reuter, V.E., Motzer, R.J., Chaganti, R.S., 2010. Genomic deregulation during metastasis of renal cell carcinoma implements a myofibroblast-like program of gene expression. *Cancer Research*. **70**, 9682-9692.
- Lopez-Novoa, J.M. & Nieto, M.A., 2009. Inflammation and EMT: an alliance towards organ fibrosis and cancer progression. *EMBO Molecular Medicine*. **1**, 303-314.
- Ma, X., Jana, S.S., Conti, M.A., Kawamoto, S., Claycomb, W.C., Adelstein, R.S., 2010. Ablation of nonmuscle myosin II-B and II-C reveals a role for nonmuscle myosin II in cardiac myocyte karyokinesis. *Molecular Biology of the Cell*. **21**, 3952-3962.
- Ma, X., Kawamoto, S., Hara, Y., Adelstein, R.S., 2004. A point mutation in the motor domain of nonmuscle myosin II-B impairs migration of distinct groups of neurons. *Molecular Biology of the Cell*. **15**, 2568-2579.
- Ma, X., Kovačs, M., Conti, M.A., Wang, A., Zhang, Y., Sellers, J.R., Adelstein, R.S., 2012. Nonmuscle myosin II exerts tension but does not translocate actin in vertebrate cytokinesis. *Proceedings of the National Academy of Sciences of the United States of America*. **109**, 4509-4514.
- Maelandsmo, G.M., Florenes, V.A., Nguyen, M.T., Flatmark, K., Davidson, B., 2009. Different expression and clinical role of S100A4 in serous ovarian carcinoma at different anatomic sites. *Tumour Biology : The Journal of the International Society for Oncodevelopmental Biology and Medicine*. **30**, 15-25.
- Maelandsmo, G.M., Hovig, E., Skrede, M., Engebraaten, O., Flørenes, V.A., Myklebost, O., Grigorian, M., Lukanidin, E., Scanlon, K.J., Fodstad, Ø., 1996. Reversal of the in vivo metastatic phenotype of human tumor cells by an anti-CAPL (mts1) ribozyme. *Cancer Research*. **56**, 5490-5498.
- Malanchi, I., Santamaria-Martínez, A., Susanto, E., Peng, H., Lehr, H.-., Delaloye, J.-., Huelsken, J., 2012. Interactions between cancer stem cells and their niche govern metastatic colonization. *Nature*. **481**, 85-91.
- Malashkevich, V.N., Dulyaninova, N.G., Ramagopal, U.A., Liriano, M.A., Varney, K.M., Knight, D., Brenowitz, M., Weber, D.J., Almo, S.C., Bresnick, A.R., 2010.

- Phenothiazines inhibit S100A4 function by inducing protein oligomerization. *Proceedings of the National Academy of Sciences of the United States of America*. **107**, 8605-8610.
- Malashkevich, V.N., Varney, K.M., Garrett, S.C., Wilder, P.T., Knight, D., Charpentier, T.H., Ramagopal, U.A., Almo, S.C., Weber, D.J., Bresnick, A.R., 2008. Structure of Ca²⁺-bound S100A4 and its interaction with peptides derived from nonmuscle myosin-IIA. *Biochemistry*. **47**, 5111-5126.
- Manders, E.M., Stap, J., Brakenhoff, G.J., van Driel, R., Aten, J.A., 1992. Dynamics of three-dimensional replication patterns during the S-phase, analysed by double labelling of DNA and confocal microscopy. *Journal of Cell Science*. **103 (Pt 3)**, 857-862.
- Mani, S.A., Guo, W., Liao, M.-., Eaton, E.N., Ayyanan, A., Zhou, A.Y., Brooks, M., Reinhard, F., Zhang, C.C., Shipitsin, M., Campbell, L.L., Polyak, K., Brisken, C., Yang, J., Weinberg, R.A., 2008. The Epithelial-Mesenchymal Transition Generates Cells with Properties of Stem Cells. *Cell*. **133**, 704-715.
- Manolakis, A.C., Kapsoritakis, A.N., Tiaka, E.K., Potamianos, S.P., 2011. Calprotectin, calgranulin C, and other members of the s100 protein family in inflammatory bowel disease. *Digestive Diseases and Sciences*. **56**, 1601-1611.
- Marenholz, I., Heizmann, C.W., Fritz, G., 2004. S100 proteins in mouse and man: From evolution to function and pathology (including an update of the nomenclature). *Biochemical and Biophysical Research Communications*. **322**, 1111-1122.
- Mathias, R.A., Wang, B., Ji, H., Kapp, E.A., Moritz, R.L., Zhu, H.J., Simpson, R.J., 2009. Secretome-based proteomic profiling of Ras-transformed MDCK cells reveals extracellular modulators of epithelial-mesenchymal transition. *Journal of Proteome Research*. **8**, 2827-2837.
- Matsubara, D., Niki, T., Ishikawa, S., Goto, A., Ohara, E., Yokomizo, T., Heizmann, C.W., Aburatani, H., Moriyama, S., Moriyama, H., Nishimura, Y., Funata, N., Fukayama, M., 2005. Differential expression of S100A2 and S100A4 in lung adenocarcinomas: clinicopathological significance, relationship to p53 and identification of their target genes. *Cancer Science*. **96**, 844-857.
- Matsumoto, K., Irie, A., Satoh, T., Ishii, J., Iwabuchi, K., Iwamura, M., Egawa, S., Baba, S., 2007. Expression of S100A2 and S100A4 predicts for disease progression and patient survival in bladder cancer. *Urology*. **70**, 602-607.
- Matsumura, F. & Hartshorne, D.J., 2008. Myosin phosphatase target subunit: Many roles in cell function. *Biochemical and Biophysical Research Communications*. **369**, 149-156.
- Matsuura, I., Lai, C.-., Chiang, K.-., 2010. Functional interaction between Smad3 and S100A4 (metastatin-1) for TGF- β -mediated cancer cell invasiveness. *Biochemical Journal*. **426**, 327-335.

- McAllister, S.S., Gifford, A.M., Greiner, A.L., Kelleher, S.P., Saelzler, M.P., Ince, T.A., Reinhardt, F., Harris, L.N., Hylander, B.L., Repasky, E.A., Weinberg, R.A., 2008. Systemic Endocrine Instigation of Indolent Tumor Growth Requires Osteopontin. *Cell*. **133**, 994-1005.
- Mejlvang, J., Kriajevska, M., Vandewalle, C., Chernova, T., Sayan, A.E., Berx, G., Mellon, J.K., Tulchinsky, E., 2007. Direct Repression of Cyclin D1 by SIP1 Attenuates Cell Cycle Progression in Cells Undergoing an Epithelial Mesenchymal Transition. *Molecular Biology of the Cell*. **18**, 4615-4624.
- Meng, S., Tripathy, D., Frenkel, E.P., Shete, S., Naftalis, E.Z., Huth, J.F., Beitsch, P.D., Leitch, M., Hoover, S., Euhus, D., Haley, B., Morrison, L., Fleming, T.P., Herlyn, D., Terstappen, L.W., Fehm, T., Tucker, T.F., Lane, N., Wang, J., Uhr, J.W., 2004. Circulating tumor cells in patients with breast cancer dormancy. *Clinical Cancer Research : An Official Journal of the American Association for Cancer Research*. **10**, 8152-8162.
- Milton, D.L., Schneck, A.N., Ziech, D.A., Ba, M., Facemyer, K.C., Halayko, A.J., Baker, J.E., Gerthoffer, W.T., Cremo, C.R., 2011. Direct evidence for functional smooth muscle myosin II in the 10S self-inhibited monomeric conformation in airway smooth muscle cells. *Proceedings of the National Academy of Sciences of the United States of America*. **108**, 1421-1426.
- Miranda, K.J., Loeser, R.F., Yammani, R.R., 2010. Sumoylation and nuclear translocation of S100A4 regulate IL-1 β -mediated production of matrix metalloproteinase-13. *Journal of Biological Chemistry*. **285**, 31517-31524.
- Mischke, D., Korge, B.P., Marenholz, I., Volz, A., Ziegler, A., 1996. Genes Encoding Structural Proteins of Epidermal Cornification and S100 Calcium-Binding Proteins Form a Gene Complex ("Epidermal Differentiation Complex") on Human Chromosome 1q21. *Journal of Investigative Dermatology*. **106**, 989-992.
- Miyazaki, N., Abe, Y., Oida, Y., Suemizu, H., Nishi, M., Yamazaki, H., Iwasaki, M., Inoue, H., Ueyama, Y., Nakamura, M., 2006. Poor outcome of patients with pulmonary adenocarcinoma showing decreased E-cadherin combined with increased S100A4 expression. *International Journal of Oncology*. **28**, 1369-1374.
- Moreno-Bueno, G., Peinado, H., Molina, P., Olmeda, D., Cubillo, E., Santos, V., Palacios, J., Portillo, F., Cano, A., 2009. The morphological and molecular features of the epithelial-to-mesenchymal transition. *Nature Protocols*. **4**, 1591-1613.
- Murakami, N., 1995. Phospholipid binding, phosphorylation by protein kinase C, and filament assembly of the COOH terminal heavy chain fragments of nonmuscle myosin II isoforms MIIA and MIIB. *Biochemistry*. **34**, 16046-16055.
- Murakami, N., Chauhan, V.P.S., Elzinga, M., 1998. Two nonmuscle myosin II heavy chain isoforms expressed in rabbit brains: Filament forming properties, the effects of phosphorylation by protein kinase C and casein kinase II, and location of the phosphorylation sites. *Biochemistry*. **37**, 1989-2003.

- Murakami, N., Kotula, L., Hwang, Y.-., 2000. Two distinct mechanisms for regulation of nonmuscle myosin assembly via the heavy chain: Phosphorylation for MIIB and Mts 1 binding for MIIA. *Biochemistry*. **39**, 11441-11451.
- Nam, E.H., Lee, Y., Park, Y.K., Lee, J.W., Kim, S., 2012. ZEB2 upregulates integrin alpha5 expression through cooperation with Sp1 to induce invasion during epithelial-mesenchymal transition of human cancer cells. *Carcinogenesis*. **33**, 563-571.
- Negrini, S., Gorgoulis, V.G., Halazonetis, T.D., 2010. Genomic instability an evolving hallmark of cancer. *Nature Reviews Molecular Cell Biology*. **11**, 220-228.
- Newman, G.R. & Hobot, J.A., 1987. Modern acrylics for post-embedding immunostaining techniques. *The Journal of Histochemistry and Cytochemistry : Official Journal of the Histochemistry Society*. **35**, 971-981.
- Nguyen, D.X., Bos, P.D., Massagué, J., 2009. Metastasis: From dissemination to organ-specific colonization. *Nature Reviews Cancer*. **9**, 274-284.
- Niederman, R. & Pollard, T.D., 1975. Human platelet myosin. II. In vitro assembly and structure of myosin filaments. *Journal of Cell Biology*. **67**, 72-92.
- North, A.J., 2006. Seeing is believing? A beginners' guide to practical pitfalls in image acquisition. *The Journal of Cell Biology*. **172**, 9-18.
- O'Halloran, T.J., Ravid, S., Spudich, J.A., 1990. Expression of Dictyostelium myosin tail segments in Escherichia coli: Domains required for assembly and phosphorylation. *Journal of Cell Biology*. **110**, 63-70.
- Oida, Y., Yamazaki, H., Tobita, K., Mukai, M., Ohtani, Y., Miyazaki, N., Abe, Y., Imaizumi, T., Makuuchi, H., Ueyama, Y., Nakamura, M., 2006. Increased S100A4 expression combined with decreased E-cadherin expression predicts a poor outcome of patients with pancreatic cancer. *Oncology Reports*. **16**, 457-463.
- Okada, H., Danoff, T.M., Kalluri, R., Neilson, E.G., 1997. Early role of Fsp1 in epithelial-mesenchymal transformation. *AJP - Renal Physiology*. **273**, F563-574.
- Oren, M., 2003. Decision making by p53: Life, death and cancer. *Cell Death and Differentiation*. **10**, 431-442.
- Orre, L.M., Pernemalm, M., Lengqvist, J., Lewensohn, R., Lehtiö, J., 2007. Up-regulation, modification, and translocation of S100A6 induced by exposure to ionizing radiation revealed by proteomics profiling. *Molecular and Cellular Proteomics*. **6**, 2122-2131.
- Oskarsson, T., Acharyya, S., Zhang, X.H.-., Vanharanta, S., Tavazoie, S.F., Morris, P.G., Downey, R.J., Manova-Todorova, K., Brogi, E., Massagué, J., 2011. Breast cancer cells produce tenascin C as a metastatic niche component to colonize the lungs. *Nature Medicine*. **17**, 867-874.

- Oskarsson, T. & Massagué, J., 2012. Extracellular matrix players in metastatic niches. *EMBO Journal*. **31**, 254-256.
- Ostendorp, T., Leclerc, E., Galichet, A., Koch, M., Demling, N., Weigle, B., Heizmann, C.W., Kroneck, P.M.H., Fritz, G., 2007. Structural and functional insights into RAGE activation by multimeric S100B. *EMBO Journal*. **26**, 3868-3878.
- Österreicher, C.H., Penz-Österreicher, M., Grivennikov, S.I., Guma, M., Koltsova, E.K., Datz, C., Sasik, R., Hardiman, G., Karin, M., Brenner, D.A., 2011. Fibroblast-specific protein 1 identifies an inflammatory subpopulation of macrophages in the liver. *Proceedings of the National Academy of Sciences of the United States of America*. **108**, 308-313.
- Overall, C.M. & Blobel, C.P., 2007. In search of partners: Linking extracellular proteases to substrates. *Nature Reviews Molecular Cell Biology*. **8**, 245-257.
- Page-McCaw, A., Ewald, A.J., Werb, Z., 2007. Matrix metalloproteinases and the regulation of tissue remodelling. *Nature Reviews Molecular Cell Biology*. **8**, 221-233.
- Pankov, R., Endo, Y., Even-Ram, S., Araki, M., Clark, K., Cukierman, E., Matsumoto, K., Yamada, K.M., 2005. A Rac switch regulates random versus directionally persistent cell migration. *Journal of Cell Biology*. **170**, 793-802.
- Patterson, G., Davidson, M., Manley, S., Lippincott-Schwartz, J., 2010. Superresolution imaging using single-molecule localization. *Annual Review of Physical Chemistry*. **61**, 345-367.
- Pathuri, P., Vogeley, L., Luecke, H., 2008. Crystal Structure of Metastasis-Associated Protein S100A4 in the Active Calcium-Bound Form. *Journal of Molecular Biology*. **383**, 62-77.
- Pedersen, K.B., Nesland, J.M., Fodstad, Ø., Mælandsmo, G.M., 2002. Expression of S100A4, E-cadherin, α - and β -catenin in breast cancer biopsies. *British Journal of Cancer*. **87**, 1281-1286.
- Peinado, H., Olmeda, D., Cano, A., 2007. Snail, ZEB and bHLH factors in tumour progression: An alliance against the epithelial phenotype? *Nature Reviews Cancer*. **7**, 415-428.
- Petrie, R.J., Doyle, A.D., Yamada, K.M., 2009. Random versus directionally persistent cell migration. *Nature Reviews Molecular Cell Biology*. **10**, 538-549.
- Philimonenko, A.A., Janacek, J., Hozak, P., 2000. Statistical evaluation of colocalization patterns in immunogold labeling experiments. *Journal of Structural Biology*. **132**, 201-210.
- Picone, R., Ren, X., Ivanovitch, K.D., Clarke, J.D., McKendry, R.A., Baum, B., 2010. A polarised population of dynamic microtubules mediates homeostatic length control in animal cells. *PLoS Biology*. **8**, e1000542.

- Pollard, T.D. & Borisy, G.G., 2003. Cellular Motility Driven by Assembly and Disassembly of Actin Filaments. *Cell*. **112**, 453-465.
- Prior, I.A., Muncke, C., Parton, R.G., Hancock, J.F., 2003. Direct visualization of Ras proteins in spatially distinct cell surface microdomains. *The Journal of Cell Biology*. **160**, 165-170.
- Qian, B.-., Li, J., Zhang, H., Kitamura, T., Zhang, J., Campion, L.R., Kaiser, E.A., Snyder, L.A., Pollard, J.W., 2011. CCL2 recruits inflammatory monocytes to facilitate breast-tumour metastasis. *Nature*. **475**, 222-225.
- Rabut, G. & Ellenberg, J., 2005. Photobleaching Techniques to Study Mobility and Molecular Dynamics of Proteins in Live Cells: FRAP, iFRAP and FLIP. *Live Cell Imaging: A Laboratory Manual*. Cold Spring Harbor Laboratory Press. 101.
- Ravasi, T., Hsu, K., Goyette, J., Schroder, K., Yang, Z., Rahimi, F., Miranda, L.P., Alewood, P.F., Hume, D.A., Geczy, C., 2004. Probing the S100 protein family through genomic and functional analysis. *Genomics*. **84**, 10-22.
- Rety, S., Sopkova, J., Renouard, M., Osterloh, D., Gerke, V., Tabaries, S., Russo-Marie, F., Lewit-Bentley, A., 1999. The crystal structure of a complex of p11 with the annexin II N-terminal peptide. *Nature Structural Biology*. **6**, 89-95.
- Revenu, C. & Gilmour, D., 2009. EMT 2.0: shaping epithelia through collective migration. *Current Opinion in Genetics and Development*. **19**, 338-342.
- Rhim, A.D., Mirek, E.T., Aiello, N.M., Maitra, A., Bailey, J.M., McAllister, F., Reichert, M., Beatty, G.L., Rustgi, A.K., Vonderheide, R.H., Leach, S.D., Stanger, B.Z., 2012. EMT and dissemination precede pancreatic tumor formation. *Cell*. **148**, 349-361.
- Richards, T.A. & Cavalier-Smith, T., 2005. Myosin domain evolution and the primary divergence of eukaryotes. *Nature*. **436**, 1113-1118.
- Ricketson, D., Johnston, C.A., Prehoda, K.E., 2010. Multiple tail domain interactions stabilize nonmuscle myosin II bipolar filaments. *Proceedings of the National Academy of Sciences of the United States of America*. **107**, 20964-20969.
- Ridley, A.J., 2011. Life at the leading edge. *Cell*. **145**, 1012-1022.
- Ridley, A.J., Schwartz, M.A., Burridge, K., Firtel, R.A., Ginsberg, M.H., Borisy, G., Parsons, J.T., Horwitz, A.R., 2003. Cell Migration: Integrating Signals from Front to Back. *Science*. **302**, 1704-1709.
- Rintala-Dempsey, A.C., Rezvanpour, A., Shaw, G.S., 2008. S100-annexin complexes--structural insights. *The FEBS Journal*. **275**, 4956-4966.
- Rivard, C.J., Brown, L.M., Almeida, N.E., Maunsbach, A.B., Pihakaski-Maunsbach, K., Andres-Hernando, A., Capasso, J.M., Berl, T., 2007. Expression of the calcium-binding

- protein S100A4 is markedly up-regulated by osmotic stress and is involved in the renal osmoadaptive response. *Journal of Biological Chemistry*. **282**, 6644-6652.
- Robertson, K.D., 2005. DNA methylation and human disease. *Nature Reviews Genetics*. **6**, 597-610.
- Rohde, D., Ritterhoff, J., Voelkers, M., Katus, H.A., Parker, T.G., Most, P., 2010. S100A1: A multifaceted therapeutic target in cardiovascular disease. *Journal of Cardiovascular Translational Research*. **3**, 525-537.
- Ronen, D., Rosenberg, M.M., Shalev, D.E., Rosenberg, M., Rotem, S., Friedler, A., Ravid, S., 2010. The positively charged region of the myosin IIC non-helical tailpiece promotes filament assembly. *Journal of Biological Chemistry*. **285**, 7079-7086.
- Rosty, C., Ueki, T., Argani, P., Jansen, M., Yeo, C.J., Cameron, J.L., Hruban, R.H., Goggins, M., 2002. Overexpression of S100A4 in pancreatic ductal adenocarcinomas is associated with poor differentiation and DNA hypomethylation. *The American Journal of Pathology*. **160**, 45-50.
- Rudland, P.S., Platt-Higgins, A., Renshaw, C., West, C.R., Winstanley, J.H.R., Robertson, L., Barraclough, R., 2000. Prognostic significance of the metastasis-inducing protein S100A4 (p9Ka) in human breast cancer. *Cancer Research*. **60**, 1595-1603.
- Rusakov, D.A., Davies, H.A., Stewart, M.G., Schachner, M., 1995. Clustering and co-localization of immunogold double labelled neural cell adhesion molecule isoforms in chick forebrain. *Neuroscience Letters*. **183**, 50-53.
- Ryan, D.G., Taliana, L., Sun, L., Wei, Z.-., Masur, S.K., Lavker, R.M., 2003. Involvement of S100A4 in stromal fibroblasts of the regenerating cornea. *Investigative Ophthalmology and Visual Science*. **44**, 4255-4262.
- Ryckman, C., Vandal, K., Rouleau, P., Talbot, M., Tessier, P.A., 2003. Proinflammatory activities of S100: Proteins S100A8, S100A9, and S100A8/A9 induce neutrophil chemotaxis and adhesion. *Journal of Immunology*. **170**, 3233-3242.
- Sakaguchi, M., Miyazaki, M., Inoue, Y., Tsuji, T., Kouchi, H., Tanaka, T., Yamada, H., Namba, M., 2000. Relationship between contact inhibition and intranuclear S100C of normal human fibroblasts. *Journal of Cell Biology*. **149**, 1193-1206.
- Salama, I., Malone, P.S., Mihaimed, F., Jones, J.L., 2008. A review of the S100 proteins in cancer. *European Journal of Surgical Oncology*. **34**, 357-364.
- Sandquist, J.C., Swenson, K.I., DeMali, K.A., Burridge, K., Means, A.R., 2006. Rho kinase differentially regulates phosphorylation of nonmuscle myosin II isoforms A and B during cell rounding and migration. *Journal of Biological Chemistry*. **281**, 35873-35883.

- Sandquist, J.C. & Means, A.R., 2008. The C-Terminal Tail Region of Nonmuscle Myosin II Directs Isoform-specific Distribution in Migrating Cells. *Molecular Biology of the Cell*. **19**, 5156-5167.
- Santamaria-Kisiel, L., Rintala-Dempsey, A.C., Shaw, G.S., 2006. Calcium-dependent and -independent interactions of the S100 protein family. *Biochemical Journal*. **396**, 201-214.
- Sanz-Moreno, V., Gadea, G., Ahn, J., Paterson, H., Marra, P., Pinner, S., Sahai, E., Marshall, C.J., 2008. Rac Activation and Inactivation Control Plasticity of Tumor Cell Movement. *Cell*. **135**, 510-523.
- Sato, Y., Harada, K., Itatsu, K., Ikeda, H., Kakuda, Y., Shimomura, S., Ren, X.S., Yoneda, N., Sasaki, M., Nakanuma, Y., 2010. Epithelial-mesenchymal transition induced by transforming growth factor- β 1/snail activation aggravates invasive growth of cholangiocarcinoma. *American Journal of Pathology*. **177**, 141-152.
- Sayan, A.E., Griffiths, T.R., Pal, R., Browne, G.J., Ruddick, A., Yagci, T., Edwards, R., Mayer, N.J., Qazi, H., Goyal, S., Fernandez, S., Straatman, K., Jones, G.D.D., Bowman, K.J., Colquhoun, A., Mellon, J.K., Kriaievska, M., Tulchinsky, E., 2009. SIP1 protein protects cells from DNA damage-induced apoptosis and has independent prognostic value in bladder cancer. *Proceedings of the National Academy of Sciences of the United States of America*. **106**, 14884-14889.
- Schlessinger, K., McManus, E.J., Hall, A., 2007. Cdc42 and noncanonical Wnt signal transduction pathways cooperate to promote cell polarity. *Journal of Cell Biology*. **178**, 355-361.
- Schneider, M., Hansen, J.L., Sheikh, S.P., 2008. S100A4: A common mediator of epithelial-mesenchymal transition, fibrosis and regeneration in diseases? *Journal of Molecular Medicine*. **86**, 507-522.
- Sellers, J.R., 2000. Myosins: A diverse superfamily. *Biochimica Et Biophysica Acta - Molecular Cell Research*. **1496**, 3-22.
- Sellers, J.R. & Knight, P.J., 2007. Folding and regulation in myosins II and V. *Journal of Muscle Research and Cell Motility*. **28**, 363-370.
- Shewan, A.M., Maddugoda, M., Kraemer, A., Stehbens, S.J., Verma, S., Kovacs, E.M., Yap, A.S., 2005. Myosin 2 is a key Rho kinase target necessary for the local concentration of E-cadherin at cell-cell contacts. *Molecular Biology of the Cell*. **16**, 4531-4542.
- Shibue, T. & Weinberg, R.A., 2009. Integrin β 1-focal adhesion kinase signaling directs the proliferation of metastatic cancer cells disseminated in the lungs. *Proceedings of the National Academy of Sciences of the United States of America*. **106**, 10290-10295.
- Silacci, P., Mazzolai, L., Gauci, C., Stergiopulos, N., Yin, H.L., Hayoz, D., 2004. Gelsolin superfamily proteins: key regulators of cellular functions. *Cellular and Molecular Life Sciences : CMLS*. **61**, 2614-2623.

- Sleeman, J.P. & Thiery, J.P., 2011. SnapShot: The epithelial-mesenchymal transition. *Cell*. **145**, 162-162.e1.
- Small, J.V., Isenberg, G., Celis, J.E., 1978. Polarity of actin at the leading edge of cultured cells. *Nature*. **272**, 638-639.
- Smutny, M., Cox, H.L., Leerberg, J.M., Kovacs, E.M., Conti, M.A., Ferguson, C., Hamilton, N.A., Parton, R.G., Adelstein, R.S., Yap, A.S., 2010. Myosin II isoforms identify distinct functional modules that support integrity of the epithelial zonula adherens. *Nature Cell Biology*. **12**, 696-702.
- Solomon, E., Borrow, J., Goddard, A., 1991. Chromosome aberrations and cancer. *Science*. **254**, 1153-1160.
- Sorci, G., Agneletti, A.L., Donato, R., 2000. Effects of S100A1 and S100B on microtubule stability. An in vitro study using triton-cytoskeletons from astrocyte and myoblast cell lines. *Neuroscience*. **99**, 773-783.
- Spector, D. & Goldman, R., 2006. *Basic Methods in Microscopy: Protocols and Concepts from Cells: A Laboratory Manual*. Cold Spring Harbor Laboratory Press.
- Sprague, B.L. & McNally, J.G., 2005. FRAP analysis of binding: proper and fitting. *Trends in Cell Biology*. **15**, 84-91.
- Srinivasan, S., Wang, F., Glavas, S., Ott, A., Hofmann, F., Aktories, K., Kalman, D., Bourne, H.R., 2003. Rac and Cdc42 play distinct roles in regulating PI(3,4,5)P3 and polarity during neutrophil chemotaxis. *The Journal of Cell Biology*. **160**, 375-385.
- Stein, U., Arlt, F., Walther, W., Smith, J., Waldman, T., Harris, E.D., Mertins, S.D., Heizmann, C.W., Allard, D., Birchmeier, W., Schlag, P.M., Shoemaker, R.H., 2006. The Metastasis-Associated Gene S100A4 Is a Novel Target of β -catenin/T-cell Factor Signaling in Colon Cancer. *Gastroenterology*. **131**, 1486-1500.
- Streicher, W.W., Lopez, M.M., Makhatadze, G.I., 2010. Modulation of quaternary structure of S100 proteins by calcium ions. *Biophysical Chemistry*. **151**, 181-186.
- Strutz, F., Okada, H., Lo, C.W., Danoff, T., Carone, R.L., Tomaszewski, J.E., Neilson, E.G., 1995. Identification and characterization of a fibroblast marker: FSP1. *The Journal of Cell Biology*. **130**, 393-405.
- Su, Y.L., Raftery, M.J., Goyette, J., Hsu, K., Geczy, C.L., 2009. Oxidative modifications of S100 proteins: Functional regulation by redox. *Journal of Leukocyte Biology*. **86**, 577-587.
- Suzuki, H., Onishi, H., Takahashi, K., Watanabe, S., 1978. Structure and function of chicken gizzard myosin. *Journal of Biochemistry*. **84**, 1529-1542.

- Takeda, K., Kishi, H., Ma, X., Yu, Z.-., Adelstein, R.S., 2003. Ablation and mutation of nonmuscle myosin heavy chain II-B results in a defect in cardiac myocyte cytokinesis. *Circulation Research*. **93**, 330-337.
- Takenaga, K., Nakamura, Y., Endo, H., Sakiyama, S., 1994a. Involvement of S100-related calcium-binding protein pEL98 (or mts1) in cell motility and tumor cell invasion. *Japanese Journal of Cancer Research*. **85**, 831-839.
- Takenaga, K., Nakamura, Y., Endo, H., Sakiyama, S., 1994b. Involvement of S100-related calcium-binding protein pEL98 (or mts1) in cell motility and tumor cell invasion. *Japanese Journal of Cancer Research : Gann*. **85**, 831-839.
- Takenaga, K., Nakamura, Y., Sakiyama, S., 1997a. Expression of antisense RNA to S100A4 gene encoding an S100-related calcium-binding protein suppresses metastatic potential of high-metastatic Lewis lung carcinoma cells. *Oncogene*. **14**, 331-337.
- Takenaga, K., Nakanishi, H., Wada, K., Suzuki, M., Matsuzaki, O., Matsuura, A., Endo, H., 1997b. Increased expression of S100A4, a metastasis-associated gene, in human colorectal adenocarcinomas. *Clinical Cancer Research*. **3**, 2309-2316.
- Tarabykina, S., Griffiths, T.R.L., Tulchinsky, E., Mellon, J.K., Bronstein, I.B., Kriajevska, M., 2007. Metastasis-associated protein S100A4: Spotlight on its role in cell migration. *Current Cancer Drug Targets*. **7**, 217-228.
- Tarabykina, S., Kriajevska, M., Scott, D.J., Hill, T.J., Lafitte, D., Derrick, P.J., Dodson, G.G., Lukanidin, E., Bronstein, I., 2000. Heterocomplex formation between metastasis-related protein S100A4 (Mts1) and S100A1 as revealed by the yeast two-hybrid system. *FEBS Letters*. **475**, 187-191.
- Tarabykina, S., Scott, D.J., Herzyk, P., Hill, T.J., Tame, J.R.H., Kriajevska, M., Lafitte, D., Derrick, P.J., Dodson, G.G., Maitland, N.J., Lukanidin, E.M., Bronstein, I.B., 2001. The dimerization interface of the metastasis-associated protein S100A4 (Mts1): In vivo and in vitro studies. *Journal of Biological Chemistry*. **276**, 24212-24222.
- Taylor, S., Herrington, S., Prime, W., Rudland, P.S., Barraclough, R., 2002. S100A4 (p9Ka) protein in colon carcinoma and liver metastases: Association with carcinoma cells and T-lymphocytes. *British Journal of Cancer*. **86**, 409-416.
- They, M., 2010. Micropatterning as a tool to decipher cell morphogenesis and functions. *Journal of Cell Science*. **123**, 4201-4213.
- They, M., Pepin, A., Dressaire, E., Chen, Y., Bornens, M., 2006. Cell distribution of stress fibres in response to the geometry of the adhesive environment. *Cell Motility and the Cytoskeleton*. **63**, 341-355.
- Thiery, J.P., 2003. Epithelial-mesenchymal transitions in development and pathologies. *Current Opinion in Cell Biology*. **15**, 740-746.
- Thiery, J.P., 2002. Epithelial-mesenchymal transitions in tumour progression. *Nature Reviews.Cancer*. **2**, 442-454.

- Thiery, J.P., Acloque, H., Huang, R.Y.J., Nieto, M.A., 2009. Epithelial-Mesenchymal Transitions in Development and Disease. *Cell*. **139**, 871-890.
- Trybus, K.M., Huiatt, T.W., Lowey, S., 1982. A bent monomeric conformation of myosin from smooth muscle. *Proceedings of the National Academy of Sciences of the United States of America*. **79**, 6151-6155.
- Tsoporis, J.N., Izhar, S., Leong-Poi, H., Desjardins, J.-., Huttunen, H.J., Parker, T.G., 2010. S100B interaction with the receptor for advanced glycation end products (RAGE): A novel receptor-mediated mechanism for myocyte apoptosis postinfarction. *Circulation Research*. **106**, 93-101.
- Tsoporis, J.N., Marks, A., Haddad, A., Dawood, F., Liu, P.P., Parker, T.G., 2005. S100B expression modulates left ventricular remodeling after myocardial infarction in mice. *Circulation*. **111**, 598-606.
- Tsuna, M., Kageyama, S., Fukuoka, J., Kitano, H., Doki, Y., Tezuka, H., Yasuda, H., 2009. Significance of S100A4 as a prognostic marker of lung squamous cell carcinoma. *Anticancer Research*. **29**, 2547-2554.
- Tulchinsky, E., Grigorian, M., Tkatch, T., Georgiev, G., Lukanidin, E., 1995. Transcriptional regulation of the mts1 gene in human lymphoma cells: The role of DNA-methylation. *Biochimica Et Biophysica Acta - Gene Structure and Expression*. **1261**, 243-248.
- Urban, E., Jacob, S., Nemethova, M., Resch, G.P., Small, J.V., 2010. Electron tomography reveals unbranched networks of actin filaments in lamellipodia. *Nature Cell Biology*. **12**, 429-435.
- Valastyan, S. & Weinberg, R.A., 2011. Tumor metastasis: Molecular insights and evolving paradigms. *Cell*. **147**, 275-292.
- Valsesia-Wittmann, S., Magdeleine, M., Dupasquier, S., Garin, E., Jallas, A.-., Combaret, V., Krause, A., Leissner, P., Puisieux, A., 2004. Oncogenic cooperation between H-Twist and N-Myc overrides failsafe programs in cancer cells. *Cancer Cell*. **6**, 625-630.
- van den Bos, C., Roth, J., Koch, H.G., Hartmann, M., Sorg, C., 1996. Phosphorylation of MRP14, an S100 protein expressed during monocytic differentiation, modulates Ca(2+)-dependent translocation from cytoplasm to membranes and cytoskeleton. *Journal of Immunology (Baltimore, Md.: 1950)*. **156**, 1247-1254.
- van Dieck, J., Fernandez-Fernandez, M.R., Veprintsev, D.B., Fersht, A.R., 2009. Modulation of the oligomerization state of p53 by differential binding of proteins of the S100 family to p53 monomers and tetramers. *The Journal of Biological Chemistry*. **284**, 13804-13811.
- Van Roy, F. & Berx, G., 2008. The cell-cell adhesion molecule E-cadherin. *Cellular and Molecular Life Sciences*. **65**, 3756-3788.

- Vandewalle, C., Comijn, J., De Craene, B., Vermassen, P., Bruyneel, E., Andersen, H., Tulchinsky, E., Van Roy, F., Berx, G., 2005. SIP1/ZEB2 induces EMT by repressing genes of different epithelial cell-cell junctions. *Nucleic Acids Research*. **33**, 6566-6578.
- Vandewalle, C., Van Roy, F., Berx, G., 2009. The role of the ZEB family of transcription factors in development and disease. *Cellular and Molecular Life Sciences : CMLS*. **66**, 773-787.
- Venkov, C.D., Link, A.J., Jennings, J.L., Plieth, D., Inoue, T., Nagai, K., Xu, C., Dimitrova, Y.N., Rauscher III, F.J., Neilson, E.G., 2007. A proximal activator of transcription in epithelial-mesenchymal transition. *Journal of Clinical Investigation*. **117**, 482-491.
- Vicente-Manzanares, M., Choi, C.K., Horwitz, A.R., 2009. Integrins in cell migration--the actin connection. *Journal of Cell Science*. **122**, 199-206.
- Vicente-Manzanares, M., Koach, M.A., Whitmore, L., Lamers, M.L., Horwitz, A.F., 2008. Segregation and activation of myosin IIB creates a rear in migrating cells. *Journal of Cell Biology*. **183**, 543-554.
- Vicente-Manzanares, M., Ma, X., Adelstein, R.S., Horwitz, A.R., 2009. Non-muscle myosin II takes centre stage in cell adhesion and migration. *Nature Reviews Molecular Cell Biology*. **10**, 778-790.
- Vicente-Manzanares, M., Newell-Litwa, K., Bachir, A.I., Whitmore, L.A., Horwitz, A.R., 2011. Myosin IIA/IIB restrict adhesive and protrusive signaling to generate front-back polarity in migrating cells. *The Journal of Cell Biology*. **193**, 381-396.
- Wang, F., Kovács, M., Hu, A., Limouze, J., Harvey, E.V., Sellers, J.R., 2003. Kinetic mechanism of non-muscle myosin IIB. Functional adaptations for tension generation and maintenance. *Journal of Biological Chemistry*. **278**, 27439-27448.
- Wang, Y.Y., Ye, Z.Y., Zhao, Z.S., Tao, H.Q., Chu, Y.Q., 2010. High-level expression of S100A4 correlates with lymph node metastasis and poor prognosis in patients with gastric cancer. *Annals of Surgical Oncology*. **17**, 89-97.
- Wear, M.A. & Cooper, J.A., 2004. Capping protein: new insights into mechanism and regulation. *Trends in Biochemical Sciences*. **29**, 418-428.
- Wei, C., Wang, X., Chen, M., Ouyang, K., Song, L.-., Cheng, H., 2009. Calcium flickers steer cell migration. *Nature*. **457**, 901-905.
- Wei, Q. & Adelstein, R.S., 2000. Conditional expression of a truncated fragment of nonmuscle myosin II-A alters cell shape but not cytokinesis in HeLa cells. *Molecular Biology of the Cell*. **11**, 3617-3627.
- Winterbourn, C.C. & Hampton, M.B., 2008. Thiol chemistry and specificity in redox signaling. *Free Radical Biology and Medicine*. **45**, 549-561.

- Wolf, K. & Friedl, P., 2011. Extracellular matrix determinants of proteolytic and non-proteolytic cell migration. *Trends in Cell Biology*. **21**, 736-744.
- Wolf, K., Mazo, I., Leung, H., Engelke, K., Von Andrian, U.H., Deryugina, E.I., Strongin, A.Y., Bröcker, E.-., Friedl, P., 2003. Compensation mechanism in tumor cell migration: Mesenchymal-amoeboid transition after blocking of pericellular proteolysis. *Journal of Cell Biology*. **160**, 267-277.
- Wyckoff, J.B., Wang, Y., Lin, E.Y., Li, J.-., Goswami, S., Stanley, E.R., Segall, J.E., Pollard, J.W., Condeelis, J., 2007. Direct visualization of macrophage-assisted tumor cell intravasation in mammary tumors. *Cancer Research*. **67**, 2649-2656.
- Wylie, S.R. & Chantler, P.D., 2008. Myosin IIC: A third molecular motor driving neuronal dynamics. *Molecular Biology of the Cell*. **19**, 3956-3968.
- Wylie, S.R. & Chantler, P.D., 2001. Separate but linked functions of conventional myosins modulate adhesion and neurite outgrowth. *Nature Cell Biology*. **3**, 88-92.
- Xie, R., Schlumbrecht, M.P., Shipley, G.L., Xie, S., Bassett, R.L., Jr, Broaddus, R.R., 2009a. S100A4 mediates endometrial cancer invasion and is a target of TGF-beta1 signaling. *Laboratory Investigation; a Journal of Technical Methods and Pathology*. **89**, 937-947.
- Xie, R., Schlumbrecht, M.P., Shipley, G.L., Xie, S., Bassett, R.L., Broaddus, R.R., 2009b. S100A4 mediates endometrial cancer invasion and is a target of TGF-beta1 signaling. *Laboratory Investigation*. **89**, 937-947.
- Xu, J., Lamouille, S., Derynck, R., 2009. TGF-beta-induced epithelial to mesenchymal transition. *Cell Research*. **19**, 156-172.
- Xu, J., Wang, F., Van Keymeulen, A., Herzmark, P., Straight, A., Kelly, K., Takuwa, Y., Sugimoto, N., Mitchison, T., Bourne, H.R., 2003. Divergent signals and cytoskeletal assemblies regulate self-organizing polarity in neutrophils. *Cell*. **114**, 201-214.
- Yammani, R.R., 2012. S100 proteins in cartilage: Role in arthritis. *Biochimica Et Biophysica Acta - Molecular Basis of Disease*. **1822**, 600-606.
- Yang, J., Mani, S.A., Donaher, J.L., Ramaswamy, S., Itzykson, R.A., Come, C., Savagner, P., Gitelman, I., Richardson, A., Weinberg, R.A., 2004. Twist, a master regulator of morphogenesis, plays an essential role in tumor metastasis. *Cell*. **117**, 927-939.
- Yang, J. & Weinberg, R.A., 2008. Epithelial-Mesenchymal Transition: At the Crossroads of Development and Tumor Metastasis. *Developmental Cell*. **14**, 818-829.
- Yilmaz, M. & Christofori, G., 2009. EMT, the cytoskeleton, and cancer cell invasion. *Cancer and Metastasis Reviews*. **28**, 15-33.
- Yonemura, Y., Endou, Y., Kimura, K., Fushida, S., Bandou, E., Taniguchi, K., Kinoshita, K., Ninomiya, I., Sugiyama, K., Heizmann, C.W., Schafer, B.W., Sasaki, T.,

2000. Inverse expression of S100A4 and E-cadherin is associated with metastatic potential in gastric cancer. *Clinical Cancer Research : An Official Journal of the American Association for Cancer Research*. **6**, 4234-4242.
- Yoon, C.S., Hyung, W.J., Lee, J.H., Chae, Y.S., Won, N.H., Yeom, B.W., Choi, J.S., 2008. Expression of S100A4, E-cadherin, alpha- and beta-catenin in gastric adenocarcinoma. *Hepato-Gastroenterology*. **55**, 1916-1920.
- Zhang, S., Wang, G., Fernig, D.G., Rudland, P.S., Webb, S.E.D., Barraclough, R., Martin-Fernandez, M., 2005a. Interaction of metastasis-inducing S100A4 protein in vivo by fluorescence lifetime imaging microscopy. *European Biophysics Journal*. **34**, 19-27.
- Zhang, S., Wang, G., Liu, D., Bao, Z., Fernig, D.G., Rudland, P.S., Barraclough, R., 2005b. The C-terminal region of S100A4 is important for its metastasis-inducing properties. *Oncogene*. **24**, 4401-4411.
- Zhou, Y., Yang, W., Kirberger, M., Lee, H.-., Ayalasomayajula, G., Yang, J.J., 2006. Prediction of EF-hand calcium-binding proteins and analysis of bacterial EF-hand proteins. *Proteins: Structure, Function and Genetics*. **65**, 643-655.
- Zhukova, L., Zhukov, I., Bal, W., Wyslouch-Cieszynska, A., 2004. Redox modifications of the C-terminal cysteine residue cause structural changes in S100A1 and S100B proteins. *Biochimica Et Biophysica Acta - Molecular Cell Research*. **1742**, 191-201.
- Zimmer, D.B., Wright Sadosky, P., Weber, D.J., 2003. Molecular mechanisms of S100-target protein interactions. *Microscopy Research and Technique*. **60**, 552-559.